Host and Viral Determinants of Reovirus Oncolysis

by

Adil Mohamed

A thesis submitted in partial fulfillment of the requirements for the degree of

Doctor of Philosophy

in

Virology

Department of Medical Microbiology and Immunology
University of Alberta

ABSTRACT

Mammalian orthoreovirus (reovirus) is a non-pathogenic virus that naturally infects through the enteric and respiratory routes. Reoviruses are non-enveloped and have a 10-segment double stranded RNA (dsRNA) genome encased in 2 concentric capsid shells. Representative isolates of each of the 3 reovirus serotypes include [(Type 1 Lang (T1L), Type 2 Jones (T2J), Type 3 Dearing (T3D) and Type 3 Abney (T3A)]. A proprietary variant of T3D (REOLYSIN®) is currently being evaluated as an oncolytic virotherapy in Phase I/II/III clinical trials for a multitude of cancers. However, in most clinical trials, REOLYSIN® treatment does not improve efficacy over standard of care. Therefore, in order to enhance REOLYSIN® efficacy as an oncolytic virus, there needs to be an improved understanding of mechanisms of reovirus replication both from a virus and host cell perspective.

The first chapter of our studies include an in-depth phenotypic and genotypic characterization of laboratory T3D strains. We demonstrate for the first time that oncolytic properties differ between T3D laboratory strains. Specifically, compared to $T3D^{KC}$ and $T3D^{TD}$, $T3D^{PL}$ had enhanced replication in cancer cell lines and demonstrated improved *in-vivo* tumor regression. Reassortment analysis and site-directed mutagenesis identified 3 genes (S4, M1, L3) and specific polymorphisms that account for replication differences between $T3D^{TD}$ and $T3D^{PL}$. Gene-function analysis determined that accelerated $T3D^{PL}$ replication kinetics was linked to i) M1 gene modulating superior inherent viral core transcriptase activity and filamentous virus factory morphology, ii) S4, M1 and L3 gene impacting suppression of RIG-I/MDA5 dependent signaling, iii) S4 gene mediating a heightened RIG-I/MDA5 independent signaling and iv) L3 gene governing large viral factories. An extensive phylogenetic comparison identified that current T3D laboratory strains have diverged from the original clinical T3D isolate, and laboratory specific virus propagation methodologies likely contributed to this divergence. Finally, the proprietary REOLYSIN® isolate was resolved to be identical in amino acid sequence to our laboratory T3D strain ($T3D^{PL}$), making our findings from this study directly applicable to improving our understanding of REOLYSIN®.

The second chapter involved functional characterization of host cell p38 MAPK signaling during reovirus replication. It was previously determined that the ras-p38 MAPK-IFN axis affected reovirus replication during multiple rounds of replication but the role of p38 MAPK during initial reovirus replication was unknown. We demonstrated that initial reovirus replication is diminished following p38 MAPK signaling inhibition using a panel of specific p38 MAPK inhibitors. Specifically, the efficiency of reovirus outer capsid cleavage was diminished following p38 MAPK inhibitor treatment and was specifically linked to reduced i) virion endocytosis and ii) endosome to lysosome transition. Additionally, we identified a beneficial role of p38 MAPK signaling during secondary reovirus amplification. Therefore, an active p38 MAPK signaling pathway enhanced various reovirus replication steps to facilitate productive infection. By assessing reovirus replication in a panel of breast cancer cell lines and subsequent microarray analysis, we identified MAPK11 (p38β) as a potential prognostic marker for reovirus

uncoating. Moreover, we propose the utilization of methodical prognostic markers specific for reovirus replication steps, rather than global prognostic markers as is currently performed.

Overall, our studies uncover novel virus and host cell determinants of reovirus replication and not only increases our appreciation of inter-laboratory reovirus diversity but also directly impacts our current understating of REOLYSIN®.

TABLE OF CONTENTS

LIST OF TABLES

LIST OF FIGURES

LIST OF ABBREVIATIONS

ATCC	American Type Culture Collection
ATF2	Cyclic AMP-dependent transcription factor 2
BafA1	Bafilomycin A1
CAT	Chloramphenicol acetyltransferase
CatB	Cathepsin B
CatG	Cathepsin G
CatL	Cathepsin L
CatS	Cathepsin S
cDNA	Complementary deoxyribonucleic acid
CHT	Chymotrypsin
CNS	Central nervous system
Con A	Concanamycin A
CQ	Chloroquine
CsCl	Cesium chloride
DI	Defective interfering
DKO	Double-knockout
DNA	Deoxyribonucleic acid
dsRNA	double stranded ribonucleic acid
ECHO-7	enteric cytopathogenic human orphan type 7
EEA1	Early endosome antigen 1
eEF2	Eukaryotic elongation factor 2

EGF	Epidermal growth factor
EGFR	Epidermal growth factor receptor
ELISA	Enzyme-linked immunosorbent assay
EMBL	European Molecular Biology Laboratory
FDA	Food and Drug Administration
GAPDH	Glyceraldehyde 3-phosphate dehydrogenase
GDI	Guanine nucleotide dissociation inhibitor
GM-CSF	Granulocyte-macrophage colony-stimulating factor
GPCR	G protein-coupled receptors
GPI	Glycosylphosphatidylinositol
GTase	Guanylyltransferase
HAT	Human airway trypsin-like protease
HER-2	Human epidermal growth factor receptor 2
hJAM	Human junction adhesion molecule
hpi	Hour post infection
Hsp27	Heat shock protein 27
HSV-1	Herpes simplex virus 1
ICAM-1	Intercellular Adhesion Molecule 1
IFN	Interferons
IP-10	Interferon gamma-induced protein 10
IRF3/7	interferon regulatory factor 3/7
ISG	Interferon stimulated genes
ISVP	Intermediate subvirion particle

JAM	Junction adhesion molecule
LAMP	Lysosomal-associated membrane protein
M	Microfold
MAPK	Mitogen activated protein kinase
MDA5	Melanoma Differentiation-Associated protein 5
MEF	Mouse embryonic fibroblast
MEL	Mouse erythroleukemia
MNK1	MAP kinase-interacting serine/threonine-protein kinase 1
MOI	Multiplicity of infection
mRNA	Messenger ribonucleic acid
MSK1	Mitogen and stress activated protein kinase 1
MT	Microtubule
mTORC1	Mammalian target of rapamycin complex 1
MβCD	Methyl-β-cyclodextrin
$Na_2{}^{51}CrO_4$	Sodium chromate
NE	Neutrophil elastase
Neu5Ac	α-linked 5-N-acetyl neuraminic acid
NFκB	Nuclear factor kappa light chain enhancer of activated B cells
NgR1	Nogo receptor
NH_4Cl	Ammonium chloride
NTPase	nucleotide triphosphatase
PAF	Platelet activating factor
PAFR	Platelet activating factor receptor

PCR	Polymerase chain reaction
PI-PLC	Phosphatidylinositol-specific phospholipase C
PKR	Protein kinase RNA
pNPP	para-Nitrophenylphosphate
RANKL	Receptor activator of nuclear factor kappa-B ligand
RBC	Red blood cell
RIG-I	Retinoic acid-inducible gene I
RNA	Ribonucleic acid
RT-PCR	Real time polymerase chain reaction
SAM	S-adenosyl methionine
SIV	Simian immunodeficiency virus
SLL	α-sialyllactose
ssRNA	single stranded ribonucleic acid
T1L	Type 1 Lang
T2J	Type 2 Jones
T3A	Type 3 Abney
T3D	Type 3 Dearing
TLR	Toll like receptor
TNFα	Tumor necrosis factor α
TPC2	Two-pore channel subtype 2
UV	Ultraviolet
V-ATPase	Vacuolar ATPase
VF	Viral factory

CHAPTER 1: INTRODUCTION

1.1 CANCER BURDEN

According to the World Health Organization, cancer is the second leading cause of death, with 8.8 million global deaths per year [1, 2]. In Canada, cancer causes the highest mortality, accounting for almost 30% of all deaths. The Canada Cancer Society have presented striking and grim 2017 statistics; over 200,000 Canadians will be diagnosed with cancer and close to 80,000 will die of cancer in 2017 alone [3]. There is an urgent need for solving what is now termed the cancer epidemic. Various initiatives in cancer research over the past few decades have improved our understanding of cancer biology and etiology, and together with advancements in patient care, have allowed patients diagnosed with cancer to live longer and improve their quality of life. However, the costs associated with these achievements, compounded by the rising cancer incidence, have put immense pressure on government budgets and the health care system. Direct cancer related costs represent 7% of the total Canadian healthcare spending budget. In addition to government funding, numerous charitable organizations also contribute towards alleviation of the cancer burden. In Canada, of the more than 2.7 billion dollars spent by charities and the government towards the fight against cancer, 20% funds cancer research, 25% supports patient awareness and advocacy and 55% goes towards fundraising, salaries and overhead costs [4].

1.2 CANCER TREATMENT

Cancer treatments can be broadly divided into 4 categories; surgery, radiation, chemotherapy and immunotherapy [5]. The treatment options available are highly dependent on the cancer stage, which is a description of the cancer size, location, metastasis level and cell type.

The TNM cancer staging system is used to report all cancer types except for blood, brain and spinal cord cancers. T, N, and M describe cancer status at the primary site, nearby lymph nodes and metastatic sites, respectively. The letter (T, N, M) is followed by a number, which provides additional information such as size of tumor and number of cancer containing lymph nodes [6]. Improvements in imaging techniques and the discovery of novel cancer biomarkers have made cancer staging more accurate and led to better treatment regimen planning [7]. Treatment strategies usually involve a combination of more than one therapy. For example, in the case of a solid tumor, surgery would be used to resect the tumor mass, and chemotherapy and/or radiation would be used to target the cancer cells around the tumor margin and metastatic tumor sites [5].

1.2.1 Conventional cancer therapies

Conventional cancer therapies (chemotherapy, radiation) are commonly associated with severe side effects since they target dividing cells, which include both cancer and normal cells. Targeted cancer therapies include small molecule inhibitors and monoclonal antibodies that are designed to block or interfere with specific molecules present or active only in cancer cells. Two classical examples of targeted therapies are Herceptin® and Zelboraf®. Herceptin® specifically targets and inhibits human epidermal growth factor receptor 2 (HER2), whose downstream signaling controls cell proliferation and cell cycle. Over-expression of HER2 on the cell surface is a feature on certain aggressive breast cancers. On the other hand, Zelboraf® uniquely binds and inhibits a mutated form of BRAF (BRAF V600E), which accounts for enhanced growth signaling in many skin cancers [8]. Recently, biological therapies such as bacteria and viruses are being pursued as targeted cancer therapies. Biological therapies offer several advantages over conventional cancer therapies: i) tumor homing and targeting ii) intratumoral amplification iii) easily modifiable [9].

1.2.2 Biological cancer therapies

The use of biological therapies as a cancer therapy were reported in the late 19th century by several physicians and professors. However, Dr. William Coley is recognized as being the first to systematically administer his "toxin" to a large number of human patients. In 1891, Dr. Coley, a clinician-scientist at the New York Hospital, became curious following the spontaneous remission of an inoperable neck tumor in a patient who developed erysipelas, a *Streptococcus pyogenes* infection of the skin [10]. Similar instances of cancer remission after a bacterial infection had previously been reported, including one dating back to 1725 in Paris, where patients with syphilis (*Treponema pallidum*) were often cured of tumors and developed fewer tumors than the average population [11, 12]. Convinced by these observations, Dr. Coley injected 3 sarcoma patients with live Streptococcal cultures. These injections proved to be very toxic and 2 of the 3 patients died of infection, even with observable tumor shrinkage [10, 13]. In an attempt to lower toxicity, future studies involved using heat-inactivated cultures of *Streptococcus pyogenes* and *Serratia marcescens*, a mixture commonly referred to as Coley's toxin [10, 14-16]. Even though Dr. Coley reported numerous tumor remission successes with his toxin, the rest of the medical field remained sceptical of the results. Poor patient follow-ups, non-standard toxin preparations, and different administration routes, made Dr. Coley's findings un-reproducible by other physicians. Eventually, due to political and hierarchical conflicts of interest, in addition to the impending development of radiation therapy, the Coley's toxin was un-registered by the United States Food and Drug Administration (FDA) [10, 17-19]. Recent studies focussed on reproducing Dr. Coley's findings and re-assessing his patients' follow-ups, demonstrated a significant tumor regression and remission in 20-50% of patients with Coley's toxin regimen [10, 20, 21]. Dr. Coley had reported that the sustained fever triggered by his toxin

was likely the key to cancer remission [22]. With our current knowledge on toll like receptors (TLRs), cytokines and the role of immune system activation in cancer, it is now widely recognized that Dr. Coley's findings were the first reports of cancer immunotherapy. Our improved understanding of the tumor microenvironment and genetic technology advancements has resulted in the pursuit of revisiting the use of live bacteria for targeted cancer therapy. Observations that solid tumors possess regions of low oxygen due to poor and disorganized vascularization are the basis for the use of genetically modified live attenuated strains of obligate (Bifidobacterium, Clostridium) or facultative (Salmonella, Listeria) anaerobic bacteria as tumor homing and targeting oncolytic bacteria [23, 24]. *Clostridium novyi*-NT, *Salmonella typhimirium* (VNP20009 and TAPET-CD) and *Listeria monocytogenes* (ANZ-100 and CRS-207) are currently undergoing phase I and II clinical trials [24].

1.2.3 Oncolytic viruses

The first reports of a virus having the potential to treat tumors were made by Italian clinicians in the late 1890s to early 1900s, when patients with cervical cancer underwent remission following administration of the rabies vaccine. In one instance a patient's cervical tumor shrank following a rabid dog bite [25-27]. The rabies vaccine used at the time was developed by Louis Pasteur, who attenuated the pathogenic rabies virus by repeated passaging in rabbits. Each rabbit passage involved spinal cord extraction and drying to progressively inactivate the virus. Since then, advancements in the field of virology, including the development of cell culture techniques, microscopical visualization of viruses and animal models for viruses and cancer, a number of viruses have been evaluated as cancer therapies [28]. The first reported oncolytic virus human clinical trial was performed in 1949 using Hepatitis B virus on patients with Hodgkin's lymphoma. Of the 22 patients in the trial, 14 developed hepatitis and 7 had

improvements in clinical symptoms [28, 29]. Trials were also performed in the 1950s using West Nile virus and adenovirus with limited success [28, 30, 31]. In 1974, a highly controversial trial on 90 terminally ill cancer patients was performed using a non-attenuated strain of the mumps virus. It was reported that 37 patients had either complete tumor regression or regression of more than 50%, while 42 patients had regression of less than 50% [28, 32]. All these early trials had similar ethical concerns with using pathogenic human viruses and uncontrolled virus inoculums, which in some instances included unpurified human sera and tissue extracts [28]. Pioneering studies Dr. Alice Moore in the 1950's, with oncolytic viruses and animal models of cancer are highly under-appreciated, and her work deserves more recognition by the oncolytic virus field. Dr. Moore's research: i) demonstrated in controlled experiments that multiple viruses can be oncolytic *in-vivo*, ii) established the concept that *in-vivo* oncolytic virus efficacy can be enhanced by repeated passage in cancer cells *in-vitro*, iii) recognized that specific oncolytic virus efficacy depends on tumor type (melanoma, sarcoma, carcinoma) and iv) observed that virus replication in tumors to high titres does not always cause tumor regression [33-48].

1.2.3.1 Clinically approved oncolytic viruses

In 2004, RIGVIR®, an unmodified enteric cytopathogenic human orphan type 7 (ECHO-7) was the first ever oncolytic virus to be granted regulatory approval. RIGVIR® was initially approved for use in Latvia to treat melanoma and has since been approved for use in Georgia and Armenia in 2015 and 2016, respectively [49, 50]. ONCORINE®, a genetically attenuated adenovirus was approved in 2005 for the treatment of head and neck cancer in China [49, 51]. In 2015, T-VEC®, a modified herpes simplex virus, became the first FDA-approved oncolytic virus for the treatment of advanced melanoma. T-VEC® has since been approved for use in Australia and Europe [52]. Currently, numerous oncolytic viruses are being pursued in European,

American and Canadian clinical trials, of which five viruses comprise a majority of the studies; i) Herpes Simplex Virus 1 (T-VEC®), ii) Vaccinia Virus (JX-594®), iii) Coxsackievirus A21 (CAVATAK®), iv) Adenovirus (DNX-2401®) and v) Mammalian orthoreovirus (REOLYSIN®) [53, 54]. Oncolytic viruses achieve their tumor specificity by targeting unique features of cancer cells. Most oncolytic viruses in clinical trials are genetically modified to primarily improve cancer cell specificity, and occasionally to minimize any potential of pathogenicity [53]. The strategic design of T-VEC® will be discussed as an example.

1.2.3.2 T-VEC®

T-VEC® is a genetically modified herpes simplex virus type 1 (HSV-1) strain JS1, originally isolated from an otherwise healthy volunteer with a cold sore, exclusively for the pursuit of oncolytic studies. It was reasoned that human HSV-1 isolation was necessary since the HSV-1 laboratory strains being utilized for oncolytic studies had been attenuated due to repeated passaging in non-human cell lines, and hence not optimal as oncolytic viruses [55]. HSV-1 encoded ICP34.5 is involved in neurovirulence and antiviral interferon (IFN) suppression [56]. As a result, most HSV-1 oncolytic viruses are ICP34.5-null to minimize pathogenicity. In a panel of human cancer cell lines, using both wild-type and ICP34.5-null viruses, it was demonstrated that human isolated HSV-1 strain JS1 was more cytolytic compared to the HSV-1 strain 17+, a highly virulent laboratory adapted HSV-1 virus backbone used in oncolytic clinical trials. In addition to the ICP34.5 gene deletion in HSV-1 strain JS1, oncolytic activity was further enhanced by deletion of the ICP47 gene and replaced by the US11 gene [55]. ICP47 functions to suppress surface expression of peptides on major histocompatibility complex class I (MHC-I), resulting in inhibition of immune cell detection of virus infected cells [55, 57]. The US11 protein is expressed late during HSV-1 infection and serves to block protein kinase RNA (PKR)

activation and restrict PKR induced anti-viral signaling and PKR modulated host protein translation [55, 58, 59]. ICP47 is expressed early during HSV-1 infection and hence replacement of ICP47 with US11 results in earlier expression of US11 and improved inhibition of PKR mediated signaling [60]. JS1Δ34.5/ICP47 exhibited enhanced tumor clearance *in-vivo*, relative to JS1Δ34.5, demonstrating a functional benefit of ICP47 deletion and early US11 expression in oncolytic activity. To further stimulate host anti-tumor immunity, the gene encoding the cytokine granulocyte-macrophage colony-stimulating factor (GM-CSF) was replaced in place of the deleted ICP34.5 gene [55]. GM-CSF is a potent immune recruiting and activating cytokine that has been observed to function in anti-tumor immunity [61]. Using a contralateral tumor model, it was demonstrated that JS1+GM-CSFΔ34.5/ICP47 administration into the primary tumor resulted in enhanced tumor regression of the secondary non-injected tumor compared to JS1Δ34.5/ICP47. The primary injected tumor regressed to a similar extent in JS1+GM-CSFΔ34.5/ICP47 and JS1Δ34.5/ICP47 treatments [55]. In summary, T-VEC® is a minimal cell adapted human isolated HSV-1 strain with genetic modifications to eliminate pathogenicity and enhance anti-viral and anti-tumor immunity.

1.2.3.3 REOLYSIN®

Most oncolytic viruses undergoing clinical trials are genetically modified, however a few wild-type unmodified viruses are also being pursued. Examples include: i) PARVORYX®, a parvovirus H1 strain, ii) CAVTAK®, a coxsackie virus A21 strain, iii) REOLYSIN®, Mammalian orthoreovirus type 3 Dearing strain [53, 54]. REOLYSIN® is under trademark by Oncolytics Biotech Inc., based in Calgary, Alberta. REOLYSIN® has undergone numerous phase I/II clinical trials in a wide range of cancers and has an excellent safety profile with the maximum tolerable dose yet to be attained. Most patients administered REOLYSIN® respond

with transient (less than 6hrs) mild flu-like symptoms such as chills, fever and headache [62, 63]. All current REOLYSIN® clinical trials are in combination with chemotherapies and immunotherapies. Most trials with REOLYSIN® and various combination therapies have demonstrated minimal overall survival benefit. The inclusion of tumor prognostic markers such as EGFR, BRAF and KRAS, (i.e. signalling pathways known to enhance reovirus replication), slightly improve overall survival statistics, suggesting the need for identification of additional prognostic markers [63-67]. A recent phase II clinical trial in advanced or metastatic breast cancer demonstrated promising results, with a doubling in overall survival for patients receiving REOLYSIN® in combination with chemotherapy (21 months) compared to patients who received chemotherapy alone (10.8months) [68]. These results make REOLSYIN® the first intravenously delivered oncolytic virus in a randomized study to display a statistically significant advantage in overall survival, and approval for a phase III study has been granted by the FDA [62]. Pre-clinical studies have established an important role of host immune system activation during REOLYSIN® therapy for maximum therapeutic efficacy [63]. Early phase I/II clinical trials are currently underway in pancreatic cancer and myeloma with REOLYSIN® in combination with immune system activating therapies [62]. Better understanding of reovirus structure, reovirus replication and host responses to reovirus infection will assist in designing next generation REOLYSIN® variants and in selection of optimal chemo- and immuno-therapy combinations.

1.3 REOVIRUS

1.3.1 Background

Mammalian orthoreovirus (reovirus) species belong to the *Orthoreovirus* genus and *Reoviridae* family and consists of icosahedral, non-enveloped viruses with segmented dsRNA

genomes [69-72]. Members of the *Orthoreovirus* genus can be classified as being either fusogenic or non-fusogenic; the former causing multinucleated syncytial cells during virus infection [73-75]. The fusogenic potential has been extensively characterized and is encoded by a fusion-associated small transmembrane (FAST) protein [76, 77] . All *Mammalian orthoreovirus* isolates are classified as non-fusogenic, while members of the *Avian orthoreovirus*, *Baboon orthoreovirus* and *Reptilian orthoreovirus* species are fusogenic [75, 78]. *Pteropine orthoreovirus* isolates consist of both fusogenic and non-fusogenic viruses [79-81]. It is important to note that although *Baboon orthoreoviruses* and *Pteropine orthoreoviruses* are of mammalian origin, they are not classified as *Mammalian orthoreoviruses*.

Reoviruses are commonly isolated from a wide range of vertebrate hosts; Humans, Monkeys, Mice, Dogs, Cattle, Pigs [82-86]. More than 90% of the human population is seropositive for reovirus, indicative of its highly ubiquitous nature [87, 88]. Based on serum neutralization assays, S1 gene sequence, and/or S1 electropherotype, reoviruses are classified into three serotypes; type 1, type 2 and type 3 [69, 89-92]. Prototypic human isolated clinical isolates commonly studied in research laboratories include type 1 Lang (T1L), type 2 Jones (T2J), type 3 Dearing (T3D) and type 3 Abney (T3A) [69, 93].

1.3.2 Disease burden

In humans, reoviruses are commonly isolated from both healthy children and children with gastrointestinal illness [69]. A study on human volunteers inoculated intranasally with each of the three reovirus serotypes isolated from humans, 8 of 28 individuals developed illness which was defined as malaise, rhinorrhea, cough, sneezing, pharyngitis and headache. The illness was self-limiting and lasted for 4 to 7 days. Accordingly, reovirus was designated as an orphan (non-

pathogenic) human virus. It is important to note that all volunteers in the study were healthy adult males aged 21 to 38 years old and were seropositive for reovirus prior to the experiment [94]. In a controlled experiment performed on young (less than 1 year old) monkeys (*Macaca radiata*) using various inoculation routes (oral/nasal, intragastric, intravenous) with human reovirus serotype 3, it was observed that reovirus could no longer be isolated from rectal and throat swabs after 14 days post inoculation and 13 of the 17 animals developed mild fever and diarrhea which lasted 6 to 15 days. No inflammation of the liver, heart or pancreas was detected in any of the monkeys [95, 96].

In a separate study, a serotype 1 reovirus isolated from a lung of a dog that died with a respiratory illness, was assessed for pathogenicity in multiple animal models including dogs, monkeys (*Macaca fascicularis*), rabbits, guinea pigs, hamsters and ferrets. The dogs used in the experiment were 8-week old weanling pups. All four dogs were infected intranasally and at 6-8 days post inoculation, developed fever and respiratory illness (cough, nasal watery discharges and foamy saliva). Histopathology at 13 days post inoculations determined interstitial pneumonitis. However, none of the other animal models tested had any clinical signs of disease, suggesting potential host-specificity of the reovirus isolate used [97]. In mouse models, reovirus pathogenesis is highly dependent on the reovirus serotype, laboratory strain, inoculation route, infection dose, mouse age, mouse strain and laboratory location. The consensus observation in mouse models is that weanling (21-28 day old) and adult mice are asymptomatic to reovirus infection. In summary: i) humans and monkeys infected with human reovirus isolates result in either asymptomatic infection or causes a mild self-limiting gastrointestinal/respiratory infection and ii) mice infected with human isolates of reovirus produce highly variable results.

There have been 2 recent reports of reovirus being isolated from the cerebrospinal fluid of human infants, one a 6.5-week old with meningitis and the second an 8-week old with bacterial sepsis and gastrointestinal distress [98-100]. Even though there is no causal evidence, these reports suggest that age and/or immune status could potentially play a role in human pathogenesis by reovirus. Additionally, there has been an increasing number of *Pteropine orthoreoviruses* from bats being isolated and identified from humans with acute respiratory infection, indicating that reovirus host-specificity is plastic and has the potential of expanding its host range [101-103].

1.3.3 Genome composition

The reovirus genome is packaged within the viral core and is composed of 10 dsRNA segments; 4 small (S1, S2, S3, S4), 3 medium (M1, M2, M3), 3 large (L1, L2, L3) [91]. The 10 genome segments encode 12 proteins, 8 structural (σ1, σ2, σ3, μ1, μ2, λ1, λ2, λ3) (Figure 1.2) and 4 non-structural (σ1s, σNS, μNS, μNSC). S1 encodes σ1 and σ1s, S2 encodes σ2, S3 encodes σNS, S4 encodes σ3, M1 encodes μ2, M2 encodes μ1, M3 encodes μNS and μNSC, L1 encodes λ3, L2 encodes λ2 and L3 encodes λ1 (Table 1.1, [104-106]). Note that the naming of reovirus dsRNA segments and proteins was based on electrophoretic molecular weights and therefore can get confusing, for example L1 (slowest migrating L genome segment) encodes λ3 (fastest migrating large reovirus protein) (Figure 1.1). The S1 segment produces two proteins by means of alternative start codon usage; relative to the AUG start site at position 13 which expresses σ1, translation initiation at an alternative frame AUG at position 71 results in expression of σ1s [92]. On the other hand, the μNSC protein is an in-frame translation product that is 40 amino acids smaller in length relative to μNS [107, 108].

1.3.4 Genome packaging

Each genome segment has 5' and 3' untranslated regions (UTRs) of varying lengths and sequences, however the initial sequence at the 5' end (GCTA) and the final sequence at the 3' end (CATC) are the same for all 10 genome segments [109-112]. Both the 5' and 3' sequences are required for packaging, as complete deletion of either does not produce functional virions [111, 113, 114]. The 5' end is the gene assortment determinant, and the 10 genes with their unique 5' ends are required for functional assembly of virions [114]. Deletion analyses determined that the minimum packaging signal length differed between genome segments; S2 gene 5' 96 nucleotides (nt) and 3' 98nt, M2 gene 5' 124nt and 3' 172nt, L1 gene 5' 129nt and 3' 139nt. Using various combinations of the minimum 5' and 3' packaging signals of the S2, M1 and L1 genes flanking the chloramphenicol acetyltransferase (CAT) reporter gene, it was observed that the 5' minimum packaging signal was the determinant of gene assortment [111, 113-117]. For example, combining the 5' 96nt S2 and 3' 172nt M1 (5' S2-CAT-M1 3') was capable of replacing the reovirus S2 gene and generate infectious virions [114]. Furthermore, studies have also demonstrated that 5' UTR secondary structure is important for reovirus genome packaging. The first study utilized combinations of the 5' and 3' packaging signals from T1L and T3D serotypes and assessed feasibility of forming functional virions. The CAT gene flanked with 5' T1L-L1 and 3' T3D-L1 packaging signals did not generate functional T3D virions and was further investigated. The 5' packaging signal of the L1 gene from T1L and T3D differ at 3 positions; A46G, A60G and C81U. Following assessment of single site revertants, only the 5' T1L-L1 packaging signal with a T3D reversion at position 81 (T1L-C81U) generated functional virions (in combination with a 3' T3D-L1). Using a secondary structure prediction tool, the 5' ends of T3D-L1 and T1L-C81U had identical loop structures and were distinct from single site

reversions (T1L-A46G, T1L-A60G) as well as double site reversions (T1L-A46G/A60G, T1L-A46G/C81U, T1L-A60G/C81U) [117]. In the second study, addition of a 300bp Simian immunodeficiency virus (SIV)-gag sequence to the 5' end of the L1 gene only generated functional virions when wobble base mutagenesis was performed on the SIV-gag sequence to generate RNA secondary structure with similar energy burden of the 5' end of the L1 gene [115]. Therefore, both sequence and secondary structure of the 5' end are important for reovirus genome packaging.

1.3.5 Virion composition

(Figure 1.2)

The 10 reovirus genome segments are packaged within the viral core capsid consisting of 120 copies of the λ1 shell stabilized in place by 150 copies of the σ2 clamp. Within the viral core at the base of each vertex is 1 copy of λ3 RNA-dependent RNA polymerase (10-12 copies per virion) and 2 copies of the μ2 polymerase cofactor (20-24 copies per virion). It is unclear if all 12 vertices are occupied by λ3 and μ2. Some models propose that only 10 vertices are occupied, each with 1 dsRNA genome, λ3 and μ2. Each vertex is composed of a pentameric λ2 turret-like complex (60 copies per virion) where nascent viral mRNA is capped by λ2 enzymatic activities and extruded from the viral core [118-123]. Surrounding the viral core is an outer capsid composed of heterohexameric complexes of μ1 coated by σ3 (600 copies each per virion), with σ3 exposed on the exterior [120, 123-125]. The trimeric σ1 cell attachment protein (36 copies per virion) is located at each vertex and is held in place by the flap domain of the λ2 turret-like complex interacting with the σ1 tail domain [120, 123, 126-128].

1.3.6 Replication

(Figure 1.3)

1.3.6.1 Cell binding

1.3.6.1.1 Sialic acid (low affinity binding receptor)

Reovirus binding to the host cell is mediated by viral σ1 and cell surface molecules. The hemagglutination assay is a classical method that utilizes erythrocyte surface sialic acid mediated agglutination as a measure of virion, bacteria or antibody concentration [129-131]. Sialic acids were first predicted to be involved in reovirus binding following the observation that reovirus mediated erythrocyte agglutination and that agglutination was abolished when sialic acids were depleted by neuraminidase treatment [132]. The importance of sialic acids and other glycans during reovirus cell binding are dependent on both host cell type and reovirus serotype.

Comparing T1 reovirus infectivity in L929 (mouse fibroblast cell line) and MEF (mouse embryonic fibroblast) cell lines, neuraminidase treatment only diminished reovirus infectivity in MEF cells [133], suggesting that sialic acid binding is dispensable for T1 reovirus infection in L929 cells. Many studies on reovirus and sialic acid binding utilize isogenic viruses T3SA+ and T3SA- which were identified by understanding and manipulation of a bovine reovirus field isolate (T3C44) capable of binding cells independent of sialic acids. Similar to MEF cells, reovirus binding to the mouse erythroleukemia (MEL) cell line is highly dependent on sialic acid binding. Adaptation of T3C44 on MEL cells generated a reovirus variant dependent on sialic acid for cell binding with a single site amino acid L204P change in the σ1 cell attachment protein. To eliminate the impact of confounding mutations in other genes, two isogenic T1L

reassortants were generated, one with T3C44 P204 σ1 (T3SA+) and the second with T3C44 204L σ1 (T3SA-). T3SA+ and T3SA- differ only in the S1 gene encoding σ1 cell attachment protein at amino acid L204P, rendering the virus containing P204 capable of binding to sialic acid (T3SA+) and L204 incapable of binding sialic acid (T3SA-). Viral yield following infection of T3SA+ and T3SA- in MEL cells resulted in T3SA+ infection producing 2500 times higher viral yield relative to T3SA-, validating sialic acid dependency [134].

Using specific glycan array screening, it was determined that T1L reovirus σ1 has a preference for binding GM2 glycan while T3D reovirus σ1 selectively binds α-linked 5-N-acetyl neuraminic acid (Neu5Ac) sialylated glycans [133]. Sequence and crystal structure analysis have determined that sialic acid binding occurs at the head domain of T1L and at the body domain of T3D [133, 135]. Sialic acids also play a role in the context of reovirus infection via the intestinal route. Peroral infection of mice with T3SA- or T3SA+ reovirus strains demonstrated that T3SA+ strain had enhanced spread to distant organs and lethality, relative to T3SA-. Interestingly, intestinal infection was similar between T3SA+ and T3SA-, suggesting that reovirus binding to sialic acid was likely important for reovirus access to and spread via the systemic system [136]. Using sialic acid competition assays on fixed intestinal sections, T1L was observed to specifically bind to M cells in a MAL I and MAL-II dependent manner. MAL I and MAL II are plant generated lectins that bind sialic acids linked α2-3 to galactose [137]. Therefore, sialylated glycans are important for reovirus binding during intestinal infection *in-vivo* and in cell culture *in-vitro*.

1.3.6.1.2 Junction adhesion molecule-A (JAM-A) (high affinity binding receptor)

Reovirus (T3SA+ and T3SA-) binding competition assays performed in the presence of σ1 monoclonal antibody (9BG5) and/or α-sialyllactose (SLL) proposed the presence of a high avidity σ1 head domain binding receptor, in addition to the low avidity σ1 body domain binding sialic acid. Pre-incubation of T3SA- with SLL had no effect on virus infection, as anticipated, while the pre-incubation with 9BG5 antibody lowered virus infection, suggesting a second virus binding molecule. When T3SA+ was used, individual pre-treatment with SLL and 9BG5 diminished virus infection, whereas combining both SLL and 9BG5 had an additive inhibitory effect on virus infection, further indicating the presence of a virus binding moiety other than sialic acid. Kinetics of attachment and temporal competition assays demonstrated that sialic acids accelerate initial viral binding but do not initiate virus entry into the cell. Conversely, the binding receptor inhibited by 9BG5 enables high affinity virus binding and triggers viral entry and subsequent infection. The 9BG5 monoclonal antibody is serotype specific and binds to reovirus serotype 3 σ1 head domain [134].

In search of the σ1 head binding receptor, the reovirus resistant COS-7 monkey fibroblast-like cell line was transfected with a cDNA library generated from the reovirus susceptible NT2 human neuronal precursor cell line, and the top 0.5% of cells with highest T3SA- binding were sorted. Plasmids from sorted cells were isolated, further enriched over three rounds of T3SA- binding and sequenced for identity. All four clones that conferred enhanced T3SA- binding encoded human junction adhesion molecule (hJAM). Overexpression of hJAM enhanced reovirus binding, whereas hJAM antibody pre-treatment diminished reovirus binding. Furthermore, in a cell-independent surface plasmon resonance assay, reovirus virions were found to directly bind hJAM [138]. JAM is an immunoglobulin superfamily transmembrane protein

expressed on a wide array of tissues and cell types and functions in regulating tight junction barriers and immune cell extravasation. There are three isoforms of JAM, namely JAM-A, JAM-B, JAM-C. Subsequent expression studies have delineated the JAM-A isoform as the high avidity reovirus receptor [139].

Using a JAM-A knockout (JAM-A -/-) mouse model, it was observed that JAM-A is not required for intestinal reovirus replication following peroral infection. However, systemic reovirus dissemination and replication in distant organs (spleen, liver, heart, brain) following peroral infection is dependent on JAM-A. Additionally, relative to primary endothelial cells from JAM+/+ mice, reovirus infection in JAM-A -/- cells was highly attenuated, suggesting that systemic dissemination of reovirus is determined by JAM-A dependent infection of endothelial cells [140].

1.3.6.1.3 Nogo receptor (NgR1) (neuron targeting receptor)

In-vivo pathogenesis models have demonstrated that in the absence of a functional immune system to prevent reovirus systemic spread, reovirus has tropism for the central nervous system (CNS). Following intracranial virus inoculation and assessment of reovirus (T3SA-) infection and histopathology of the brain in JAM +/+ and JAM-/- mice, it was observed that reovirus infection in the brain occurred independent of JAM-A. Additionally, reovirus infection was similar between JAM-A +/+ and JAM-A -/- in primary cortical neuron cell culture *in-vitro*, collectively implying the presence of neural receptors of reovirus other then JAM-A [140].

Using a whole genome siRNA knockdown screen, Nogo Receptor (NgR1) was identified as a top candidate receptor that mediates CNS reovirus infection. NgR1 is a glycosylphosphatidylinositol (GPI)-anchored membrane protein primarily expressed in the CNS

on the surface of neurons, and to a lesser extent on epithelial cells [141, 142]. Using reovirus resistant CHO cells, it was demonstrated that expression of NgR1 enhanced reovirus binding and infection. Treatment of NgR1 expressing CHO cells with GPI cleaving phosphatidylinositol-specific phospholipase C (PI-PLC) or pre-incubation of reovirus with soluble NgR1, diminished reovirus infection. Antibodies against NgR1 reduced reovirus infection of primary cortical neurons as well as NgR1 expressing CHO cells. Therefore, the evidence strongly suggests that NgR1 mediates reovirus binding and infection in the CNS [143].

Signaling initiated following NgR1 binding to its ligands (Nogo proteins, myelin-associated glycoprotein (MAG), oligodendrocyte myelin glycoprotein (OMgp) and B lymphocyte stimulator (BLyS)), modulate actin cytoskeleton controlling Rho-associated protein kinases (ROCKs) and inhibit neuronal axon growth. As a result, pharmacological inhibition of either NgR1 or its cognate ligands are being pursued as a means to aid in recovery from CNS injuries [144]. It has yet to be determined if reovirus binding triggers Ngr1 mediated signaling, and if this signaling cascade contributes to the observed reovirus mediated CNS pathology. In conclusion, reovirus binding is host cell type dependent and mediated by three host factors; surface glycan sialic acids, tight junction JAM-A and neuronal NgR1.

1.3.6.2 Endocytosis

1.3.6.2.1 β1 integrin (endocytosis trigger)

Following reovirus binding to the cell surface, virion internalization is initialized. Reovirus infection in resistant CHO cells transfected with either JAM-A or JAM-A lacking its cytoplasmic domain, was equivalent, implying that a trigger other than JAM-A binding/signaling was important for reovirus entry. Identification of integrin binding motifs (RGD and KGE) on

the λ2 turret protein led to the evaluation of the role of integrins during reovirus infection. Using a panel of antibodies against RGD (α3, α5, αv, β1, αvβ3, αvβ5) and KGE (α1, α2, α6) motifs, only antibodies against β1 integrin were capable of lowering reovirus infection. Relative to β1 integrin knockout GD25 cells, reovirus infection in β1 integrin wildtype GD25β1A cells was considerable higher, albeit similar reovirus binding to both cell lines. Confocal microscopy demonstrated that reovirus internalization was attenuated in GD25 cells (β1 integrin -/-) compared to GD25β1A cells (β1 integrin +/+) [145]. Therefore, reovirus binding to β1 integrin mediates reovirus entry and infection. In addition to the identification of λ2-integrin binding motifs, sequence analysis performed on other reovirus outer capsid proteins have identified the α4β1 binding IDSS motif on σ3. Therefore, the role of viral proteins other than λ2 are likely but have yet to be determined [146].

Signaling following β1 integrin binding is important for adaptor protein and clathrin recruitment for endocytosis, and for endocytic compartment sorting. Mutational analysis demonstrated that β1 integrin cytoplasmic NPXY motifs (Y783/Y795) are required for correct sorting and transport of internalized reovirus endosomes [147]. Therefore, following reovirus binding to sialic acid and JAM-A (and Ngr1), interaction of λ2 (and maybe σ3) with β1 integrin transmits signals triggering endocytosis and subsequent endosome sorting and transport for successful and efficient reovirus infection.

1.3.6.2.2 Non-polarized cell entry

(Figure 1.4)

Reovirus entry has been extensively studied for both virions and intermediate subvirion particles (ISVPs). ISVPs are generated during enzyme mediated outer capsid cleavage either extracellularly by intestinal enzymes (trypsin, chymotrypsin and pancreatin), or intracellularly in late endosomes and endo-lysosomes by cathepsin B and L. Briefly, proteolytic cleavage of reovirus outer capsid proteins results in formation of an ISVP which lacks outer capsid σ3 and has μ1 cleaved to a truncated δ protein (discussed in detail in "reovirus uncoating" section 1.3.6.3). In addition to virions, ISVP entry mechanisms were also studied to better understand intestinal reovirus infection (discussed in detail in "intestinal M cell entry" section 1.3.6.2.4)

Virion and ISVP entry into cells exploit various endocytic routes for cell entry. It is well established that virion entry into cells is mostly (~80%) dependent on dynamin, clathrin and caveolae, and to a lesser (~20%) extent on dynamin-independent routes [146, 148]. However, ISVP entry into cells is highly dependent on the cell culture system used.

In some instances, it was observed that ISVP entry occurs directly at the plasma membrane without the need for endocytosis. L cells were incubated with media containing sodium chromate ($Na_2{}^{51}CrO_4$) overnight and after multiple washes to remove excess sodium chromate, cells were adsorbed with reovirus virions, ISVPs or cores. As a measure of plasma membrane permeation, ^{51}Cr release in the media was measured at 90min post reovirus adsorption. ISVPs released 38-58% of total ^{51}Cr, while virions and cores released only 1.3-4.2% of total ^{51}Cr, thereby suggesting that ISVP entry perturbed the plasma membrane causing intracellular ^{51}Cr leakage. Electron micrographs of reovirus infected L cells demonstrated that as early as 5min post ISVP adsorption, cytoplasmic cores were observed. At 15min post adsorption, 80% cytoplasmic cores were observed, with the remaining enclosed within vesicles. On the other hand, virions were primarily vesicle enclosed following entry and only 7% cytoplasmic cores

were observed at 15min post adsorption [149, 150]. These results suggest that ISVP entry disrupts the plasma membrane and mostly by-passes the requisite endosomal trafficking steps that virions undergo for cytoplasmic core release.

In other studies, ISVP entry was observed to be dynamin dependent, clathrin independent, caveolae dependent and lipid raft mediated. Using cells treated with dynasore, an inhibitor of dynamin, entry of both virions and ISVPs was diminished, suggesting a role of dynamin during virion and ISVP entry. Pre-treatment with chlorpromazine, a drug that interferes with clathrin assembly, inhibited virion infection but not ISVP infection in GD25β1A (β1 integrin +/+) cells, indicating a clathrin independent route of ISVP entry. Genistein is used to block Src kinase mediated endocytosis and is used as an inhibitor of cavelolar mediated endocytosis. In L929, A549 and HEK293 cells, both virion and ISVP infectious virus yields were inhibited following genistein pre-treatment. In HeLa cells, genistein pre-treatment also inhibited virion infection but had no effect on ISVP infection [146]. Therefore, it seems likely that the ISVP endocytosis route preference is cell-type dependent. In L929 cells pre-treated with the membrane cholesterol depleting drug, methyl-β-cyclodextrin (MβCD), virus yield following virion infection was attenuated whereas ISVP infection yield was unaffected [146]. Cholesterol depletion would diminish lipid rafts formation, membrane fluidity and receptor coalescing, suggesting these factors are integral during virion entry but dispensable during ISVP entry.

1.3.6.2.3 Polarized cell entry

In contrast to all other studies that utilized non-polarized cells, one study utilized polarized epithelial cells to mimic *in-vivo* intestinal cell organization, and single virion tracking with 4D live cell microscopy. They observed that both reovirus and ISVP enter the cell via

endocytosis, mediated primarily by a clathrin and dynamin dependent mechanism [148]. Endocytosed vesicles systematically transition from an early endosome to a late endosome and finally to an endo-lysosome, with a change in membrane receptors, pH and enzyme activity at every stage. Unlike ISVPs that escape promptly following endocytic vesicle internalization, virions escape at the late endosome and endo-lysosome stages. Using fluorescently labeled reovirus, internalization and compartmentalization were identified and monitored using plasmid-based expression of fluorescently tagged AP2 (clathrin-mediated endocytic vesicles), Rab5 (early endosomes) and Rab7 (late endosomes). Both virions and ISVPs were observed to interact with endocytic vesicles during internalization, suggesting clathrin-mediated mechanisms of entry. Virions were found to temporally transition from early to late endosomes, while ISVPs minimally interacted with either early or late endosomes. Virion trafficking to late endosomes and lysosomes facilitates enzyme-mediated ISVP generation and subsequent endosome escape into the cytoplasm [148]. Therefore, virions and ISVPs have distinct endocytic trafficking routes in both polarized and non-polarized cells.

1.3.6.2.4 Intestinal M cell entry

(Figure 1.5)

The polarized cell study raised an interesting debate as to the directional nature of reovirus infection in the natural enteric (and respiratory) environment. Growing evidence supports the idea that luminal reovirus is internalized by microfold (M) cells at the apical surface, followed by infection of epithelial and/or endothelial cells through the basolateral surface. Subsequent reovirus release occurs into the lumen through the apical surface of epithelial cells or into the systemic system through the apical surface of endothelial cells. M cells

are specialized phagocytic cells that transport microbes and antigens from the mucosal surface into Peyer's patches for recognition and processing by immune cells [151, 152]. The first evidence of preferential M cell infection by reovirus was provided in 1981 using electron microscopy assessment of mouse ileal sections. Closed ileal loops were generated in anesthetized mice, and loops were inoculated with T1 reovirus. At 30min post inoculation, reovirus was found to be adhered primarily on the surface of M cells and was rarely observed bound to absorptive cells. By 1hr post inoculation, virions were primarily enclosed within vesicles in the M cells, and in some instances, virions were observed to be released into the extracellular space on the basolateral surface. At 1 hour post infection (hpi), virions observed on absorptive cells were always on the cell surface and no evidence of virion endocytosis was observed [153].

Follow-up studies further defined reovirus intestinal infection by identifying that ISVPs are required for M cell adsorption and transport. Using a similar closed ileal loop model system but with luminal contents flushed out and replaced with phosphate buffer saline (PBS), reovirus virions, ISVP or cores were inoculated in the presence or absence of protease inhibitors. Protease inhibitors functioned to block enzyme activity and consequent virion to ISVP conversion. In the presence of protease inhibitors, ISVPs adhered to M cells to a greater extent compared to virions or cores. Virions inoculated in the absence of protease inhibitors had higher adherence to M cells relative to virions inoculated in the presence of protease inhibitors. These observations suggest that proteolytic processing of virions to ISVPs was required for efficient intestinal M cell binding and entry [154]. In week-old mice, M cells constituted 7.4% of the intestine, in contrast to less than 1% in newborn mice. It was observed that in newborn mice reovirus adsorbed onto a wide array of intestinal cell types including M cells, undifferentiated cells and absorptive cells. However, in week-old mice, reovirus adsorbed primarily onto M cells, and to a lesser extent on

undifferentiated cells and absorptive cells. These results suggest the intestinal architecture and composition impacts reovirus infection and also re-enforces the importance of M cells in reovirus intestinal entry [155].

Recent studies have also validated the importance of M cells using an innovative strategy of intestinal M cell manipulation. Receptor activator of nuclear factor kappa-B ligand (RANKL) in necessary and sufficient for M cell differentiation from intestinal epithelial precursor cells. Relative to wild type untreated mice, RANKL knockout or RANKL neutralizing antibody treated mice had strikingly diminished intestinal M cells, which was restored following administration of exogenous RANKL. M cell quantification was performed visually using fluorescence and scanning electron microscopy and functionality was determined by assessing the uptake of fluorescent beads or enteric bacteria (*Salmonella enterica* serovar Typhimurium, *Yersinia enterocolitica*) [156]. In the context of reovirus, mice treated with RANKL neutralizing antibody had diminished reovirus intestinal replication, relative to isotype antibody treated or untreated mice. Additionally, using fluorescence microscopy of intestinal tissue sections, it was observed the reovirus protein (anti-σNS) staining was primarily observed in M cells (anti-GP2) and adjacent enterocytes, suggesting that reovirus transported through M cells infected and replicated in adjacent enterocytes [157]. Therefore, in the intestine, reovirus virions are proteolytically processed to ISVPs, preferentially bind and enter M cells, and infect neighbouring enterocytes through tight junctions or basolaterally. It has been observed that σ1 on virions exist in a folded conformation and upon conversion of virions to ISVPs, σ1 exists in an extended conformation [120, 126]. The extended σ1 form may contribute to exposing cell surface receptor binding sites, a potential evolutionary mechanism to initiate virus-cell binding only when in an optimal environment.

1.3.6.2.5 Apical vs basolateral surface entry

Reovirus has been shown to preferentially infect polarized epithelial cells in transwell culture through the basolateral surface rather than the apical surface. JAM-A staining on these polarized cells was primarily present on the basolateral surface and to a much lesser extent on the apical surface. In the presence of JAM-A neutralizing antibody, basolateral reovirus infection was diminished, suggesting that JAM-A levels likely determined preferential reovirus infection through the basolateral route. Interestingly, following basolateral surface reovirus infection, progeny virus was only isolated from the apical surface media wash, suggesting a directional infection and apical surface virus shedding mechanism [158]. Reovirus binding and entry *in-vivo* is therefore a very complex and systematic process. The evidence supports the idea that virion uncoating to ISVP in the intestinal lumen promotes ISVP adsorption to and transport through M cells and into the basolateral milieu where JAM-A expression on adjacent epithelial (or endothelial) cells facilitate reovirus infection. Reovirus progeny is released into the apical surface intestinal lumen (or bloodstream) for subsequent dissemination.

1.3.6.2.6 Serotype specific entry

It is important to point out that results summarized above with respect to reovirus interaction with M cells were performed in the context of reovirus serotype T1L. Studies comparing intestinal infection with T1L and T3D reovirus have been performed and it was observed that similar to T1L, T3D reovirus can also adhere to and be transported by M cells. However, unlike T1L reovirus, T3D reovirus was non-selective and adhered to all other intestinal cell types (absorptive, goblet, tuft) [159]. Using reassortant analysis, it was deciphered that the S1 gene encoding the σ1 cell attachment protein was the determining factor for the

differential T3D and T1L absorptive cell interaction. It was also observed that T3D reovirus underwent a drastic drop in titre following inoculation, unlike T1L reovirus whose titre was stable. At the time, it was concluded that T3D internalization into absorptive cells was an abortive infection and resulted in the reduced titre [160]. An alternate explanation was provided by recent findings using site-directed mutagenesis which have shown that only two serotype 3 reovirus isolates, T3D and T3C31, have a proteolytic cleavage site at position 249 of the σ1 neck domain, while all other serotype 1 and 3 reovirus isolates do not. A single amino acid switch at position 249 conferred T3D σ1 incapable of proteolytic cleavage and intestinal inoculation did not result in a titre reduction [161]. In a subsequent study using fixed intestinal sections, it was also observed that T1L ISVPs had enhanced binding to M cells relative to T3D ISVPs and that this phenotype was determined by σ1 [137]. T3D ISVPs used in this study were not modified at position 249, and therefore likely constituted a truncated σ1. Therefore, it is very important to note and take into consideration that the commonly used laboratory reovirus T3D strain possesses a protease cleavage susceptible σ1 cell attachment protein that restricts intestinal infection.

1.3.6.3 Capsid uncoating

(Figure 1.6)

During the natural route of intestinal infection, reovirus undergoes systematic cleavage of its outer capsid proteins. Peroral inoculation of radiolabeled reovirus in mice, followed by intestine luminal content analysis at 0, 5, 10, 30 and 120min post inoculation, showed that reovirus outer capsid proteins (σ3 and μ1) were temporally degraded. Specifically, at 0min, some degradation of outermost capsid protein σ3 was observed, suggesting that i) σ3 is very

susceptible to intestinal enzymes and was cleaved during the time it took for sacrificing the mice and harvesting the intestine or ii) σ3 was cleaved during stomach passage. Virus harvested from the stomach at 10 or 30min post inoculation had intact virions, strongly suggesting that σ3 degradation was occurring after passage through the stomach, likely in the intestine. At 5min post inoculation in the intestine, almost all σ3 was degraded and μ1 cleavage to δ had initiated. As previously mentioned, virions lacking σ3 and μ1 completely cleaved into δ are classified as ISVPs. Virions were fully converted to ISVPs by 30min post inoculation in the intestine and ISVPs were also observed at 120min post inoculation, suggesting that ISVPs were stable in the intestinal environment [162].

During infection, ISVPs but not virions, have been shown to bypass the need for intracellular lysosomal mediated uncoating, since ISVPs can infect cells in the presence of lysosomal pH neutralizing ammonium chloride (NH_4Cl). Therefore, monitoring reovirus infection in cells treated with NH_4Cl can be used as a measure of ISVP concentration in a mixture of ISVP and virions. Virions were treated with purified trypsin and collected at various timepoints post incubation. It was observed that virus infection in the presence of NH_4Cl increased with trypsin incubation time and correlated with the levels of ISVP which were determined by monitoring σ3 degradation and μ1 to δ cleavage. In the intestinal lumen, ISVPs increased over time and attained a maximal level at 7hr post inoculation, after which ISVP levels dropped to basal inoculum levels by 15hr post inoculation, further suggesting ISVP stability in the intestine [162]. In summary, the outer capsid proteins (σ3 and μ1) of reovirus virions are cleaved in the intestine into stable and infectious ISVPs.

Similar to the previously described *in-vivo* reovirus M cells binding assay, studies were performed by addition of protease inhibitors during reovirus infection of closed ileal loops *in-*

vivo, but instead of observing luminal cell adherence, samples were assessed for productive reovirus infection [154, 162, 163]. Virions inoculated with protease inhibitors restricted reovirus intestinal infection, whereas ISVP infection was unaffected by the addition of protease inhibitors. As discussed previously, generation of ISVPs were observed to be important for facilitating adhesion to intestinal M cells, and likely also mediated enhanced infection [154, 162, 163]. Intestinal enzymes are therefore important for proteolytic processing of virions into ISVPs and facilitate efficient reovirus M cell binding and overall infection in the intestine.

1.3.6.3.1 Intestinal uncoating

In the stomach, the major gastric enzyme is a low pH activated protease, pepsin. Active proteases in the small intestine include chymotrypsin and trypsin. Proteases function to break down large proteins into smaller peptides. Peptidases such as carboxypeptidase and aminopeptidase further breakdown peptides into individual amino acids for absorption [164]. In the presence of purified gastrointestinal proteases (pepsin, trypsin, chymotrypsin), reovirus undergoes differential cleavage of outer capsid proteins depending on the enzyme used. Protease-specific cleavage fragments have been observed for σ1, σ3 and μ1. Using σ1 isolated from radiolabeled, urea disrupted reovirus T1L and T3D preparations, it was observed that T1L σ1 was resistant to trypsin and chymotrypsin cleavage, while T3D σ1 was cleaved by both enzymes. Furthermore, T3D σ1 had differential trypsin and chymotrypsin cleavage fragments [165]. Monitoring cleavage of σ3 over a time course using various proteases (trypsin, chymotrypsin, pepsin) followed by mass spectrometry, identified the details of protease specific cleavage sites for σ3 [166]. Comparing the reovirus protein composition (via SDS-PAGE) from virus incubated with specific enzymes (pepsin, trypsin, chymotrypsin) to virus isolated from the intestinal tract, it was observed that digestion with chymotrypsin resulted in ISVPs resembling

intestinal ISVPs. Pepsin treatment only degraded σ3, leaving μ1 intact, while trypsin treatment degraded σ3 and cleaved μ1 to δ, similar to chymotrypsin, but the δ fragment observed with trypsin digest was smaller in size relative to chymotrypsin digest δ fragment [163].

Enzymes from sources such as papain (papaya), bromelain (pineapple), pronase (bacteria *Streptomyces griseus*), proteinase K (fungi *Tritirachium album*) and fibrinolysin, have all been reported to digest reovirus virions into ISVPs [167]. Reovirus outer capsid proteins are therefore susceptible to a wide range of proteases. Reovirus virions are highly stable in the environment and resist temperature (50°C to -70°C) and pH (pH 4 to pH 10) changes [168-170].

1.3.6.3.2 Respiratory uncoating

Relative to the intestinal route of infection, reovirus infection through the respiratory route is much less studied. Membrane bound proteases such as human airway trypsin-like protease (HAT) and TMPRSS2 were shown to be expressed on the surface of bronchiolar epithelial cells. *In-vitro* reovirus incubation with purified HAT resulted in almost complete degradation of σ3 and minimal cleavage of μ1 to δ, suggesting that HAT was not a strong chymotrypsin-like virion to ISVP converting enzyme. HAT digested reovirus samples resulted in similar viral yields when infected in the presence or absence of E64D (a cathepsin B, L and calpain inhibitor), suggesting that HAT digested virions could by-pass the intracellular uncoating steps, and were ISVP-like [171].

Based on the observation that mice challenged intranasally with LPS were more susceptible to reovirus infection, it was proposed that proteases such as neutrophil elastase (NE), cathepsin G (CatG) and chymase, released by immune cells during respiratory inflammation contribute towards reovirus virion to ISVP conversion. When used in purified form in reovirus

digest assays, NE, CatG and chymase, were all capable of efficiently degrading σ3. In contrast, μ1 to δ cleavage occurs in order of most to least efficient, NE, chymase and CatG and with all being much less efficient compared to chymotrypsin. Furthermore, reovirus digested by these immune proteases are also resistant to E64D treatment, suggesting an ISVP-like phenotype [172]. Therefore, proteases present in the respiratory environment potentially have a functional benefit towards reovirus infection.

1.3.6.3.3 Intracellular uncoating

In the absence of extracellular proteases, reovirus virions are internalized, and similar to observations during reovirus digestion by chymotrypsin, intracellular uncoating of virions to ISVPs is marked by σ3 degradation and μ1 to δ cleavage. Intracellular uncoating depends on lysosomal proteolysis, since various strategies to inhibit transport to lysosomes (Concanamycin A (conA), Bafilomycin A1 (BafA1), NH_4Cl, Chloroquine (CQ)) inhibited intracellular virion to ISVP conversion and virus replication. ConA and BafA1 are inhibitors of vacuolar proton-ATPase while NH_4Cl and CQ are weak bases. Hence, ConA, BafA1, NH_4Cl and CQ are all reagents that function in increasing lysosomal pH and inherently inhibit enzymes whose activity depends on low pH. ISVP infection and replication was unaffected by cell treatment with ConA, BafA1, NH_4Cl or CQ, suggesting endosomal acidification is not a requirement during ISVP infection [173, 174].

Proteases present in the lysosome function to process endosome cargo and were proposed to also contribute to proteolytic processing of reovirus virions to ISVPs during intracellular infection. Endosomal enzymes important during reovirus uncoating include cathepsin B (CatB) and cathepsin L (CatL). E64D, a cysteine protease inhibitor attenuated reovirus uncoating, while

pepstatin A, an aspartic protease inhibitor did not alter reovirus replication. Treatment of virions with purified cysteine proteases CatB and CatL resulted in the formation of ISVPs. Contrastingly, virions treated with CatD, an aspartic protease, did not result in ISVPs [175-177]. This subset of data suggested that cysteine proteases were likely important during intracellular reovirus uncoating.

Using wild-type and knockout (CatB or CatL) fibroblast cell lines, in combination with specific CatB and CatL inhibitors, it was observed that intracellular uncoating was mediated primarily by CatL. Inhibiting CatB individually did not impact intracellular ISVP formation, however inhibition of both CatB and CatL had a more profound abrogation on reovirus uncoating compared to CatL inhibition individually [178]. Whether reovirus uncoating is mediated by stepwise enzymatic cleavage, for example CatL cleavage preceded by CatB, has yet to be determined. Additionally, persistent reovirus infected L cells (LX cells) that no longer support parental reovirus uncoating were discovered to possess diminished CatB and CatL enzyme activity [179, 180]. Therefore, CatB and CatL enzymes are important during the intracellular reovirus disassembly processes.

1.3.6.4 Membrane perturbation

(Figure 1.3, 1.6)

Following virion uncoating, the viral core needs to penetrate the cell membrane (endosome or plasma) and be released into the cytoplasm to initiate viral RNA transcription and protein translation. Reovirus uncoating is associated with degradation of σ3 and cleavage of μ1 to δ, of which the later step is important for membrane perturbation. Reovirus ISVPs, but not virions or cores, have the capacity to induce red blood cell (RBC) hemolysis and intracellular

^{51}Cr leakage, suggesting the membrane disturbing property is unique to the ISVP form [149, 181, 182]. It was determined that ISVP membrane perturbation efficiency was driven by an ion (Cs^+) dependent μ1 conformation change, because of two major observations: i) addition of KCl, RbCl and CsCl, but not NaCl and LiCl, enhanced chymotrypsin-mediated reovirus capsid digestion, and ii) enhanced intracellular ^{51}Cr leakage by T3A ISVPs relative to T1L ISVPs was associated with the M2 gene encoding μ1 [150, 183]. Furthermore, T1L ISVPs demonstrated increased hemolytic activity relative to T3D ISVPs, and was dependent on both CsCl and the M2 gene.

Using mutational analysis of μ1 and characterization of μ1 cleavage fragments, ISVPs are now classified into two categories; ISVP and ISVP*. ISVPs are virions lacking σ3 and μ1 cleaved into μ1δ and φ, while ISVP*s are ISVPs lacking σ1, μ1N and φ [184-186]. The μ1 protein is N-terminally myristoylated and the μ1N fragment is released via auto-cleavage. Both these properties are important for ISVP* membrane perturbation. Plasmid transfection and mutational analysis identified μ1 G2 and N42 as the sites for N-terminal myristoylation and μ1N auto-cleavage, respectively. N-terminal myristoylation is a requirement for μ1N auto-cleavage, suggesting a virion conformational change after myristoylation [185, 187]. Prior to the advent of the plasmid based reverse genetics system, re-coating of viral cores with baculovirus purified reovirus capsid proteins was the strategy of choice to study the function of reovirus proteins. Briefly, chymotrypsin generated and purified viral cores were incubated with baculovirus generated and purified outer capsid proteins (σ1, σ3, μ1). Recoated viral cores were found to possess similar structural and functional properties to native virions. Relative to the wild-type μ1, viral cores re-coated with a N42A μ1 mutant were found to display diminished i) ISVP mediated hemolysis, and ii) intracellular ISVP endosomal escape, revealing that μ1N fragment release mediates membrane perturbation [185]. Further studies determined that the fragments

important for ISVP* membrane perturbation include μ1N and φ. Using RBC membranes loaded with fluorescent labeled dextrans, along with virion derived or synthetic μ1 fragments, it was observed that μ1N is sufficient for membrane pore formation. Although φ can associate with membranes, it is not sufficient for pore formation. However, φ was observed to be required for optimal hemolytic activity of μ1N. Building on the previous observation of ISVP*s associating with membranes, using synthetic μ1N and ISVPs, it was observed that ISVPs were recruited to membranes. The current model proposes that membrane pore formation by μ1N (and φ) recruits ISVP*s to the membrane vicinity. Using the RBC membrane model, ISVP*s did not translocate across a membrane with μ1N-formed pores, suggesting potential host factor involvement in ISVP* membrane perturbation [186]. With this new-found knowledge of ISVPs and ISVP*s, it would be interesting to re-visit the discrepancies observed during ISVP cell entry and determine if ISVPs at various transition stages to ISVP* are differentially capable of direct plasma membrane penetration.

1.3.6.5 Viral mRNA transcription

Reovirus core particles are transcriptionally active and initiate viral RNA synthesis upon release into the cytoplasm [188]. The viral core capsid is composed of a λ1 shell held together by the σ2 clamp. The viral RNA dependent RNA polymerase λ3 and polymerase co-factor μ2 are packaged within the core capsid and are situated at the base of the λ2 vertex [112, 119]. Viral mRNA is synthesized by the λ3 polymerase using the negative sense strand of the dsRNA genome as a template [112, 189]. Newly synthesized viral mRNA is extruded through the cylindrical channel formed by λ2 pentamers at each vertex. The λ2 channel is not only a gateway for the viral mRNA to leave the viral core but is also a multi functional enzyme complex that adds a 5' cap onto the viral mRNA. The base of λ2 constitutes a guanylyltransferase (GTase)

which converts GTP to GMP and attaches GMP to the 5' terminal diphosphate end of viral mRNA [119]. As discussed previously, all 10 reovirus gene segments have a GCTA sequence at the 5' end [110, 112]. The presence of two methyltransferase domains on λ2 catalyze the methylation at positions N7 of the newly added guanine cap and at position 2'O of the terminal mRNA guanine. The current model predicts a single S-adenosyl methionine (SAM) methyl donor binding pocket in λ2 which is accessible by both methyltransferases. Specifically, following methylation of terminal guanine N7, and release of the SAM by-product, a second SAM binds and facilitates methylation at cytosine 2'O [190, 191]. Therefore, newly synthesized mRNA constitutes a 5' cap structure similar to a eukaryotic cap 1. The 5' terminal triphosphate has to be processed to a diphosphate by a nucleotide triphosphatase (NTPase) prior to 5'cap addition by the GTase onto the viral mRNA. Two reovirus core proteins, λ1 and μ2, have been observed to possess NTPase activity, however, whether one or both of these proteins are involved in newly synthesized mRNA terminal dephosphosphorylation has yet to be determined [192, 193].

1.3.6.6 Virion assembly

During reovirus assembly, a positive sense RNA strand for each gene is packaged within the viral core. The precise mechanisms for single gene preference and core assembly are unknown. "Empty" reoviruses which lack the dsRNA genome but are otherwise similar in protein composition to "full" virions are routinely isolated from virus preparations and can be separated during CsCl gradient centrifugation [194, 195]. Based on this observation, two models can be proposed i) reovirus assembly does not require interactions with positive sense RNA segments, ii) empty virions are composed of one or more protein variants generated during the error prone virus replication process, which allow virus assembly in the absence of genomic viral

RNA. Synthesis of the negative strand occurs within the viral core using the positive strand as a template, by the λ3 viral RNA dependent RNA polymerase. Assessment of various replication steps of a μ2 temperature sensitive mutant, demonstrated that μ2 is important in negative strand synthesis [196]. Studies dating back to 1974 have demonstrated that within the virion, the positive strand of the reovirus dsRNA genome is 5' capped, while the negative strand has a 5' diphosphate end. The current model suggests that during reovirus assembly, 5' capped positive sense viral RNA segments are packaged and following negative sense RNA synthesis within the viral core, the 5' end of the negative strand is dephosphorylated [110, 197]. The viral core NTPase (λ1 and/or μ2) mediating negative strand 5' dephosphosphorylation, and the importance of negative strand 5' dephosphosphorylation, have yet to be investigated.

1.3.6.7 Viral factories

(Figure 1.7)

1.3.6.7.1 μ2 – viral factory scaffold

The majority of reovirus mRNA transcription, protein synthesis and virus assembly occur within distinct cytoplasmic compartments known as viral factories [198-200]. The non-structural reovirus protein μNS (M3 gene) and minor structural protein μ2 (M1 gene) are fundamental factors of viral factory initiation and morphology, respectively [201, 202]. Of all the characterized reovirus isolates, only the field isolated T3C12 and the T3D strains originating from the Bernard Fields laboratory ($T3D^F$, $T3D^N$) form round "globular" factories. All other reovirus field isolates and laboratory strains, irrespective of serotype, form fibrous "filamentous" factories [203]. Using a panel of T1L and $T3D^F$ reassortment viruses, the M1 gene encoding μ2 protein was classified as the determinant of viral factory morphology [201]. M1 gene sequence

analysis and reovirus factory morphology characterization of field and laboratory strain isolates, identified a single site serine to proline polymorphism at amino acid position 208 that switches virus factory morphology from globular to filamentous [203, 204]. The importance of the M1 P208S polymorphism in virus factory morphology classification was further confirmed using reverse genetics analysis with isogenic T1L and $T3D^F$ strains only differing in M1 P208S. Colocalization fluorescence microscopy on reovirus infected cells and cells transfected with M1 gene expressing plasmid, demonstrated that P208 μ2 filamentous morphology culminates from μ2 localizing to and associating with microtubules. S208 μ2 on the other hand does not associate with microtubules and remains cytoplasmic. Addition of microtubule disrupting drug nocodazole resulted in reovirus encoding P208 μ2 forming globular factories further confirming the role of microtubule association in filamentous factory morphology [201].

1.3.6.7.2 μNS – viral core shield

Unlike other genes, transfection of a plasmid encoding the M3 gene (μNS protein) results in formation of globular cytoplasmic inclusions, very similar to those formed during $T3D^F$, $T3D^N$ and T3C12 reovirus infection. However, when M3 is transfected along with M1 (P208), μNS localized to microtubules, suggesting μNS and μ2 interact [205]. Additional studies using truncated μNS variants have identified μNS domains important in interacting with μ2 as well as other viral proteins (σNS, σ2, λ1, λ2) [206]. Therefore, μNS likely plays a role in viral protein recruitment to viral factories and subsequent viral core particle assembly. The observation that the proteins found to interact with μNS are reovirus core proteins led to investigations into μNS playing a role in reovirus core particle recruitment to viral factories [206]. Incubation of baculovirus generated μNS with reovirus virions, ISVPs or cores, followed by CsCl density gradient centrifugation resulted in increased density only with the core and μNS mixture.

Subsequent Western blot analysis using μNS specific antibody determined that the increased density band corresponded to the presence of μNS with viral cores. Electron microscopic assessment of the CsCl gradient purified viral cores and μNS mixture revealed large core complex formation, indicative of μNS forming a matrix around viral cores. Interestingly, μNS complexed viral cores retained their transcription and methylation activities, demonstrating that λ2 vertex channels remain unobstructed for new viral RNA release [207]. During reovirus infection, μNS interacts with viral mRNA, that could function in either modulating translation efficiency and/or genome segregation and packaging [208]. The close interaction of μNS with viral cores could explain the observed μNS-RNA complex formation. Purified reovirus cores have the capacity to be recoated with outer capsid proteins, which inhibits core transcriptase activity [209]. However, μNS complexed viral cores could not be recoated with outer capsid proteins [207]. During reovirus infection, outer capsid proteins are present at high concentrations, and μNS-core interactions could suggest a potential preventative mechanism in maintaining core transcriptase activity during replication [207]. To demonstrate the ability of μNS to recruit reovirus cores, cells were transfected with μNS encoding plasmid for 6 hours, followed by infection with empty ISVPs in the presence of cycloheximide for 90 minutes. Empty ISVPs were generated using chymotrypsin digestion of empty virions. The use of ISVPs allowed for immediate viral core release into the cytoplasm with minimal endosomal processing. To eliminate confounding effects of new viral mRNA and protein synthesis, empty ISVPs were utilized. Microscopical assessment using μNS and reovirus core specific antibodies demonstrated that viral cores localized to μNS globular inclusions [207]. In conclusion, the present model proposes that i) μNS coalesces viral cores into transcriptionally active complexes, ii) μNS-core

complexes interact with μ2 and merge into large viral factories (globular of filamentous), iii) μNS-core complexes maintain core transcriptase activity by inhibiting outer capsid assembly.

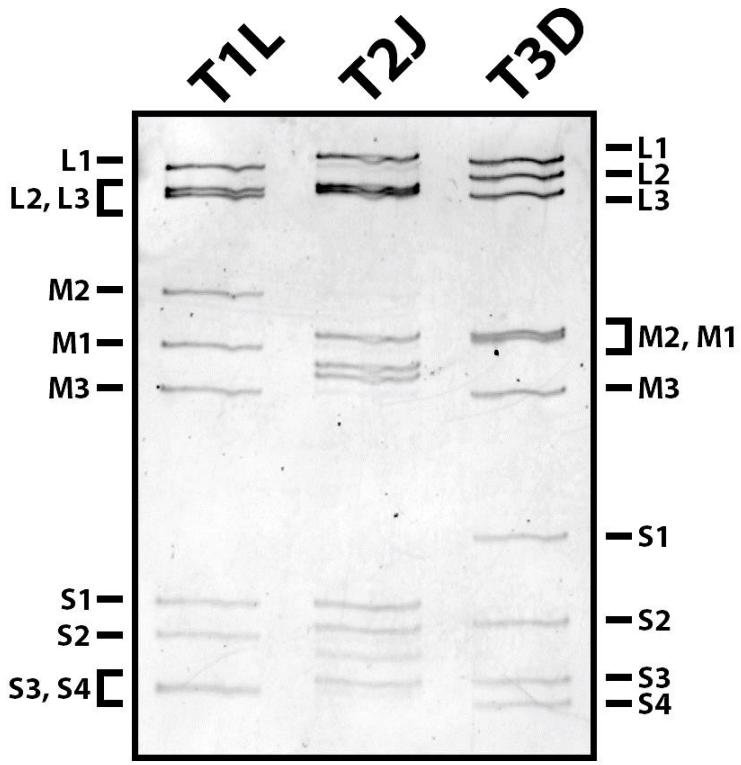

Figure 1.1: Double stranded RNA genome segment profile (electropherotype) of reovirus serotypes T1L, T2J and T3D. RNA was Trizol extracted from CsCl purified reovirus preparations and separated by SDS-PAGE. Segments of dsRNA were stained with ethidium bromide and imaged using a GE® ImageQuant LAS4010 imager.

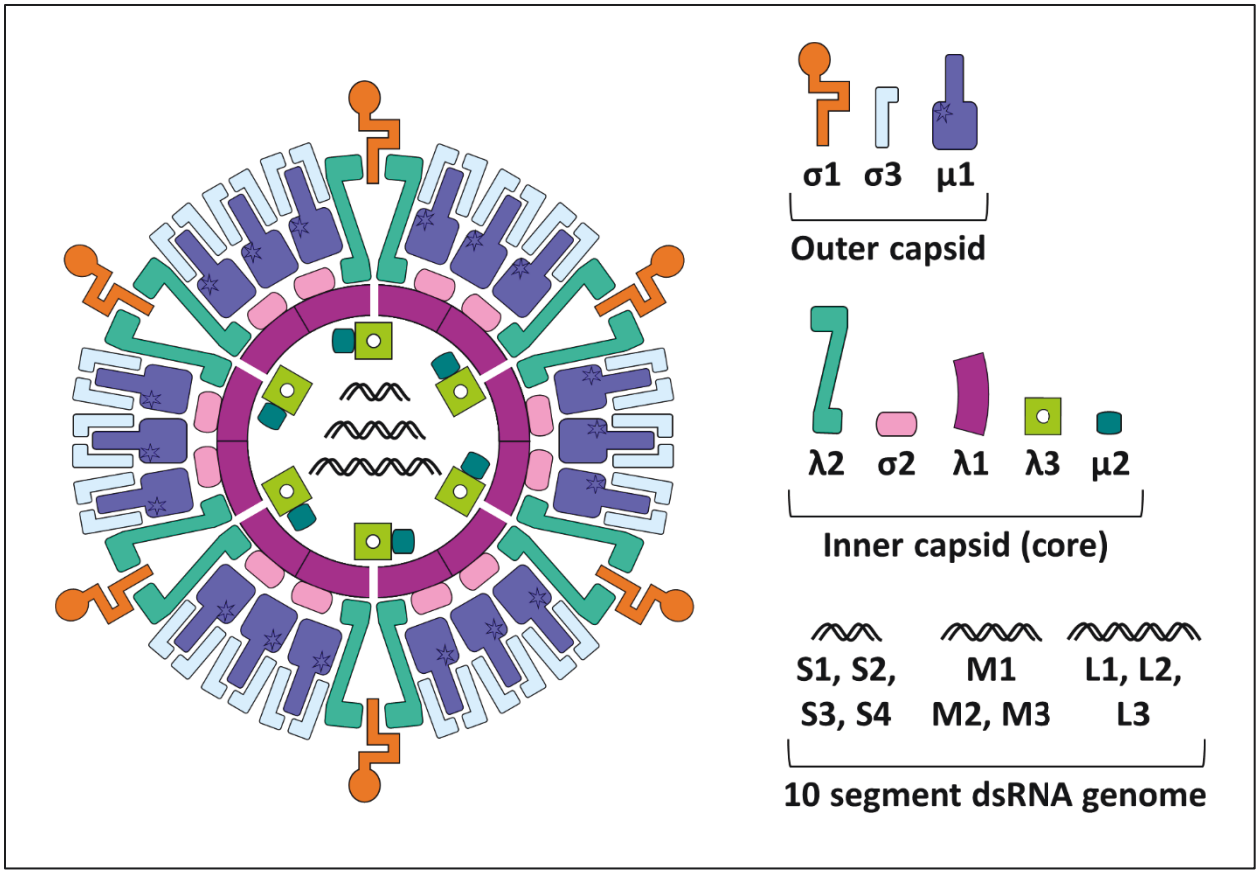

Figure 1.2. Diagrammatic representation of reovirus virion. Outer capsid proteins include σ1, σ3 and μ1. Inner capsid (core) proteins include λ2, σ2, λ1. Within the viral core are λ3, μ2 and 10 segments of dsRNA genome. Please note that the proteins count and dsRNA genome segments on the figure do not represent actual copies. See table 1.1 for specific genome segment details and virion protein copy counts.

Gene Segment	Gene length	Protein	Protein copies per virion
S1	1416	σ1	36
		σ1s	Non-structural
S2	1331	σ2	150
S3	1198	σNS	Non-structural
S4	1196	σ3	600
M1	2304	μ2	20-24
M2	2303	μ1	600
M3	2241	μNS	Non-structural
		μNSC	Non-structural
L1	3854	λ3	10-12
L2	3916	λ2	60
L3	3901	λ1	120

Table 1.1. Summary of reovirus genome and protein composition. The reovirus genome includes 10 dsRNA segments classified by length into three categories; small (S1, S2, S3, S4), medium (M1, M2, M3), large (L1, L2, L3). The S1 and M3 genes are translated into 2 proteins. All other genes only produce 1 protein. Reovirus produces 12 proteins, of which 8 are structural (σ1, σ2, σ3, μ1, μ2, λ1, λ2, λ3) and 4 are non-structural (σ1s, σNS, μNS, μNSC).

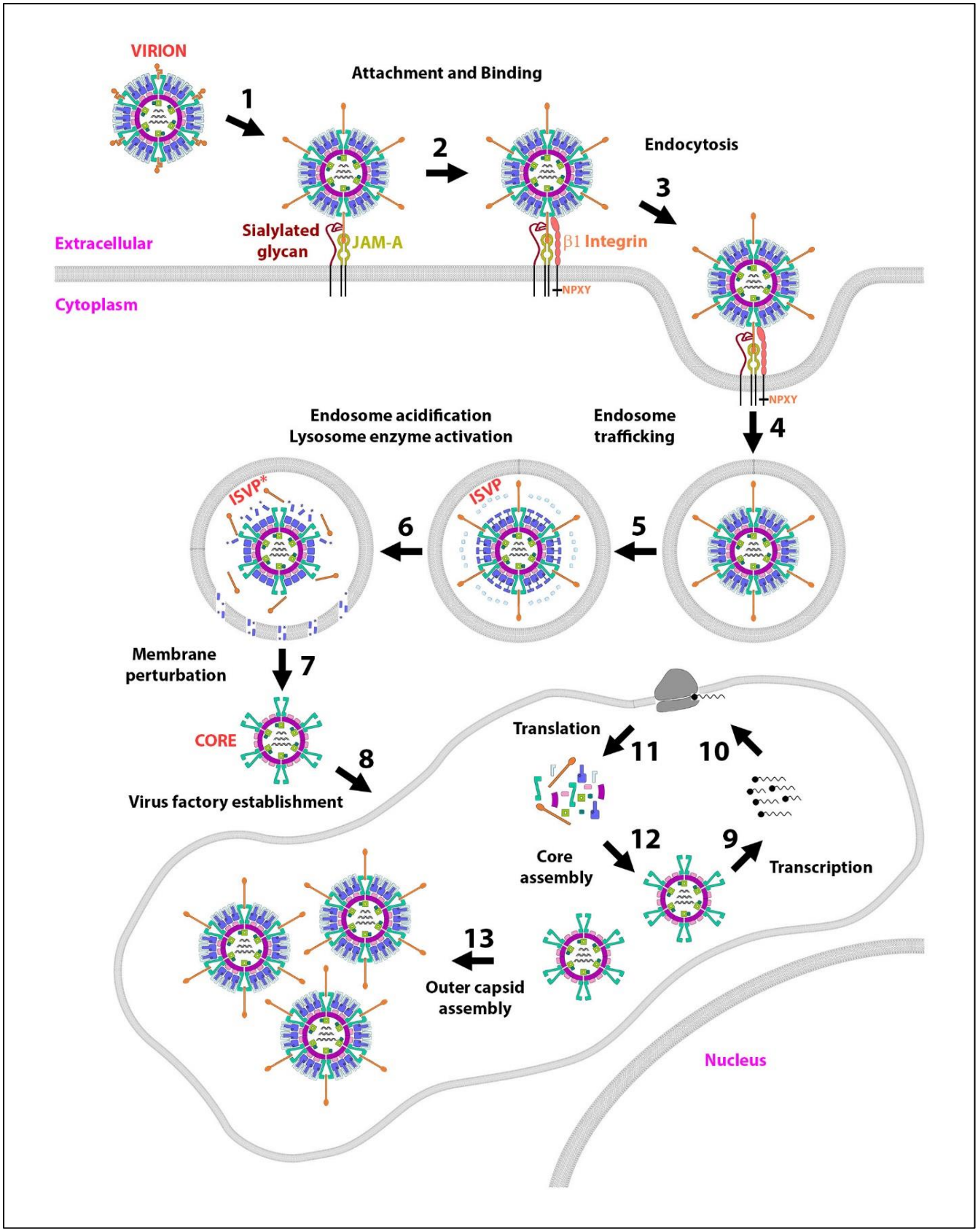
VIRION
Attachment and Binding
1
2
Endocytosis
3
Extracellular
Sialylated glycan
JAM-A
β1 Integrin
NPXY
Cytoplasm
NPXY
Endosome acidification
Lysosome enzyme activation
Endosome trafficking
4
ISVP*
ISVP
6
5
Membrane perturbation
7
CORE
8
Virus factory establishment
Translation
11
10
12
9
Core assembly
Transcription
13
Outer capsid assembly
Nucleus

Figure 1.3. Summary of reovirus intracellular replication. 1) Virion protruding cell attachment protein σ1 initially attaches with low affinity to the cell surface via sialylated glycans, followed by JAM-A mediated high affinity binding. **2 and 3)** Interaction of β1 integrins to the outer exposed region of λ2 initiates the endocytosis trigger by signaling through the NPXY motif. **4)** Internalized virions traffic through the endosome pathway from early to late endosomes/endo-lysosome. **5 and 6)** The acidified environment and activity of lysosomal enzymes (cathepsin B and L) in the late endosome/endo-lysosome compartments mediate cleavage of virion outer capsid proteins. **5)** Degradation of σ3 and cleavage of μ1 into particle associated μ1δ and φ results in generation of an infectious subvirion particle (ISVP). **6)** Additional cleavage of μ1 results in release of μ1N, φ and σ1, producing an ISVP* (Specific details of steps 5 and 6 are described in Fig 1.6). **7)** Released μ1N and φ fragments associate with and disrupt the endosomal membrane layer, allowing viral core release into the cytoplasm. **8)** The core particle initiates viral mRNA transcription and host-mediated viral protein translation resulting in establishment of a viral factory where further virus amplification occurs. (Details of step 8 are provided in Fig 1.7). **9-12)** In the viral factory, core particles produce viral mRNA that is translated into proteins by viral factory surface-associated ribosome complexes. Viral proteins and mRNA assemble into progeny viral cores. Following negative strand synthesis within the assembled core, these progeny viral cores further contribute and amplify viral mRNA and proteins. **13)** At later stages during virus replication core particles are coated by outer capsid proteins μ1, σ3 and σ1 resulting in cessation of virus replication and induction of cell death pathways and subsequent virion release.

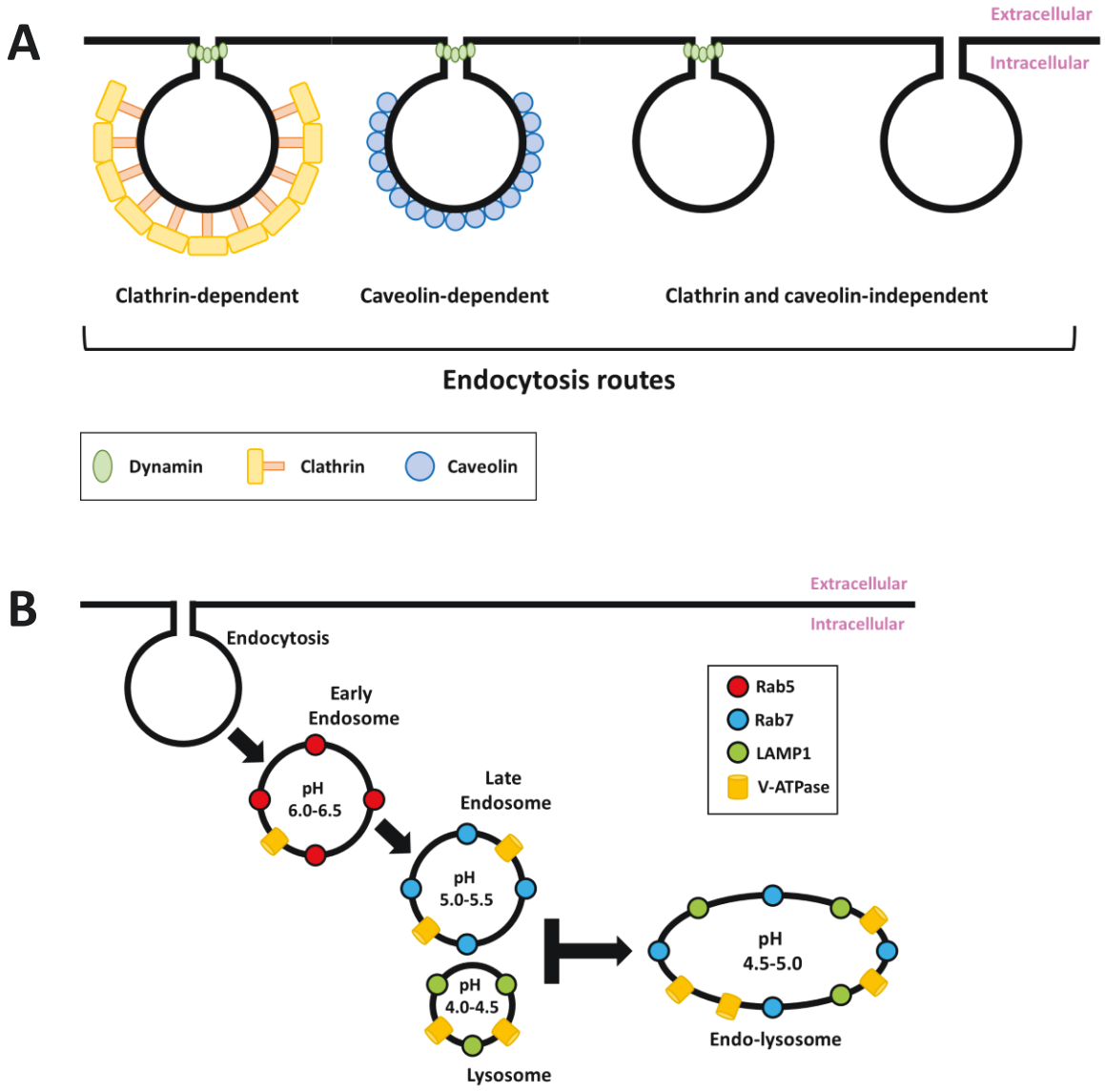

Figure 1.4. Routes of endocytic entry. A) Most endocytic pathways utilize a "ring" of dynamin proteins to detach and release the membrane bound endosome. Clathrin coated endosomes involve a complex signaling cascade and recruitment of adaptor proteins and clathrin. Cholesterol-rich regions are present in caveolin dependent and clathrin/caveolin-independent endosomes. B) Endocytic vesicles undergo systematic trafficking from early to late endosomes. Late endosome fusion with lysosomes result in formation of an endo-lysosome containing active lysosomal enzymes.

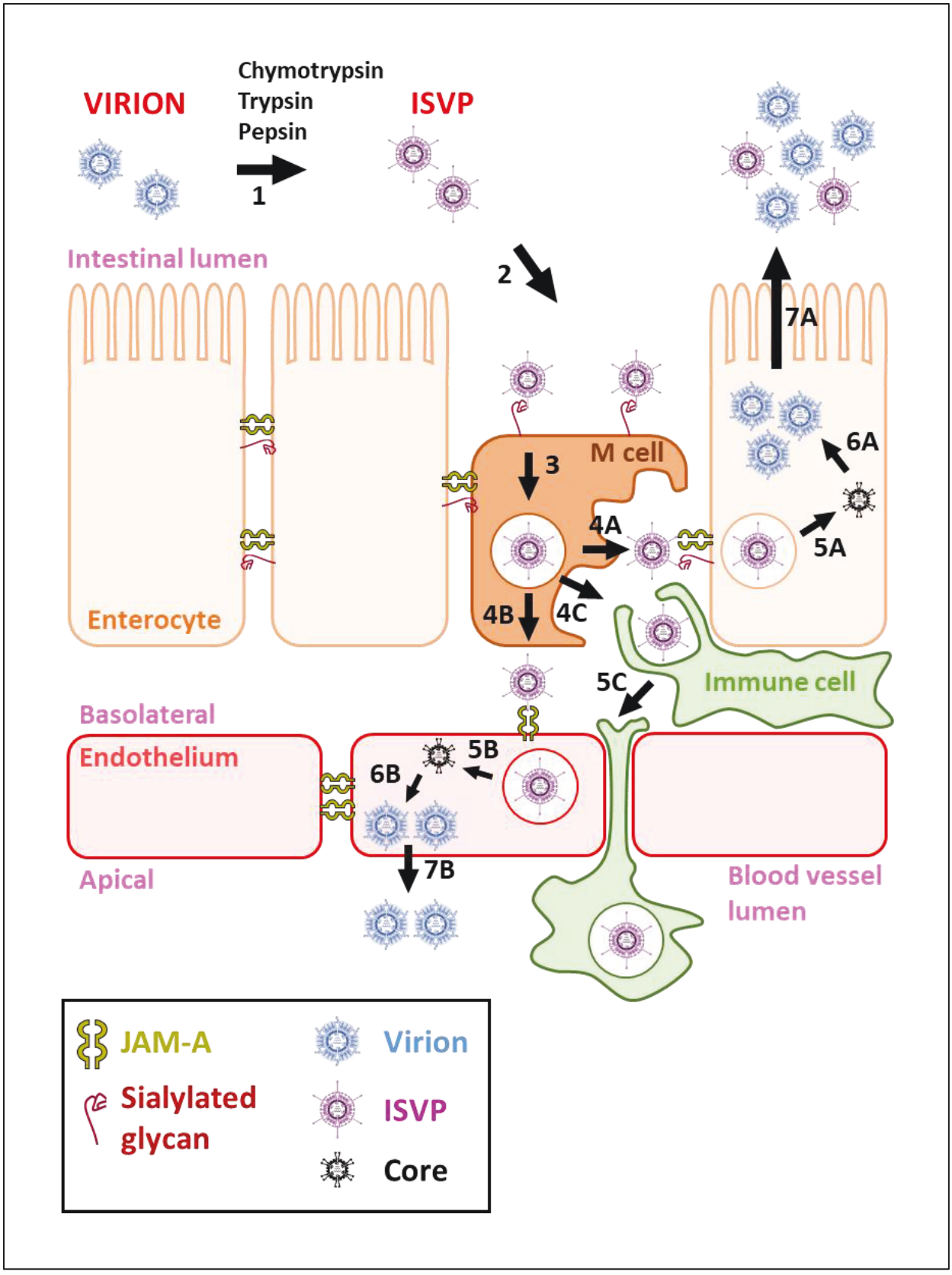
VIRION
Chymotrypsin
Trypsin
Pepsin
1
ISVP
Intestinal lumen
2
7A
M cell
3
6A
4A
5A
4B
4C
Enterocyte
Immune cell
5C
Basolateral
Endothelium
5B
6B
7B
Apical
Blood vessel lumen
JAM-A
Sialylated glycan
Virion
ISVP
Core

Figure 1.5. Model of intestinal reovirus infection and dissemination. 1) Following reovirus ingestion and passage through the stomach, intestinal proteolytic enzymes (chymotrypsin, tryspin and pepsin) cleave virion outer capsid proteins, generating an ISVP (described in Fig 1.6). **2)** ISVP σ1 facilitates attachment to phagocytic M cells via surface expressed sialylated glycans. **3)** ISVPs are internalized and traffic through M cells. **4)** ISVPs are released from the M cell and can attach and bind to JAM-A expressing adjacent enterocytes **(4A)**, basolateral endothelial layer **(4B)** and/or be phagocytosed by immune cells (dendritic cells, macrophages) **(4C)**. **5A-B and 6A-B)** Reovirus amplification occurs in enterocytes **(5A, 6A)** and endothelial cells **(5B, 6B)**. **7A, 7B)** Progeny virions are released back into the intestinal lumen **(7A)** or bloodstream **(7B)**. Following release into the intestinal lumen, some progeny virions are converted into ISVPs and initiate a second replication cycle **(7A)**. **5C)** Immune cells containing phagocytosed ISVPs extravasate the endothelial cell layer into the blood stream. For simplicity, only JAM-A and sialylated glycans are depicted as tight junction molecules.

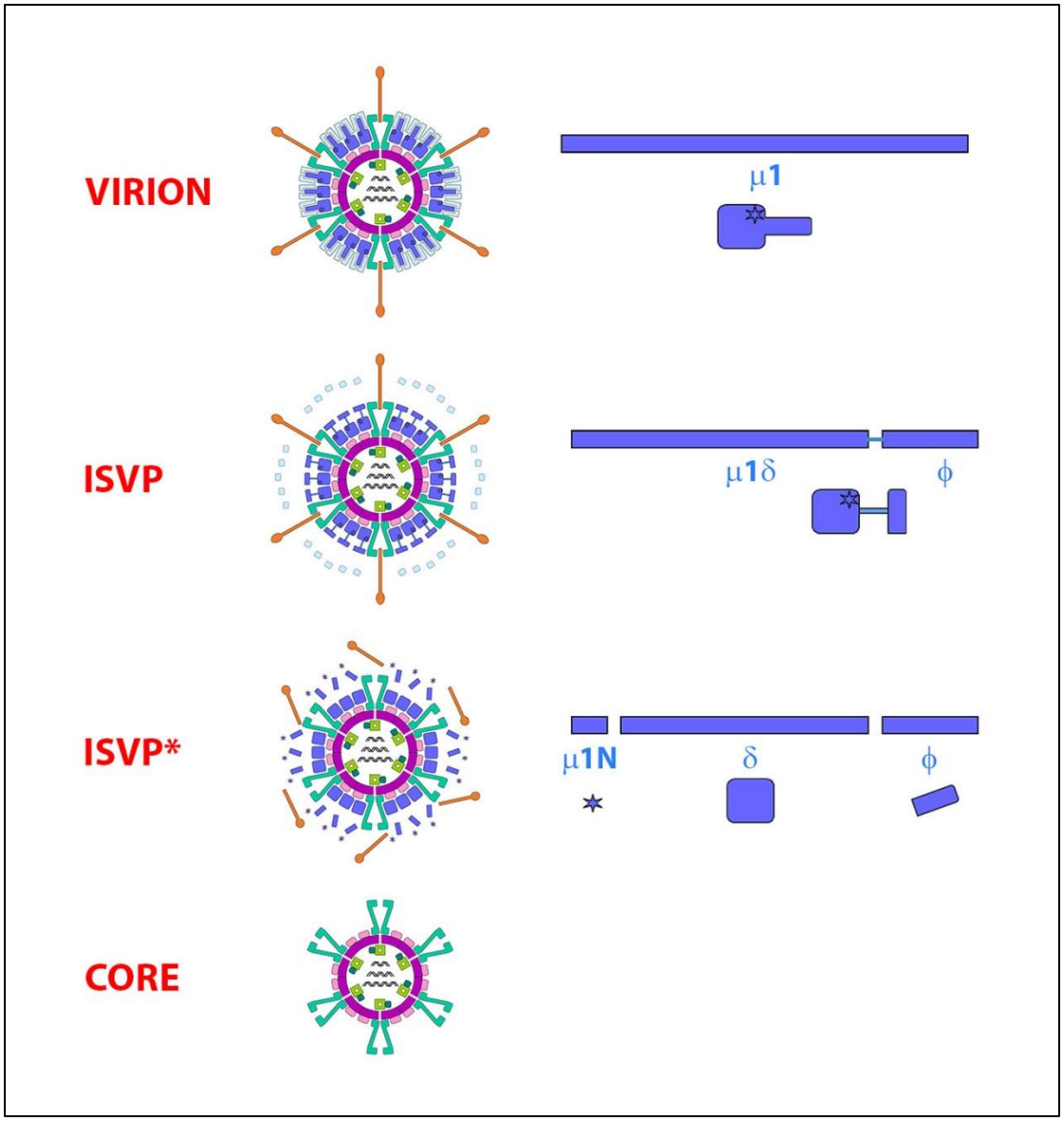

Figure 1.6. Intermediates of reovirus outer capsid disassembly. During intracellular or extracellular enzymatic exposure, reovirus transitions from an intact virion to an ISVP, ISVP* and core. Virions consist of a full-length μ1 protein. ISVPs are generated following degradation of σ3 and particle associated cleavage of μ1 into μ1δ and φ. Further enzymatic processing results in release of μ1N, φ and σ1, resulting in an ISVP*. The δ protein from ISVP* is either removed during membrane perturbation or during extended chymotrypsin treatment *in-vitro*. The viral core particle lacks all outer capsid proteins (σ1, σ3, μ1).

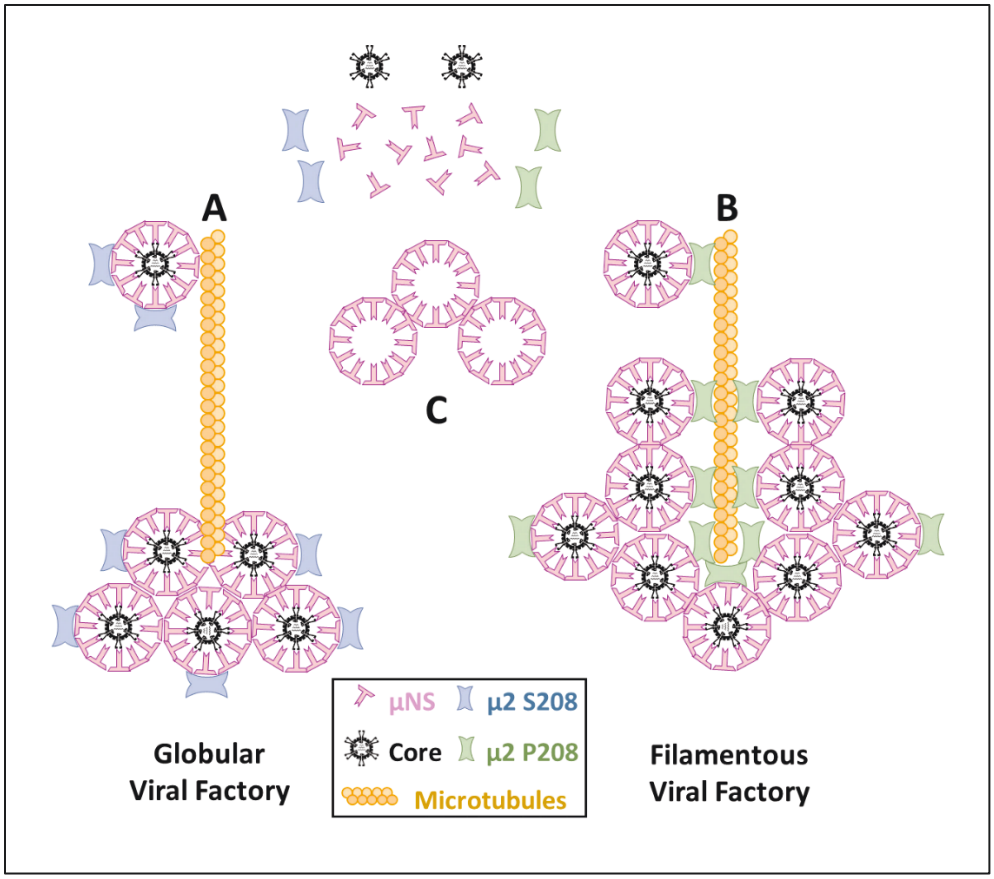

Figure 1.7. Model for viral factory establishment. Following viral core release into the cytoplasm and initiation of viral mRNA transcription and protein translation, viral proteins μ2 and μNS contribute towards viral factory establishment. A and B) The μNS protein interacts with the viral core resulting in aggregation and viral factory establishment [207]. The size and morphology of virus factories are dependent on interaction of μ2 with microtubules (and μNS). A) Viral factory morphology is globular with a μ2 S208 that cannot interact with microtubules. When microtubules are disrupted, the globular factories reduce in size and increase in number [210]. B) With a μ2 P208 that interacts with microtubules, viral factories are filamentous in morphology. Disruption of microtubules results in filamentous to globular factory conversion [210]. C) In the absence of other viral proteins, μNS forms cytoplasmic globular factory-like aggregates.

1.4. PROJECT OBJECTIVES

As discussed in Chapter 1.2.3.3, the efficacy of REOLYSIN® in clinical trials as a cancer therapy needs to be improved. Based on reports by Oncolytics Biotech Inc, REOLYSIN® is a proprietary isolate of T3D. Various laboratories, including ours, are striving to enhance reovirus oncolytic potency. Given that a number of studies have demonstrated that single amino acid changes in the reovirus genome can alter reovirus replication, we decided to better characterize various T3D laboratory strains in relation to REOLYSIN®. To improve efficacy, all current clinical trails use REOLYSIN® in combination with chemotherapies, radiation or immunotherapies, indicating host signaling can benefit REOLYSIN® therapy. Our studies focussed on 2 primary objectives:

1. Improve our understanding of reovirus oncolysis by comparative (phenotypic and genetic) analysis of T3D laboratory strains.
2. Delineate the function of cellular p38 MAPK signaling during reovirus replication.

MATERIALS AND METHODS

Cell lines

All cell lines were grown at 37°C at 5% CO_2 and all media was supplemented with 1x antibiotic antimycotics (A5955, Millipore Sigma). Except for NIH/3T3 media that was supplemented with 10% NCS (N4637, Millipore Sigma), all other media was supplemented with 10% FBS (F1051, Millipore Sigma). L929, NIH/3T3, H1299, ID8, HCT 116 and B16-F10 cell lines (Dr. Patrick Lee, Dalhousie University), Huh7.5 (Dr. Michael Houghton, University of Alberta) and BHK-21-BSR T7/5 (Dr. Ursula Buchholz, NIAID) were generous gifts. BT-549, Hs578T, MCF7, T-47D, MDA-MB-231 and MDA-MB468 cell lines were purchased from ATCC as part of the NCI-60 cell line panel. L929 cell line was cultured in MEM (M4655, Millipore Sigma) supplemented with 1× non-essential amino acids (M7145, Millipore Sigma) and 1mM sodium pyruvate (S8636, Millipore Sigma). L929 cell line in suspension were cultured in Joklik's modified MEM (pH 7.2) (M0518, Millipore Sigma) supplemented with 2g/L sodium bicarbonate (BP328, Fisher Scientific), 1.2g/L HEPES (BP310, Fisher Scientific), 1× non-essential amino acids (M7145, Millipore Sigma) and 1mM sodium pyruvate (S8636, Millipore Sigma). H1299, ID8, BT-549, Hs578T, MCF7, T-47D, MDA-MB-231 and MDA-MB468 cell lines were cultured in RPMI (R8758, Millipore Sigma). NIH/3T3, B16-F10, Huh7.5, HCT 116 and BHK-21-BSR T7/5 cell lines were cultured in DMEM (D5796, Millipore Sigma) supplemented with 1mM sodium pyruvate (S8636, Millipore Sigma). BHK-21-BSR T7/5 cell line was selected in media containing 1mg/ml G418 (A1720, Millipore Sigma) every second passage. All cell lines were routinely assessed for mycoplasma contamination using 0.5µg/ml Hoechst 33352 (H1399, ThermoFisher Scientific) staining or PCR (G238, ABM).

Reovirus stocks

Seed stock lysates of T1L, T2J, T3D-PL (Dr. Patrick Lee, Dalhousie University), T3D-KC (Dr. Kevin Coombs, University of Manitoba) and T3D-TD (Dr. Terence Dermody, University of Pittsburgh) were gifts in kind. T3D-ATCC (ATCC® VR-824) was purchased from American Type Culture Collection. Reovirus lysates were plaque purified and second or third passage L929 cell lysates were used as spinner culture inoculums.

Plaque Purification

Media was removed from confluent L929 cell monolayers in 6 well plates. Reovirus lysates were diluted in MEM (no additives) and 200µl of the dilution was added to each well. Virus inoculum was incubated for 1hr at 37°C, while rocking gently every 5-10min. Virus inoculum was removed prior to addition of 3ml agar overlay which constituted an equal ratio of 2% Agar and 2X MEM (Temin's modification, no phenol red, 11935046, ThermoFisher Scientific) supplemented with 20% FBS, 2× non-essential amino acids (M7145, Millipore Sigma), 2mM sodium pyruvate (S8636, Millipore Sigma) and 2x antibiotic antimycotics (A5955, Millipore Sigma). The agar overlays were allowed to solidify for 30 minutes at room temperature and incubated at 37°C until plaques were clearly visible. Isolated plaques were selected and marked on the plate base using a sharpie. Using sterile cotton plugged glass pasteur pipets and rubber bulbs, agar plugs over selected plaques were carefully extracted, dispensed into 1.5ml microcentrifuge tubes with 200µl of MEM (no additives) and incubated overnight at 4°C.

Reovirus Passaging

Following overnight incubation, plaque isolated agar plug in MEM was diluted in 1:1 in 100µl MEM (no additives). Media was removed from 60-80% confluent L929 cell monolayers in 6 well plates and 200µl of diluted plaque isolated agar plug was added to the well. Following incubation for 1hr at 37°C (rocking gently every 5-10min), 2ml cell culture media was added to each well. Cell death was monitored microscopically every 12-24hrs. When more than 80% cell death was attained, each well was scraped using a sterile plastic cell lifter (08100240, Fisher Scientific) and transferred to 2ml microcentrifuge tube. This was referred to as passage 1. Following 3 freeze/vortex/thaw cycles, virus concentration in passage 1 lysate was determined using plaque assay.

Lysate from passage 1 was serially diluted in MEM (no additives) such that a final dilution of MOI 1-3 (assuming 1.1×10^7 cells) in 1ml was attained. Media was removed from 60-80% confluent (1.1×10^7 cells at 80%) L929 cells in a $55cm^2$ dish and 1ml passage 1 lysate dilution was added. Following incubation for 1hr at 37°C, while rocking gently every 5-10min, 9ml cell culture media was added. Cell death was monitored microscopically every 12-24hrs. When more than 80% cell death was attained, dish was scraped using a sterile plastic cell lifter (08100240, Fisher Scientific) and transferred to a 15ml conical centrifuge tube. This was referred to as passage 2. Following 3 freeze/vortex/thaw cycles, virus concentration in passage 2 lysate was determined using plaque assay.

T3D-PL, T3D-KC and T3D-TD lysates from passage 2 or PL-RG, TD-RG, TD+PL-S4, TD+PL-M1, TD+PL-L3, PL+TD-S4, PL+TD-M1 and PL+TD-L3 lysates from passage 1, were serially diluted in MEM (no additives) such that a final dilution of MOI 1-3 (assuming 3×10^7 cells) in 6ml was attained. Media was removed from 2 $150cm^2$ dishes with 60-80% confluent (3×10^7 cells at 80%) L929 cells and 3ml passage 2 lysate dilution was added to each dish.

Following incubation for 1hr at 37°C, while rocking gently every 5-10min, 15ml cell culture media was added to each dish. Cell death was monitored microscopically every 12-24hrs. When more than 80% cell death was attained, both dishes were scraped using a sterile plastic cell lifter (08100240, Fisher Scientific), pooled and transferred to a 50ml conical centrifuge tube. Following 3 freeze/vortex/thaw cycles, virus concentration was determined using plaque assay. This passage was used as the inoculum for large scale spinner culture amplification.

Large Scale Reovirus Amplification

Four 150cm^2 dishes with 100% confluent L929 cell monolayers were detached using trypsin, were resuspended in 500ml JMEM culture media and added to sterile 2L flat bottom flask (10-035G, Fisher Scientific) with stir bar and aluminum foil cover. Flask containing cells was incubated at 37°C with low speed stirring in either a large chamber incubator or a water bath, neither of which had CO_2 regulation. Cell density was monitored every 24hrs by removing a 1ml aliquot and performing a trypan blue cell count using either a haemocytometer or Biorad TC-20 cell counter. When cell density reached approximately 1×10^6 cells/ml, 700ml JMEM culture media was added to the flask. Cell density was monitored every 12-24hrs and at approximately 1×10^6 cells/ml (1.2×10^9 cells/1200ml/flask), virus lysates were diluted in MEM (no additives) and added to the flask at an MOI 1-3. Cell density and death was monitored every 12-24hrs. At 50-70% cell death, cells were collected by centrifugation at 1000g for 15min at 4°C. The cell pellet from each flask was resuspended in 15ml homogenization buffer (10mM Tris pH 7.4, 250mM NaCl, 10mM β-mercaptoethanol, 1× protease inhibitor cocktail), transferred to a 50ml conical centrifuge tube and frozen at -80°C. Frozen cell pellets were thawed at 4°C and vortexed for 5min on maximum speed. Per cell pellet, 10ml vertel XF (Dymar Chemicals Limited, ON, Canada) was added, vortexed for 5min on maximum speed and probe sonicated for

30sec on maximum amplitude ensuring a homogenous emulsification. Following centrifugation at 4000rpm for 10min at 4°C, the top (reddish-pink color) layer was separated into a new 50ml conical centrifuge tube. Ten ml of vertel XF (Dymar Chemicals Limited, ON, Canada) was added to the top layer, vortexed for 5min on maximum speed and probe sonicated for 30sec on maximum amplitude ensuring a homogenous emulsification. Following centrifugation at 4000rpm for 10min at 4°C, the top (reddish-pink color) layer was separated into a new 50ml conical centrifuge tube and layered on a CsCl gradient (9ml 1.4g/cc, 9ml 1.2g/cc) in SW28 ultra clear tubes. Tubes were topped up with PBS, weight balanced on a digital scale and centrifuged at 100,000g at 4°C for 6-12hrs. Reovirus separates into two white bands signifying top component empty virions and bottom layer full virions. The bottom band was extracted using a needle (19-22Ga) and syringe (5-10ml) and loaded into dialysis tubing (10-20KDa). Extracted virus was dialyzed in dialysis buffer (150mM NaCl, 10mM $MgCl_2$, 10mM Tris pH 7.4) with 3 buffer changes, the first after 1-3hrs, the second after 3-6hrs and third after 6-12hrs. The dialyzed virus was transferred into a 15ml conical centrifuge tube and allowed any precipitate to settle at 4°C for 12hrs. The supernatant was aliquoted into 1.5ml microcentrifuge tubes and stored at 4°C. Virus concentration was determined using plaque assay

Reovirus plaque assays

Reovirus dilutions were added to 100% confluent L929 cells for 1hr at 37°C with gentle rocking every 10 minutes, followed by addition of agar overlay (1:1 ratio of 2% agar 2× JMEM media). Overlays were allowed to solidify for 30 minutes at room temperature and incubated at 37°C. When plaques became visible (3-7 days post infection), 4% formaldehyde solution (33314, Alfa Aesar) was added to the overlay for 30 minutes. Formaldehyde was discarded, agar overlays were carefully scooped out and cells were further fixed with methanol for 5min. Methanol was

discarded, and cells were stained with crystal violet solution (1% crystal violet (C581, Fisher Scientific) in 50% ethanol and 50% water) for 10min and rinsed with water. For cell lines other than L929, after methanol staining, plaques were stained using immunocytochemistry with rabbit anti-reovirus pAb. Plaques were scanned on the ImageQuant LAS4010 imager (GE Healthcare Life Sciences), and plaque area was measured using ImageQuant TL software (GE Healthcare Life Sciences).

Virus Infections

Refer to Table 1.1 for reagent volumes. Reovirus (purified stock, cell lysate, plaque isolated agar plug) was diluted in MEM (no additives). Cell culture media was aspirated from 90-100% confluent cell monolayers. Virus inoculum was added to each well and incubated for 1hr with gentle rocking every 5-10min to allow for virus adsorption. The virus inoculum was aspirated and the monolayer was washed once with MEM (no additives). Cell culture media was added and the incubated at 37°C. Note that a "wash" in the above protocol constitutes addition of reagent, gently rocking back and forth twice and aspiration of reagent.

Refer to Table 1.1 for reagent volumes. When samples were assessed and or standardized for virus binding, cells (90-100% confluent cell monolayers) were pre-incubated at 4°C for 30min. Cell culture media was aspirated, virus inoculum was added to each well and incubated at 4°C for 1hr with gentle rocking every 5-10min to allow for virus adsorption. The virus inoculum was aspirated and the monolayer was washed twice with ice-cold MEM (no additives). Cell culture media was added and the incubated at 37°C. During virus adsorption, the cell plates, virus inoculum and MEM (no additives) were always kept on ice or the 4°C fridge. Note that a

"wash" in the above protocol constitutes addition of reagent, gently rocking back and forth twice and aspiration of reagent.

When minimal cell culture media manipulation was required (e.g p38 MAPK assessment), virus inoculum was spiked directly to the cell culture media.

Immunocytochemistry

Colorimetric infectivity assay: Refer to Table 1.1 for reagent volumes. Following reovirus infection (***Virus infection*** or ***Reovirus plaque assay*** protocols), cell culture media was aspirated, or agar overlays were removed, and cell monolayers were washed once with PBS. Cells were fixed with methanol or 4% paraformaldehyde, washed twice with PBS, and incubated with blocking buffer (3% BSA/PBS/0.1% Triton X-100) for 1 hour at room temperature. Blocking buffer was aspirated and primary antibody (rabbit anti-reovirus pAb) diluted in blocking buffer for a final concentration of 1:10,000 was added and incubated overnight at 4°C. Samples were washed 3 × 5minutes with PBS/0.1% Triton X-100. Secondary antibody diluted in blocking buffer (goat anti-rabbit AP) was added and incubated for 1-3hrs at room temperature. Samples were washed 3 × 5minutes with PBS/0.1% Triton X-100. NBT/BCIP substrate diluted in AP buffer (100mM Tris pH 9.5, 100mM NaCl, 5mM $MgCl_2$) was added and infected cells were monitored for black/purple staining using microscopy. 100× NBT/BCIP substrate stocks were diluted as follows in dimethylformamide (DMF) (D4551, Millipore Sigma): NBT (30mg/1ml) (B8503, Millipore Sigma), BCIP (15mg/1ml) (N6639, Millipore Sigma). When infected cells had stained a dark purple color, substrate was removed and reactions were stopped by adding PBS/5mM EDTA. Note that a "wash" in the above protocol constitutes addition of reagent, gently rocking back and forth twice and aspiration of reagent.

Fluorescence infectivity assay: Refer to Table 1.1 for reagent volumes. Following reovirus infection (***Virus infection*** protocol), cell culture media was aspirated, and cell monolayers were washed once with PBS. Cells were fixed with 4% paraformaldehyde, washed twice with PBS, and incubated with blocking buffer (3% BSA/PBS/0.1% Triton X-100) for 1 hour at room temperature. Blocking buffer was aspirated and primary antibody (rabbit anti-reovirus pAb) diluted in blocking buffer for a final concentration of 1:10,000 was added and incubated overnight at 4°C. Samples were washed 3 × 5minutes with PBS/0.1% Triton X-100. Secondary antibody diluted in blocking buffer (goat anti-rabbit Alexa Fluor 488) was added and incubated for 1-3hrs at room temperature. Samples were washed 3 × 5minutes with PBS/0.1% Triton X-100. Nuclei were stained with 0.5µg/ml Hoechst 33352 (H1399, ThermoFisher Scientific) for 15min and stained samples were visualized and imaged using EVOS FL Auto Cell Imaging System (ThermoFisher Scientific). Note that a "wash" in the above protocol constitutes addition of reagent, gently rocking back and forth twice and aspiration of reagent.

Immunofluorescence

Refer to Table 1.1 for reagent volumes. Cells were seeded on #1.5 thickness coverslips. Following reovirus infection (***Virus infection*** protocol), cell culture media was aspirated, and cell monolayers were washed once with PBS. Cells were fixed with 4% paraformaldehyde, washed twice with PBS, and incubated with blocking buffer (3% BSA/PBS/0.1% Triton X-100) for 1 hour at room temperature. Blocking buffer was aspirated and primary antibody (mouse anti-σNS 3E10 conjugated to Alexa Fluor 568, mouse-anti-σ3 10G10 conjugated to Alexa Fluor 647, rabbit anti-µ2 pAb) diluted in blocking buffer was added and incubated overnight at 4°C. Primary mAbs mouse anti-σNS and mouse-anti-σ3 10G10 were conjugated to Alexa Fluor 568 and Alexa Fluor 647, respectively, using APEX antibody labeling kits as per manufacturer's

protocol (ThermoFisher Scientific). Samples were washed 3 × 5minutes with PBS/0.1% Triton X-100. Secondary antibody diluted in blocking buffer (goat anti-rabbit Alexa Fluor 488) was added and incubated for 1-3hrs at room temperature. Samples were washed 3 × 5minutes with PBS/0.1% Triton X-100. Nuclei were stained with 0.5µg/ml Hoechst 33352 (H1399, ThermoFisher Scientific) for 15min. Coverslips were mounted on microscope slides using 10µl SlowFade Diamond (S36967, ThermoFisher Scientific) and visualized using an Olympus IX-81 spinning disk confocal microscope (Quorum Technologies). Note that a "wash" in the above protocol constitutes addition of reagent, gently rocking back and forth twice and aspiration of reagent.

Flow cytometry: Cell culture media was aspirated and cell monolayers were rinsed with PBS (1ml/12well). PBS was discarded and trypsin (200µl/12well) was added and incubated until cells detached. Tryspin in detached cells was quenched with cell culture media (1ml/12well). Volumes of PBS, trypsin and cell culture media were scaled up/down according to well size. Detached cells were centrifuged and washed with 1ml PBS. Refer to Table 1.1 for reagent volumes. PBS was aspirated, cell pellet was gently resuspended in 4% paraformaldehyde and incubated at 4°C for 30min. Samples were centrifuged and washed with 1ml PBS/0.1% Triton X-100 (wash buffer). Wash buffer was aspirated, cell pellet was gently resuspended in 3% BSA/wash buffer (blocking buffer) and incubated at 1 hour at room temperature for 30min. Samples were spiked with primary antibody (rabbit anti-reovirus pAb) diluted in blocking buffer for a final concentration of 1:10,000 and incubated overnight at 4°C. Samples were centrifuged and washed twice with 1ml wash buffer. Wash buffer was aspirated, and cell pellet was gently resuspended in secondary antibody diluted in blocking buffer (goat anti-rabbit Alexa Fluor 647 at 1:1:2,000 dilution) and incubated for 1-3hrs at room temperature. Samples were centrifuged

and washed twice with 1ml wash buffer. Wash buffer was aspirated, and cell pellet was gently resuspended in 500µl PBS. Samples were processed using a FACSCanto (BD Biosciences) and data was analyzed using FSC Express 5 (De Novo Software). Total cells were gated using FSC-A and SSC-A, while single cells were gated using FSC-A and FSC-H. A minimum of 10,000 total cells were collected for each sample. Note that a "wash" in the above protocol constitutes aspiration of supernatant, resuspension of pellet and centrifugation. Prior to fixation, cells were centrifuged at 500g for 5min at 4°C. After fixation, cells were centrifuged at 1,000g for 5min at 4°C.

RNA extraction and RT-PCR

Cells were lysed in TRI Reagent® (T9424, Millipore Sigma) and the aqueous phase was separated following chloroform extraction as per TRI Reagent® protocol. Ethanol was mixed with the aqueous phase and RNA isolation protocol was continued as per GenElute Mammalian Total RNA Miniprep kit (RTN350, Millipore Sigma) protocol. RNA was eluted using RNAse free water and total RNA was quantified using Biodrop DUO (Biodrop). Using 1µg RNA per 20µl reaction, cDNA synthesis was performed with random primers (48190011, ThermoFisher Scientific) and M-MLV reverse transcriptase (28025013, ThermoFisher Scientific) as per M-MLV reverse transcriptase protocol. Following a 1/8 cDNA dilution, RT-PCR reactions were executed as per SsoFast EvaGreen Supermix (1725204, Bio-Rad) protocol using a CFX96 system (Bio-Rad).

Western blot analysis

Cells were washed with PBS and lysed in RIPA buffer (50mM Tris pH 7.4, 150mM NaCl, 1% IGEPAL CA-630 (NP-40), 0.5% sodium deoxycholate) supplemented with protease

inhibitor cocktail (11873580001, Roche) and phosphatase inhibitors (1mM sodium orthovanadate, 10mM β-glycerophosphate, 50mM sodium fluoride). For each 12 well, 100µl lysis buffer was used and volume was scaled up/down according to well size. Following addition of 5× protein sample buffer (250mM Tris pH 6.8, 5% SDS, 45% glycerol, 9% β-mercaptoethanol, 0.01% bromophenol blue) for a final 1× protein sample buffer, samples were heated for 5min at 100°C and loaded onto SDS-acrylamide gels. After SDS-PAGE, separated proteins were transferred onto nitrocellulose membranes using the Trans-Blot® Turbo™ Transfer System (Bio-Rad). Membranes were blocked with 3% BSA/TBS-T (blocking buffer) and incubated with primary and secondary antibodies (5ml blocking buffer, primary and secondary antibody per mini (7×8.5cm) membrane). Membranes were washed 3×5min with TBS-T after primary and secondary antibodies. (10ml wash buffer per mini (7×8.5cm) membrane). Membranes with HRP-conjugated antibodies were exposed to ECL Plus Western Blotting Substrate (32132, ThermoFisher Scientific) (2ml substrate per mini (7×8.5cm) membrane) for 2min at room temperature. Prior to visualization, membranes were rinsed with TBT. Membranes were visualized using ImageQuant LAS4010 imager (GE Healthcare Life Sciences), and densitometric analysis was performed by using ImageQuant TL software (GE Healthcare Life Sciences). Note that a "wash" in the above protocol constitutes addition of reagent, gently rocking back and forth twice and removal of reagent.

Double-stranded genomic reovirus RNA visualization

RNA was extracted from CsCl purified reovius preparations (~1×10^{10} virus particles) using TRI Reagent LS (T3934, Millipore Sigma) as per manufacturer's protocol. Purified RNA was diluted in 4× Laemmli sample buffer (1610747, Bio-Rad), and separated on an 8% SDS-acrylamide gel for 22 hours at 6mA (per gel) at 4°C. RNA was stained using ethidium bromide

(0.5 μg/mL) for 1hr at room temperature, gels were destained with TAE (40mM Tris, 5 mM sodium acetate, 1 mM EDTA [pH 7.5]) for 2hrs at room temperature and gels were imaged on ImageQuant LAS4010 imager (GE Healthcare Life Sciences).

Flow cytometry binding assay

L929 cells were detached with CellStripper (Corning), diluted and aliquoted (5×10^{10} cells/sample/ml), pre-chilled at 4°C for 30min and bound with normalized virions at 4°C for 1 hour. Unbound virus was washed off and cell-bound virus was quantified using flow cytometry following sequential binding with rabbit anti-reovirus pAb and goat anti-rabbit Alexa Fluor 488. After secondary antibody staining, samples were fixed with 4% paraformaldehyde for 30 minutes at 4°C. Following a wash with PBS to remove 4% paraformaldehyde, cell pellet was gently resuspended in 500μl PBS. Samples were processed using a FACSCanto (BD Biosciences) and data was analyzed using FSC Express 5 (De Novo Software). Total cells were gated using FSC-A and SSC-A, while single cells were gated using FSC-A and FSC-H. A minimum of 10,000 total cells were collected for each sample. All steps were performed at 4°C on a microcentrifuge tube rotator and FACS buffer (PBS/5% FBS) was used as the diluent and wash buffer. Prior to fixation, cells were centrifuged at 500g for 5min at 4°C. After fixation, cells were centrifuged at 1,000g for 5min at 4°C. Volumes of reagents as per 12 well in Table 1.1. Two wash steps were performed following virus binding and primary and secondary antibody incubation. Note that a "wash" in the above protocol constitutes centrifugation, aspiration of supernatant, resuspension of pellet in wash buffer, centrifugation and aspiration of wash buffer.

Agarose gel separation of reovirus

Purified virions (5×10^{10} virus particles) diluted in 5% Ficoll and 0.05% bromophenol blue were run on a 0.7% agarose gel in TAE buffer (40mM Tris, 5 mM sodium acetate, 1 mM EDTA [pH 7.5]) for 12 hours at room temperature, stained with Imperial total protein stain for 2hrs at room temperature, destained overnight in TAE buffer and visualized on the ImageQuant LAS4010 imager (GE Healthcare Life Sciences)

***In-vitro* reovirus core transcription assay**

Reovirus cores were generated by incubating purified virions with chymotrypsin (CHT) (C3142, Millipore Sigma) at 14µg/ml for 2 hours at 37C. CHT digest reactions were halted by adding protease inhibitor cocktail (11873580001, Roche) and incubating at 4°C. Reovirus cores were pelleted by centrifugation at 100,000g for 2 hours at 4°C, and reconstituted in 100mM Tris pH 8. Transcription reactions were assembled on ice to include 100mM Tris pH 8, 10mM MgCl2, 100µg/ml pyruvate kinase (P7768, Millipore Sigma), 3.3mM phosphoenol pyruvate (P0564, Millipore Sigma), 0.32 units/µl RNaseOUT (10777019, ThermoFisher Scientific), 0.2mM rATP, 0.2mM rCTP, 0.2mM rGTP, 0.2mM rUTP and 1×1011 virus cores per 150µl reaction. Negative control samples were set up without rATP. Reactions were allowed to proceed at 40°C and at indicated timepoints, 40µl transcription aliquots were added to 400ul TRI Reagent LS (T3934, Millipore Sigma) containing 3ng of mouse GAPDH RNA (*in-vitro* transcribed using T7 RiboMAX (Promega), as per manufacturer's protocol). Using 10µg glycogen (R0551, ThermoFisher Scientific) as a carrier according to manufacturer's instructions, RNA was purified, converted to cDNA (28025013, ThermoFisher Scientific) using random primers (48190011, ThermoFisher Scientific) and RT-PCR (1725204, Bio-Rad) performed to quantify

reovirus S4, reovirus M2 and mouse GAPDH. Values were standardized to GAPDH and plotted relative to 0 hours post transcription. For high throughput transcription assays, reactions were set up similar, aliquoted into RT-PCR 96-well tubes and spiked with 10× final SYBR Green II (S7564, ThermoFisher Scientific). Relative fluorescence was measured at 5-minute intervals for 2 hours in a CFX96 system (Bio-Rad).

In-vivo oncolysis experiments

Fifteen six-week-old female C57BL/6 mice were injected subcutaneously in the hind flank with 1×105 B16-F10 cells per 100ul per mouse. When tumors become palpable (~14 days post B16-F10 cell injection), a total of 3 equivalent doses (5×108 pfu/100ul) were inoculated intratumorally at 2-day intervals. The negative control group was inoculated with PBS. Tumor volumes were measured in 3 dimensions using digital calipers every 2 days. Mice were sacrificed when either tumors became too large (200mm3), and/or tumors had visible signs of necrosis and ulceration.

Resazurin Cell Viability Assay

Resazurin stock solution was prepared at 440μM in PBS and stored in aliquots at 4°C. Immediately prior to addition to wells, resazurin stock solution was dilution 1/10 in PBS and 10ul was added per well. Samples were read on the FLUOstar Optima (BMG Lab Tech) plate reader every 30min for 2hrs, until signal saturation. Fluorescence was measured at excitation 520nm an emission 584nm.

Radiolabeled (S^{35}) reovirus virions

Media was removed from 90-100% confluent L929 cells in a 55cm^2 dish and 1ml reovirus dilution was added at MOI 10. Following incubation for 1hr at 37°C, while rocking gently every 5-10min, 9ml cell culture media was added. At 9hpi, cell culture media was removed, cell monolayers were washed with methionine/cysteine free media and replaced with methionine/cysteine free media supplemented with 35S-methionine at 100µCi/ml and dialyzed FBS at 10% final. At 20hpi, cells were washed 3 times with PBS and lysed in RIPA (50mM Tris pH 7.4, 150mM NaCl, 1% IGEPAL CA-630 (NP-40), 0.5% sodium deoxycholate) supplemented with protease inhibitor cocktail (11873580001, Roche). Per 55cm^2 dish, cells were lysed in 1.5ml RIPA. Lysed cells were centrifuged at 600g for 5min at 4°C and supernatant was layered onto a 20% sucrose (in PBS). Per 1.5ml RIPA, 300ul 20% sucrose cushion. Sucrose layered samples were centrifuged at 100,000g for 90min at 4°C. RIPA and sucrose were carefully removed with a pipet virus pellet was resuspended in PBS (350µl PBS/55cm^2/1.5ml RIPA). Note that a "wash" in the above protocol constitutes addition of reagent, gently rocking back and forth twice and aspiration of reagent.

Fluorescent (Alexa Fluor 546) labeled reovirus virions

Succinimidly ester Alexa Fluor 546 (A20002, ThermoFisher Scientific) was dissolved in methanol (1ml/mg), aliquoted into 20 tubes (50µg/tube) and desiccated in a vacuum centrifuge. Desiccated aliquots were stored at -20C and dissolved in DMSO prior to use. Each 50µg aliquot was dissolved in 86.25µl DMSO for a 500µM stock solution. Reovirus stock was diluted to 3×10^{12} particles per 500ul in freshly made 0.2µm filter sterilized 0.05M sodium bicarbonate (pH 8.5) and 12µl of 500µM Alexa Fluor 546 dye was added (12µM final dye concentration).

Virus/sodium bicarbonate/Alexa Fluor 546 dye was incubated on a rotator in the dark at 4°C for 90min, followed by an overnight dialysis (MWCO 10-20KDa) in PBS. Labeled virus concentration was determined using plaque assay and stored in the dark at 4°C.

Lentivirus production and stable cell line generation

Lentivirus was generated as per MISSION® Lentiviral Packaging Mix protocol (SHP001, Millipore Sigma) using 6 well plates. Lentivirus containing supernatants were collected every 12hrs for 72hrs. Pooled lentivirus collections were centrifuged at 600g for 10min at 4°C, and the supernatant was 0.45µm filter sterilized, aliquoted and stored at -80°C.

Lentivirus stock was diluted in cell culture media supplemented with sequabrene (S2667, Millipore Sigma) at 8µg/ml final. Dilutions ranged from 1/3 to 1/36. Media was aspirated from 12 well plates with cells at 50-60% cell confluency, 500µl lentivirus dilution was added to each well and allowed to incubate at 37°C for 12hrs. Lentivirus was aspirated and replaced with cell culture media for an additional 12-24hrs until cells became confluent. At 100% confluency, cells were trypsinized, transferred to a 6 well plate and incubated at 37°C for 12hrs. Cell culture media was replaced with media supplemented with puromycin (2µg/ml for NIH/3T3 cell line) and cell death was monitored by microscopy. Cells not treated with lentivirus but exposed to puromycin supplemented media were used to determine when untransduced cells were killed. When lentivirus transduced cells reached 90-100% confluency, cells, were trypsinized and transferred to 55cm2 flask with media supplemented with puromycin. Lowest lentivirus dilution with minimal (0-10%) cell death was selected for further assessment. Puromycin selection was performed every second passage.

Nucleic Acid Purification

The following kits were used for purification of nucleic acids and protocols were followed as per manufacturer. GenElute™ Plasmid Miniprep Kit (PLN350, Millipore Sigma), GenElute™ HP Plasmid Midiprep Kit (NA0200, Millipore Sigma), GenElute™ Mammalian Total RNA Miniprep Kit (RTN350, Millipore Sigma), QIAquick PCR Purification Kit (28106, Qiagen), PureLink™ Quick Gel Extraction Kit (K210012, Fisher Scientific).

Chemically Competent Bacteria

Stbl3 bacteria stock was a kind gift from Dr. Mary Hitt, university of Alberta. Stbl3 stock was single colony isolated on LB agar plates (per 1L: 10g bacto tryptone, 5g bacto yeast extract, 10g NaCl, 20g bacto agar, pH 7.0) without antibiotics. A single colony was inoculated into 5ml LB and incubated for 16hrs at 37°C and 220rpm. The 5ml culture was transferred into 500ml LB and incubated at 37°C and 220rpm. OD_{600} was monitored every 30min-1hr until OD_{600} 0.4-0.6 was attained). The 500ml culture was transferred into ice cold centrifuge tubes and incubated on ice for 10min. The culture was centrifuged at 3,000g for 10min at 4°C. The media was carefully decanted, and the cell pellet was resuspended in 150ml of ice cold sterile 0.1M $MgCl_2$. Cells were centrifuged at 3,000g for 10min at 4°C and supernatant was carefully decanted. Cell pellet was resuspended in 100ml of ice cold sterile 0.1M $CaCl_2$ and incubated on ice for 20min. Cells were centrifuged at 3,000g for 10min at 4°C and supernatant was carefully decanted. Cell pellet was resuspended in 50ml of ice cold sterile 0.1M $CaCl_2$ with 10% glycerol and centrifuged at 3,000g for 10min at 4°C. Cell pellet was resuspended in 2ml of ice cold sterile 0.1M $CaCl_2$ with 10% glycerol, aliquoted into 100ul per tube, flash frozen with liquid nitrogen and stored at -80°C.

Bacteria Transformation

For chemically competent Stbl3 bacteria, aliquot was thawed on ice, 30µl of bacteria was mixed with 10-100ng of plasmid DNA or 5µl ligation reaction (20µl total) and incubated on ice for 30min. Bacteria/DNA sample was heat shocked at 42°C for 90sec and incubated on ice for 2-5min. Heat shocked bacteria/DNA sample was gently mixed with 500µl LB and incubated at for 30min at 30°C and 220rpm. Following recovery incubation, 10ul, 40ul and 200ul of culture was spread on each of 3 LB/agar/antibiotic plates and incubated at room temperature for 30min to allow culture to adsorb into agar. Plates were incubated inverted at 37°C for 14-16hrs or 30°C for 24-28hrs. Single isolated bacteria colonies were selected, inoculated into 4ml (miniprep) or 50ml (midiprep) LB/antibiotic and incubated for 37°C for 14-16hrs or 30°C for 24-28hrs, followed by plasmid purification.

Colony PCR

A single colony was selected and resuspended into 50µl sterile PBS or water. Using 4ul bacteria suspension, a 20ul reaction was set-up using Taq DNA polymerase (10342020, ThermoFisher Scientific) and gene specific primers as per manufacturer's protocol. PCR product insert (4ul at 1ng/ul) was used as a positive control. Completed reactions were run on an agarose gel and bacteria clones matching both expected size and positive control were selected for downstream analysis.

T3D^{PL} and T3D^{TD} reverse genetics system

L929 cells in 6well plates were infected with T3D-PL or T3D-TD at an MOI of 3 and cell lysates were collected at 24hpi in TRI Reagent® (T9424, Millipore Sigma). Total RNA was

purified using as per TRI Reagent® protocol. Using 1µg RNA per 20µl reaction, cDNA synthesis was performed with pooled forward and reverse gene specific primers for all 10 genes, and M-MLV reverse transcriptase (28025013, ThermoFisher Scientific) as per M-MLV reverse transcriptase protocol. Using cDNA (2µl) as a template, each gene segment was PCR amplified (100µl total reaction) using a gene specific primer set with iProof High Fidelity PCR kit (BioRad), as per manufacturer's protocol. PCR products were purified using QIAquick PCR Purification Kit (28106, Qiagen). S1, M1, M2, M3, L1, L2 and L3 gene segments were gel extracted using PureLink™ Quick Gel Extraction Kit (K210012, Fisher Scientific). All purified PCR products were double digested with CpoI (FD0744, ThermoFisher Scientific) and NotI (FD0594, ThermoFisher Scientific) and purified using QIAquick PCR Purification Kit (28106, Qiagen).

Vector pBacT7-S1T3D (addgene plasmid #33282) was double digested with CpoI (FD0744, ThermoFisher Scientific) and NotI (FD0594, ThermoFisher Scientific), and vector backbone (5716bp fragment) was gel extracted using PureLink™ Quick Gel Extraction Kit (K210012, Fisher Scientific). Gel extracted vector backbone was treated using alkaline phosphatase (EF0654, ThermoFisher Scientific) as per manufacturer's protocol, and purified using QIAquick PCR Purification Kit (28106, Qiagen).

Ligation reactions were performed with a 1:5 ratio of vector:insert using T4 DNA Ligase (15224017, ThermoFisher Scientific) in a 20ul reaction as per manufacturer's protocol. Ligation reactions were transformed into Stbl3 chemically competent bacteria and transformants were selected on LB/agar/carbnecillin (100 µg/ml) plates. For each gene, 8 bacteria colonies were selected for colony PCR validation. Positive bacteria clones were inoculated into 50ml LB/carbnecillin (100 µg/ml) culture for amplification and midiprep plasmid purification using

GenElute™ HP Plasmid Midiprep Kit (NA0200, Millipore Sigma). All plasmids except T3D-L1 were amplified at 37°C for 14-16hrs. T3D-L1 plasmids were amplified at 30°C for 24-28hrs. All plasmids were sequenced to validate inserted gene sequences.

Reassortant reovirus generation

BHK-21-BSR T7/5 cells were seeded in 12 well plates and transfected when cells reached 80-90% confluency. Volumes below are for a single 12 well reaction: 0.35µg of each of 10 reovirus genes and 0.8µg C3P3 (T7 RNA Polymerase linked with $(G_4S)_4$ to NP8686 African Swine Fever Virus capping enzyme) were diluted in 50µl Opti-MEM (31985070, ThermoFisher Scientific). 11µl *Trans*IT®-LT1 (MIR2300, Mirus Bio) was diluted in 50µl Opti-MEM and incubated for 10 minutes at room temperature. LT1 and plasmid dilutions were combined and incubated for 20 minutes at room temperature. Cell media was replaced with 500µl fresh media and transfection mixture was added dropwise to each well. Following a 16-18 hour incubation at 37°C, media was replaced with 750µl fresh media and incubated for an additional 3-5days. Lysates were scraped, collected and plaqued on L929 cells following three freeze/thaw cycles.

Table 1.2. Reagent volumes.

	Volume per well					
Plate	Culture media	Virus dilution	Agar overlay	4% (para) formaldehyde	Methanol	1% crystal violet
6 well	2 ml	200 µl	3 ml	1 ml	2 ml	2 ml
12 well	1 ml	100 µl	1.5 ml	500 µl	1 ml	1 ml
24 well	500 µl	50 µl	750 µl	250 µl	500 µl	500 µl
48 well	250 µl	50 µl		100 µl	250 µl	
96 well	125 µl	50 µl		50 µl	125 µl	
	Volume per well					
Plate	Blocking and permeabilization buffer	Antibody (1° or 2°) or Hoechst 33352 dilution	Wash buffer	NBT/BCIP substrate dilution	PBS/5mM EDTA	pNPP substrate dilution
6 well	800 µl	400 µl	2 ml	400 µl	2 ml	
12 well	400 µl	200 µl	1 ml	200 µl	1 ml	
24 well	200 µl	100 µl	500 µl	100 µl	500 µl	
48 well	100 µl	50 µl	250 µl	50 µl	250 µl	
96 well	50 µl	50 µl	125 µl	50 µl	125 µl	200 µl

Table 1.3. Antibodies.

Antibody	Dilution (Application)	Catalogue Number	Source
Rabbit anti-reovirus pAb	1:10,000 (WB, FC, ICC)		Dr. Patrick Lee (Dalhousie University)
Rabbit anti-σ1C pAb	1:1,000 (WB)		Dr. Roy Duncan (Dalhousie University)
Rabbit anti-µ2 pAb	1:1,000 (IF)	In-house	ProSci Inc
Mouse anti-σNS mAb	1:100 (IF)	3E10	DSHB
Mouse anti-σ3 mAb	1:100 (IF)	10G10	DSHB
Mouse anti-σ3 mAb	1:500 (WB)	4F2	DSHB
Rabbit anti-RIG-I mAb	1:1,000 (WB)	3743	CST
Rabbit anti-IRF3 pAb	1:1,000 (WB)	sc-9082	SCBT
Rabbit anti-P-IRF3 mAb	1:1,000 (WB)	4947	CST

Rabbit anti-P-p38 mAb	1:1,000 (WB)	9215S	CST
Rabbit anti-p38α pAb (p38 TOTAL)	1:500 (WB)	sc-535	SCBT
Rabbit anti-p38α pAb	1:1,000 (WB)	9218	CST
Rabbit anti-p38β mAb	1:1,000 (WB)	2339	CST
Rabbit anti-p38δ mAb	1:1,000 (WB)	2308	CST
Rabbit anti-p38γ pAb	1:1,000 (WB)	2307	CST
Rabbit anti-P-MKK3/6 pAb	1:1,000 (WB)	9231S	CST
Rabbit anti-P-MSK1 pAb	1:1,000 (WB)	9595	CST
Rabbit anti-P-MNK1 pAb	1:1,000 (WB)	2111S	CST
Rabbit anti-P-eEF2 pAb	1:1,000 (WB)	2331S	CST
Rabbit anti-P-ATF2 mAb	1:1,000 (WB)	5112S	CST
Mouse anti-β-actin mAb	1:500 (WB)	47778	SCBT
Goat anti-rabbit HRP	1:10,000 (WB)	111-035-144	JIR
Goat anti-mouse HRP	1:10,000 (WB)	115-035-146	JIR
Goat anti-rabbit AP	1:10,000 (ICC)	111-055-144	JIR
Goat anti-rabbit Alexa Fluor 647	1:2,000 (WB, FC)	111-605-144	JIR
Goat anti-rabbit Alexa Fluor 488	1:2,000 (FC, ICC)	111-545-144	JIR
Goat anti-mouse Alexa Fluor 647	1:2,000 (WB, FC)	115-605-146	JIR

WB: Western blot, FC: Flow cytometry, ICC: Immunocytochemistry, DHSB: Developmental Hybridoma Studies Bank, SCBT: Santa Cruz Biotechnology, JIR: Jackson ImmunoResearch, CST: Cell Signaling Technology, HRP: horseradish peroxidase, AP: alkaline phosphatase, pAb: polyclonal antibody, mAb: monoclonal antibody.

Table 1.4. List of live cell manipulating reagents.

Reagent	Stock	Diluent
SB202190	100mM	DMSO
SB203580	50mM	DMSO
SB202474	50mM	DMSO
Anisomycin	18.85mM	DMSO
BIRB796	125.6mM	DMSO
Nocodazole	10mM	DMSO
Paclitaxel	2.5mM	DMSO
Ammonium chloride (NH_4Cl)	4M	H_2O
Hydrogen peroxide (H_2O_2)	100mM	H_2O

Table 1.5. Reverse genetics cloning primer sequences.

Primer Name	Sequence
NotI-T7pr-S1-Fwd	ATAAGAATGCGGCCGCTAAACTATTAATACGACTCACTATAGCTATTGGTCGGATGGATCC
S1-Rbz-CpoI-Rev	CCAGGTCGGACCGCGAGGAGGTGGAGATGCCATGCCGACCCGATGAAATGCCCCAGTGCC
NotI-T7pr-S2-Fwd	ATAAGAATGCGGCCGCTAAACTATTAATACGACTCACTATAGCTATTCGCTGGTCAGTTATG
S2-Rbz-CpoI-Rev	CCAGGTCGGACCGCGAGGAGGTGGAGATGCCATGCCGACCCGATGAATGTGTGGTCAGTCG
NotI-T7pr-S3-Fwd	ATAAGAATGCGGCCGCTAAACTATTAATACGACTCACTATAGCTAAAGTCACGCCTGTCG
S3-Rbz-CpoI-Rev	CCAGGTCGGACCGCGAGGAGGTGGAGATGCCATGCCGACCCGATGATTAGGCGTCACCCAC
NotI-T7pr-S4-Fwd	ATAAGAATGCGGCCGCTAAACTATTAATACGACTCACTATAGCTATTTTTGCCTCTTCCCAG
S4-Rbz-CpoI-Rev	CCAGGTCGGACCGCGAGGAGGTGGAGATGCCATGCCGACCCGATGAATGAAGCCTGTCCCA
NotI-T7pr-M1-Fwd	ATAAGAATGCGGCCGCTAAACTATTAATACGACTCACTATAGCTATTCGCGGTCATGGCT
M1-Rbz-CpoI-Rev	CCAGGTCGGACCGCGAGGAGGTGGAGATGCCATGCCGACCCGATGAAGCGCGTACGTAGTC
NotI-T7pr-M2-Fwd	ATAAGAATGCGGCCGCTAAACTATTAATACGACTCACTATAGCTAATCTGCTGACCGTTAC
M2-Rbz-CpoI-Rev	CCAGGTCGGACCGCGAGGAGGTGGAGATGCCATGCCGACCCGATGATTTGCCTGCATCCCT
NotI-T7pr-M3-Fwd	ATAAGAATGCGGCCGCTAAACTATTAATACGACTCACTATAGCTAAAGTGACCGTGGTCAT
M3-Rbz-CpoI-Rev	CCAGGTCGGACCGCGAGGAGGTGGAGATGCCATGCCGACCCGATGAATGGGGGTCGGGAA
NotI-T7pr-L1-Fwd	ATAAGAATGCGGCCGCTAAACTATTAATACGACTCACTATAGCTACACGTTCCACGACAAT
L1-Rbz-CpoI-Rev	CCAGGTCGGACCGCGAGGAGGTGGAGATGCCATGCCGACCCGATGAGTTGACGCACCACG
NotI-T7pr-L2TD-Fwd	ATAAGAATGCGGCCGCTAAACTATTAATACGACTCACTATAGCTAAAAGGCGCGATGGCG
NotI-T7pr-L2PL-Fwd	ATAAGAATGCGGCCGCTAAACTATTAATACGACTCACTATAGCTAAATGGCGCGATGGCG
L2-Rbz-CpoI-Rev	CCAGGTCGGACCGCGAGGAGGTGGAGATGCCATGCCGACCCGATGAATTAGGCGCGCTCAC
NotI-T7pr-L3-Fwd	ATAAGAATGCGGCCGCTAAACTATTAATACGACTCACTATAGCTAATCGTCAGGATGAAGC

L3-Rbz-CpoI-Rev	CCAGGTCGGACCGCGAGGAGGTGGAGATGCCATGCCGACCCGATGAATCGGCCCAACTAGC

Note that L2 gene forward primers were unique for T3D-PL and T3D-TD.

Table 1.6. RT-PCR primer sequences.

Primer Name	Primer Sequence
ReoS4-F	GGAACATTGTGAGAGCAGCA
ReoS4-R	GCAAGCTAGTGGAGGCAGTC
ReoM2-F	ACGATGTCCCCACTATCAGC
ReoM2-R	GATTGCTTCGGCTATCTTCG
mGAPDH-F	TGGCAAAGTGGAGATTGTTGCC
mGAPDH-R	AAGATGGTGATGGGCTTCCCG
mIfnb1-F	CCCTATGGAGATGACGGAGA
mIfnb1-R	CTGTCTGCTGGTGGAGTTCA
mIfna4-F	CTGCTGGCTGTGAGGACATA
mIfna4-R	AGGAAGAGAGGGCTCTCCAG
mRigI-F	GCCCCTACTGGTTGTGGAAA
mRigI-R	GTGAGAACACAGTTGCCTGC
mRsad-F	ATGGTTCAAGGACTATGGGGAG
mRsad-R	TTGACCACGGCCAATCAGAG
mMx1-F	TCTGTGCAGGCACTATGAGG
mMx1-R	ACTCTGGTCCCCAATGACAG
mIfi44-F	TGACATGGCAGCAAGAAAAG
mIfi44-R	CTGCACACTCGCCTTGTAAA
mCxcl10-F	ATGACGGGCCAGTGAGAATG
mCxcl10-R	CATCGTGGCAATGATCTCAACA
mCcl4-F	CAGCTGTGGTATTCCTGACCAA
mCcl4-R	AGCTGCTCAGTTCAACTCCA
mCcl5-F	CTGCTGCTTTGCCTACCTCT
mCcl5-R	CGAGTGACAAACACGACTGC
mIl6-F	CTCTGCAAGAGACTTCCATCCA
mIl6-R	GACAGGTCTGTTGGGAGTGG
mCxcl1-F	ACCGAAGTCATAGCCACACTC
mCxcl1-R	CTCCGTTACTTGGGGACACC
mCxcl2-F	CCCAGACAGAAGTCATAGCCAC
mCxcl2-R	TGGTTCTTCCGTTGAGGGAC
mFas-F	GTCCTGCCTCTGGTGCTTG
mFas-R	AGCAAAATGGGCCTCCTTGA

mCsf2-F	ATGCCTGTCACGTTGAATGA
mCsf2-R	CCGTAGACCCTGCTCGAATA
hMAPK14-F	TGCACATGCCTACTTTGCTC
hMAPK14-R	ATCATAAGGATCGGCCACTG
hMAPK11-F	GCTGTGAACGAGGACTGTGA
hMAPK11-R	CGCTTCAGCTGGTCAATGTA
hMAPK13-F	TGTCAGTGTGGGACACCAGT
hMAPK13-R	GGGTCCTGCGGTTAAGTACA
hMAPK12-F	AGCCCCAGGTCCAGAAGTAT
hMAPK12-R	GCTTGAAGCTGAGCACCTCT
hGAPDH-F	GAGTCAACGGATTTGGTCGT
hGAPDH-R	GACAAGCTTCCCGTTCTCAG

Table 1.7 shRNA sequences.

TRC ID	Sequence	Label	Clone	Target gene	Species	Additional information
TRCN0000000509	CCGGGCCGTATAGGATGTCAGACAACTCGAGTTGTCTGACATCCTATACGGCTTTTT	shMAPK14	1	MAPK14	Human	In-house shRNA library glycerol stocks
TRCN0000000510	CCGGCCATGTTCAGTTCCTTATCTACTCGAGTAGATAAGGAACTGAACATGGTTTTT	shMAPK14	2	MAPK14	Human	In-house shRNA library glycerol stocks
TRCN0000000511	CCGGCCATGAGGCAAGAAACTATATCTCGAGATATAGTTTCTTGCCTCATGGTTTTT	shMAPK14	3	MAPK14	Human	In-house shRNA library glycerol stocks
TRCN0000010051	CCGGGTTACGTGTGGCAGTGAAGAACTCGAGTTCTTCACTGCCACACGTAACTTTTT	shMAPK14	4	MAPK14	Human	In-house shRNA library glycerol stocks
TRCN0000010053	CCGGGACATAATTCACAGGGACCTACTCGAGTAGGT	shMAPK14	5	MAPK14	Human	In-house shRNA library glycerol stocks

	CCCTGTGAATTATGTCTTTTT					
TRCN0000009972	CCGGGAACAACATCGTCAAGTGCCACTCGAGTGGCACTTGACGATGTTGTTCTTTTT	shMAPK11	6	MAPK11	Human	In-house shRNA library glycerol stocks
TRCN0000195286	CCGGCACGTTCAATTCCTGGTTTACCTCGAGGTAAACCAGGAATTGAACGTGTTTTTTG	shMAPK11	7	MAPK11	Human	In-house shRNA library glycerol stocks
TRCN0000199575	CCGGGCCACGTCCATCGAGGACTTCCTCGAGGAAGTCCTCGATGGACGTGGCTTTTTTG	shMAPK11	8	MAPK11	Human	In-house shRNA library glycerol stocks
TRCN0000196579	CCGGGAGAATCTACACGCATGTATGCTCGAGCATACATGCGTGTAGATTCTCTTTTTTG	shMAPK11	9	MAPK11	Human	In-house shRNA library glycerol stocks
TRCN0000199347	CCGGCCTGTCCTCTTCTGGCTACTGCTCGAGCAGTAGCCAGAAGAGGACAGGTTTTTTG	shMAPK11	10	MAPK11	Human	In-house shRNA library glycerol stocks
TRCN0000006145	CCGGCTGGATGACTTCACGGACTTTCTCGAGAAAGTCCGTGAAGTCATCCAGTTTTT	shMAPK12	12	MAPK12	Human	In-house shRNA library glycerol stocks
TRCN0000006146	CCGGCATCTTGAATTGGATGCGCTACTCGAGTAGCGCATCCAATTCAAGATGTTTTT	shMAPK12	13	MAPK12	Human	In-house shRNA library glycerol stocks
TRCN0000006147	CCGGCTGGACGTATTCACTCCTGATCTCGAGATCAGGAGTGAATACGTCCAGTTTTT	shMAPK12	14	MAPK12	Human	In-house shRNA library glycerol stocks

TRCN0000006148	CCGGCCAGGTCCAGAAGTATGATGACTCGAGTCATCATACTTCTGGACCTGGTTTTT	shMAPK12	15	MAPK12	Human	In-house shRNA library glycerol stocks
TRCN0000006149	CCGGGCCCTTCCAGTCCGAGCTGTTCTCGAGAACAGCTCGGACTGGAAGGGCTTTTT	shMAPK12	16	MAPK12	Human	In-house shRNA library glycerol stocks
TRCN0000055428	CCGGGCGCAACTTCTATGACTTCTACTCGAGTAGAAGTCATAGAAGTTGCGCTTTTT	shMAPK13	17	MAPK13	Human	In-house shRNA library glycerol stocks
TRCN0000000827	CCGGCCGTTTGATGATTCCTTAGAACTCGAGTTCTAAGGAATCATCAAACGGTTTTT	shMAPK13	18	MAPK13	Human	In-house shRNA library glycerol stocks
TRCN0000197055	CCGGGATGCTCAAAGGCCTTAAGTACTCGAGTACTTAAGGCCTTTGAGCATCTTTTTTG	shMAPK13	19	MAPK13	Human	In-house shRNA library glycerol stocks
TRCN0000009978	CCGGCCCTTTCAGTCCGAGATCTTCCTCGAGGAAGATCTCGGACTGAAAGGGTTTTT	shMAPK13	20	MAPK13	Human	In-house shRNA library glycerol stocks
TRCN0000009981	CCGGTCTGTGGGCTGTATCATGGCACTCGAGTGCCATGATACAGCCCACAGATTTTT	shMAPK13	21	MAPK13	Human	In-house shRNA library glycerol stocks
TRCN0000103885	CCGGGCAAAGATATTCTGCGCCAAACTCGAGTTTGGCGCAGAATATCTTTGCTTTTTG	shRIG-I		DDX58 (RIG-I)	Mouse	In-house shRNA library glycerol stocks
	CCTAAGGTTAAGTCGCCCTCGCTCGAGCGAGGGCGACTTAACCTTAGG	shSCR				Addgene plasmid #1864 (Sarbassov D.D. *et al.* 2005. Science)

	ACCGGACACTCG AGCACTTTTTGAA TTC	shEMPTY				pLKO.1 empty vector control with 18bp stuffer sequence (Cat# RHS4080)
	TACAACAGCCAC AACGTCTAT	shGFP		eGFP		TRC lentiviral eGFP shRNA positive control (Cat# RHS4459)

CHAPTER 2: T3D LABORATORY STRAIN CHARACTERIZATION

2.1 RESULTS: PHENOTYPIC CHARACTERIZATION

2.1.1 $T3D^{PL}$ has enhanced oncolytic potency compared to $T3D^{KC}$ and $T3D^{TD}$

The prototypic serotype 3 reovirus (Dearing, T3D) has been propagated in different laboratories for almost 60 years, and previous comparisons between T3D laboratory strains found that $T3D^{C}$ (from Cashdollar laboratory) and $T3D^{F/N}$ (from Nibert laboratory) exhibit different respiratory pathogenesis *in-vivo* and in cell signaling *in-vitro* [211, 212]. Surprisingly however, similar *in-vitro* replication kinetics were observed between these two T3D laboratory strains [213]. We noticed that compared to published $T3D^{C}$ and $T3D^{F/N}$ replication kinetics *in-vitro*, our laboratory T3D strain had enhanced replication kinetics. Given that laboratories across the globe use distinct sources of reovirus for understanding virus replication, innate and cellular responses to viruses, and reovirus-mediated oncolysis, it seemed important to reveal differences among laboratory strains. We therefore sought to compare the *in-vitro* replication potency, innate signalling, and oncolytic activities of various T3D laboratory strains.

First, the *in-vitro* growth kinetics was assessed for four T3D strains; $T3D^{PL}$ (Patrick Lee, Dalhousie University), $T3D^{KC}$ (Kevin Coombs, University of Manitoba), $T3D^{TD}$ (Terence Dermody, University of Pittsburgh) and $T3D^{ATCC}$ (American Type Culture Collection). All four strains were plaque purified, amplified on L929 mouse fibroblasts most commonly used to propagate reovirus, and cesium chloride purified. Plaque area was then compared among reovirus strains, as a measure of overall efficiency of virus infection and cell-to-cell spread. On L929 cells, $T3D^{PL}$ produced plaques that were clearly observed at 2-3 dpi (Fig 2.26). In contrast, $T3D^{KC}$ and $T3D^{TD}$ plaques were only visible at 6-7dpi. Reovirus plaques were fixed at 7dpi and

plaques visualized by crystal violet staining (Fig 2.1A). $T3D^{PL}$ had the largest average plaque size of 1644, $T3D^{KC}$ and $T3D^{TD}$ had the smallest average plaque sizes of 42 and 32, respectively, and $T3D^{ATCC}$ had an intermediate average plaque size of 225 (Fig 2.1B). $T3D^{PL}$ originated from the Wolfgang K. Joklik laboratory (Duke University) while $T3D^{KC}$ and $T3D^{TD}$ originated from the Bernard N. Fields laboratory (Harvard Medical School); The T3D strain from the B.N. Fields laboratory was originally obtained from the W. K. Joklik laboratory [214-217]. The depositor of $T3D^{ATCC}$, W. Adrian Chappell, was affiliated with the Centre for Disease Control (Atlanta), but could not be linked to any reovirus laboratories or publications and therefore the passage history of $T3D^{ATCC}$ was unknown. Since we could not trace the origins of $T3D^{ATCC}$ to discern the propagation history, it was omitted from further experiments; although laboratories using $T3D^{ATCC}$ should note that it clearly has distinct replication kinetics.

To assess if the differences observed between T3D strains in L929 cells also translated to differences in other cell lines, we performed virus plaque assays on a panel of mouse (ID8 ovarian cancer, B16-F10 melanoma) and human (Huh7.5 hepatocellular carcinoma, H1299 non-small cell lung carcinoma) tumorigenic cell lines. For cell lines other than L929s, virus plaques or infected cell foci were detected by immunocytochemical staining with anti-reovirus polyclonal serum, as plaques were not always discernable with crystal violet on cells that do not form perfect monolayers. In all cell lines tested, plaques or foci formed by $T3D^{PL}$ were larger than $T3D^{KC}$ and $T3D^{TD}$ (Fig 2.1C, 2.2A). Enhanced clearing of cells in the center of plaques was also obvious for $T3D^{PL}$ relative to $T3D^{KC}$ and $T3D^{TD}$, suggesting $T3D^{PL}$ had enhanced ability to replicate, spread and kill cancer cells *in-vitro.* This is the first report, to our knowledge, of differences in *in-vitro* replication between T3D laboratory strains.

It was previously demonstrated that variants of T3D with enhanced replication potency *in-vitro* correlated with improved oncolytic efficacy *in-vivo* [218]. On this basis, we similarly compared the *in-vivo* oncolytic efficacy between $T3D^{PL}$ and $T3D^{TD}$. We utilized the aggressive B16-F10 syngeneic melanoma mouse model as a preliminary measure of virus replication mediated tumor clearance. B16-F10 cells were implanted subcutaneously into the hind flank of six-week old female C57BL/6 mice. The plaque size morphology of $T3D^{PL}$ and $T3D^{TD}$ was confirmed in-vitro prior to use in animals (Fig 2.2A), and when tumors were palpable, equivalent doses (5×108 pfu/dose) of $T3D^{PL}$ and $T3D^{TD}$ were injected intra-tumorally at 2-day intervals, for a total of 3 doses (Fig 2.2B). PBS was injected as a negative control. Tumor volumes were monitored every 2 days. Compared to the PBS control group, both $T3D^{PL}$ and $T3D^{TD}$ showed improved tumor regression (Fig 2.2C). However, $T3D^{TD}$ only marginally controlled tumor growth while $T3D^{PL}$ reliably controlled tumor growth in all mice.

Kaplan Meier animal survival plots could not be applied to this study because as per the strict animal ethics protocol, mice had to be sacrificed when either tumors became too large ($600mm^3$), or if they showed any signs of necrosis and ulceration; having different causes of death made survival curves uninformative with respect to oncolysis. Necrosis was especially evident in $T3D^{PL}$ treated mice, causing a dry scab at the tumor site that peeled off and resulted in exposed flesh and need to sacrifice the mouse despite that the tumor was cleared. Additionally, we found it crucial to begin treatment with reovirus when tumor volumes were less than $20mm^3$; otherwise mice did not survive past the final dose of treatment due to aggressive tumor growth. Overall, this tumor regression study is first report, to our knowledge, of differential *in-vivo* oncolytic capabilities between T3D laboratory strains. An in-depth characterization was performed to potentially identify novel mechanisms mediating reovirus oncolysis.

2.1.2 T3D^{KC} and T3D^{TD} have lower virion σ1 levels relative to T3D^{PL}

Previous studies demonstrated that modifications to outer capsid proteins such as σ1, σ3 and μ1 can impact reovirus infectivity [218-220]. To determine if virion architecture contributes to differences in T3D^{PL}, T3D^{KC} and T3D^{TD} replication, we assessed virion genomic dsRNA and protein composition. RNA was extracted from purified reovirus preparations and separated by SDS PAGE. Resolution of reovirus genomic dsRNA segments using SDS-PAGE produces a unique electropherotype depending on reovirus serotype. Specifically, the distinct band position of the S1 segment was long-used as an indicator of reovirus serotype. T3D^{PL}, T3D^{KC} and T3D^{TD} had a similar dsRNA electropherotype that was distinct from T1L and T2J (Fig 2.3A), and similar to previous reports of T3D dsRNA pattern [221-223]. These results suggest that the T3D laboratory strains likely diversified within the T3D serotype rather than undergoing reassortment with serotypes 1 or 2.

Virion structural proteins of purified T3D^{PL}, T3D^{KC} and T3D^{TD} preparations were then visualized by Imperial^{TM} total protein staining or Western blot analysis using reovirus protein specific antibodies. The ratio of capsid proteins λ1/2, μ1C, σ2 and σ3 were similar between T3D^{PL}, T3D^{KC} and T3D^{TD} (Fig 2.3B). However, for equivalent capsid protein (σ3), T3D^{KC} and T3D^{TD} had lower average levels of σ1 compared to T3D^{PL} (Fig 2.3B, 2.3C). The σ1 protein is a trimer that extends from channels generated by pentameric λ2 proteins at vertices of reovirus particles, and functions as the cell-attachment protein. Not all reovirus virion vertices need to be occupied by σ1; in fact, reovirus particles can have 0-to-12 σ1 trimers depending on the sequence of σ1 or λ2 [218, 224]. Since Western blotting gave us an average level of virion σ1, we utilized agarose gel separation of full virions as a method to distinguish virions based on σ1 levels. More than 80% of T3D^{PL} virions had a range of 7-12 σ1 trimers/virion. Contrastingly,

only 28% and 6% of $T3D^{KC}$ and $T3D^{TD}$ virions had a range of 7-12 σ1 trimers/virion, respectively. Close to 50% of $T3D^{KC}$ and $T3D^{TD}$ virions had a range of 3-6 σ1 trimers/virion. $T3D^{KC}$ and $T3D^{TD}$ had 24% and 48% of virions with 0-2 σ1 trimers/virion, respectively (Fig 2.3D).

2.1.3 $T3D^{PL}$ has increased cell binding compared to $T3D^{KC}$ and $T3D^{TD}$

We and others have previously observed that 3 or more σ1 trimers/virion are necessary and sufficient for virion binding to cells [127, 218, 224]. Since σ1 levels differed between the T3D strains, with $T3D^{KC}$ and $T3D^{TD}$ having a larger percentage of 0-2 σ1 trimers/virion relative to $T3D^{PL}$, we compared the binding efficiency of the three laboratory strains. Equal virions were adsorbed onto L929 cells at 4°C for 1 hour, and bound virions per cell were assessed using flow cytometry. Assessment of reovirus binding using flow cytometry is linear over a wide range (81-fold) of virus dilutions (Fig 2.4A, 2.4B). $T3D^{KC}$ and $T3D^{TD}$ bound cells at 60% and 40% efficiency of $T3D^{PL}$, which correlated closely to their respective σ1 trimers/virion ratio (Fig 2.4C).

Binding of reovirus via σ1 is mediated primarily by cell surface sialic acids and junction adhesion molecule – A (JAM-A). As depicted in Figure 2.4D, for serotype T3D, σ1 sialic acid binding occurs at the body domain (amino acids 198-204, red spheres), while JAM-A binding occurs at the head domain (amino acids 311-455); both of which have been very well characterized. The difference in σ1 at amino acid 408 (orange spheres) between $T3D^{PL}$ and $T3D^{KC}$/$T3D^{TD}$ is located in the head domain but not at the JAM-A binding interface (light purple spheres) and therefore is less likely to contribute to the differential virion cell binding levels. No differences are present between the T3D strains in sialic acid – σ1 binding domain (Fig 2.4D).

Differences observed in binding efficiency between $T3D^{PL}$, $T3D^{KC}$ and $T3D^{TD}$ are most likely due to virion σ1 levels, and we previously demonstrated that T3D variants with reduced virion σ1 levels possess mutations in the σ1 anchor tail domain (amino acids 1-27) or the λ2 flap domain (amino acids 1023-1289, orange ribbon). Interestingly, $T3D^{PL}$ and $T3D^{KC}$/$T3D^{TD}$ differ in the anchor domain σ1 at amino acid 22 and in the λ2 methyltransferase (yellow ribbon) and flap interacting domain at amino acids 504 (red spheres) and 509 (green spheres); these differences are more-likely to explain the variation in σ1 levels between $T3D^{PL}$ and $T3D^{KC}$/$T3D^{TD}$. Additionally, $T3D^{KC}$ has a unique difference in the λ2 flap domain at amino acid 1069 (blue spheres), which could explicate the intermediate level of σ1 levels in $T3D^{KC}$ (Fig 2.4E).

2.1.4 $T3D^{PL}$, $T3D^{KC}$ and $T3D^{TD}$ have similar entry kinetics

Following attachment to cells, reovirus undergoes endocytosis and trafficking to lysosomes where cathepsins L and B mediate virus uncoating [146, 225-228]. Specifically, during reovirus uncoating, the outermost σ3 protein is degraded, and μ1C is cleaved to the membrane-destabilizing products δ, μ1N and φ. The resulting intermediate subviral particle (ISVPs) is capable of penetrating membranes and delivering the final reovirus core particle to the cytoplasm [182, 184, 186, 229-231]. Numerous studies have demonstrated that reovirus particle infectivity of ISVPs is higher than whole virions in both reovirus susceptible and resistant cell lines [232-234]. Therefore, efficient reovirus uncoating is a crucial mediator for successful infection. Standardizing for virus binding, cleavage of σ3 and μ1C was monitored by Western blot analysis at various timepoints post infection. Complete cleavage of σ3 was observed by 3hpi and coincided with initiation of μ1C to δ cleavage (Fig 2.5A). The rate of μ1C cleavage to δ was quantified as a percentage of δ to δ + μ1C standardized to β actin (housekeeping protein). All

T3D strains had similar uncoating rates and almost complete uncoating was attained by 5hpi (Fig 2.5A, 2.5B). Unlike $T3D^{KC}$ and $T3D^{TD}$, *de-novo* synthesized μ1 and σ3 was observed at 5hpi in $T3D^{PL}$, suggesting an enhancement of protein expression during $T3D^{PL}$ infection (Fig 2.5A).

During intestinal infection, reovirus uncoating is facilitated by intestinal proteases such as chymotrypsin and trypsin. To mimic intestinal uncoating kinetics, equal particles of $T3D^{PL}$, $T3D^{KC}$ and $T3D^{TD}$ were incubated with chymotrypsin and reactions were halted at various timepoints, and reovirus protein cleavage was monitored by Imperial^{TM} coomassie staining. The levels of core proteins λ1/2 and σ2 were unchanged, indicating viral core stability during chymotrypsin incubation (Fig 2.6A). At 20min post chymotrypsin, the level of μ1C to δ cleavage was similar between $T3D^{PL}$, $T3D^{KC}$ and $T3D^{TD}$. Since no δ cleavage occurred at 10min post chymotrypsin and complete μ1C degradation was observed at 30min post chymotrypsin, a narrow timepoint between 10min and 30min would need to be performed to determine the rate of μ1C to δ cleavage (Fig 2.6A). In the case of σ3, the rate of cleavage was slower for $T3D^{PL}$ compared to $T3D^{KC}$ and $T3D^{TD}$ (Fig 2.6A, 2.6B), suggesting potential difference in intestinal virus stability between the laboratory T3D strains.

2.1.5 $T3D^{PL}$ has enhanced viral RNA transcription and protein translation over $T3D^{KC}$ and $T3D^{TD}$

Following uncoating of the outer capsid, reovirus cores that enter the cytoplasm become transcriptionally active [228, 235]. To assess core transcriptase activity and overall accumulation of viral RNA, we used quantitative RT-PCR for viral RNA over the course of infection. S4 and M2 viral RNAs were used as representative viral genes, while GAPDH housekeeping gene was used for standardization between samples. Over 12hpi, viral RNA synthesis for $T3D^{PL}$ had a

steeper slope, indicating faster rate of viral transcription compared to $T3D^{KC}$/$T3D^{TD}$ (Fig 2.7A, 2.7B). The rate of viral RNA transcription was similar between $T3D^{KC}$ and $T3D^{TD}$. Before viral RNA saturation at 8hpi, $T3D^{PL}$ had 77 and 85-fold higher levels of S4 viral RNA compared to $T3D^{KC}$ and $T3D^{TD}$, respectively (Fig 2.7A). Differences in viral M2 RNA were even greater, with $T3D^{PL}$ having 92 and 133-fold higher levels than $T3D^{KC}$ and $T3D^{TD}$, respectively (Fig 2.7B). We anticipated that the increased amount of viral RNA during $T3D^{PL}$ infection would translate into elevated viral proteins. Using Western blot analysis with a polyclonal anti-reovirus antibody, we observed substantially higher accumulation of $T3D^{PL}$ viral proteins compared to $T3D^{KC}$ and $T3D^{TD}$ at every respective timepoint from 6hpi onwards (Fig 2.7C).

In summary, compared to $T3D^{KC}$ and $T3D^{TD}$, $T3D^{PL}$ had increased cell binding, which correlated to higher σ1 trimers per virion. When standardized for equal virus-cell binding, $T3D^{PL}$, $T3D^{KC}$ and $T3D^{TD}$ had similar entry and uncoating kinetics, however a post-uncoating step facilitated by enhanced core transcriptase activity, resulted in expedited $T3D^{PL}$ viral RNA transcription and protein translation.

2.1.6 $T3D^{PL}$ viral cores have an inherent advantage in viral mRNA transcriptase activity over $T3D^{KC}$ and $T3D^{TD}$

The finding that $T3D^{PL}$ shows higher rates of transcription does not necessarily prove that $T3D^{PL}$ cores transcribe more efficiently; as it is also possible that any step of virus replication is increased and therefore increases amplification of viral RNAs. Specifically, upon initiation of viral RNA transcription by the viral cores, viral proteins assemble and incorporate viral RNAs, generating new viral cores. These newly synthesized viral cores further contribute to the viral RNA transcription resulting in exponential amplification of viral replication [236, 237].

Accordingly, our observation that $T3D^{PL}$ has enhanced rates of viral RNA synthesis during infection could indicate either that $T3D^{PL}$ cores have inherent enhanced transcription, or that $T3D^{PL}$ has elevated viral core amplification steps (core protein translation and/or assembly). To distinguish between these possibilities, we determined inherent core transcriptase activity in the absence of protein translation and other confounding cellular variables. Virus cores were generated using chymotrypsin (CHT) digestion, as previously described [224]. High speed centrifugation was utilized to separate pelleted virus cores from CHT digestion by-products and enable resuspension of virus cores in an *in-vitro* transcription reaction compatible buffer. The purity of viral cores was confirmed by Coomassie staining and Western blot analysis; cores had the characteristic loss of outer capsid proteins (σ1, σ3 and μ1) but retained core capsid proteins (σ2, λ1, λ2) (Fig 2.8A). Transcription reactions were assembled and allowed to proceed for various time intervals. To account for variation during sample processing and to normalize between samples, each sample was spiked with *in-vitro* synthesized mouse GAPDH RNA as an internal control prior to RNA extraction. Equalized for input viral cores and following correction for GAPDH, the rate of S4, M2 and L2 viral RNA transcription was significantly higher in $T3D^{PL}$ compared to $T3D^{KC}$ and $T3D^{TD}$ (Fig 2.8B). No RNA transcription was observed in reactions lacking rATP, confirming that RNA quantified in the presence of all four rNTPs was a consequence of productive core transcription. *In-vitro* core transcription rates were linear unlike the exponential rates observed during intracellular infection (Fig 2.7A, 2.8B), supporting previous evidence for viral core amplification during reovirus infection. Therefore, $T3D^{PL}$ has an inherent transcriptase advantage within the viral cores.

2.1.7 Establishment of infection is accelerated in T3D^{PL} compared to T3D^{KC} and T3D^{TD}

A thorough assessment of the literature suggested that T3D growth curves published by the Patrick Lee laboratory differed from those published by the Kevin Coombs and Terence Dermody laboratories [213, 218, 238]. However, since these differences could be caused by laboratory specific protocols of infection and plaque assays, we performed a side-by-side single step growth curve comparison between T3D^{PL} and T3D^{TD} in L929 cells. Reovirus titres at 1hpi were similar between T3D^{PL} and T3D^{TD}, suggesting equal input virions (Fig 2.9). Relative to 1hpi, the titres at 3 and 6hpi were lower (~1 log) in both T3D^{PL} and T3D^{TD}, indicative of non-infectious viral core formation. Compared to input, 12hpi titres for T3D^{PL} increased by 3-logs while T3D^{TD} increased by 1.5-logs. T3D^{PL} titres saturated at 18hpi while T3D^{TD} titres saturated at 24hpi, and saturation titres in T3D^{PL} were 1-log higher than T3D^{TD}. T3D^{PL} therefore has a more rapid and productive replication cycle compared to T3D^{TD}.

Previous measurements of viral RNA and protein levels during infection were an overall average assessment and did not distinguish between these two possible scenarios; i) T3D^{PL} has enhanced viral RNA/protein levels per infected cell and/or ii) T3D^{PL} infects a larger proportion of cells. To monitor the kinetics of single-step reovirus infection and spread on a per-cell basis, reovirus-infected cells were visualized by immunofluorescence with polyclonal anti-reovirus antiserum at 12, 24 and 48hpi. At equivalent cell-bound virus dilutions, T3D^{PL} had increased number of infected cells compared to T3D^{KC} and T3D^{TD} at 12hp (Fig 2.10A). Virus infected cells at 24 and 48hpi in T3D^{KC}/T3D^{TD} were similar to 12 and 24hpi in T3D^{PL}, respectively, again suggesting a delayed infection for T3D^{KC}/T3D^{TD} relative to T3D^{PL}. Indicative of virus spread to neighbouring cells, infected cell foci were observed at 24hpi in T3D^{PL} compared to 48hpi in T3D^{KC}/T3D^{TD}. Unlike T3D^{KC}/T3D^{TD}, T3D^{PL} infection caused loss of HOESCHT nuclear

staining at 48hpi, suggesting enhanced cell death (Fig 2.10A). These findings suggest that for equal bound virions, $T3D^{PL}$ establishes an earlier infection, spreads more rapidly and causes higher cell death compared to $T3D^{KC}$/$T3D^{TD}$.

Flow cytometry was used as a more quantitative measure of reovirus infection and dissemination kinetics. $T3D^{PL}$ and $T3D^{TD}$ infections were normalized for cell-bound virus and processed for flow cytometry analysis with polyclonal reovirus antibodies, at 12 and 24hpi. At 12hpi, $T3D^{PL}$ and $T3D^{TD}$ had two distinct populations; a low fluorescence intensity reovirus-antigen-negative (REO-) and a high fluorescence intensity reovirus-antigen-negative (REO+) population (Fig 2.10B). The REO- population represented uninfected cells since the fluorescence intensity matched with the mock infected population. At 12hpi, the REO+ population of $T3D^{PL}$ was more distinct from the REO- population, unlike $T3D^{TD}$ whose REO+ population was a contiguous extension of the REO- population suggesting fewer virus proteins per infected cells. At 24hpi, the $T3D^{TD}$ REO+ population had a similar profile to that of $T3D^{PL}$ at 12hpi, suggesting that $T3D^{TD}$ has a population of prematurely infected cells at 12hpi that becomes established by 24hpi. At 24hpi, REO- in $T3D^{PL}$ was reduced compared to 12hpi, suggesting potential spread of $T3D^{PL}$ infection from 12 to 24hpi. For $T3D^{TD}$, 24hpi REO- was similar to 12hpi (Fig 2.10B). Therefore, in congruence with our immunofluorescence analysis, $T3D^{PL}$ was able to establish a productive infection and spread to neighbouring cells earlier than $T3D^{TD}$.

To address the possibility that the 12 to 24hpi difference in $T3D^{TD}$ REO+ population could be due to spread of infection and not due to establishment of infection, we used an antibody neutralization strategy. To validate antibody neutralization, reovirus inoculum was incubated with polyclonal anti-reovirus antibody for 30min prior to adsorption onto cells, followed by flow cytometry analysis for reovirus infection at 12hpi (Fig 2.11A; 0hpi α-Reo Ab).

The absence of a REO+ population in neutralizing antibody pre-treated samples suggested complete inhibition of initiation of infection. Similar to Figure 2.10B, in samples lacking neutralizing antibody, $T3D^{PL}$ established infection by 12hpi while $T3D^{TD}$ produced a pre-maturely infected population at 12hpi and establishing infection at 24hpi (Fig 2.11A; No Ab). Since the majority of cell-bound virions enter the cell by 2hpi [146, 225], treatment of reovirus infected cells at 3-5hpi with reovirus neutralizing antibodies would not inhibit initial reovirus infection but still sufficiently block reovirus spread. Indeed, addition of reovirus neutralizing antibodies did not affect the percent of infected cells at 12hpi (Fig 2.11A: 3hpi α-Reo Ab). Importantly, the infectivity profiles of $T3D^{TD}$ for 12 versus 24hpi were highly similar irrespective of neutralizing antibody treatment (e.g. 27.8% versus 25.9%), suggesting that the increased infection of $T3D^{TD}$ at 24hpi relative to 12hpi was due to a delay in establishment of infection rather than reovirus spread. In $T3D^{PL}$, addition of neutralizing antibody eliminated the increase in REO+ population between 12hpi and 24hpi (e.g. 23.3% versus 25.5%) and reduced the levels of infected cells at 24hpi between no antibody versus antibody neutralization (e.g. 37.5% to 25.5%), suggesting that $T3D^{PL}$ dissemination already occurs by 24hpi (Fig 2.11A).

In Figure 2.11A (3hpi α-Reo Ab), we observed a positive shift in the REO- population at 24hpi in the neutralizing antibody treated $T3D^{PL}$ samples. The neutralizing antibody used in the study was a polyclonal antibody primarily recognizing primarily μ1 and σ3, and to lesser extent σ1. A single cycle of $T3D^{PL}$ infection produces a 4-log increase in viral titres by 24hpi (Fig 2.9), resulting in potential saturation of σ1 specific antibodies which are in a minority. It is very likely that progeny virions bound only by σ3-specific antibodies, could still enter the cell via σ1 binding but not undergo successful uncoating and infection due to σ3 inaccessibility. Cells with internalized virions would cause a shift relative to uninfected cells, and the shift would be

significantly lower than productively infected samples. The absence of the population shift in pre-treated neutralizing antibody samples could be due to sufficient σ1 specific antibodies to block the entry of input virions.

Immunofluorescence was used as an additional method to confirm the flow cytometry neutralizing antibody conclusions. Equalized for cell binding, $T3D^{PL}$ and $T3D^{TD}$ infections were supplemented with anti-reovirus neutralizing antibodies at 3hpi and samples were fixed for immunofluorescence processing at 12, 24, 48 and 120hpi. Similar to flow cytometric data (Fig 2.10B, 2.11A), $T3D^{TD}$ infection increased from 12 to 24hpi, with the 24hpi infection matching $T3D^{PL}$ at 12hpi. Relative to 24hpi, $T3D^{PL}$ and $T3D^{TD}$ infections remained unchanged at 48 and 120hpi. In the absence of neutralizing antibody, $T3D^{PL}$ and $T3D^{TD}$ infections saturated at 48 and 120hpi, respectively. At 120hpi in the absence of neutralizing antibody, the cell monolayer in $T3D^{PL}$ was abolished due to extensive cell death (Fig 2.11B). Therefore, immunofluorescence analysis confirmed the capacity of the neutralizing antibody to inhibit reovirus spread and validated our conclusions that $T3D^{TD}$ infection is delayed compared to $T3D^{PL}$. The superior core transcription activity of $T3D^{PL}$ (Fig 2.7A, 2.7B, 2.8B) likely contributes to the rapid onset of infection relative to $T3D^{TD}$, although additional advantages could contribute to rapid $T3D^{PL}$ infection.

2.1.8 $T3D^{TD}$ triggers a heightened IFN-dependent signaling cascade

Upon entry into host cells, reovirus RNA is detected by cytoplasmic Retinoic acid-inducible gene I (RIG-I) and melanoma differentiation-associated protein 5 (MDA5) resulting in downstream activation of interferon regulatory factor (IRF) 3/7 and subsequent production of interferons (IFNs) and antiviral interferon stimulated genes (ISGs) [239-242]. Reovirus dsRNA

motifs being detected could potentially originate from i) unstable virus cores formed during the uncoating process release dsRNA into the cytoplasm [243] and/or ii) viral mRNA secondary structure [239]. IRF-3-dependant IFN signaling is vital for inhibiting reovirus spread to neighbouring uninfected cells [239]. However, the role of the IFN signaling triggered during the initial infection is less clearly understood.

We investigated the possibility that a heightened IFN signaling cascade delays $T3D^{TD}$ infection. Focus was placed on early infection timepoints (8-12hpi) to ensure the phenotypes observed are from the initial infection and not virus spread. Standardizing for equivalent percent of infected cells (using flow cytometry, as in Fig 2.10B), $T3D^{PL}$ – versus $T3D^{TD}$ – infected L929 cell lysates were collected and assessed for reovirus protein expression and activating IRF-3 phosphorylation by western blot analysis, and reovirus RNA, IFN mRNAs, and ISG mRNAs by qRT-PCR. Surprisingly, despite having lower levels of reovirus RNAs (Fig 2.12A; *Reovirus S4*, *M2* RNA), $T3D^{TD}$– infected cell showed more activation of IFN and ISG mRNAs relative to $T3D^{PL}$-infected cells (Fig 2.12A; expression of *Ifnα4, Ifnβ1*, *Mx1, Rsad2*). Similarly, levels of reovirus proteins were lower in $T3D^{TD}$– versus $T3D^{PL}$ – infected cells (Fig 2.12B; Reovirus μ1 and σ3 proteins), yet $T3D^{TD}$ produced higher IRF-3 phosphorylation (Fig 2.12B; P-IRF3). In other words, despite $T3D^{TD}$ having lower levels of viral pathogen associated molecular patterns (PAMPS), elevated levels of antiviral signaling were observed compared to $T3D^{PL}$. For both viruses, however, IFN signalling increased in a dose-dependent manner.

Two possibilities were proposed to explain the inverse relationship between laboratory strains with respect to replication versus innate signalling: i) $T3D^{TD}$ is a more potent inducer of IFN signalling, or ii) $T3D^{PL}$ is a more potent inhibitor of IFN activation. To distinguish between these alternatives, cells were co-infected with $T3D^{PL}$ and $T3D^{TD}$ at a high MOI to ensure that

most (>80%) cells were infected with both viruses, and cell lysates were collected for Western blot analysis of IRF-3 phosphorylation. P-IRF-3 was similar between $T3D^{TD}$ and $T3D^{PL}/T3D^{TD}$ co-infection (Fig 2.12B), suggesting that $T3D^{TD}$-dependant activation of IRF-3 could not be overcome by the presence of $T3D^{PL}$. Therefore, $T3D^{TD}$ is most likely a more potent inducer of IFN activation than $T3D^{PL}$. Furthermore, reovirus proteins were either unchanged (σ3) or only marginally reduced (μ1/μ1C) in $T3D^{PL}/T3D^{TD}$ co-infection compared to $T3D^{PL}$ despite high P-IRF-3 levels, implying that IRF-3 activation may not play a major role in differential $T3D^{PL}$ and $T3D^{TD}$ infection establishment (Fig 2.12B).

Since $T3D^{TD}$ displays delayed infection kinetics relative to $T3D^{PL}$, we determined if IFN signaling kinetics follow a similar trend. L929 cells were infected at various MOI, skewing for high infection, to assess the impact of reovirus infected cells rather than neighbouring uninfected cells. At 12hpi and 24hpi, reovirus infected cells were identified using immunocytochemistry, while RT-PCR was used to quantify reovirus (*S4*) and IFN (*Ifnβ1*) gene expression at 6hr intervals until 24hpi. At MOI 27, most cells were infected with $T3D^{PL}$ or $T3D^{TD}$ at both 12hpi and 24hpi. At MOI 3, reovirus infection increased from 12hpi to 24hpi in both $T3D^{PL}$ and $T3D^{TD}$ (Fig 2.13A). At all the MOIs, compared to $T3D^{TD}$, $T3D^{PL}$ had accelerated reovirus gene expression, similar to previous findings. On the other hand, *Ifnβ1* gene expression demonstrated an interesting trend. $T3D^{TD}$ induction of *Ifnβ1* peaked at 6hpi-12hpi and reduced from 12hpi-24hpi. $T3D^{PL}$ induced *Ifnβ1* expression to a lesser extent that $T3D^{TD}$ from 6hpi to 12hpi. However, from 12hpi to 24hpi, *Ifnβ1* expression in $T3D^{PL}$ had an increasing trend, with 24hpi expression in $T3D^{PL}$ being greater than $T3D^{TD}$ (Fig 2.13B). Differential kinetics of IFN signaling between $T3D^{PL}$ and $T3D^{TD}$ inversely correlate with reovirus replication from 0hpi-12hpi, and positively correlate from 12hpi-24hpi.

2.1.9 The heightened IFN response triggered by T3D^{TD} does not impede initial infection

Although the co-infection study suggested that IRF-3 activity does not account for differences in replication by T3D^{PL} versus T3D^{TD}, we investigated directly if delayed T3D^{TD} infection was IFN-independent. Previous knockout and knockdown studies on mouse fibroblast cell lines showed that even though RIG-I and MDA-5 are both implicated during the reovirus infection cycle, RIG-I is the more dominant trigger [239-242]. Non-transformed NIH/3T3 mouse fibroblast cells, which have an intact innate immune signaling cascade, were stably transduced with lentivirus expressing scrambled shRNA (shSCR) or RIG-I targeting shRNA (shRIG-I). Stable shRNA expressing cells were selected with 2ug/ml puromycin for at least 48hrs, a timepoint at which untransduced cells were eliminated by puromycin treatment. Relative to shSCR, RIG-I was successfully knocked down (>80%) at both the gene and protein level in shRIG-I (Fig 2.14A, 2.14B). T3D^{PL} and T3D^{TD} infection kinetics were measured using immunofluorescence at 12 and 24hpi in shSCR and shRIG-I (Fig 2.14C). T3D^{PL} infection at 12hpi matched closely to T3D^{TD} infection at 24hpi, demonstrating a similar delay previously observed in L929 cells. Infection kinetics were similar in shSCR and shRIG-I in both T3D^{PL} and T3D^{TD}, suggesting RIG-I signaling is unlikely to play a role during initial reovirus infection (Fig 2.14C).

To further validate that slow T3D^{TD} replication was independent of RIG-I, we assessed reovirus, IFN, and ISG RNA and protein levels following T3D^{PL} and T3D^{TD} infection. Similar to the trend in L929 cells, T3D^{TD} had lower reovirus gene (*S4, M2*) expression and higher IFN and ISG activation (*Ifnα4, Ifnβ1, Rsad2*, *Cxcl10*) relative to T3D^{PL} in both shSCR and shRIG-I cells (Fig 2.15). The shRIG-I cells had highly diminished IFN expression in both T3D^{PL} and T3D^{TD} compared to shSCR cells, suggesting that RIG-I is the dominant dsRNA sensor during reovirus

infection. Despite having reduced IFN gene activation, $T3D^{PL}$ and $T3D^{TD}$ RNA and protein levels in shRIG-I cells were similar to shSCR cells (Fig 2.15, 2.14A). These results strongly suggest that early RIG-I signaling does not affect initial virus replication for either reovirus laboratory strain. In summary, our data proposes a post-uncoating, IFN independent mechanism of enhanced $T3D^{PL}$ infection.

An argument could be made that 80-90% knockdown of RIG-I and subsequent 80-90% reduction of *Ifnb1* expression upon reovirus infection is not sufficient to overcome the effects of IFN antiviral effects on reovirus replication. As an alternative approach, we therefore utilized primary WT and RIG-I/MDA5 double-knockout (DKO) mouse embryonic fibroblast (MEF) cell lines to compare virus infectivity, spread and IFN signaling. First, we confirmed the absence of IFN signalling in RIG-I/MDA5 DKO cells exposed to either strain of reovirus. Quantitative RT-PCR was used to assess IFN induction and activation in WT versus RIG-I/MDA5 DKO MEFs following 12 hours of infection by $T3D^{PL}$ and $T3D^{TD}$ (at doses the produce equivalent number of productively infected cells) (Fig 2.16). As seen above in other cell lines, IFN signaling (*Ifnα4* and *Rsad2*) was higher during $T3D^{TD}$ infection relative to $T3D^{PL}$. *Ifnβ1* expression was similar between $T3D^{PL}$ and $T3D^{TD}$ likely due to gene expression saturation, as suggested by an increase in ISG (*Rsad2*) expression between $T3D^{PL}$ and $T3D^{TD}$ (Fig 2.16). Importantly RIG-I/MDA5 DKO MEFs showed no IFN signaling (*Ifnα4* and *Rsad2*) in either $T3D^{PL}$ and $T3D^{TD}$ infection, confirming that RIG-I (and MDA5) are necessary and sufficient for IFN triggering during reovirus infection. Viral RNA was also similar for $T3D^{PL}$ and $T3D^{TD}$ between WT and RIG-I/MDA5 DKO MEFs, supporting that IFN signaling does not impact initial reovirus infection. (Fig 2.16)

Having confirmed the absence of IFN signalling in RIG-I/MDA5 DKO MEFs, we used plaque assays to assess $T3D^{PL}$ and $T3D^{TD}$ overall replication and spread on WT versus RIG-I/MDA5 DKO MEFs. At equivalent virus dose, the number of reovirus-infected cell foci was similar between WT and RIG-I/MDA5 DKO MEFs for either virus, suggesting that the initial round of infection was independent of IFN signaling (Fig 2.17). $T3D^{PL}$ formed larger plaques than $T3D^{TD}$ on both WT and RIG-I/MDA5 DKO MEFs, and therefore $T3D^{PL}$ has enhanced overall replication and spread relative to $T3D^{TD}$ regardless of RIG-I/MDA5 status. The plaque size on RIG-I/MDA5 DKO MEFs was larger than WT MEFs in both $T3D^{PL}$ and $T3D^{TD}$, indicating an important role for RIG-I and MDA5 in reovirus spread (Fig 2.17).

Flow cytometry was used to determine $T3D^{PL}$ and $T3D^{TD}$ infectivity kinetics at 12 and 24hpi. At 12hpi, the percent of infected cells was similar in wild-type (WT) and RIG-I/MDA5 DKO MEFs for both $T3D^{PL}$ and $T3D^{TD}$ (Fig 2.18). In $T3D^{PL}$ WT MEF infection, percent infected cells reduced or remained the same at 24hpi compared to 12hpi, suggesting that either i) virus infected cells are cleared of infection and/or ii) infected cells are eliminated due to cell death and the second round of infections are inhibited by antiviral signaling. Contrary to WT MEFs, $T3D^{PL}$ infection of RIG-I/MDA5 DKO MEFs at 24hpi increased relative to 12hpi. $T3D^{TD}$ infection was similar at 12 and 24hpi in both WT and RIG-I/MDA5 DKO MEFs. Therefore, using the RIG-I/MDA5 DKO MEF cell line model, we strengthened our notion that $T3D^{PL}$ establishes an initial infection by 12hpi and spreads to neighbouring cells by 24hpi, while $T3D^{TD}$ initial infection continues until 24hpi. Importantly, for both $T3D^{PL}$ and $T3D^{TD}$, RIG-I/MDA5 dependent signaling does not impact initial infection but rather affects virus spread.

2.1.10 Characterization of IFN-dependent and IFN-independent reovirus signaling

Reovirus infection is known to induce cytokine expression which in-turn plays a role in pathogenesis and tumor clearance, by means of immune system regulation. Accordingly, we attempted to characterize cytokine gene expression with respect to $T3D^{PL}$ and $T3D^{TD}$ infection. Using a previously compiled microarray dataset for NIH/3T3 cells infected with $T3D^{PL}$, we identified a number of reovirus induced cytokine genes such as *Cxcl10* (Interferon gamma-induced protein 10 (IP-10)) and *Csf2* (Granulocyte-macrophage colony-stimulating factor (GM-CSF)). *Cxcl10* had already been previously assessed as being differentially regulated between $T3D^{PL}$ and $T3D^{TD}$ in a RIG-I dependent manner (Fig 2.19). Following assessment of *Csf2* expression following $T3D^{PL}$ and $T3D^{TD}$ infection in shSCR and shRIG-I NIH/3T3 cells, we observed that $T3D^{PL}$ upregulated *Csf2* expression in both shSCR and shRIG-I, indicating that *Csf2* expression was RIG-I independent. Interestingly, $T3D^{TD}$ did not induce *Csf2* expression, raising the possibility of a T3D strain specific, RIG-I dependent gene signature (Fig 2.19). Also available, were microarray datasets from $T3D^{PL}$ infected NIH/3T3 cells that were knocked down in RIG-I and Interferon-alpha/beta receptor alpha chain (IFNAR1), enabling us to identify RIG-I dependent and IFN-dependent genes, respectively. We selected and validated cytokine genes that were upregulated during $T3D^{PL}$ infection and fit into one of two categories: 1) RIG-I and IFN dependent (*Cxcl10, Ccl4, Ccl5*) and 2) RIG-I and IFN independent (*Csf2, Cxcl1, Cxcl2, Fas*). We successfully validated these microarray gene classifications using our independently generated NIH/3T3 shSCR and shRIG-I cell lines. Our data demonstrated that $T3D^{TD}$ infection upregulated RIG-I and IFN dependent genes (*Cxcl10, Ccl4, Ccl5*) to a greater extent, relative to $T3D^{PL}$ infection. However, the RIG-I and IFN independent genes (*Csf2, Cxcl1, Cxcl2, Fas*) were only upregulated during $T3D^{PL}$ infection (Fig 2.15, 2.19). Therefore, we identified a category of

genes exclusively regulated in a T3D strain specific manner, and independent of RIG-I and IFN signaling.

To confirm our gene categorization of IFN-dependent or independent, we treated L929 cells with purified IFNα or IFNβ at various concentrations (1000, 100 and 10 units/ml) and assessed gene expression using RT-PCR. Upon IFNα or IFNβ treatment, no induction of either *Ifnα4* (IFNα4), *Ifnb1* (IFNβ) was observed, endorsing their categorization as RIG-I-dependent and IFN-independent genes (Fig 2.20A). Overall, IFNβ was a potent ISG inducer compared to IFNα at equivalent concentration. *Rsad2*, *Mx1*, *Ifi44, Cxcl10*, *Ccl4* and *Il6* were upregulated by both IFNα and IFNβ in a dose dependent manner, confirming their classification as IFN-dependent genes (Fig 2.20A). In contrast, *Csf2, Cxcl1*, *Cxcl2* and *Fas* gene expression levels were unchanged following IFNα and IFNβ treatment, substantiating their classification as IFN-independent genes (Fig 2.20B).

When we extended our IFN-dependent and IFN-independent classification to cell line panel, in all four cell lines tested (NIH/3T3, L929, B16-F10, ID8), IFN-dependent genes were upregulated more by $T3D^{TD}$ than $T3D^{PL}$. But interestingly, the converse was true for IFN-independent genes, which were upregulated by $T3D^{PL}$ in a virus-dose-dependent manner but were not upregulated during $T3D^{TD}$ infection (Fig 2.12A, 2.15, 2.16, 2.19, 2.21A-C). These are the first reports of differential induction of IFN-independent genes between reovirus strains.

2.2 RESULTS: GENETIC CHARACTERIZATION

2.2.1 Genetic diversity among T3D laboratory strains

Extensive genetic and phenotypic characterizations have been performed by comparing prototypic clinical isolates of reovirus serotypes, commonly T1L and T3D. In addition to inter-serotype diversity, laboratory strains of T3D have further diverged due to laboratory-specific reovirus propagation protocols. An extensive study of the reovirus M1 gene encoding the μ2 protein from laboratory strains and environmental and clinical isolates, suggested that T3D laboratory strains originating from the Bernard N. Fields laboratory have diverged away from the original T3D isolate [203]. Nevertheless, an in-depth analysis of whole genome sequences of T3D laboratory strains has yet to be performed. We collected and assembled complete reovirus gene and amino acid sequences available on the NCBI database ($T3D^{PARENT}$, REOLYSIN®, $T3D^{JB}$, $T3D^{SB}$, $T3D^{RH}$, T3A, T1L, T2J), Addgene ($T1L^{RG}$, $T3D^{RG}$) and in-house ($T3D^{MS}$, $T3D^{PL}$, $T3D^{TD}$, $T3D^{KC}$, $T3D^{ATCC}$). T3D-PARENT includes the earliest published complete T3D sequence, which was a collaborative initiative as per NCBI BioProject PRJNA14861; S1, S2, S3, M1, M2, M3 and L1 genes were sequences from Wolfgang K. Joklik affiliated laboratories, S4 and L2 genes were sequences from the Aaron J. Shatkin laboratory while the L3 gene was a sequence from the Max L. Nibert Laboratory (Bernard N. Fields T3D strain) (Table 2.1**,** [244, 245]).

For genetic reovirus lineage assessment, we used concatenated sequences of either 10 reovirus genes [in order S1, S2, S3, S4, M1, M2, M3, L1, L2 L3] (Fig 2.22A, 2.22B) or 11 reovirus proteins [in order σ1, σ1s, σ2, σNS, σ3, μ2, μ1, μNS, λ3, λ2, λ1] (Fig 2.22C, 2.22D) from each reovirus strain to generate a phylogenetic tree using the Jukes-Cantor model and

Neighbor-Joining method (Geneious®). T2J was used as an outgroup to classify inter-serotype diversity, while T3A was used as outgroup to classify intra-serotype diversity. In both protein and nucleotide alignments, T1L was more closely related to T3D/T3A compared to T2J, validating the current doctrine in the reovirus field (Fig 2.22A, 2.22C). All T3D strains branched together, suggesting their source was from a common T3D ancestor (Fig 2.22B, 2.22D).

$T3D^{PL}$ and $T3D^{MS}$ were sequenced five years apart using independent plaque picks from a common infected cell lysate obtained from the Patrick Lee laboratory at Dalhousie University. REOLYSIN® was initially isolated from the Patrick Lee laboratory at the University of Calgary. Based on a filed patent, REOLYSIN® was isolated following three repeated passaging in HEK293 cells, with isolation of a large plaque after every passage. $T3D^{PL}$, $T3D^{MS}$ and REOLYSIN® had identical amino acid sequences, confirming their origins to the Patrick Lee laboratory. $T3D^{RG}$ plasmids were cloned by the Terence Dermody laboratory using their T3D strain ($T3D^{TD}$). We re-sequenced a $T3D^{TD}$ plaque picked from an infected cell lysate obtained from the Terence Dermody laboratory. Both $T3D^{TD}$ and $T3D^{RG}$ had identical amino acid sequences, confirming their origins to the Terence Dermody laboratory. The identical amino acid sequences of T3D strains from either the Patrick Lee ($T3D^{PL}$, $T3D^{MS}$ and REOLYSIN®) or Terence Dermody laboratories ($T3D^{TD}$ and $T3D^{RG}$) reinforces the maintenance of T3D strain homogeneity during propagation in each individual laboratory. $T3D^{PL}$, $T3D^{MS}$ and REOLYSIN® branched more closely to $T3D^{PARENT}$, while $T3D^{TD}$, $T3D^{RG}$ and $T3D^{KC}$ were the most distant (Fig 2.22B, 2.22D). Importantly, between $T3D^{PL}$ and $T3D^{TD}$ laboratory strains, there were 43 nucleotide changes accounting for 21 missense differences (Table 2.2), suggesting divergence between the two T3D laboratory strains.

2.2.2 Reassortant analysis between reovirus laboratory strains: $T3D^{PL}$ – derived S4, M1, and L3 gene segments segregate with large-plaque phenotype of $T3D^{PL}$ relative to $T3D^{TD}$

Several research studies have clearly demonstrated that single amino acid changes in the reovirus genome have the potential to radically alter phenotypic characteristics [218-220, 224]. In Chapter 2.1, we discovered that compared to $T3D^{TD}$, $T3D^{PL}$, had enhanced cell binding, accelerated replication kinetics, diminished IFN signaling and increased IFN-independent signaling. We hypothesized that phenotypic differences between $T3D^{PL}$ and $T3D^{TD}$ would correlate with specific genotypic differences between these T3D laboratory strains. Therefore, to decipher the mechanisms of enhanced $T3D^{PL}$ infection, we sought to delineate the genes involved. We performed a classical reassortment analysis to segregate genes that contribute towards $T3D^{PL}$ large plaque phenotype. $T3D^{PL}$ and $T3D^{TD}$ were coinfected at a ratio of 1:10 to favor reassortment of $T3D^{PL}$ genes in a primarily $T3D^{TD}$ background; this strategy was chosen to identify the $T3D^{PL}$ genes that contribute towards the large plaque phenotype. Reassortants were titrated on tumorigenic L929 mouse fibroblasts, and 20 large plaques were twice plaque-purified and sequenced. Since the S3 gene sequence was identical between $T3D^{PL}$ and $T3D^{TD}$, the parental origin of this gene in the reassortants could not be distinguished. Of the 20 large plaques, 8 were composed entirely of $T3D^{PL}$ genes despite a skewing of co-infection towards $T3D^{TD}$ (Fig 2.23A, 2.23B). One reassortant (B1) was in a $T3D^{PL}$ background with two $T3D^{TD}$ genes, while the remaining eleven reassortants (B2-B12) were in a $T3D^{TD}$ background with a range of 2 to 4 $T3D^{PL}$ genes. The PL-M1 gene was present in all (12/12) large reassortants, in combination with either the PL-S4 gene (9/12), PL-L3 gene (6/12), PL-M2 gene (4/12), PL-S1 gene (2/12), PL-S2 gene (2/12), PL-L1 gene (1/12) or PL-L2 gene (1/12) (Fig 2.23A).

Reassortment analysis therefore implicated the PL-M1 gene in combination with PL-S4 and/or PL-L3 genes as being most likely to be important for the $T3D^{PL}$ large plaque phenotype.

2.2.3 Generating a reverse genetics (RG) system for $T3D^{PL}$ and $T3D^{TD}$ for gene analysis

A plasmid-based RG system for reovirus was developed by the Terence Dermody laboratory in 2007 [246-248]. We had considered two alternative strategies for developing an RG system for $T3D^{PL}$ and $T3D^{TD}$: i) use site directed mutagenesis to insert $T3D^{PL}$ and $T3D^{TD}$ variations ii) clone entire $T3D^{PL}$ and $T3D^{TD}$ genes into the current RG system. We selected the latter option for the three following reasons: First, i) the site-directed mutagenesis protocol takes at least 2-3 days per reaction, with a 2-3 days sequencing wait time after every reaction. A 7-day protocol for a single reaction would make this strategy very time-consuming. Second, ii) the Quikchange II site-directed mutagenesis kit from Agilent Technologies costs close to $35/reaction, making it a very expensive strategy. Finally, iii) the site-directed mutagenesis kit would restrict us to using the base vectors of the current RG plasmids, which differ between the various genes. The differential base vectors could add unanticipated confounding variables during plasmid gene expression. Therefore, we decided to clone all of the genes from our lab stocks of $T3D^{PL}$ and $T3D^{TD}$ into the pBacT7-S1T3D base vector.

Our cloning strategy involved removing the S1 gene insert from pBacT7-S1T3D and inserting each of the $T3D^{PL}$ and $T3D^{TD}$ genes (Fig 2.24). We selected NotI and RsrII as the restriction enzyme sites at the 5' and 3' end, respectively. On the vector, NotI would digest upstream of the T7 promoter, while RsrII would digest in-between the HDV ribozyme. For the gene inserts, at the 5' end we added a NotI site and T7 promoter sequence, and at the 3' end, we added an RsrII site and the HDV ribozyme sequence removed from the vector (Fig 2.24).

Total RNA was extracted from infected $T3D^{PL}$ and $T3D^{TD}$ L929 cell lysates, and cDNA was reverse transcribed using reovirus gene specific primers. Individual reovirus genes were PCR amplified and gel-extracted if non-specific dominant bands were observed when run on an agarose gel. PCR products were digested using NotI and RsrII and column purified. The pBacT7-S1T3D vector was digested using NotI and RsrII and the 5716bp linearized fragment was gel extracted and alkaline phosphatase treated to reduce self-ligation. Digested PCR products were ligated to the linearized vector and transformed into Stbl3 *E.coli*. Transformed cells were selected on carbnecillin containing LB agar plates and colony PCR was performed to screen for insert containing colonies. Plasmids containing colonies were cultured and plasmids were column purified and sequenced for validation (Fig 2.24). Parental viruses generated using the RG system, PL-RG and TD-RG, were similar in plaque size to $T3D^{PL}$ and $T3D^{TD}$, respectively, hence validating our RG system (Fig 2.25A, 2.25B, 2.26A, 2.26B).

2.2.4 S4, M1 and L3 genes are major determinants of $T3D^{PL}$ and $T3D^{TD}$ plaque size

Our $T3D^{PL}$/$T3D^{TD}$ coinfection reassortant analysis indicated that combinations of PL-M1, PL-S4 and PL-L3 genes are likely determinants of $T3D^{PL}$ large plaque size. The reassortants we purified did not, however, reflect the potential contribution of each gene alone and/or every combination of these genes. It was also possible that while these 3 genes dominated as plaque-size determinants, other genes could less-strongly contribute to plaque size if introduced (Fig 2.23A, 2.23B). As a more comprehensive assessment of how reovirus genes could contribute to plaque size differences, we generated $T3D^{PL}$ and $T3D^{TD}$ mono-reassortants using the RG system. Mono-reassortants in either the TD-RG and PL-RG backbone (i.e. the remaining 9 genes from the opposite parent) unveiled the M1 gene as a major determinant and S4 and L3 genes as minor determinants of plaque size (Fig 2.25A, 2.25B, 2.26A, 2.26B). The remaining genes did not

show notable increase in plaque size and were therefore not further evaluated. Focusing first on the impact of $T3D^{PL}$ genes introduced into the TD-RG- backbone (Fig 2.25A, 2.25B), PL-M1 + PL-S4, PL-M1 + PL-L3 and PL-M1 + PL-S4 + PL-L3 very closely matched the PL-RG plaque size, suggesting an additive contribution by each gene. The TD-RG backbone with PL-S4 + PL-L3 produced significantly smaller plaque size than PL-RG, confirming that the PL-M1 makes the largest contribution (Fig 2.24A, 2.24B).

When we reciprocally focused on the impact of T3DTD genes introduced into the PL-RG- backbone (Fig 2.25A, 2.25B), combinations of TD-M1 + TD-S4 and TD-M1 + TD-L3 reduced the plaque size but not to the extent of TD-M1 + TD-S4 + TD-L3, again supporting that each of the three genes can make an additive contribution. The combination on TD-S4 + TD-L3 in the PL-RG backbone produced significantly larger plaques than TD-RG (Fig 2.25A, 2.25B). Finally, to determine if PL-M1 could further increase plaque size in combination with genes other than PL-S4 and PL-L3, we combined PL-M1 with the remaining 6 PL genes in the TD-RG backbone (Fig 2.27A, 2.27B). Of all the genes tested in combination with PL-M1, only PL-S4 and PL-L3 had an additive benefit on the plaque size compared to PL-M1 alone.

While the structure of μ2 (M1 gene) has yet to be solved, crystal structures for σ3 (S4 gene) and λ1 (L3 gene) are available [119, 249, 250] and were utilized to map the $T3D^{PL}$ and $T3D^{TD}$ polymorphisms within each protein 3-dimensional structure but also in the context of interacting proteins within the reovirus capsid to visualize potential impact on protein-protein associations. Interestingly, all three variations in σ3 were located in the top virion-surface and solvent exposed lobe (Fig 2.28A). The structural context of σ3 polymorphisms suggested at least three possible effects on σ3 fate and/or function. First, all three polymorphisms are proximal to the protease sensitive domain (indicated in gray) involved in degradation of reovirus σ3 outer

capsid during entry and uncoating [166, 251]; these amino acid changes therefore have the potential to influence σ3 protease sensitivity. Second, when $\sigma3_3\mu1_3$ heterohexameric structures were assembled into a six-fold axis, the localization of all three variations have the capacity to impact σ3 – σ3 capsid assembly interactions. Thirdly, the dsRNA binding activity of σ3 has been hypothesized to be mediated by σ3 dimers, specifically at lysine 236, lysine 239, arginine 291 and arginine 293 resides [250, 252-254]. When the $T3D^{PL}$ and $T3D^{TD}$ variations were mapped onto the σ3 dimer structure, D229E is directly adjacent to the proposed dsRNA-binding arginine residues and could influence dsRNA binding (Fig 2.28B). With respect to λ1, the variations between $T3D^{PL}$ and $T3D^{TD}$ were mapped in relation to λ1 – λ1 and λ1 – σ2 interactions (Fig 2.28C). The I500S variation was located at the interface between λ1 and σ2, while the Q852H variation was located at the interface between λ1 and λ1; both of which could potentially have an impact on viral core assembly and stability. In summary, the predominance of variations on the surface of σ3 and λ1 could simply reflect that internal residues are more difficult to change without destroying important protein structural determinants but could also support the importance of σ3 and λ1 interaction surfaces with other proteins or dsRNAs.

2.2.5 Identifying PL-S4, PL-M1 and PL-L3 missense variations that dictate plaque size

Between $T3D^{PL}$ and $T3D^{TD}$, there were 21 missense variations, of which 9 were distributed among S4- encoded σ3 (3 variations), M1-encoded μ2 (4 variations) and L3-encoded λ1 (2 variations) genes (Table 2.2). Previous studies have implicated the role of only 2 of these 9 variations; the σ3 protein variation at amino acid 198, and the μ2 protein variation at amino acid 208. With regards to residue 198 of σ3, it was previously found that mutation of glycine 198 to glutamic acid, valine, or tryptophan could reverse the protease hypersensitivity of σ3 conferred by another σ3 mutation (Y354H) [176, 255-257]. The σ3 E198K variation was also found

commonly introduced during either repeated passaging of T3D in cell culture or during high passage infections to generate defective interfering virion and proposed to decrease the fidelity of genome assembly and reduce virion infectivity [258]. However, if (and how) the G198K variation contributes to differential infectivity and oncolysis between $T3D^{PL}$ and $T3D^{TD}$ has not been previously characterized. The μ2 S208P variation is affiliated with microtubule association and the subsequent determination of virus factory morphology (208S globular, 208P filamentous) [201, 203, 259, 260]. The S208P variation in μ2 was also previously documented as a different between reovirus serotypes 1 (T1L) versus 3 (T3D) and linked to serotype-specific differences in myocarditis severity among neonatal mice, virus replication, cytotoxity and IFN signaling [261, 262].

To pinpoint which of the 9 amino acid variations in σ3, μ2, and λ1 accounts for the superior replication of $T3D^{PL}$ relative to $T3D^{TD}$, each of the $T3D^{PL}$ variations was introduced into the TD-backbone using site-directed mutagenesis. Reverse genetics was utilized to generate a panel of virus mutants and plaque assay was used to measure overall virus replication proficiency. We expected to see that one-or-more of the individual polymorphisms would increase plaque size of TD-RG but were surprised to learn that some of the polymorphisms also decrease replication of TD-RG (Fig 2.29A-F). Specifically, σ3 W133R variation caused a dramatic increase in plaque size and is therefore a clear determinant of $T3D^{PL}$ large-plaque phenotype. Conversely, G198K and E299D caused minimal (less than 2-fold) decrease or increase (respectively) in plaque size when introduced alone. Importantly however, when introduced along with the beneficial W133R mutations, both G198K and E299D alone or together diminished the plaque-increasing attributes of W133R (Fig 2.29A, 2.29B). Together these studies suggest that among the three variations in σ3, the W133R is the primary beneficial

variation, while G198K and E229D are inhibitory towards W133R. Of the four variations in μ2 (Q150R, S208P, R342Q, A528S), the S208P variation individually had the greatest increase in plaque size and produced plaques similar to PL-M1 (Q150R+S208P+R342Q+A528S). Q150R, R342Q, A528S variations individually had minimal impact on plaque size. In combination with S208P, the variations in R342Q or A528S, did not alter the plaque size. However, S208P in combination with Q150R had a decrease in plaque size relative to S208P individually (Fig 2.29 C, 2.29D). Therefore, the S208P variation in μ2 is the primary determinant of the large plaque phenotype. Finally, the I500S variation in λ1 individually increased the plaque size similar to PL-L3 (I500S+Q852H), while the Q852 variation did not have any impact on plaque size (Fig 2.29E, 2.29F).

2.2.6 Connecting genotypic and phenotypic differences between $T3D^{PL}$ and $T3D^{TD}$: S4 (σ3) modulates IFN-independent signaling, M1 (μ2) facilitates viral core transcriptase activity and L3 (λ1) governs virus factory size

The σ3 protein encoded by the S4 gene composes the outer-most virus capsid and plays a major role in maintaining virus stability in the environment [166, 249, 251]. Aside from its structural role, σ3 binds dsRNA binding during virus infection functions to overcome PKR signaling and to maintain viral protein translation [263, 264]. The μ2 encoded by the M1 gene also provides at least two functions during reovirus replication. Within reovirus core particles, μ2 is a λ3 polymerase cofactor, supplying NTPase activity and supporting temperature-dependent core transcriptase activity. During reovirus replication, μ2 is also a determinant of virus factory morphology, bridging tubulin to μNS which subsequently recruits other viral proteins and RNAs [119, 192, 201, 203, 265, 266]. The λ1 protein encoded by the L3 gene is a major component of the viral core inner capsid and has dsRNA binding, NTPase and RNA helicase activity [119, 193,

267, 268]. We generated mono-reassortants of S4, M1 and L3 in $T3D^{PL}$ and $T3D^{TD}$ backbones, and assessed the aspects of replication that differ between $T3D^{PL}$ and $T3D^{TD}$; viral core transcription, IFN-dependent and IFN-independent signaling and virus factory morphology.

2.2.6.1 Viral core transcriptase activity

Based on their inclusion in the viral core and RNA transcription related activities, we hypothesized that μ2 and/or λ1 are contributors to the differential $T3D^{PL}$ and $T3D^{TD}$ viral core transcriptase activity. Since six virus preparations were being used, we developed a high throughput assay for monitoring viral core transcriptase activity as an alternative approach to RT-PCR. SYBR Green II is an RNA binding dye that is commonly used in thermal shift assays to measure virus stability in real-time by binding genomic RNA released during temperature induced viral disassembly. We hypothesized that addition of SYBR Green II to the core transcription buffer could be used to measure newly synthesized viral RNA, alleviating the tedious nature of our current RT-PCR protocol. Viral cores were generated by chymotrypsin digestion and purified by high speed centrifugation as previously described (Fig 2.30A, 2.30B). SYBR Green II was added to the transcription reaction mix and fluorescence intensity was measured every 5min using the BioRad CFX96 RT-PCR machine. Similar to the RT-PCR method, the SYBR Green II method also demonstrated that $T3D^{PL}$ had a faster rate of viral RNA transcription relative to $T3D^{TD}$, as indicated by the curve slopes (Fig 2.30C). Even though the difference in transcription rates between $T3D^{PL}$ and $T3D^{TD}$ were less in the SYBR Green method compared to the RT-PCR method, $T3D^{PL}$ was consistently a faster rate relative to $T3D^{TD}$. The $T3D^{TD}$+PL-M1 and $T3D^{PL}$+TD-M1 reassortants had a similar transcription rates to $T3D^{PL}$ and $T3D^{TD}$, respectively, strongly suggesting that the M1 gene is the sole determinant of viral core transcriptase activity differing between $T3D^{PL}$ and $T3D^{TD}$ (Fig 2.30D).

2.2.6.2 IFN signaling

An unexpected difference between T3D laboratory strains was that while IFN-dependent genes were upregulated predominantly by $T3D^{TD}$, $T3D^{PL}$ tended to upregulate cytokines independent of IFN signaling (Chapter 2.1.10, Fig 2.12A, 2.15, 2.16, 2.19, 2.21A-C). Given that reovirus is undergoing clinical trials as an oncolytic therapy, and that immune system activation is known to play an important component in virus oncolysis, an understanding of the genetic determinants of distinct cytokine induction could reveal novel ways to manipulate and ideally stimulate anti-tumor immunity. Reovirus induced interferon signaling is modulated by viral RNA binding to RIG-I and MDA5 and activating IRF3 mediated signaling cascade [239, 240]. Additionally, although the dsRNA binding ability of σ3 has primarily been studied in relation to its role in blocking dsRNA recognition by PKR and retaining protein translation, dsRNA activity could certainly also impinge on RIG-I or MDA5 activation [263, 264]. Accordingly, a thorough analysis was conducted to determine which polymorphisms between $T3D^{PL}$ and $T3D^{TD}$ accounted for induction of IFN-dependent versus IFN-independent genes.

The $T3D^{PL}$ and $T3D^{TD}$ S4, M1 and L3 mono-reassortants we generated were used to assess if differential IFN activation is linked to lab strain-associated polymorphisms in σ3, μ2 and/or λ1. L929 cells were infected with each parental virus or mono-reassortant at a dose that gave the same percent of reovirus infected (i.e. reovirus antigen-positive cells by flow cytometry), with the objective to overcome confounding effects of having different cell-binding and onset of transcription. Viral and host gene expression was then quantified using qRT-PCR (Fig 2.31). $T3D^{PL}$ mono-reassortants with TD-S4, TD-M1 or TD-L3 had approximately 2-fold lower levels of viral RNA (*S4*, *M2*) relative to $T3D^{PL}$, while $T3D^{TD}$ reassortants containing PL-S4, PL-M1 or PL-L3 reassortants had approximately 2-fold higher levels of viral RNA (*S4*, *M2*) relative to

T3D^{TD}; therefore, each of S4, M1 and L3 had independent consequences on viral gene expression. Mono-reassortment of TD-S4, TD-M1 or TD-L3 into T3D^{PL} had no impact on IFN signaling (*Ifnb1*, *Ifna4*, *Mx1*, *Ccl4*) relative to T3D^{PL}. On the other hand, mono-reassortment of PL-S4, PL-M1 or PL-L3 into T3D^{TD} did significantly reduce IFN signaling (*Ifnb1*, *Ifna4*, *Mx1*, *Ccl4*) relative to T3D^{TD} (Fig 2.31). Though seemingly conflicting, the overall trend for IFN signalling did seem to correspond to the overall proficiency of virus replication. Therefore, to determine if there was a true correlation between IFN induction and virus replication, correlation plots were generated between *Ifnb1* expression and titers (12hpi) of each mono-reassortant. A strong (>0.8) correlation was observed, suggesting that efficiency of reovirus replication inversely correlates with levels of IFN induction (Fig 2.32).

2.2.6.3 IFN-independent signaling

Based on our previous observation that T3D^{PL} and T3D^{TD} differ in IFN-independent gene expression, we sought to identify if S4, M1 and/or L3 contribute towards this phenotype. A panel of IFN-independent genes (*Csf2*, *Cxcl1*, *Cxcl2*, *Fas*) was quantified by qRT-PCR among the samples of T3D^{PL}, T3D^{TD} and S4-, M1- or L3- monoreassortant- infected L929 cells (Fig 2.31). For all tested IFN-independent transcripts, high expression correlated with presence of T3D^{PL}-derived S4. In other words, viruses containing the T3D^{PL}-derived S4 consistently showed higher expression of *Csf2*, *Cxcl1*, *Cxcl2*, *Fas*, while viruses containing the T3D^{TD}-derived S4 induced lower expression of these genes (Fig 2.31). Not only is this the first time that reovirus variations in IFN-independent gene expression has been demonstrated, but we can now attribute this important phenotype to the S4-encoded σ3.

2.2.6.4 Virus factory size

The final phenotypic difference between reovirus laboratory strains that was assessed was morphology of virus factories, especially since the key variation we identified in μ2 (P208S) was previously associated with virus factory appearance [201, 203]. Specifically, a proline at position 208 of μ2 diminished microtubule association and produced globular factory morphology, while a serine produced microtubule-associated filamentous morphology. The factory morphology was therefore assessed for $T3D^{PL}$, $T3D^{TD}$ and mono-reassorants of PL-S4, PL-M1 or PL-L3 in an otherwise $T3D^{TD}$ background. Factory morphology was visualized in the ID8 mouse ovarian cancer cell line because these cells are larger in size than L929 cells, hence offering sufficient cytoplasmic area to clearly distinguish virus factories. Importantly, $T3D^{PL}$ and $T3D^{TD}$ replication differences observed in L929 cells were reproducibly observed in ID8 cells. Immunoflourescence staining and confocal microscopy provided high resolution imaging of reovirus factories. Reovirus factories were detected with specific antibodies against σNS, μ2 and σ3, and nuclei were stained using Hoechst 33342 dye. $T3D^{PL}$ and $T3D^{TD}$ exhibited prototypic filamentous and globular factory morphologies, respectively (Fig 2.34). As anticipated, globular factory morphology was determined by the M1-encoded μ2; specifically, $T3D^{TD}$ + PL-M1 had filamentous factories, while $T3D^{TD}$ + PL-S4 and $T3D^{TD}$ + PL-L3 had globular virus factories. Both μ2 and σ3 co-localized to viral factories (σNS) in all the viruses tested. In some infected cells, σ3 was localized to the nucleus in $T3D^{TD}$, $T3D^{TD}$ + PL-S4 and $T3D^{TD}$ + PL-L3 samples, suggested a potential role of M1 and virus factory morphology on σ3 nuclear translocation. Unpredictably however, globular viral factories observed in $T3D^{TD}$ + PL-L3 were larger in area than $T3D^{TD}$ or $T3D^{TD}$ + PL-S4, suggesting a novel influence of λ1 on virus factory size (Fig 2.34). Additionally, even though $T3D^{PL}$ and $T3D^{TD}$ + PL-M1 both had filamentous viral factory

morphology, the factory area in $T3D^{PL}$ was larger than $T3D^{TD}$ + PL-M1, further hinting at a potential role for a gene other than M1 (likely L3) is important in mediating factory size (Fig 2.34). As the variation in λ1 (I500S) resides at the interface between σ2 and λ1, enhanced viral capsid stability and/or assembly could contribute to increased viral factory size and should be explored further.

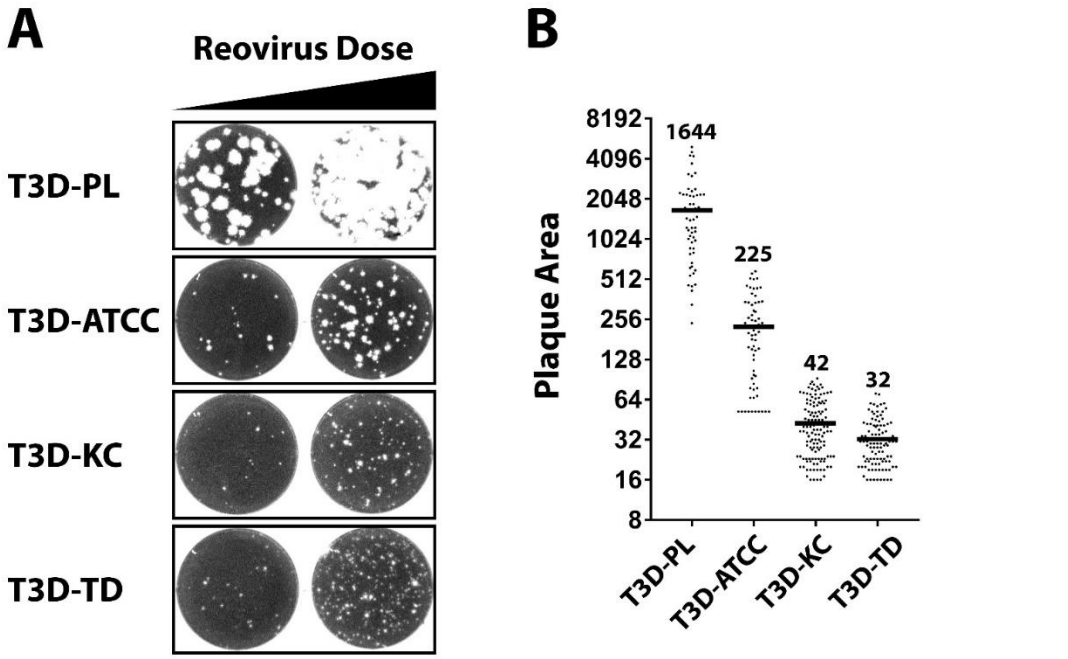
A
Reovirus Dose
T3D-PL
T3D-ATCC
T3D-KC
T3D-TD
B
Plaque Area
8192
4096
2048
1024
512
256
128
64
32
16
8
1644
225
42
32
T3D-PL
T3D-ATCC
T3D-KC
T3D-TD

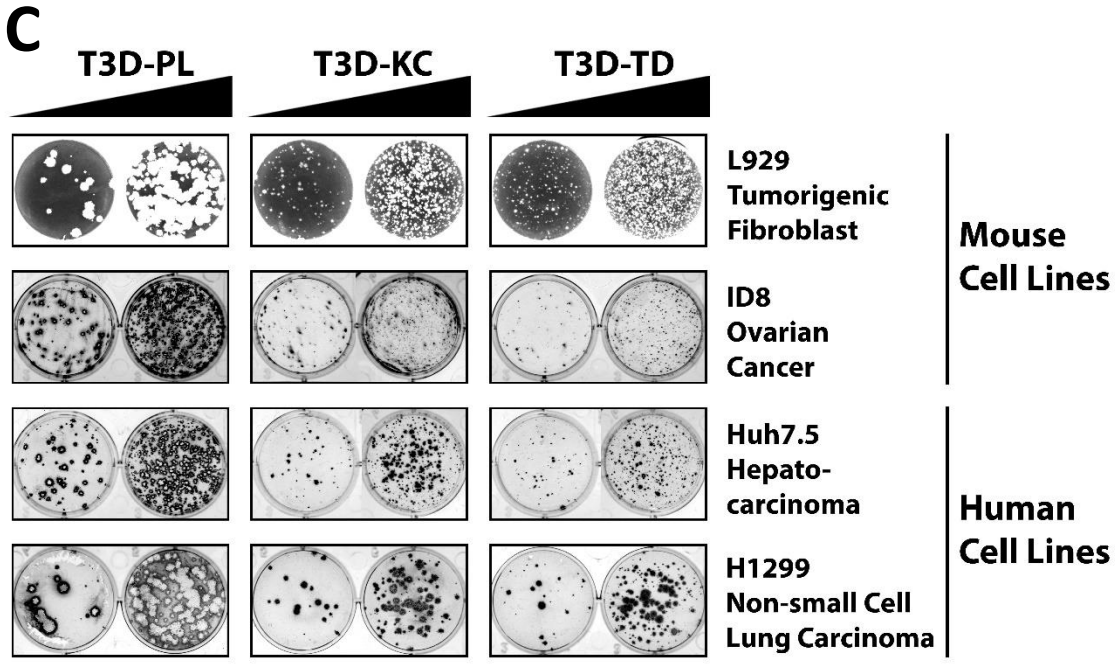
C
T3D-PL
T3D-KC
T3D-TD
L929
Tumorigenic
Fibroblast
ID8
Ovarian
Cancer
Huh7.5
Hepato-
carcinoma
H1299
Non-small Cell
Lung Carcinoma
Mouse
Cell Lines
Human
Cell Lines

Figure 2.1: T3D-PL demonstrates enhanced replication in cell lines *in-vitro*. Cell lines were infected with T3D laboratory strains ($T3D^{PL}$, $T3D^{ATCC}$, $T3D^{KC}$, $T3D^{TD}$) and overlaid with agar. Reovirus plaques or infected cell foci were visualized following staining with crystal violet (L929) or immunocytochemistry (ID8, Huh7.5, H1299). A) L929 cell line B) Quantification of plaque area in A) using ImageQuantTL colony counting add-on. Mean plaque size indicated. C) L929, ID8, Huh7.5 and H1299 cell lines.

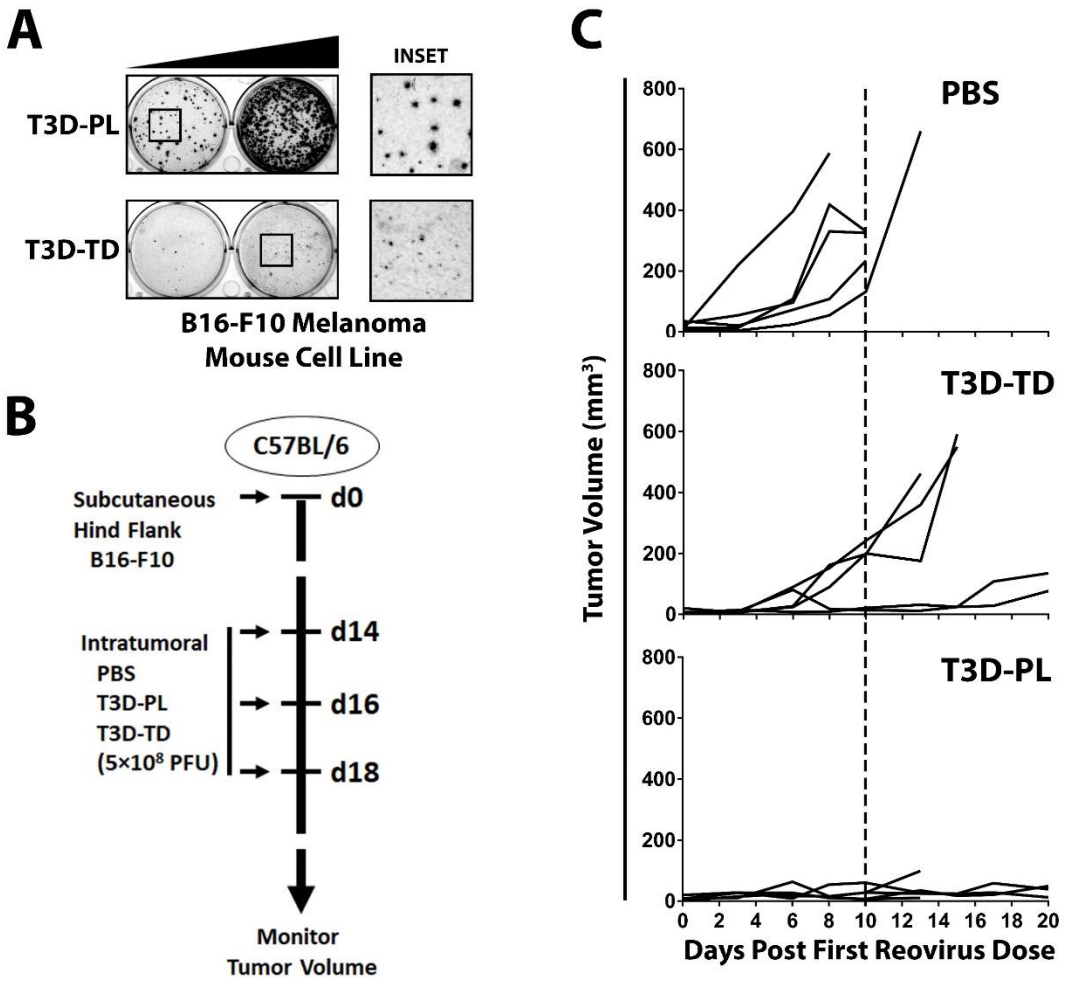

Figure 2.2: Treatment with T3D-PL resulted in improved B16-F10 in-vivo tumor regression over T3D-TD. A) B16-F10 cells were infected with $T3D^{PL}$ and $T3D^{TD}$, overlaid with agar and infected cell foci were visualized using immunocytochemistry. Inset displays a higher magnification of the indicated well region. B) Schematic experimental timeline of *in-vivo* B16-F10 tumor regression, following $T3D^{PL}$ and $T3D^{TD}$ treatment. C) Tumor volume (mm^3) measurements assessed using calipers, following first treatment dose.

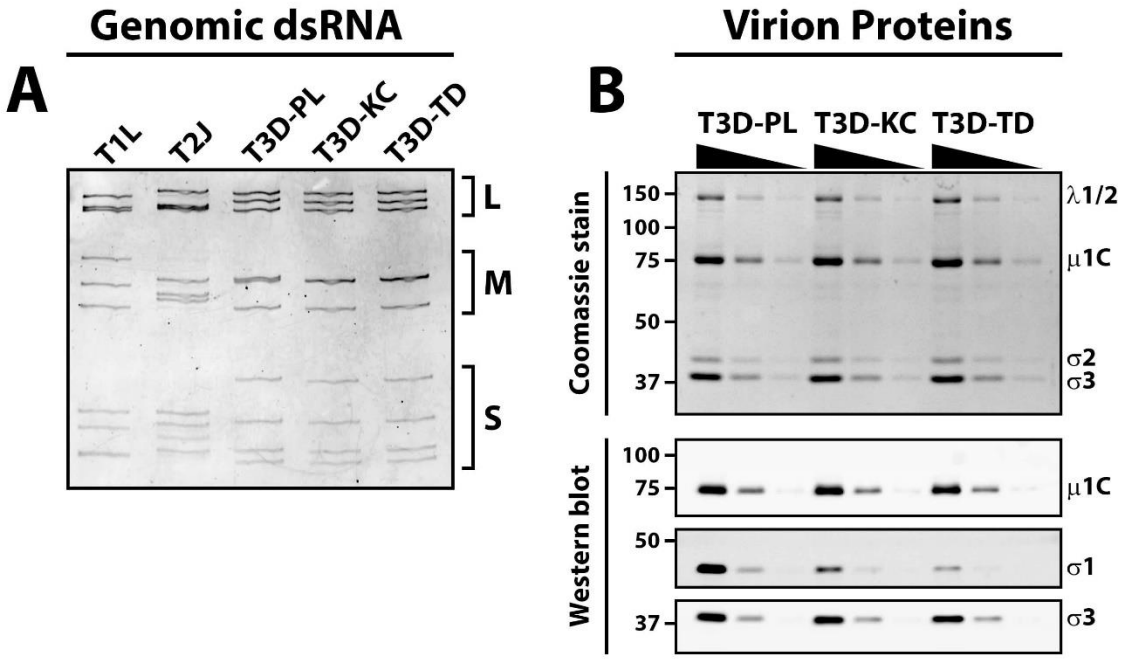

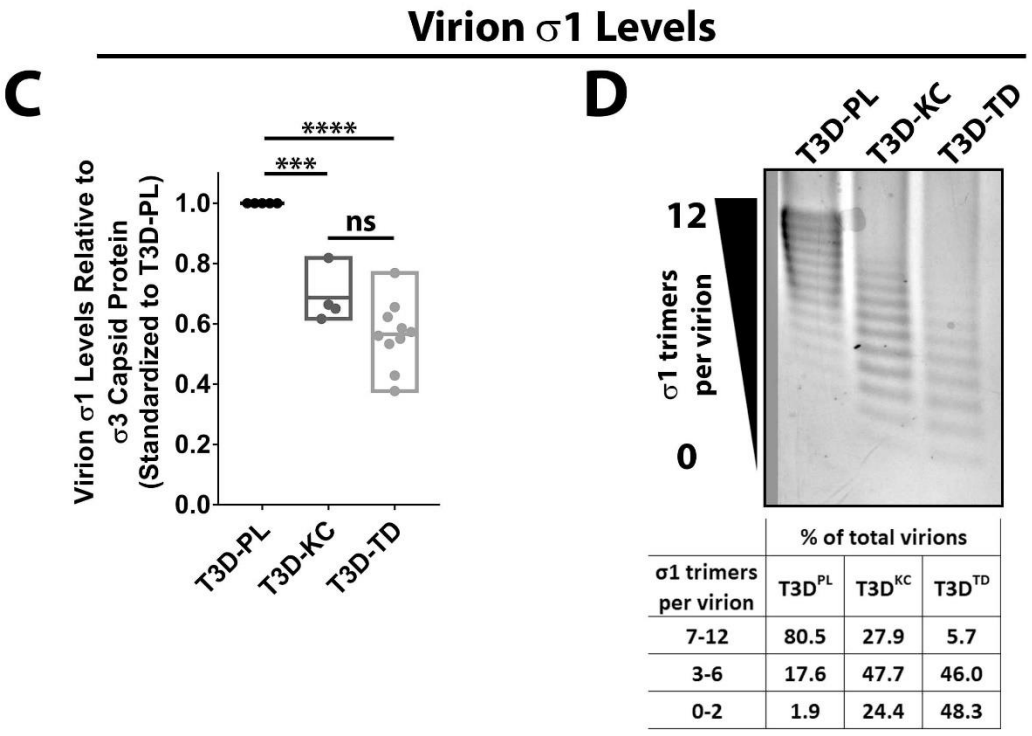

	% of total virions		
σ1 trimers per virion	$T3D^{PL}$	$T3D^{KC}$	$T3D^{TD}$
7-12	80.5	27.9	5.7
3-6	17.6	47.7	46.0
0-2	1.9	24.4	48.3

Figure 2.3: T3D-PL and T3D-TD virion genome and protein composition. A) RNA was Trizol LS extracted from CsCl purified reovirus preparations and dsRNA genome fragments were separated using SDS-PAGE followed by RNA staining using ethidium bromide. B) CsCl purified reovirus preparations were denatured in protein sample buffer with boiling and proteins were separated using SDS PAGE. Total protein was stained using Imperial^{TM} Coomassie dye, while specific reovirus proteins were identified using Western blot analysis with protein-specific antibodies. C) Densitometric band quantification of σ1 from B) using ImageQuantTL 1D gel analysis add-on. D) Agarose gel separation and Imperial^{TM} Coomassie dye staining of virions based on σ1 trimers per virion. Table indicates percentage of virions with specific σ1 timers/virion calculated using densitometric band quantification obtained with ImageQuantTL 1D gel analysis add-on. In C), $n \geq 4$, One-way ANOVA with Tukey's multiple comparisons test, *** $p < 0.0002$, **** $p < 0.0001$, ns > 0.05

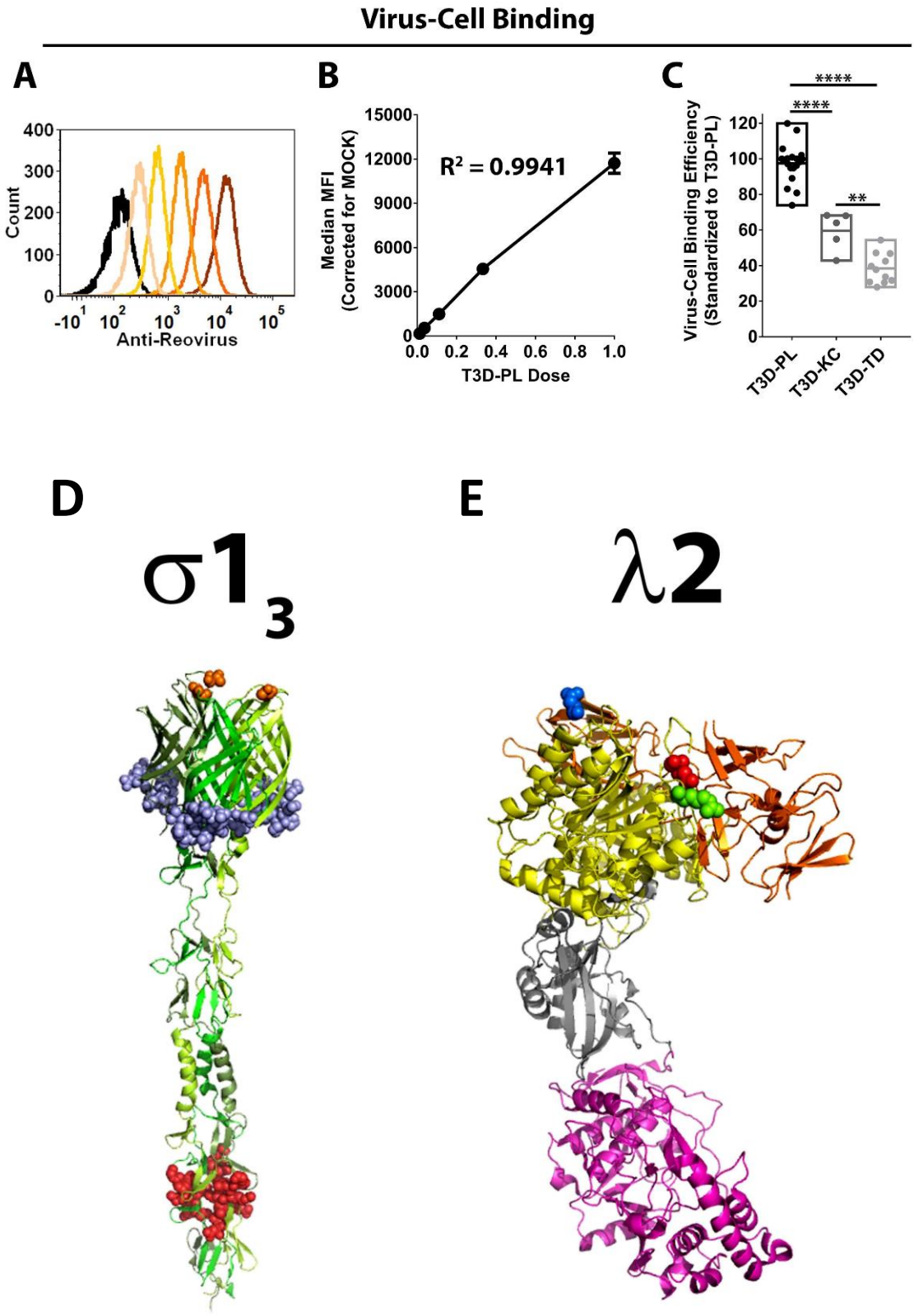
Virus-Cell Binding
A
Count
Anti-Reovirus
B
Median MFI (Corrected for MOCK)
R² = 0.9941
T3D-PL Dose
C
Virus-Cell Binding Efficiency (Standardized to T3D-PL)
****
****
**
T3D-PL
T3D-KC
T3D-TD
D
σ1 3
E
λ2

Figure 2.4: T3D-PL displays increased cell binding relative to T3D-KC and T3D-TD. A) Using non-enzymatically detached L929 cells in suspension, $T3D^{PL}$ dilutions were bound at 4°C, and following extensive washing to remove unbound reovirus, cell-bound reovirus was stained using polyclonal reovirus antibodies and mean fluorescence intensity (MFI) quantified using flow cytometry (BD FACSCanto). Black histogram = MOCK, Dark orange = highest reovirus dilution, Light orange = lowest reovirus dilution. B) Linear regression analysis of MFI determined from A), corrected for mock infected background. C) Corrected for similar particle number using Coomassie staining in Fig 2.3.B), cell binding of $T3D^{KC}$ and $T3D^{TD}$ was performed as in A) and standardized to $T3D^{PL}$ using curve from B). D) and E) Crystal structures highlighting important domains and residues, modified using PyMOL, in D) σ1 (3s6x.pdb) or E) λ2 (1ej6.pdb). D) σ1 trimer with monomers in different shades of green. Light purple spheres indicate JAM-A binding domain, red spheres indicate sialic acid binding domain and orange spheres indicate A408T. E) λ2 monomer with a gunaylyltransferase domain in pink, two methyltransferase domains, both in yellow and a flap domain in orange. Red, green and blue spheres indicate E504G, R509G and N1069T, respectively. In B), $n = 2$. In C), $n \geq 5$, One-way ANOVA with Tukey's multiple comparisons test, ** $p < 0.0021$, **** $p < 0.0001$.

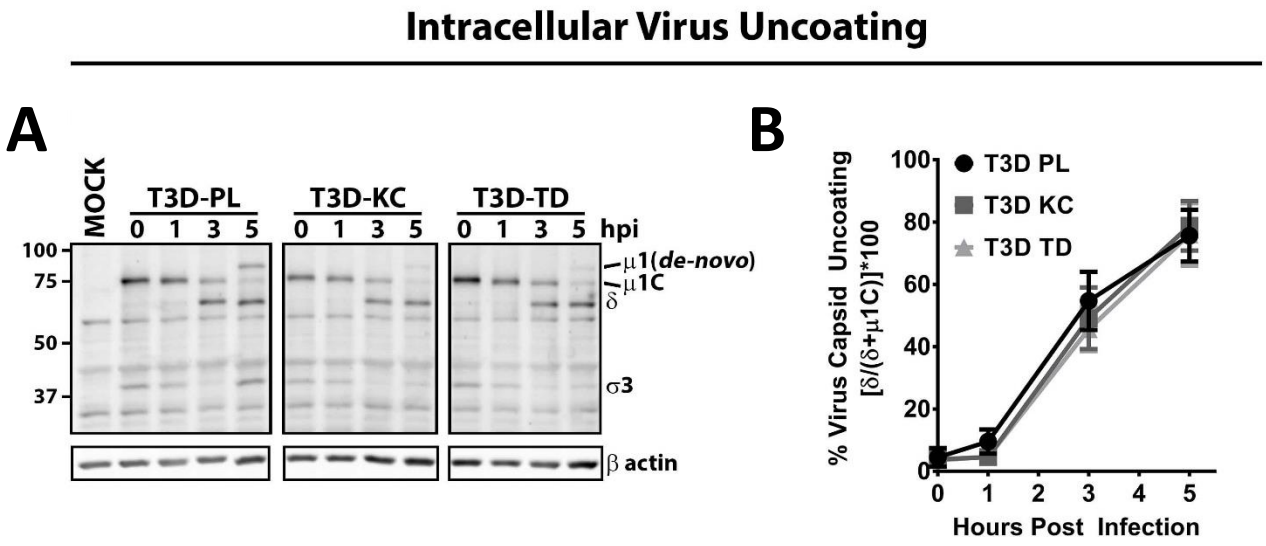

Figure 2.5: T3D-PL, T3D-KC and T3D-TD undergo similar intracellular uncoating. A) $T3D^{PL}$, $T3D^{KC}$ and $T3D^{TD}$ were bound to L929 cells at 4°C and following washing to remove unbound virions, cells were incubated at 37°C and cell lysates were collected at various timepoints post infection. Total proteins were separated using SDS PAGE and Western blot analysis with specific antibodies were used to identify reovirus proteins and β actin (loading control). B) Densitometric band quantification of μ1C and δ from A) using ImageQuantTL 1D gel analysis add-on and calculation of % virus uncoating. In B), n = 4, linear regression analysis determined the slopes are not significantly different.

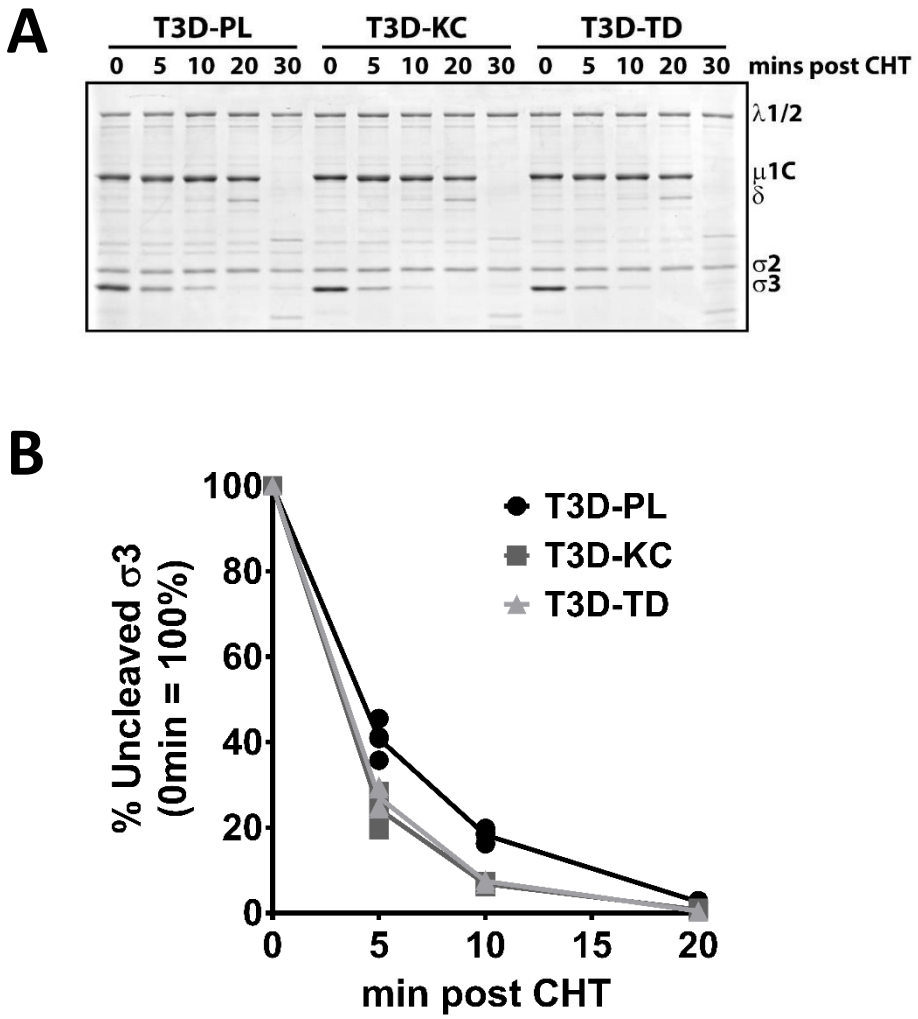

Figure 2.6. T3D-PL has slower σ3 chymotrypsin digestion kinetics relative to T3D-KC and T3D-TD. $T3D^{PL}$, $T3D^{KC}$ and $T3D^{TD}$ virus preparations were incubated with chymotrypsin (CHT) for various timepoints at 37°C. Reactions were stopped with addition of protease inhibitors and total protein was separated using SDS-PAGE and stained using Imperial™ Coomassie dye. In B), n = 2, in duplicate.

Viral mRNA Transcription

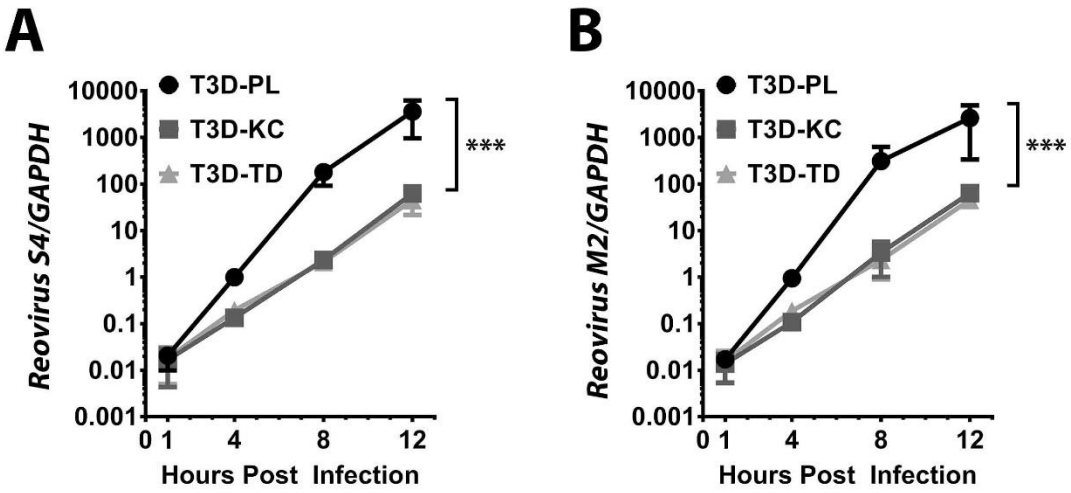

Viral Protein Translation

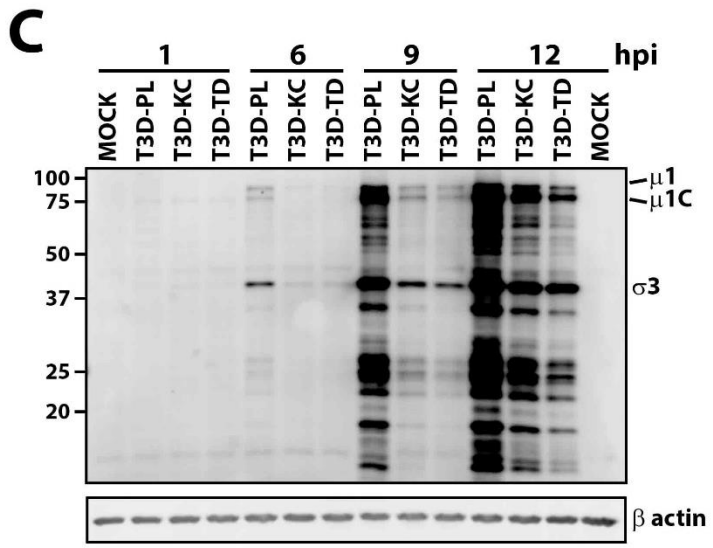

Figure 2.7: T3D-PL has accelerated viral RNA and protein translation compared to T3D-KC and T3D-TD. Similar experimental outline to Fig 2.5 A), except cell lysates were collected for RNA extraction A) and B), or protein analysis C). A) and B) Following RNA extraction and cDNA synthesis, RT-PCR was performed using gene-specific primers for reovirus S4, M2 or GAPDH. C) Total proteins were separated using SDS PAGE and Western blot analysis with specific antibodies were used to identify reovirus proteins and β actin (loading control). In A and B), n = 3, *** $p < 0.0001$, linear regression analysis determined that i) slope of T3D-PL differs from T3D-KC or T3D-TD and ii) slope of T3D-KC does not differs from T3D-TD.

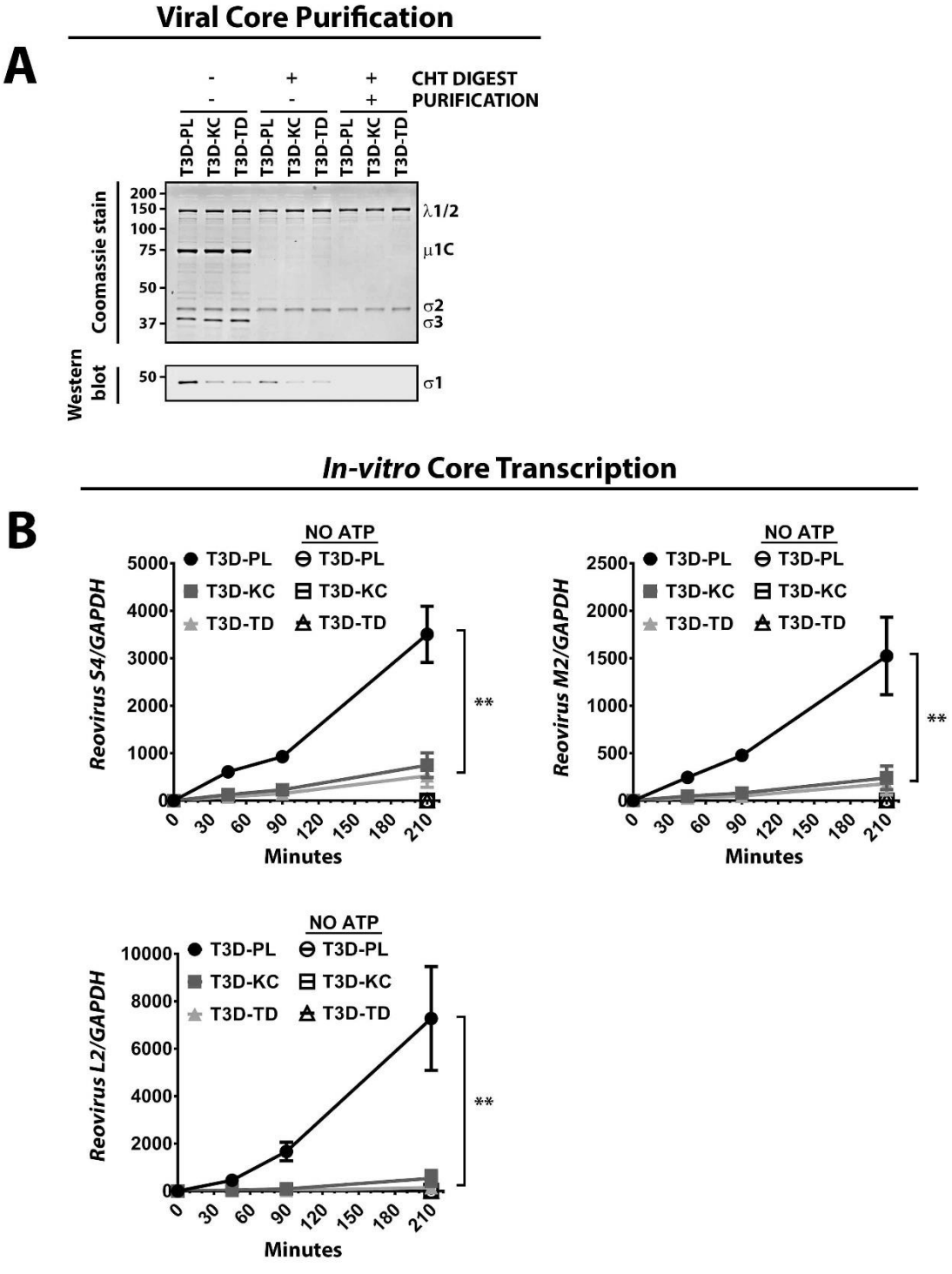
A
Viral Core Purification
CHT DIGEST
PURIFICATION
T3D-PL
T3D-KC
T3D-TD
Coomassie stain
Western blot
200
150
100
75
50
37
λ1/2
μ1C
σ2
σ3
σ1
B
In-vitro Core Transcription
NO ATP
T3D-PL
T3D-KC
T3D-TD
Reovirus S4/GAPDH
Reovirus M2/GAPDH
Reovirus L2/GAPDH
Minutes
0
30
60
90
120
150
180
210
**

Figure 2.8: T3D-PL has enhanced viral core RNA transcription activity over T3D-KC and T3D-TD. $T3D^{PL}$, $T3D^{KC}$ and $T3D^{TD}$ virus preparations were incubated with chymotrypsin (CHT) for 2 hours at 37°C. Reactions were stopped with addition of protease inhibitors and viral cores were pelleted with high speed centrifugation (100,000g) for 2 hours at 4°C. Viral cores were resuspended in 100mM Tris pH 8 and stored at 4°C. A) At every stage in viral core purification, total protein was stained using Imperial™ Coomassie dye, while reovirus σ1 protein was identified using Western blot analysis with σ1-specific antibody. B) Purified viral cores from A) were added to transcription buffer (with or without ATP) and incubated at 40°C for various timepoints. Each timepoint sample was spiked with 3ng mouse GAPDH RNA. Following RNA extraction using Trizol LS and cDNA synthesis, RT-PCR was performed using gene-specific primers for reovirus S4, M2, L2 or GAPDH. Values were standardized to respective GAPDH, and each group was normalized to the respective 0 minute timepoint. In B), $n = 3$, ** $p < 0.0021$, linear regression analysis determined that i) slope of T3D-PL differs from T3D-KC or T3D-TD and ii) slope of T3D-KC does not differs from T3D-TD.

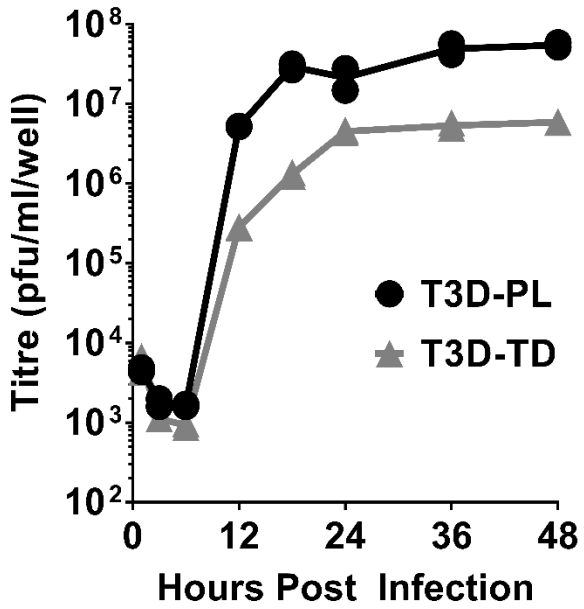

Figure 2.9: T3D-PL has enhanced virus replication kinetics relative to T3D-TD. L929 cells were infected with $T3D^{PL}$ or $T3D^{TD}$ at MOI 1 and incubated at 37°C. At each timepoint, total cells were collected by scraping and put though 3 freeze-thaw cycles. Titres in each sample were determined by plaque assay on L929 cells with crystal violet staining. n = 1, in duplicate

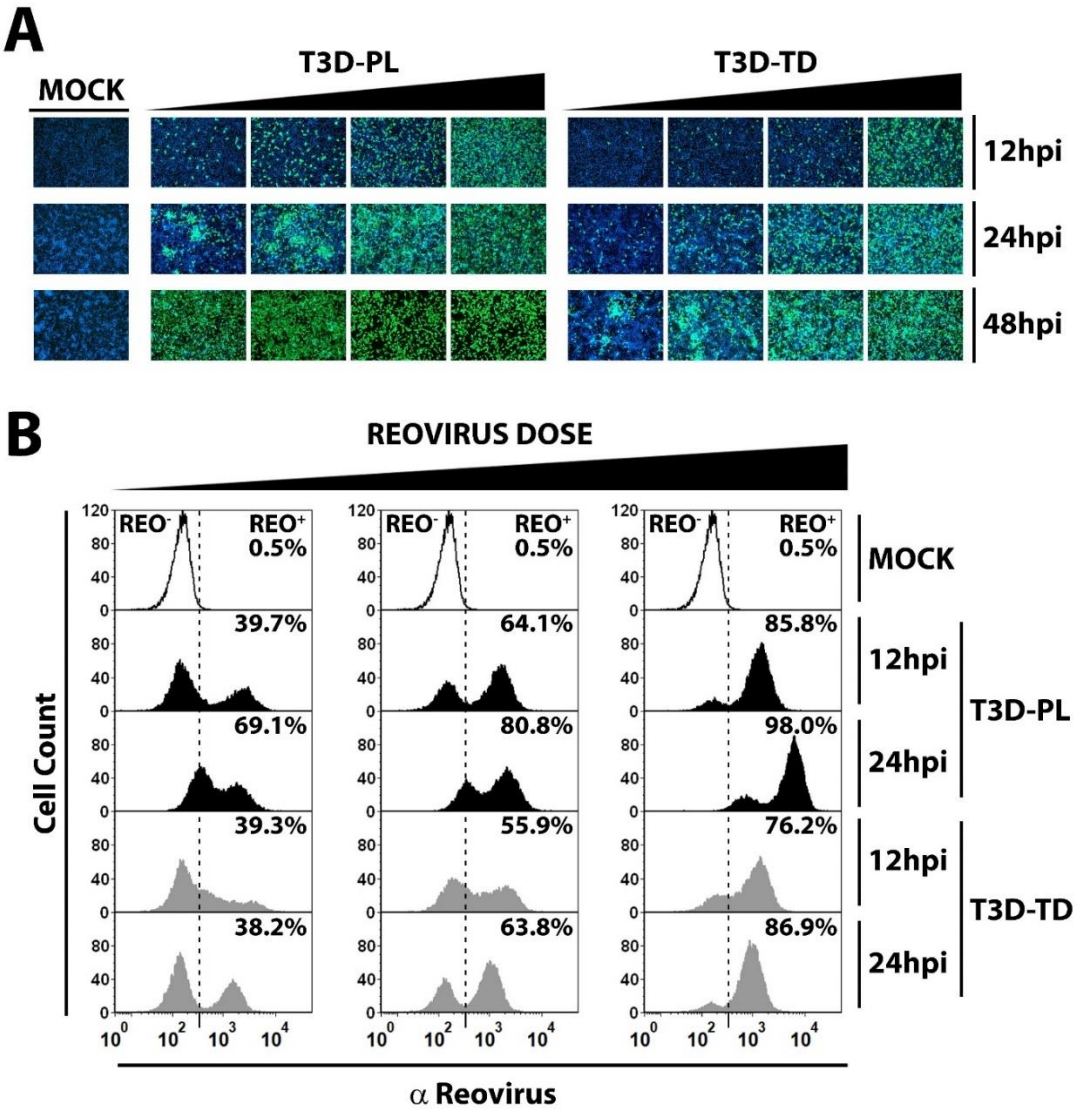

Figure 2.10: T3D-PL establishes a productive infection earlier than T3D-TD. L929 cells were infected with $T3D^{PL}$ or $T3D^{TD}$ at 1/3 virus dilutions (initial MOI 9) and incubated at 37°C for 12 or 24 hours. At each timepoint, reovirus infected cells were identified using reovirus specific primary antibody and Alexa Fluor 488 conjugated secondary antibody. A) Nuclei were stained with HOESCHT 33342 and imaged with EVOS FL Auto Cell Imaging System. Green staining represents reovirus infected cells, and blue staining represents cell nuclei. B) Reovirus infected cells were quantified using flow cytometry.

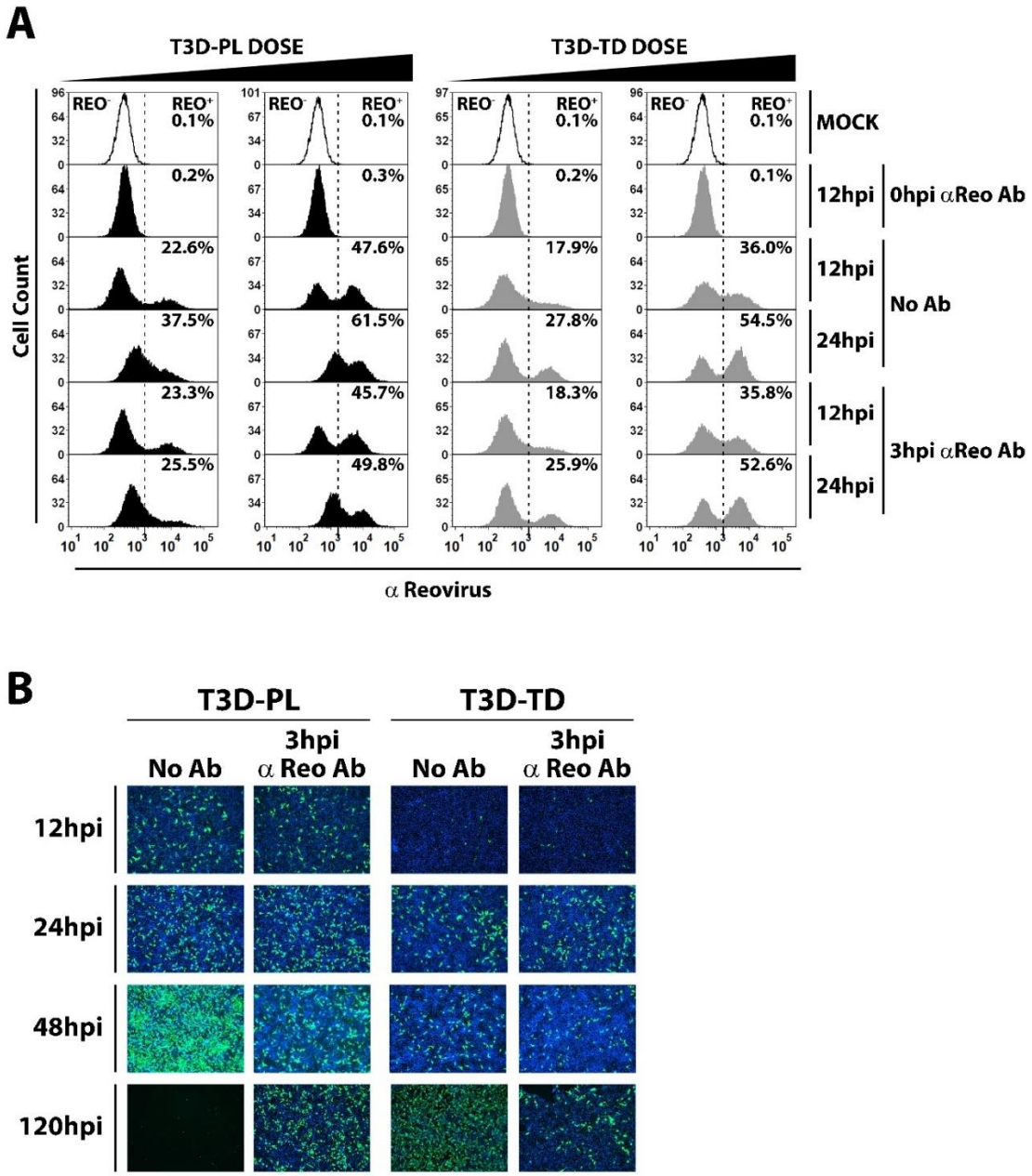

Figure 2.11: T3D-TD displays delayed establishment of infection relative to T3D-PL. L929 cells were infected with $T3D^{PL}$ or $T3D^{TD}$ at 1/3 virus dilutions (initial MOI 3) and incubated at 37°C. Polyclonal reovirus antibody was either i) incubated with reovirus inoculum for 30min prior to infection (0hpi αReo Ab) or ii) added directly to the well media at 3hpi (3hpi αReo Ab). A) Samples were processed similar to Fig 2.9 B). B) Samples were processed similar to 2.9 A).

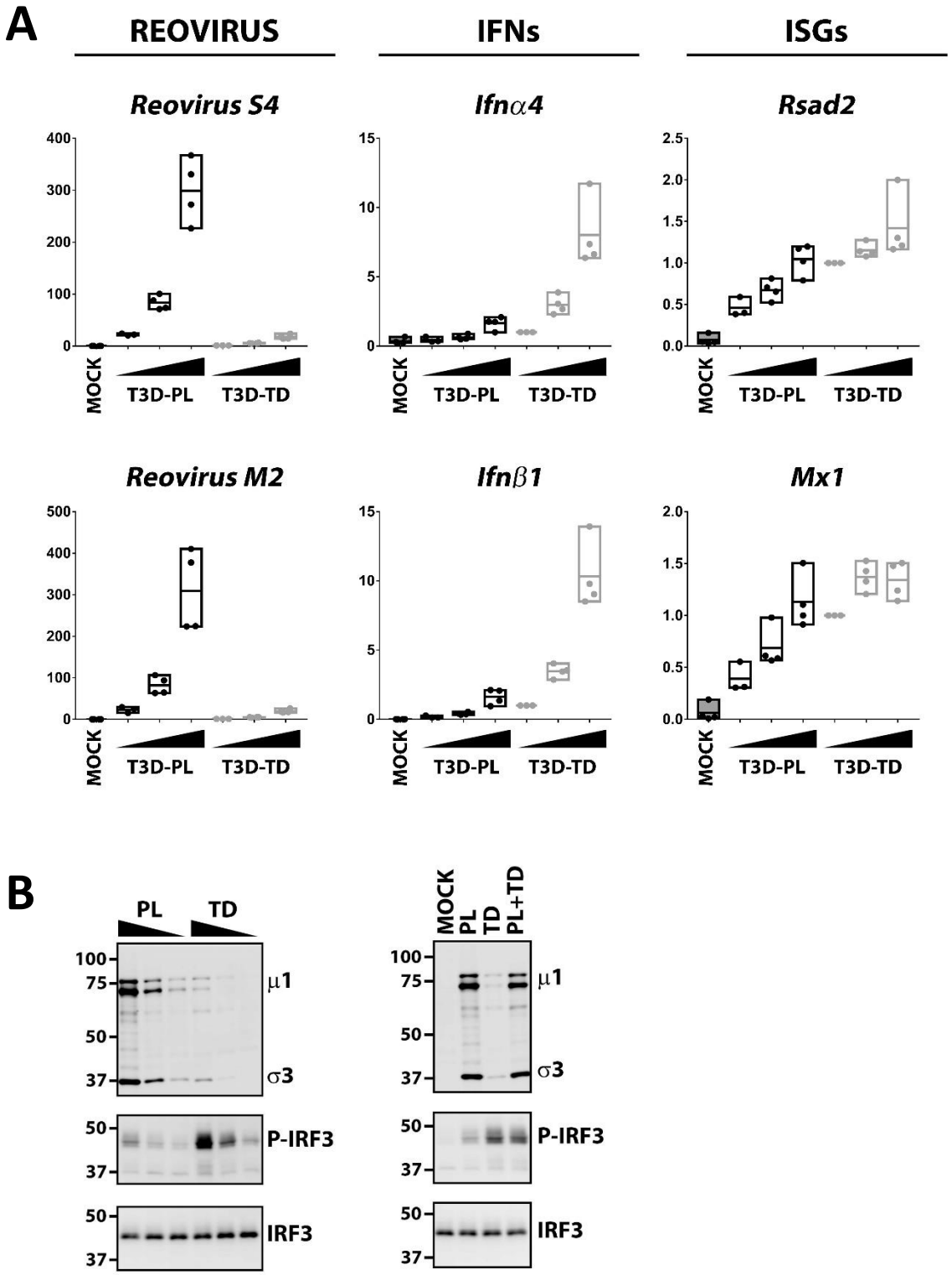
A
REOVIRUS
IFNs
ISGs
Reovirus S4
Ifnα4
Rsad2
Reovirus M2
Ifnβ1
Mx1
MOCK
T3D-PL
T3D-TD
B
PL
TD
MOCK
PL
TD
PL+TD
μ1
σ3
P-IRF3
IRF3

Figure 2.12: Compared to T3D-PL, T3D-TD stimulates a heightened IFN response. L929 cells were infected with $T3D^{PL}$ or $T3D^{TD}$ at 1/3 virus dilutions (initial MOI 9) and incubated at 37°C for 12 hours. A) Following RNA extraction and cDNA synthesis, RT-PCR was performed using gene-specific primers. Quantification was standardized to $T3D^{TD}$ MOI 1. B) Total proteins were separated using SDS PAGE and Western blot analysis with specific antibodies. In A), n = 4.

A

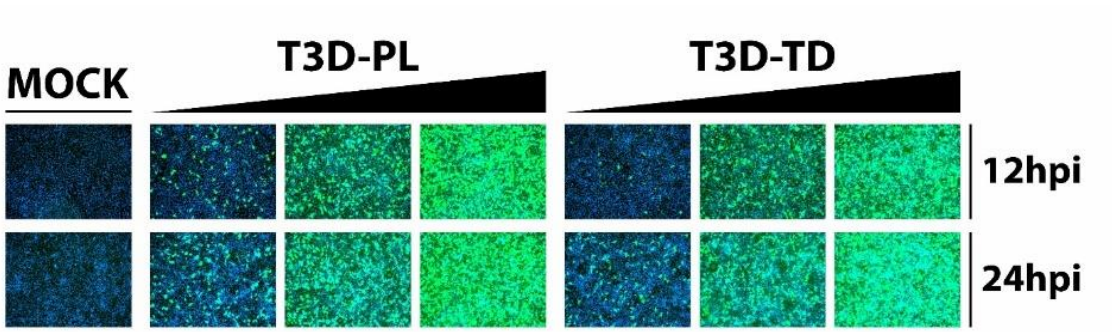
MOCK
T3D-PL
T3D-TD
12hpi
24hpi

B

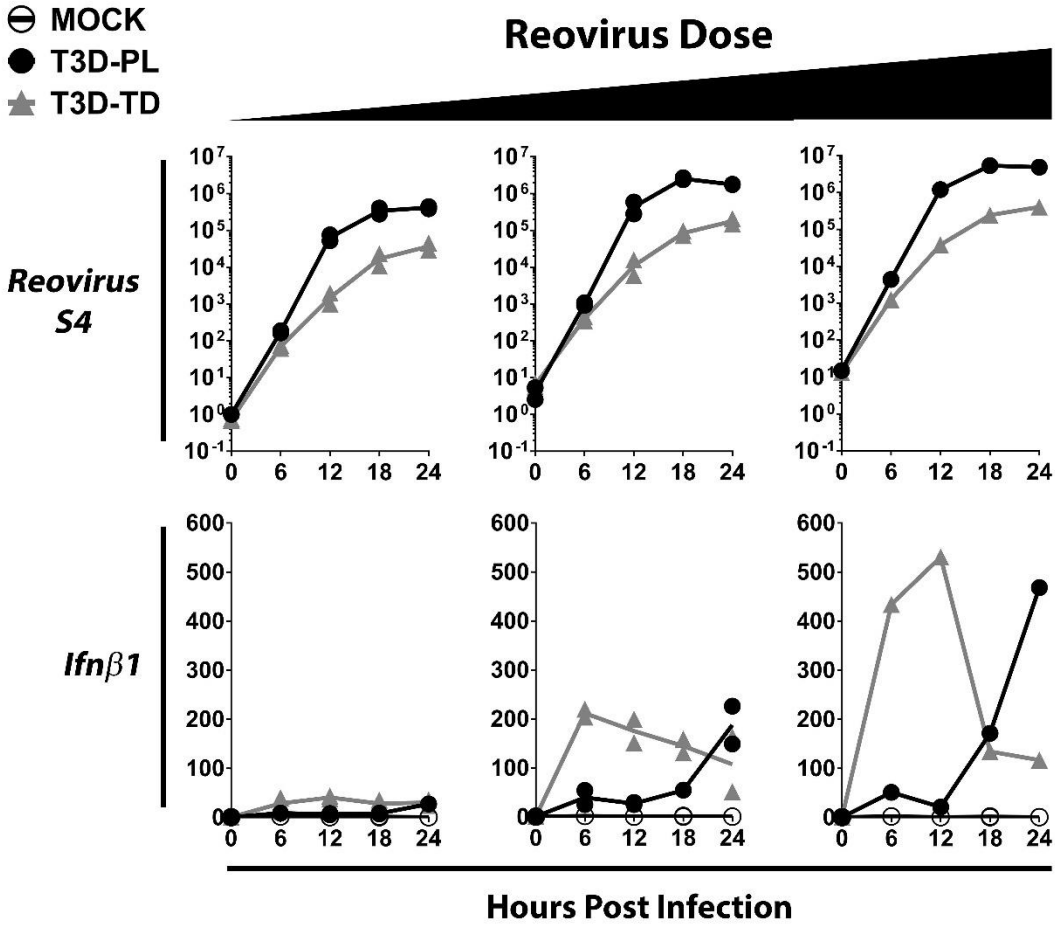
MOCK
T3D-PL
T3D-TD
Reovirus Dose
Reovirus S4
Ifnβ1
Hours Post Infection

Figure 2.13: IFN expression late during infection, increases with T3D-PL and decreases with T3D-TD. L929 cells were infected with $T3D^{PL}$ or $T3D^{TD}$ at 1/3 virus dilutions (initial MOI 27) and incubated at 37°C. A) At each timepoint, reovirus infected cells were identified using reovirus specific primary antibody and Alexa Fluor 488 conjugated secondary antibody. Nuclei were stained with HOESCHT 33342 and imaged with EVOS FL Auto Cell Imaging System. Green staining represents reovirus infected cells, and blue staining represents cell nuclei. B) Lysates were collected at each timepoint and following RNA extraction and cDNA synthesis, RT-PCR was performed using gene-specific primers (corrected for *GAPDH*). In B), MOI 9 and MOI 3 n = 2, MOI 27 n=1.

A

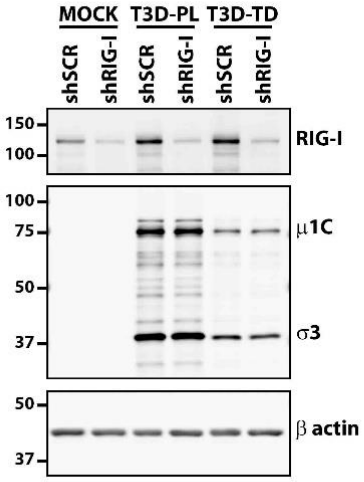
MOCK
T3D-PL
T3D-TD
shSCR
shRIG-I
shSCR
shRIG-I
shSCR
shRIG-I
150
100
RIG-I
100
75
50
37
μ1C
σ3
50
37
β actin

B

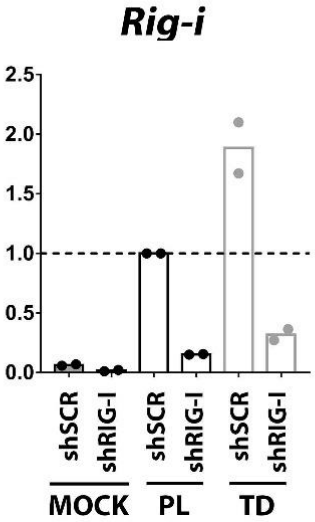
Rig-i
2.5
2.0
1.5
1.0
0.5
0.0
shSCR
shRIG-I
shSCR
shRIG-I
shSCR
shRIG-I
MOCK
PL
TD

C

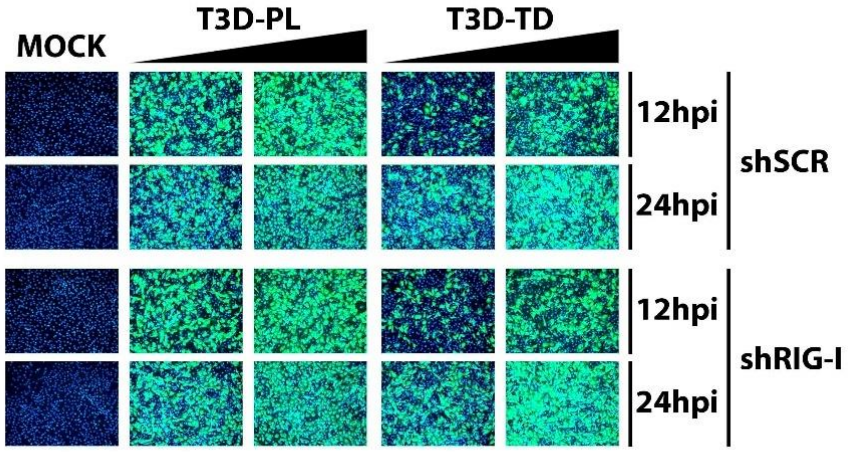
MOCK
T3D-PL
T3D-TD
12hpi
24hpi
shSCR
12hpi
24hpi
shRIG-I

Figure 2.14: RIG-I signaling does not impact initial reovirus infection. NIH/3T3 cells stably transduced with scrambled (shSCR) or RIG-I (shRIG) lentivirus were infected with reovirus at 1/3 virus dilutions (initial MOI 60) and incubated at 37°C. Samples were collected for A) Western blot analysis with specific antibodies (β actin as loading control) at 12hpi, B) RNA extraction, cDNA synthesis and RT-PCR using *Rig-I*-specific primers (corrected for *GAPDH*) at 12hpi and C) Immunocytochemistry staining of reovirus infected cells using reovirus specific primary antibody and Alexa Fluor 488 conjugated secondary antibody, and HOESCHT 33342 nuclei staining. Green staining represents reovirus infected cells, and blue staining represents cell nuclei. In B), n = 2.

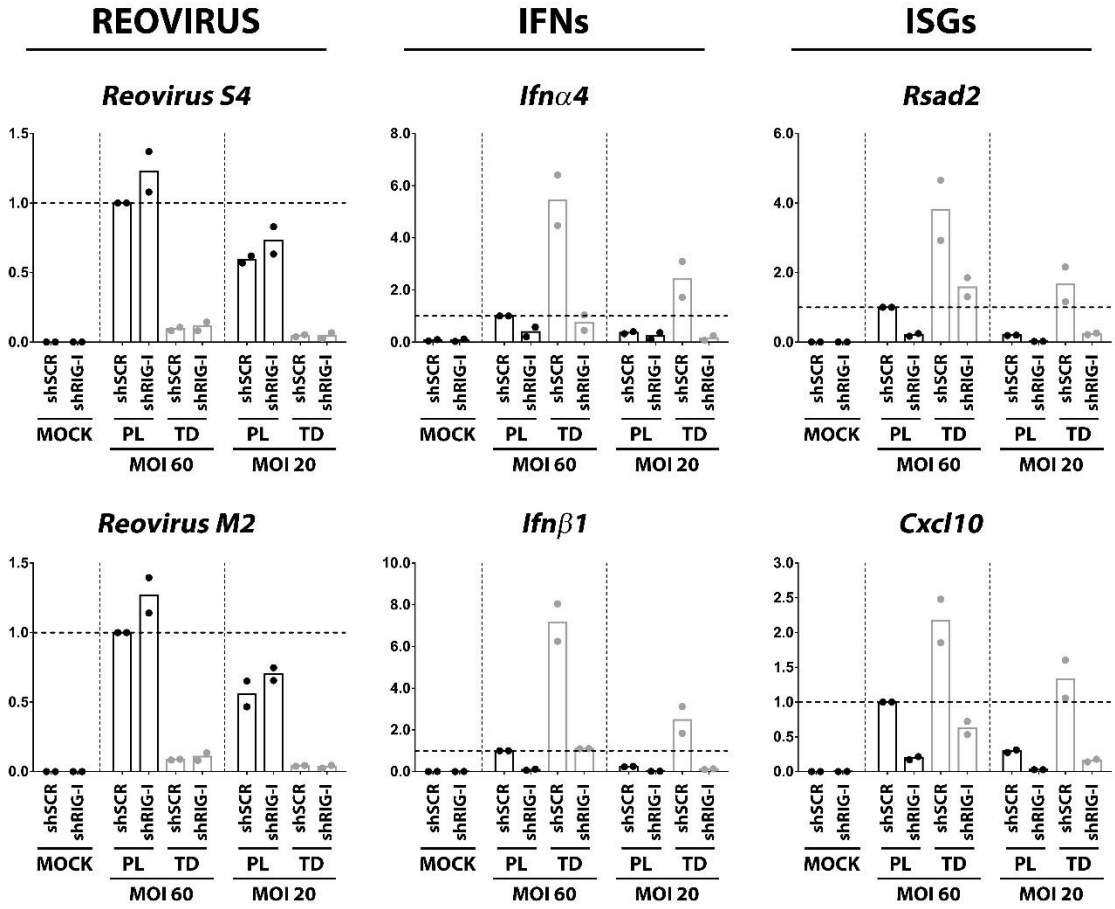

Figure 2.15: RIG-I dependent IFN signaling does not impact initial reovirus infection.

Similar to Fig 2.12**,** NIH/3T3 cells stably transduced with scrambled (shSCR) or RIG-I (shRIG) lentivirus were infected with reovirus at 1/3 virus dilutions (initial MOI 60) and incubated at 37°C. Samples were collected at 12hpi for RNA extraction, cDNA synthesis and RT-PCR using gene-specific primers (corrected for *GAPDH*) and standardized to shSCR $T3D^{TD}$ MOI 20. n = 2.

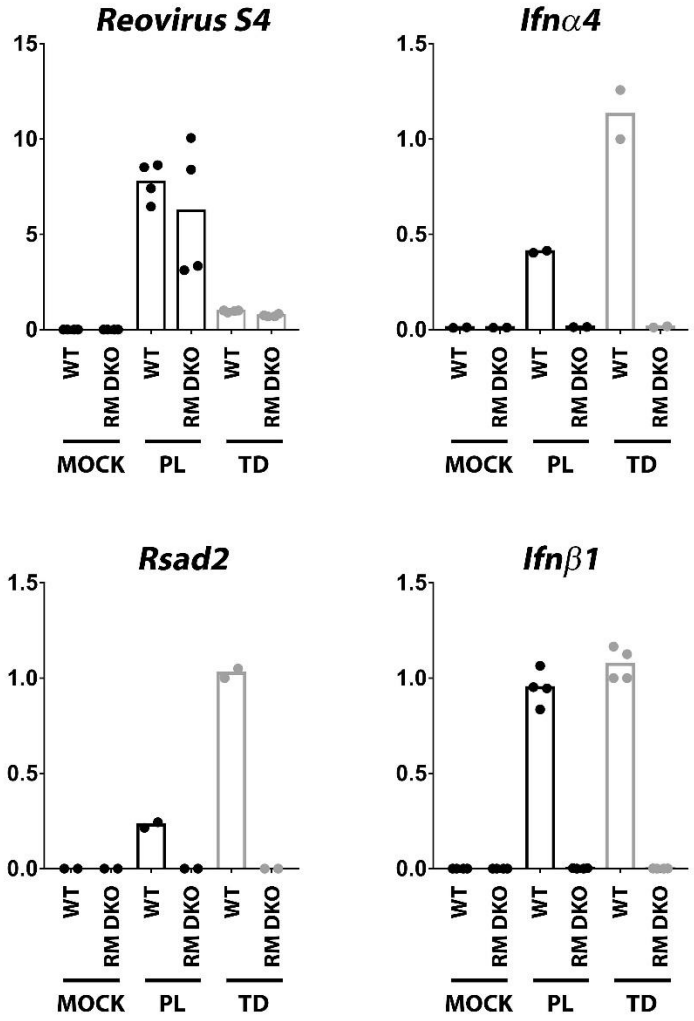

Figure 2.16: RIG-I and MDA5 dependent signaling does not impact initial reovirus infection. Wild-type (WT) or RIG-I/MDA5 double knockout (RM DKO) MEF cell lines were infected with reovirus at MOI 6 and incubated at 37°C. Samples were collected at 12hpi for RNA extraction, cDNA synthesis and RT-PCR using gene-specific primers (corrected for *GAPDH*). n = 2-4.

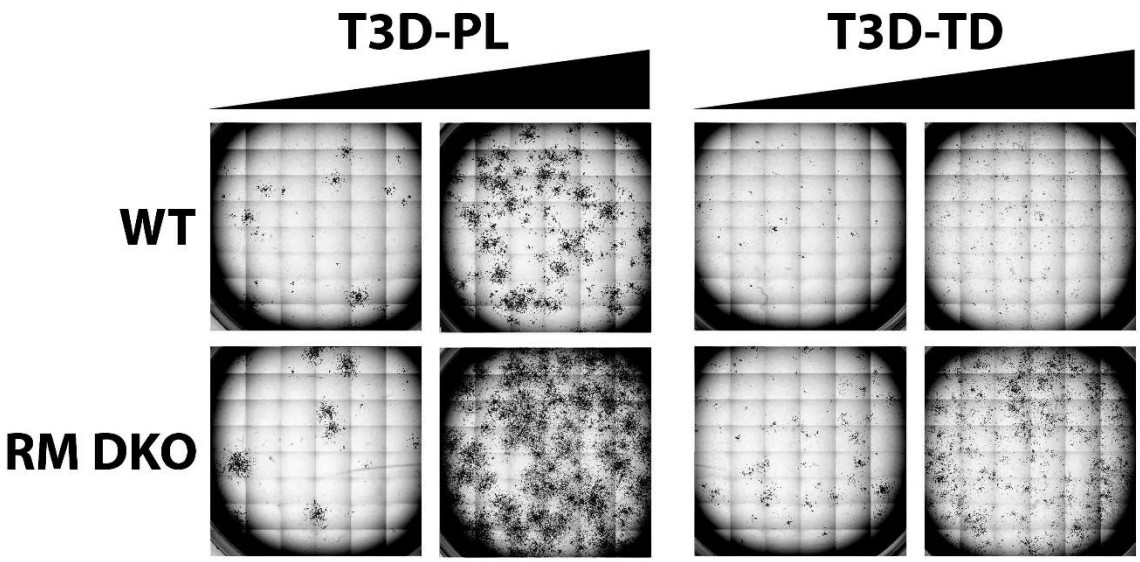

Figure 2.17: RIG-I and MDA5 dependent signaling enhanced reovirus spread. Wild-type (WT) or RIG-I/MDA5 double knockout (RM DKO) MEF cell lines were infected with reovirus and overlaid with agar. Reovirus infected cell foci were visualized following staining with immunocytochemistry.

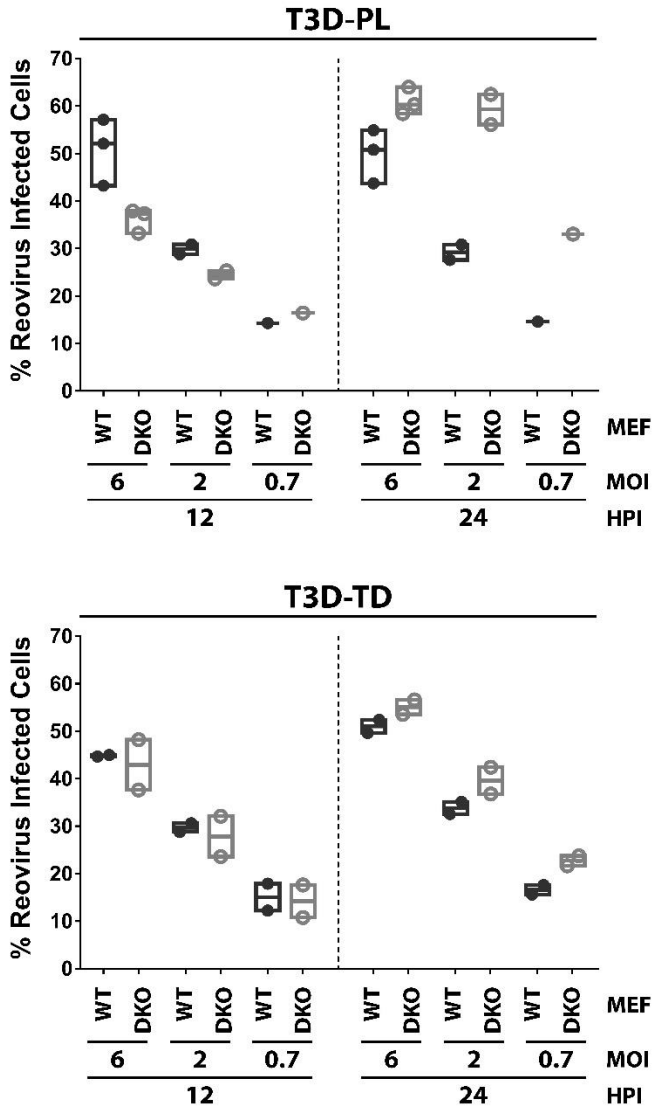

Figure 2.18: RIG-I and MDA5 dependent signaling does not impact delayed T3D-TD infection kinetics. Wild-type (WT) or RIG-I/MDA5 double knockout (RM DKO) MEF cell lines were infected with $T3D^{PL}$ or $T3D^{TD}$ at 1/3 virus dilutions (initial MOI 6) and incubated at 37°C for 12 or 24 hours. At each timepoint, reovirus infected cells were identified using reovirus specific primary antibody and Alexa Fluor 488 conjugated secondary antibody, and quantified using flow cytometry. n = 1-3.

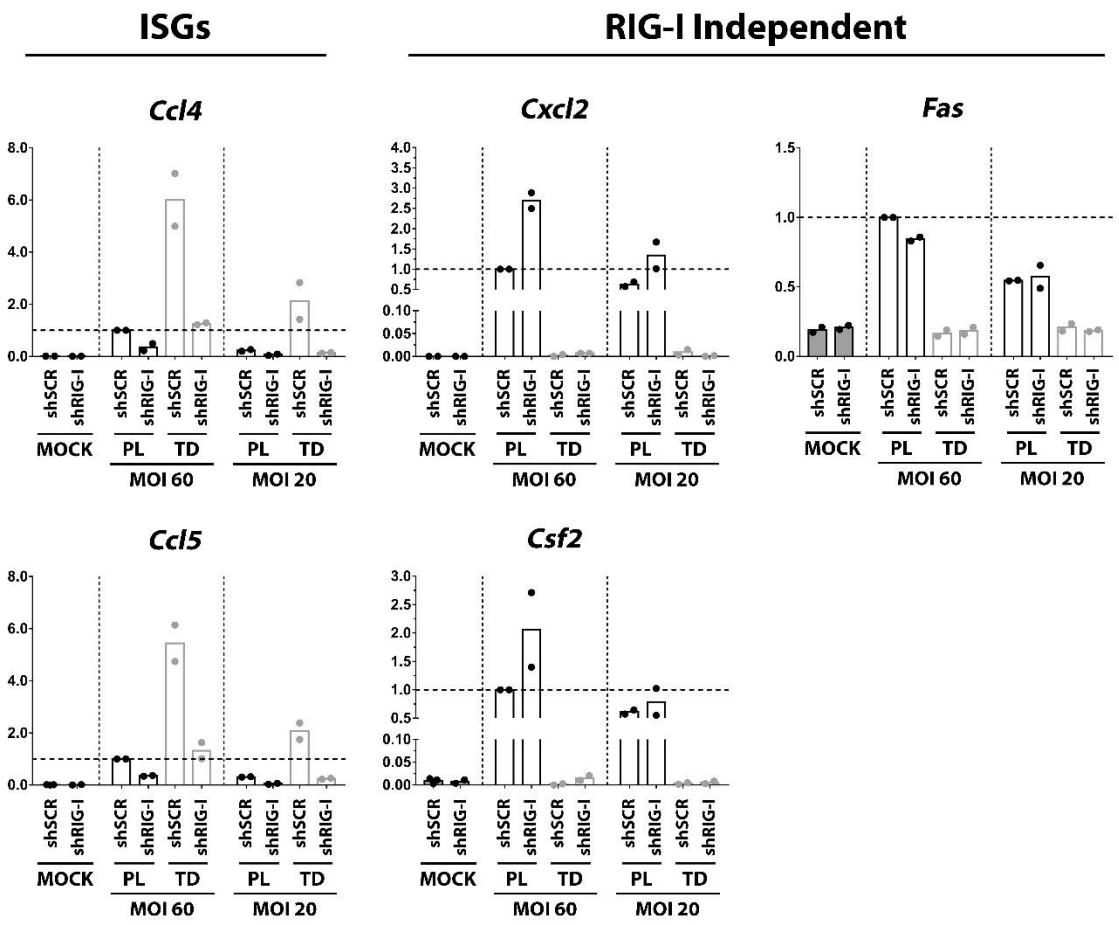

Figure 2.19: T3D-PL but not T3D-TD activates RIG-I independent signaling. Similar to Fig 2.12**,** NIH/3T3 cells stably transduced with scrambled (shSCR) or RIG-I (shRIG) lentivirus were infected with reovirus at 1/3 virus dilutions (initial MOI 60) and incubated at 37°C. Samples were collected at 12hpi for RNA extraction, cDNA synthesis and RT-PCR using gene-specific primers (corrected for *GAPDH*). n = 2

A

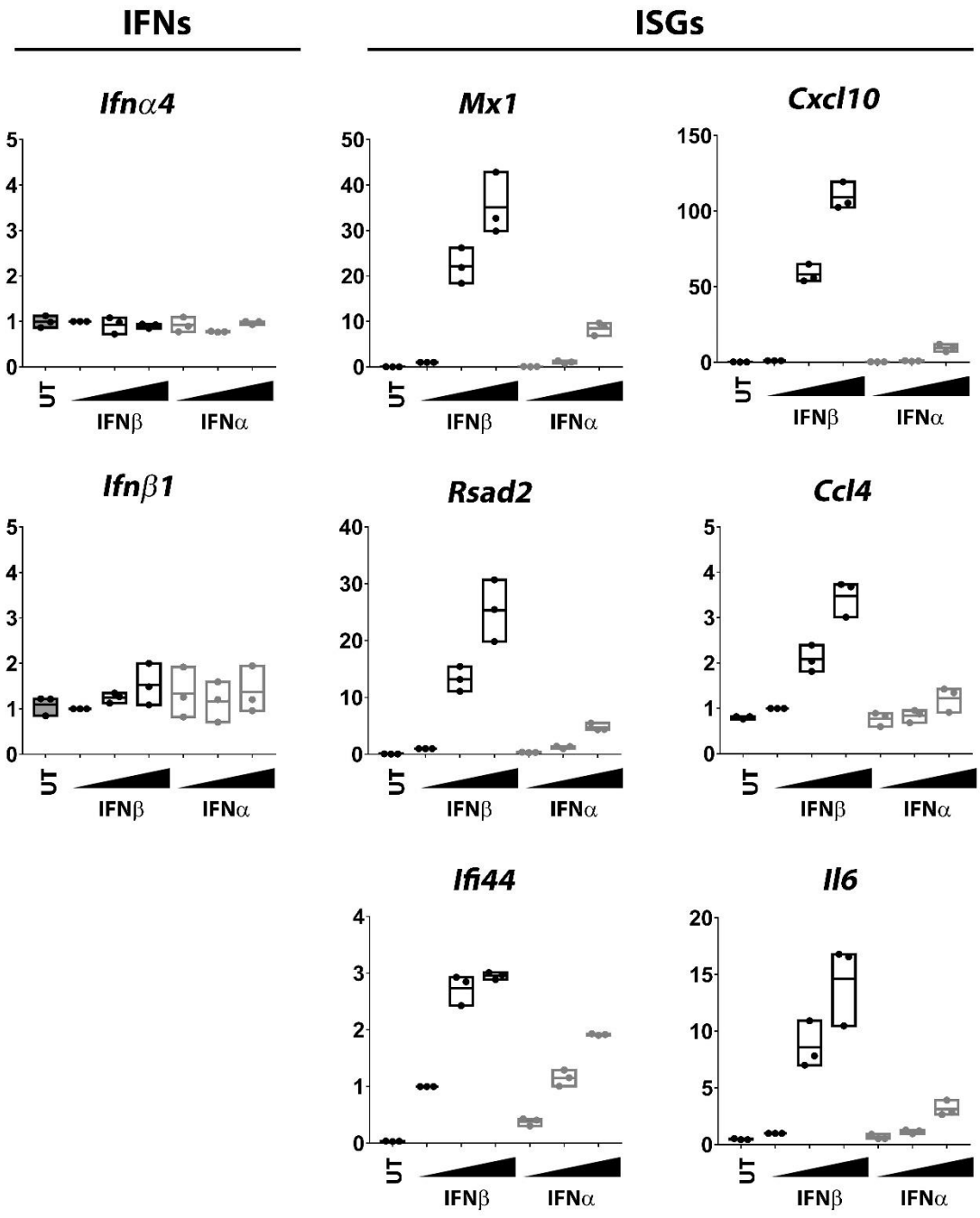
IFNs
ISGs
Ifnα4
Mx1
Cxcl10
Ifnβ1
Rsad2
Ccl4
Ifi44
Il6
UT
IFNβ
IFNα

B

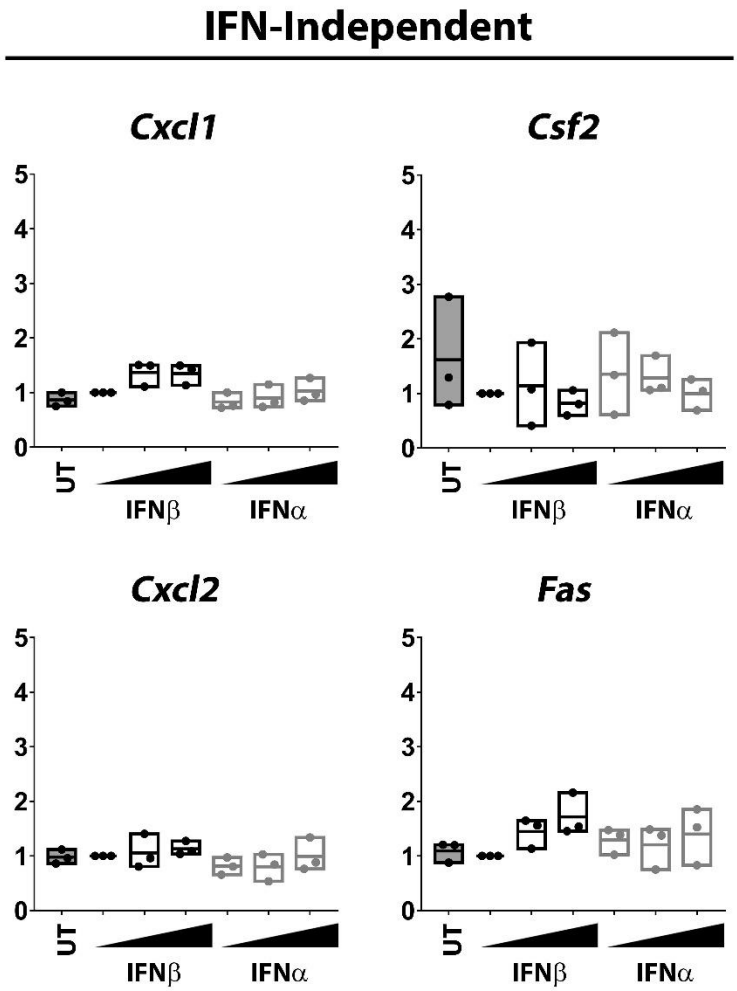

Figure 2.20: Classification of IFN-dependent and IFN-independent genes. L929 cells were treated with 1/10 dilutions (initial 1000 U/ml/12well) of purified IFNα or IFNβ for 12 hours at 37°C. Samples were collected for RNA extraction, cDNA synthesis and RT-PCR using gene-specific primers (corrected for *GAPDH*). A) IFN-dependent genes. B) IFN-independent genes IFN stimulated gene (ISG). In A and B) n = 3

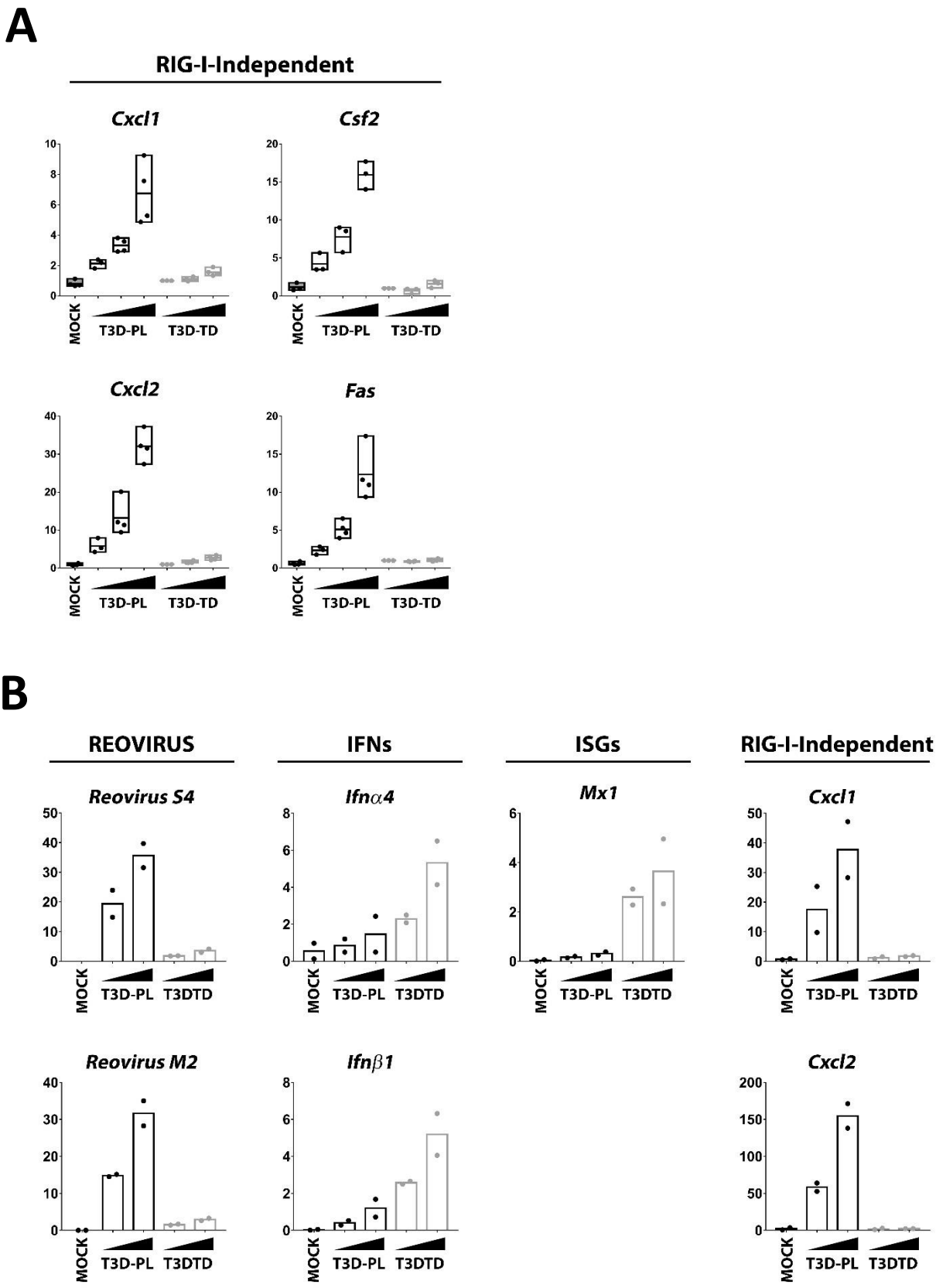
A
RIG-I-Independent
Cxcl1
Csf2
Cxcl2
Fas
MOCK
T3D-PL
T3D-TD
B
REOVIRUS
IFNs
ISGs
RIG-I-Independent
Reovirus S4
Ifnα4
Mx1
Cxcl1
Reovirus M2
Ifnβ1
Cxcl2
MOCK
T3D-PL
T3DTD

C

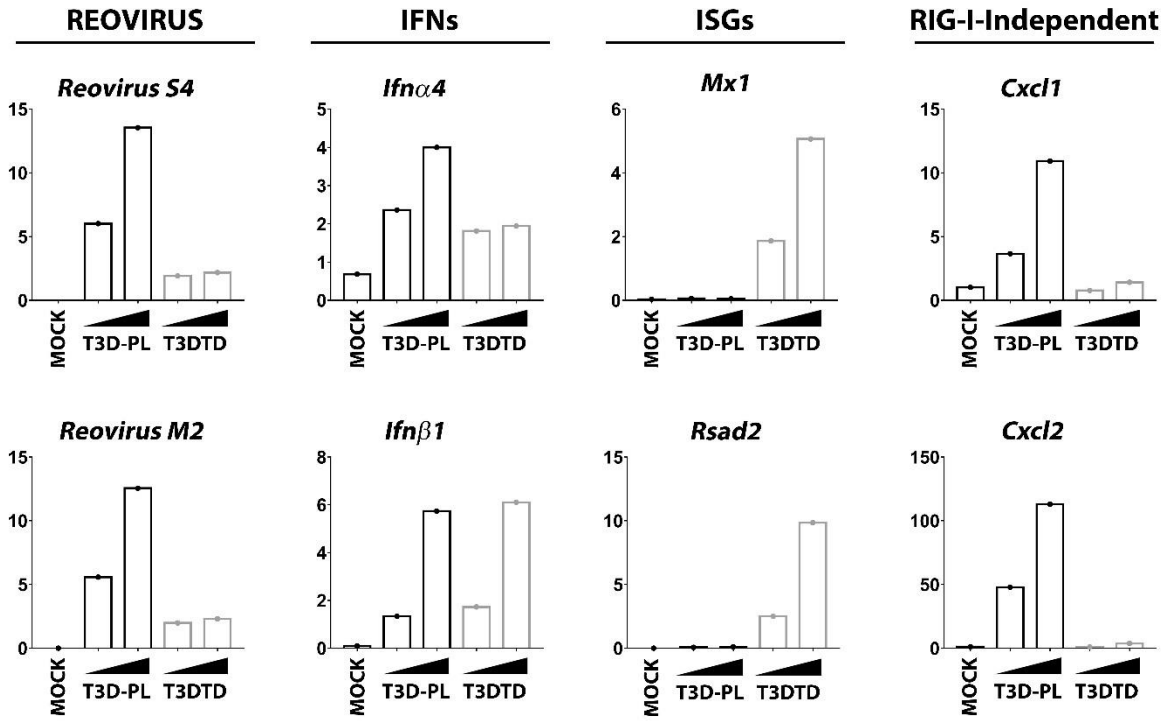

Figure 2.21: T3D-PL but not T3D-TD activates IFN-independent signaling. Cells were infected with reovirus at 1/3 virus dilutions at 37°C for 12 hours. Following RNA extraction and cDNA synthesis, RT-PCR was performed using gene-specific primers (corrected for *GAPDH*). A) L929 cells, similar to Fig 2.11 (initial MOI 9). Quantification was standardized to $T3D^{TD}$ MOI 1. B) B16-F10 (initial MOI 27) C) ID8 (initial MOI 3). In A), n = 4, B) n = 2, C) n = 1.

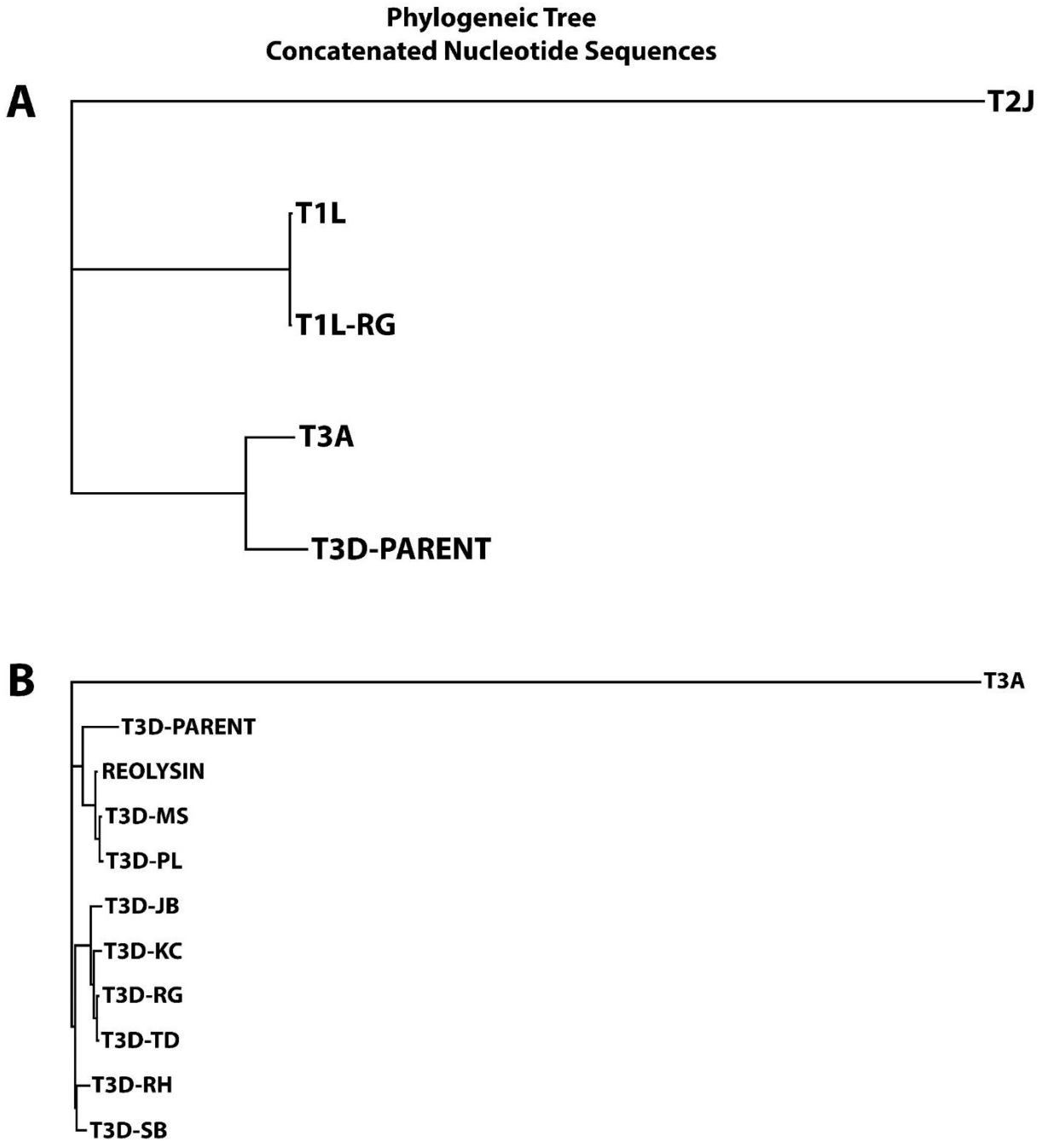
Phylogeneic Tree
Concatenated Nucleotide Sequences
A
T2J
T1L
T1L-RG
T3A
T3D-PARENT
B
T3A
T3D-PARENT
REOLYSIN
T3D-MS
T3D-PL
T3D-JB
T3D-KC
T3D-RG
T3D-TD
T3D-RH
T3D-SB

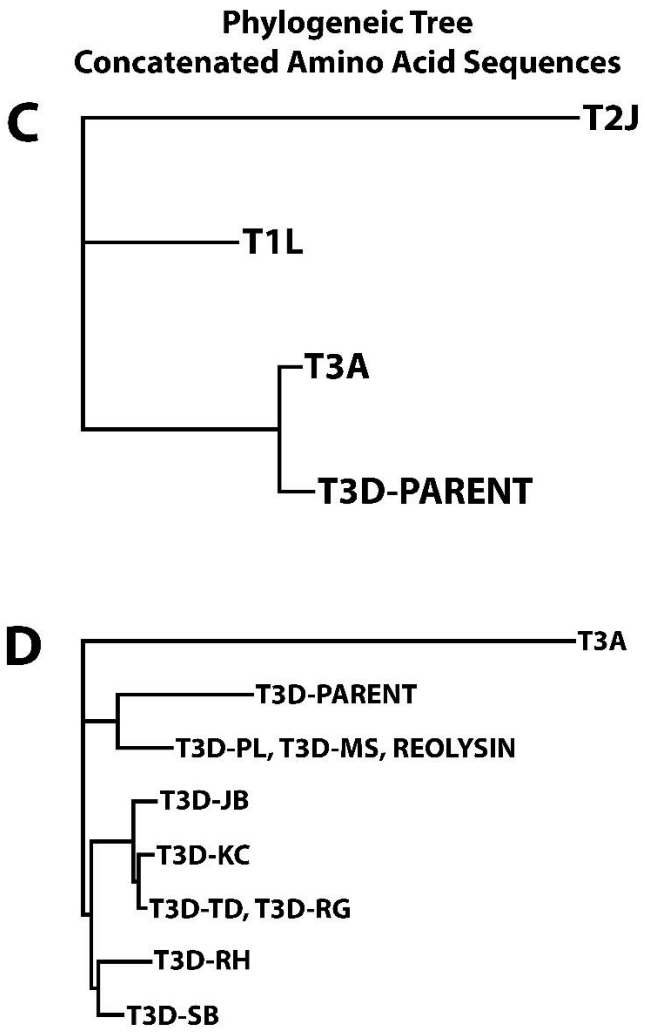

Figure 2.22: Reovirus T3D laboratory strain divergence. Phylogenetic trees were generated with concatenated complete reovirus sequences using the Geneious® tree builder add on. Assembly of phylogenetic trees was performed using the Jukes-Cantor genetic distance model and neighbour-joining tree build method. A) and B) Concatenate sequences of 10 reovirus gene segments, in order S1, S2, S3, S4, M1, M2, M3, L1, L2, L3. C) and D) Concatenate sequences of 11 reovirus proteins, in order σ1, σ1s, σ2, σNS, σ3, μ1, μ2, μNS, λ1, λ2, λ3.

A
PL/TD LARGE PLAQUE
REASSORTANTS
PL
TD
B1
B2
B3
B4
B5
B6
B7
B8
B9
B10
B11
B12
S1
S2
S3
S4
M1
M2
M3
L1
L2
L3
16
32
64
128
256
512
1024
2048
4096
Plaque Area

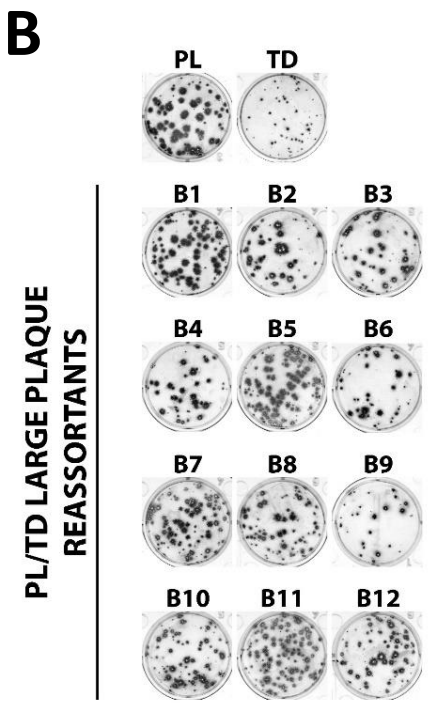

Figure 2.23: PL-M1, PL-S4 and PL-L3 genes segregated with large plaque T3D-PL/T3D-TD reassortants. L929 cells were co-infected with $T3D^{PL}$ and $T3D^{TD}$, at an MOI of 20 and 200, respectively. At 24hpi, the cell lysate was collected and following 3 freeze/thaw cycles, plaque assays were performed on L929 cells. Using $T3D^{TD}$ and $T3D^{PL}$ plaques as a reference, twenty plaques similar in size to $T3D^{PL}$ were isolated and twice plaque purified on L929 cells. RNA was isolated from plaque purified L929 cell lysates and cDNA synthesis was performed using reovirus gene-specific primers. Individual reovirus genes were amplified using high fidelity polymerase PCR, and sequenced. A) Except for the identical S3 gene, unique genetic differences in the other 9 genes were used to classify reassortant genes as $T3D^{PL}$ or $T3D^{TD}$. Quantification of plaque area in B) using ImageQuantTL colony counting add-on. B) Parental (PL and TD) and reassortant (B1-B12) infected infected L929 cells were overlaid with agar and cell foci were visualized at 4dpi following staining with immunocytochemistry.

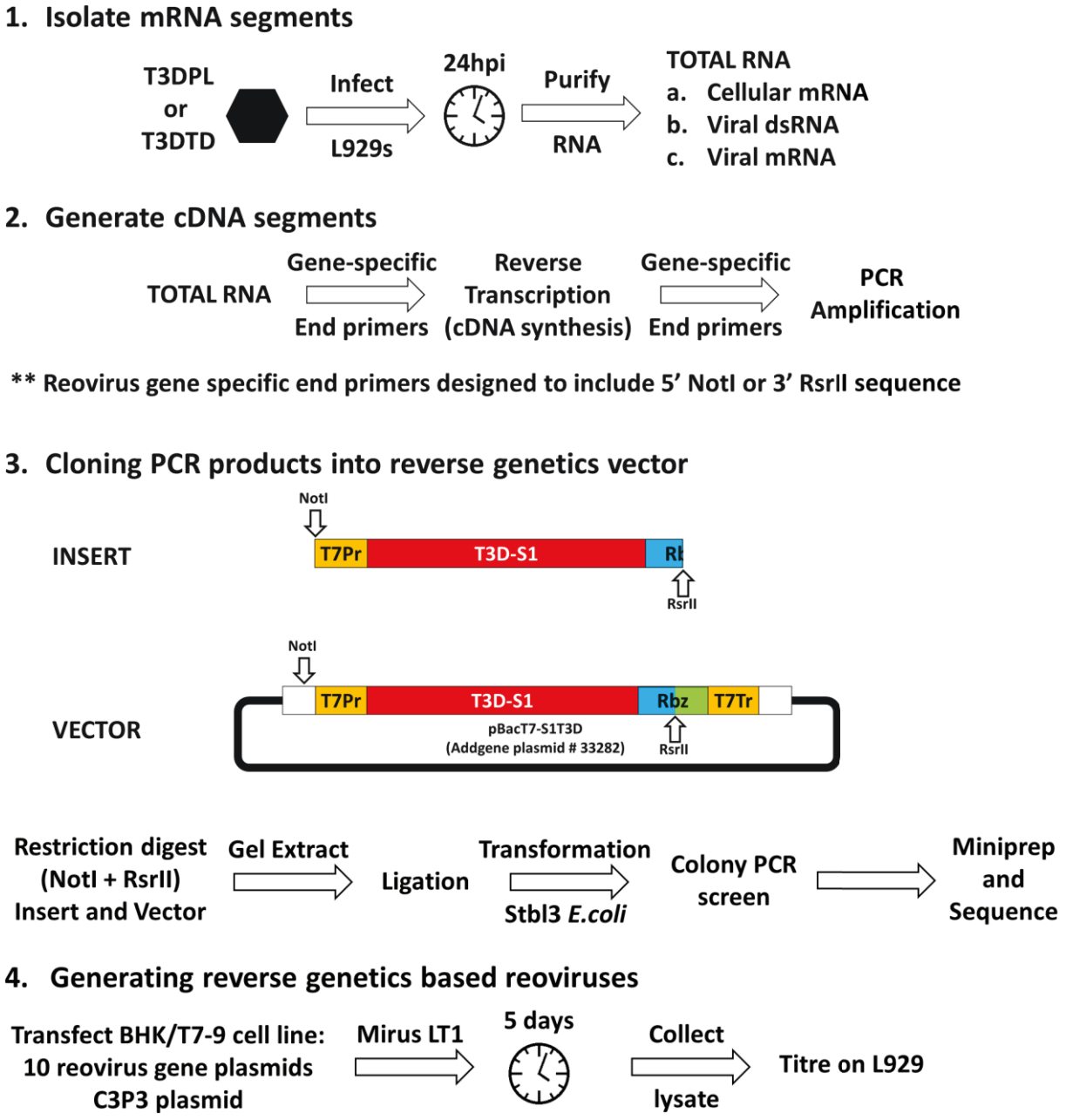

Figure 2.24: Outline of experimental strategy for design of T3D-PL and T3D-TD reverse genetics plasmids. T7Pr: T7 promoter, T7Tr: T7 terminator, Rbz: Hepatitis delta virus (HDV) ribozyme, C3P3: Plasmid encoding fusion protein containing T7 RNA polymerase and African swine fever virus capping enzyme NP868R

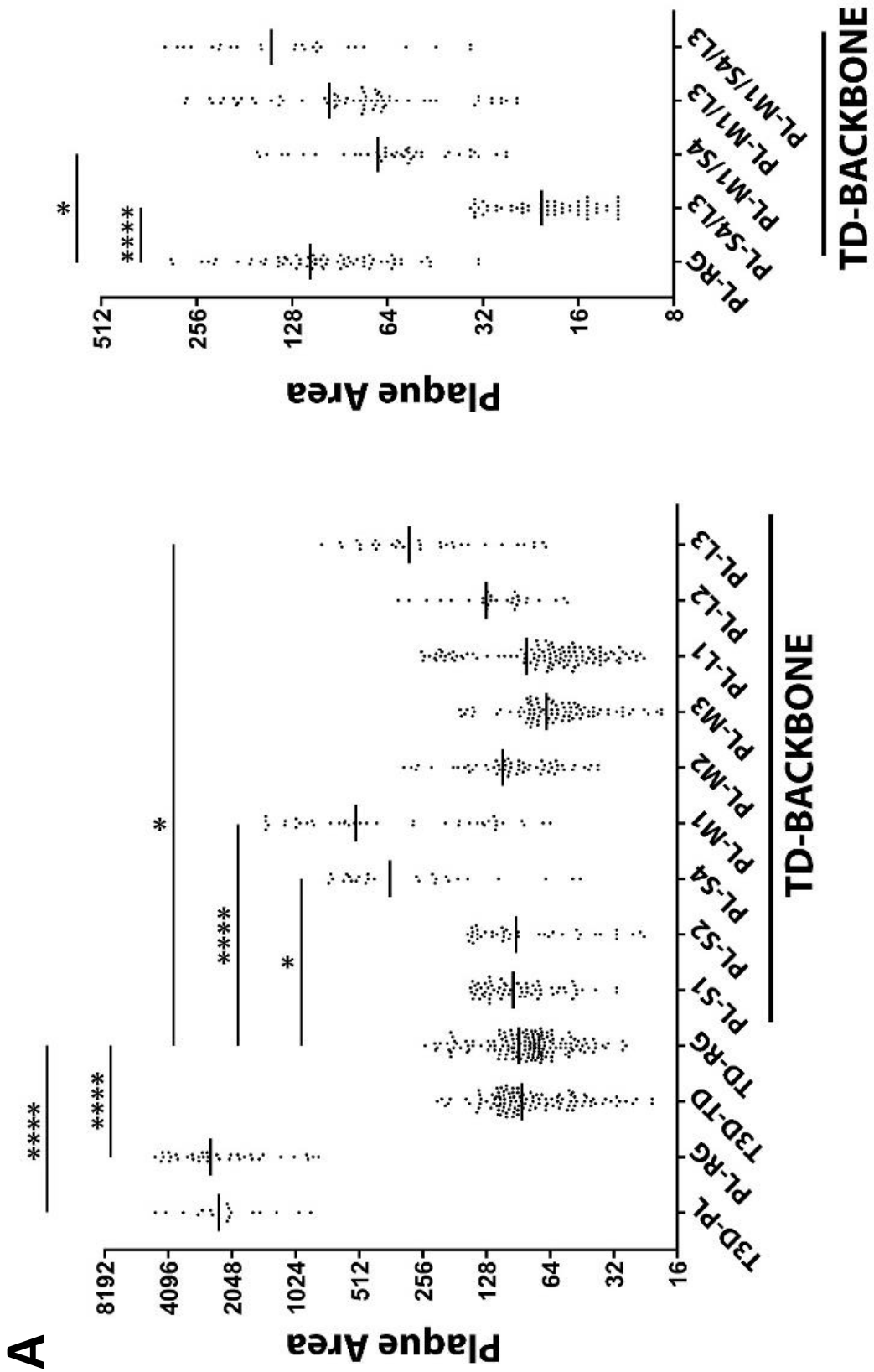
A
Plaque Area
8192
4096
2048
1024
512
256
128
64
32
16
****
****
*
****
*
T3D-PL
PL-RG
T3D-TD
TD-RG
PL-S1
PL-S2
PL-S4
PL-M1
PL-M2
PL-M3
PL-L1
PL-L2
PL-L3
TD-BACKBONE
Plaque Area
512
256
128
64
32
16
8
*
****
PL-RG
PL-S4/L3
PL-M1/S4
PL-M1/L3
PL-M1/S4/L3
TD-BACKBONE

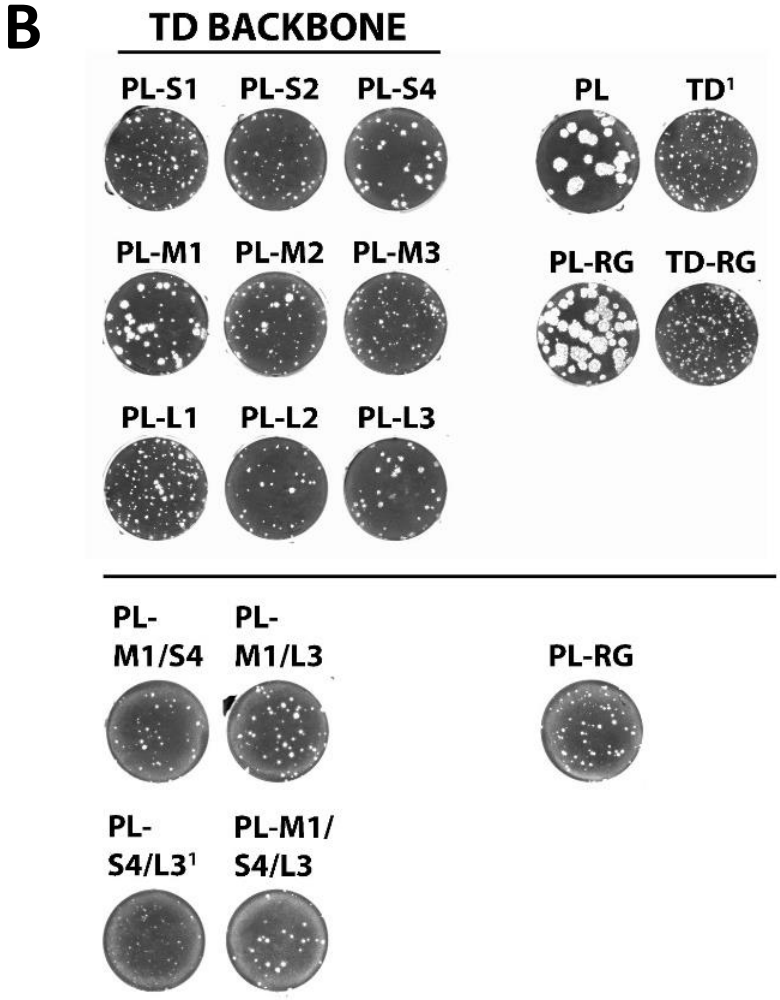

Figure 2.25: PL-M1, PL-S4 and PL-L3 genes segregated with large plaque TD backbone reassortants. BHK/T7-9 cells were transfected with plasmids encoding 10 reovirus gene segments and C3P3. At 5 days post transfection, cell lysates were collected and following 3 freeze/thaw cycles, plaqued onto L929 cells. B) Plaques were visualized following crystal violet staining and A) quantified using ImageQuantTL colony counting add-on. PL and TD are purified laboratory stocks of $T3D^{PL}$ and $T3D^{TD}$, respectively. PL-RG and TD-RG are reverse genetics generated virus lysates of $T3D^{PL}$ and $T3D^{TD}$, respectively. One-way ANOVA with Dunnett's multiple comparisons test, * $p < 0.03$, *** $p < 0.0002$, **** $p < 0.0001$. [1] Set of plaques were stopped when plaques in this well were visible

A

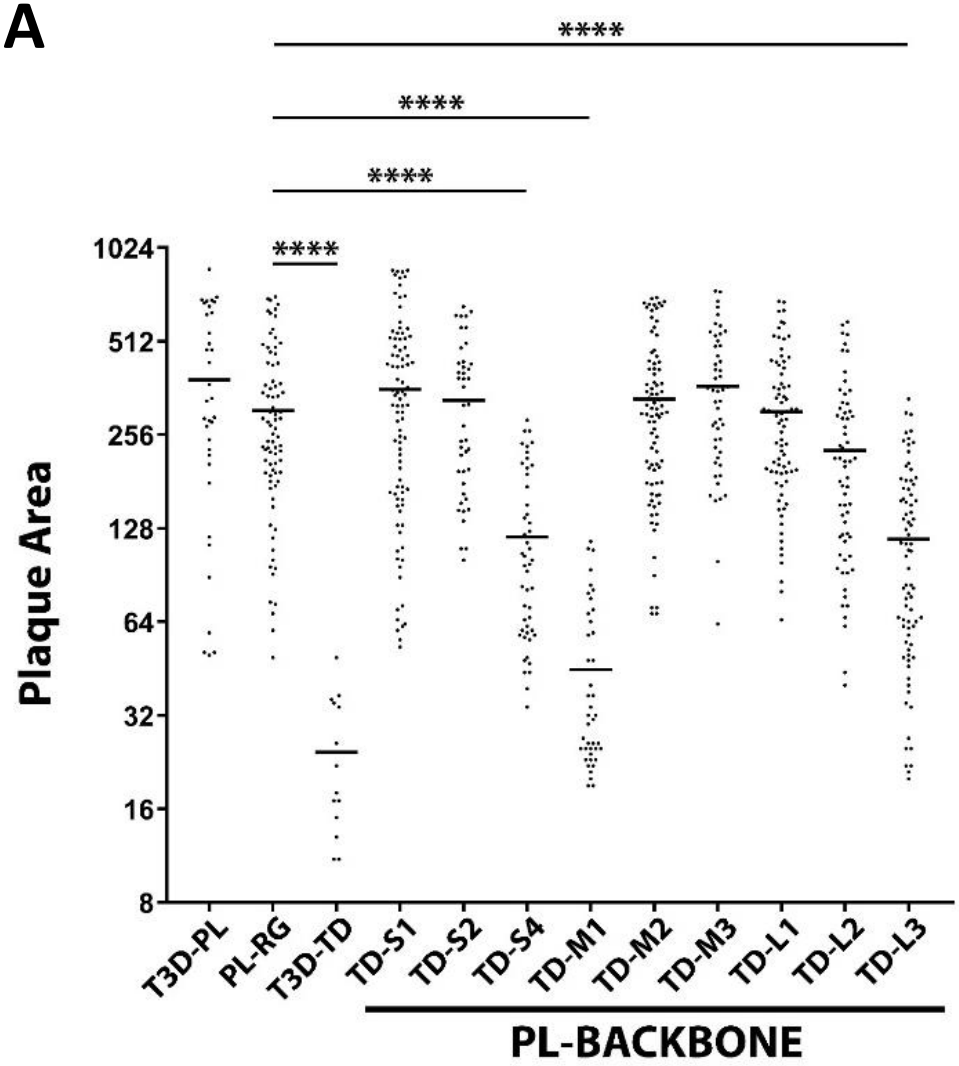
****
****
****
****
1024
512
256
128
64
32
16
8
Plaque Area
T3D-PL
PL-RG
T3D-TD
TD-S1
TD-S2
TD-S4
TD-M1
TD-M2
TD-M3
TD-L1
TD-L2
TD-L3
PL-BACKBONE

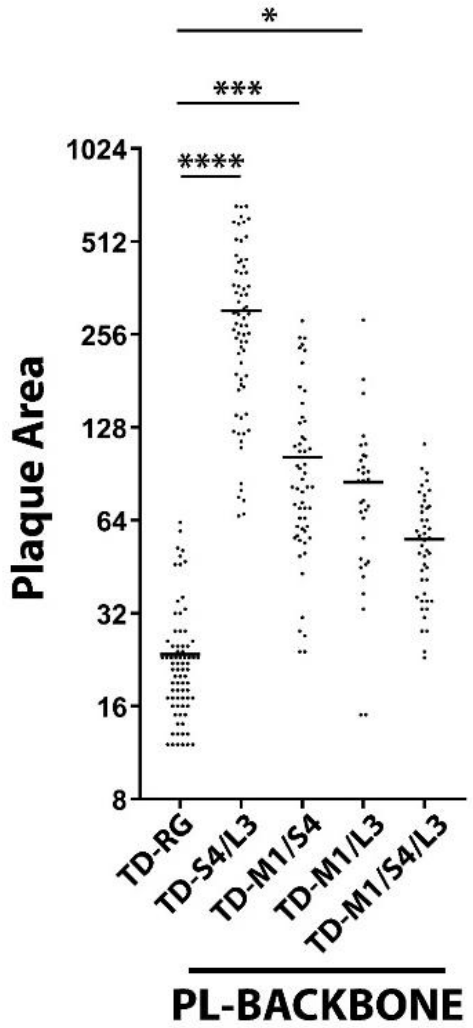
*
***
****
1024
512
256
128
64
32
16
8
Plaque Area
TD-RG
TD-S4/L3
TD-M1/S4
TD-M1/L3
TD-M1/S4/L3
PL-BACKBONE

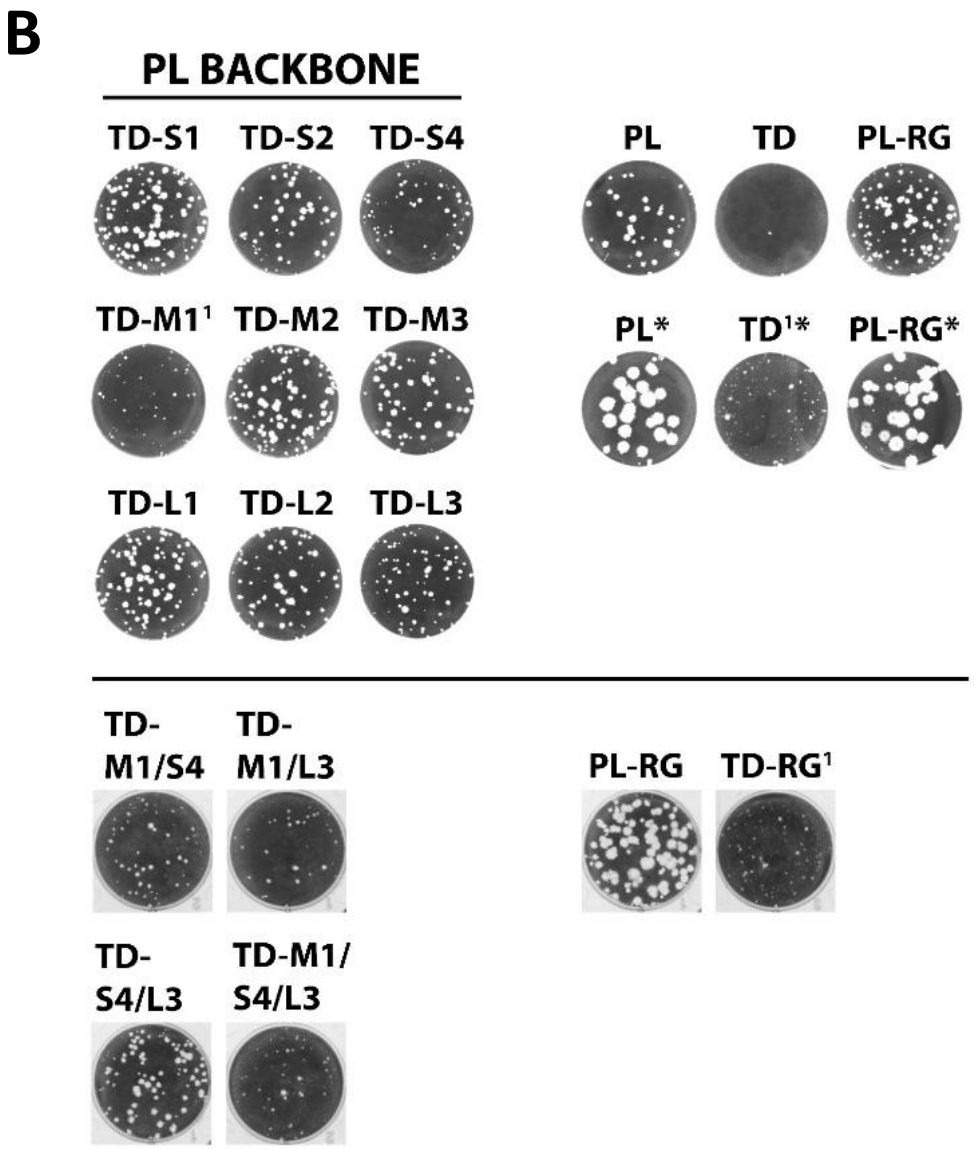

Figure 2.26: TD-S4, TD-M1 and TD-L3 genes segregated with small plaque PL backbone reassortants. A) and B) similar to Fig 2.24. One-way ANOVA with Dunnett's multiple comparisons test, * $p < 0.03$, *** $p < 0.0002$, **** $p < 0.0001$. [1] Set of plaques were stopped when plaques in this well were visible. Since T3D-TD plaques were not visible at 4dpi, plaques indicated with * were stopped at 6dpi to visualize and confirm presence of T3D-TD plaques. One-way ANOVA with Dunnett's multiple comparisons test, * $p < 0.03$, *** $p < 0.0002$, **** $p < 0.0001$.

A

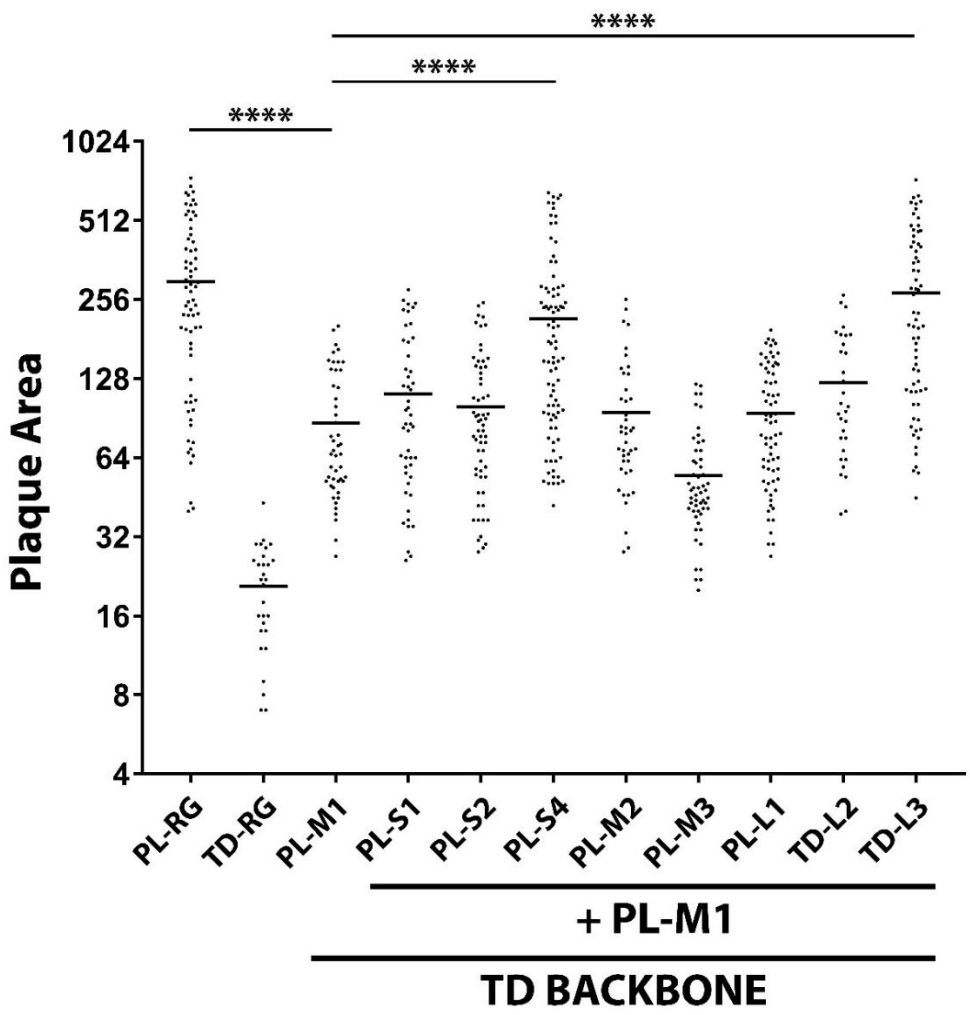
****
****
****
Plaque Area
1024
512
256
128
64
32
16
8
4
PL-RG
TD-RG
PL-M1
PL-S1
PL-S2
PL-S4
PL-M2
PL-M3
PL-L1
TD-L2
TD-L3
+ PL-M1
TD BACKBONE

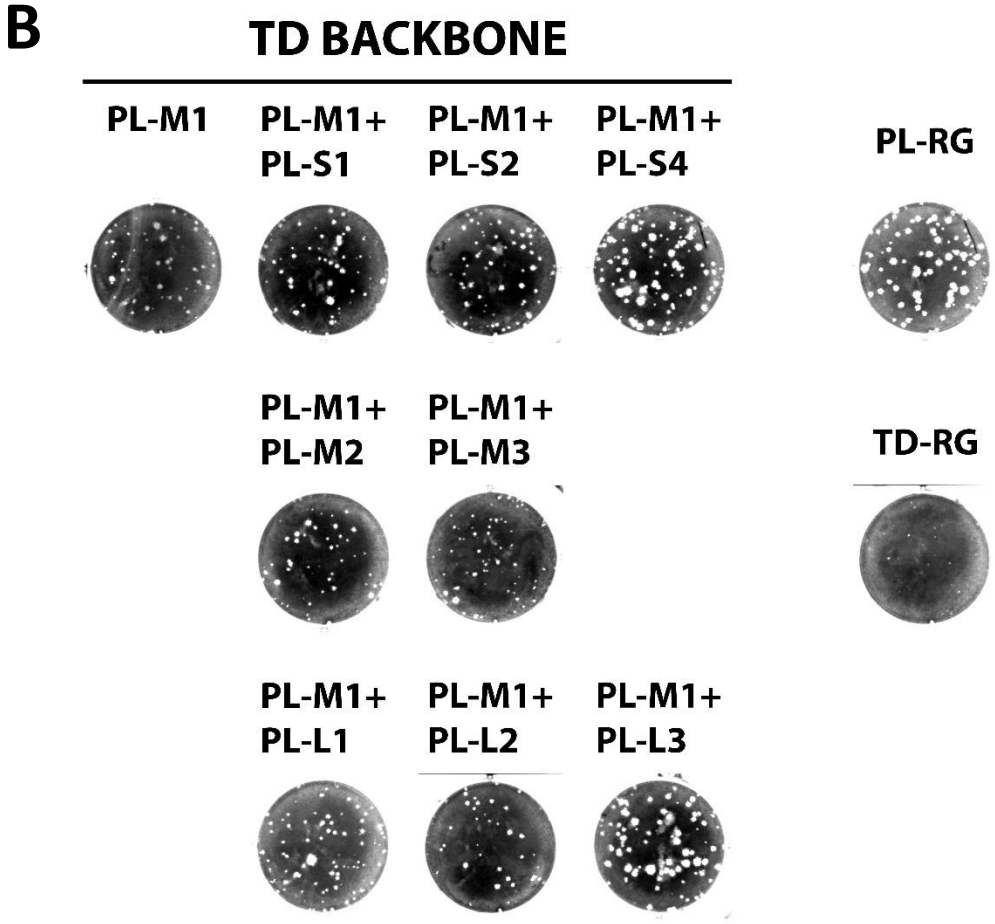

Figure 2.27: Only PL-M1 in combination with PL-S4 or PL-L3, restores PL-RG large plaque phenotype. A) and B) similar to Fig 2.24. One-way ANOVA with Dunnett's multiple comparisons test, * $p < 0.03$, *** $p < 0.0002$, **** $p < 0.0001$.

A

$\sigma 3_3 \mu 1_3$

Side

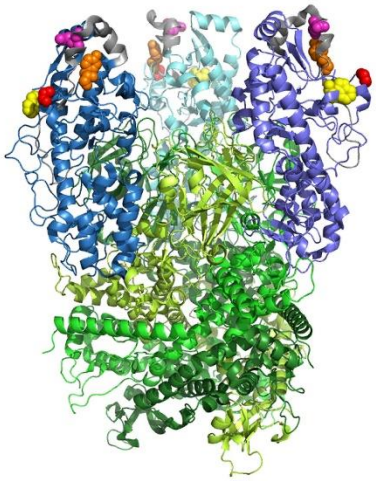

Top

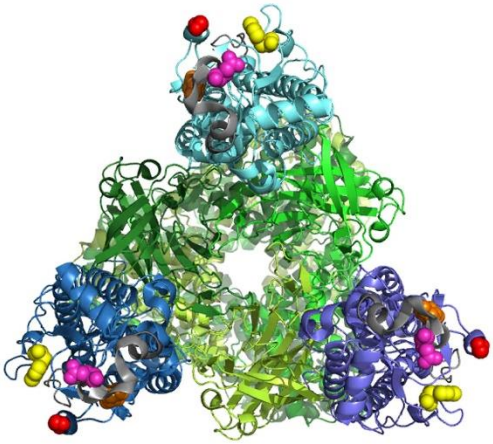

Top: 6-fold axis

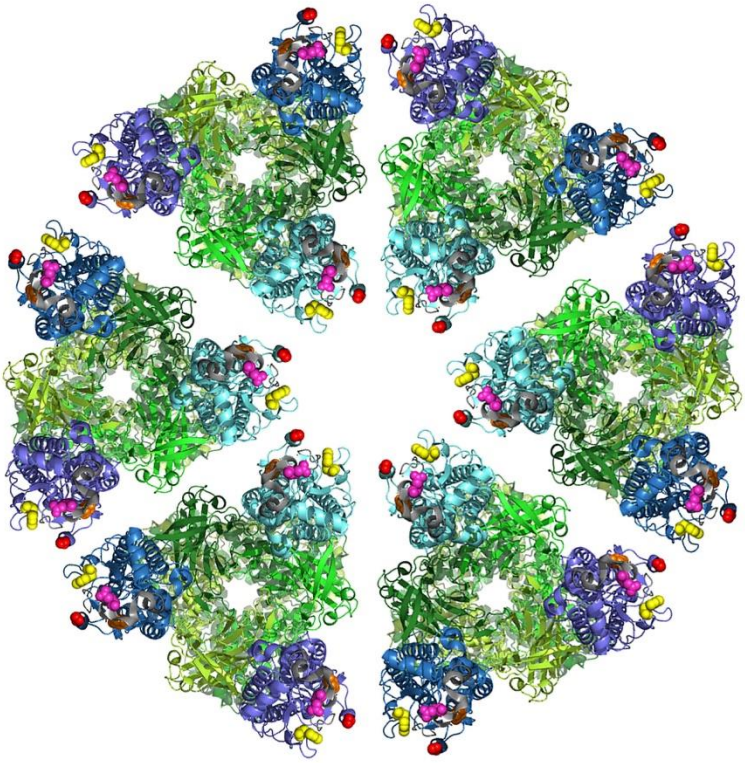

B

$\sigma 3_2$

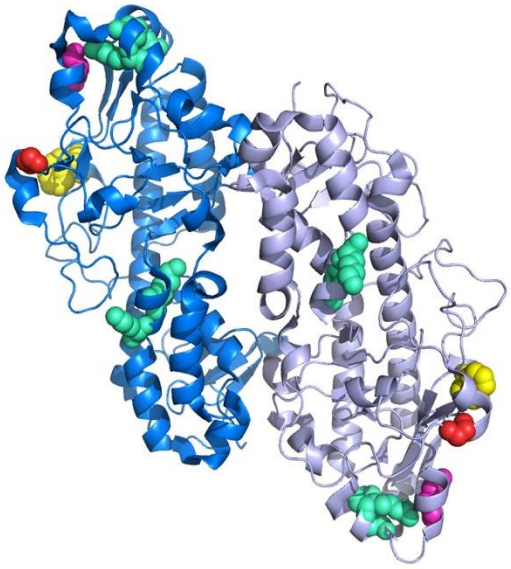

C

$\lambda 1_2 \sigma 2$

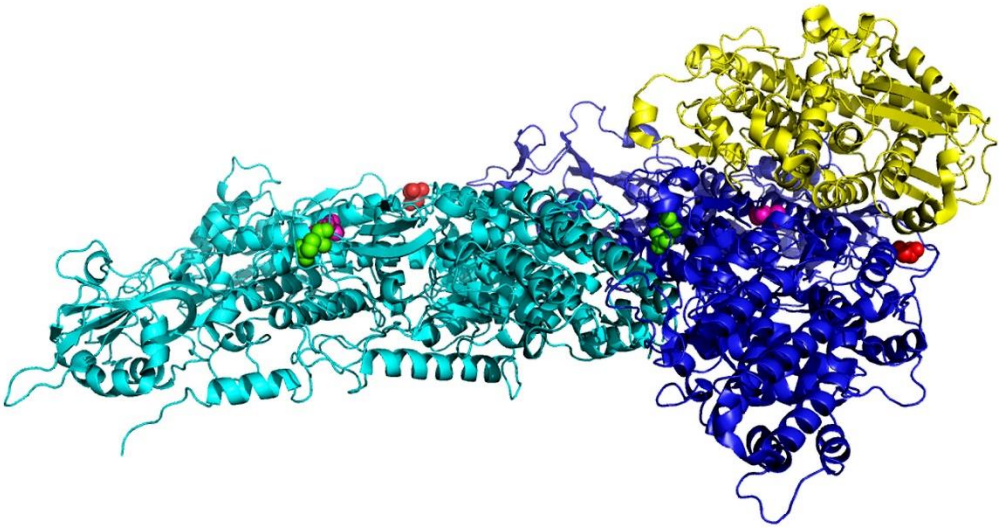

Figure 2.28: Crystal structures highlighting important residues. All structures were visualized and modified using PyMOL. A) $\sigma 3_3 \mu 1_3$ heterohexamer (1jmu.pdb). Ribbons in shades of blue indicate 3 monomers of σ3 and shades of green indicate 3 monomers of μ1. Polymorphisms in σ3 are represented by yellow spheres (W133R), red spheres (G198K), pink (E229D) and orange spheres (Y354H). B) σ3 dimer (1fn9.pdb). Ribbons in shades of blue indicate 2 monomers of σ3. Polymorphisms in σ3 are represented by yellow spheres (W133R), red spheres (G198K), pink (E229D). Regions previously determined to bind dsRNA are indicated in cyan spheres. C) $\lambda 1_2 \sigma 2$ (1ej6.pdb). Ribbons in shades of blue indicate 2 monomers of λ1, and shades of yellow indicate 1 monomer of σ2. Polymorphisms in λ1 are represented by red spheres (I500S), green spheres (8852H) and pink spheres (V1019G).

A

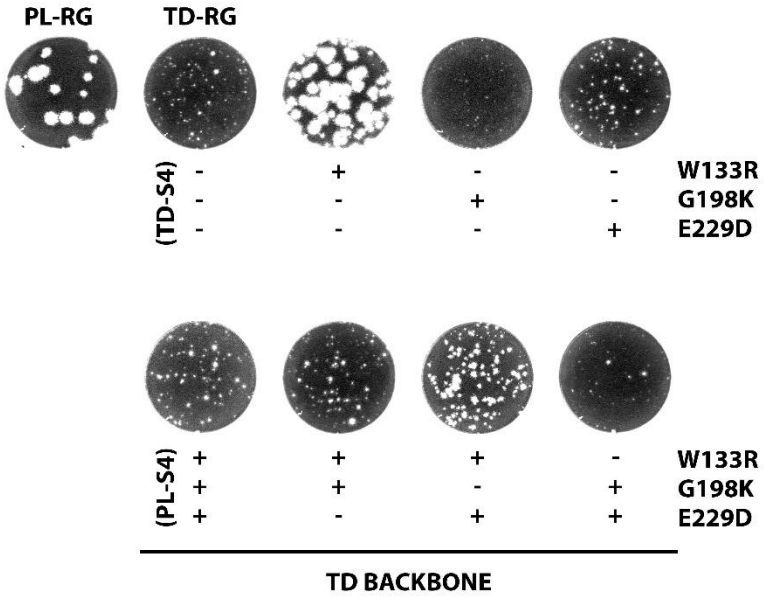
PL-RG
TD-RG
(TD-S4)
W133R
G198K
E229D
(PL-S4)
W133R
G198K
E229D
TD BACKBONE

B

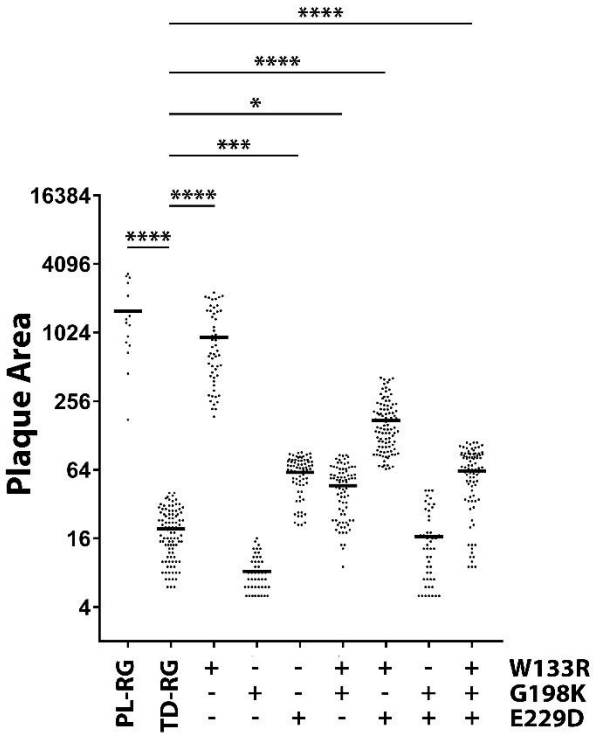
****
****
*
***
****
****
16384
4096
1024
256
64
16
4
Plaque Area
PL-RG
TD-RG
W133R
G198K
E229D

C

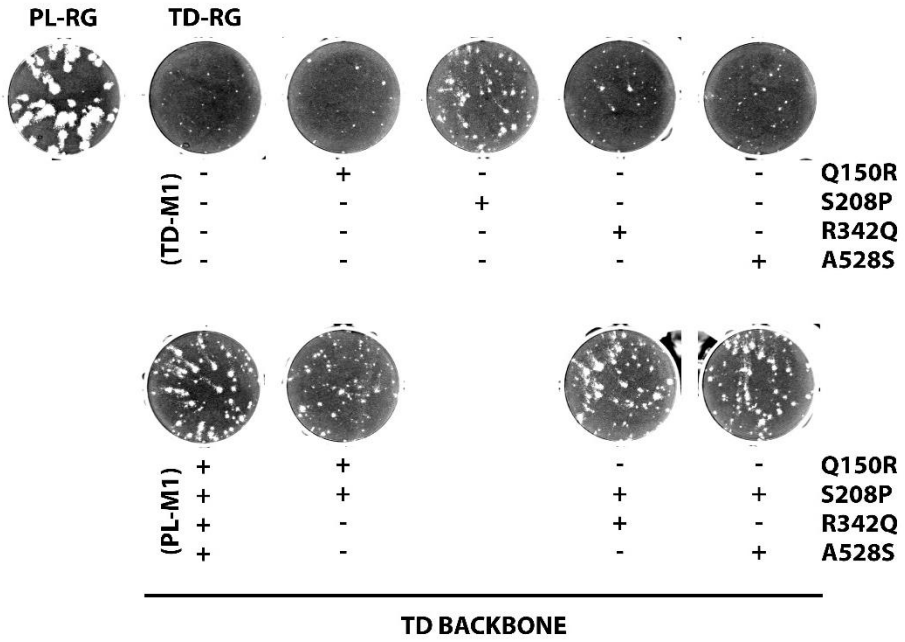
PL-RG
TD-RG
(TD-M1)
Q150R
S208P
R342Q
A528S
(PL-M1)
Q150R
S208P
R342Q
A528S
TD BACKBONE

D

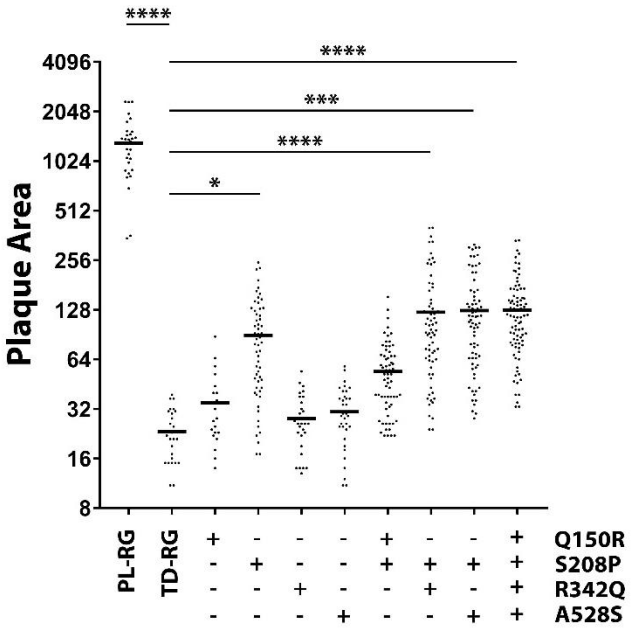
Plaque Area
4096
2048
1024
512
256
128
64
32
16
8
****
****
***
****
*
PL-RG
TD-RG
Q150R
S208P
R342Q
A528S

E

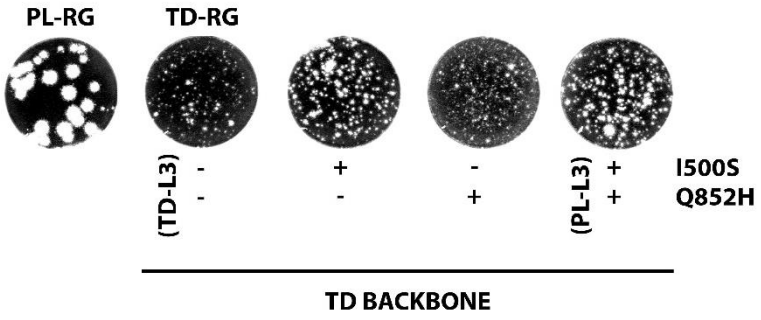
PL-RG
TD-RG
(TD-L3)
- -
+ -
- +
(PL-L3)
+ +
I500S
Q852H
TD BACKBONE

F

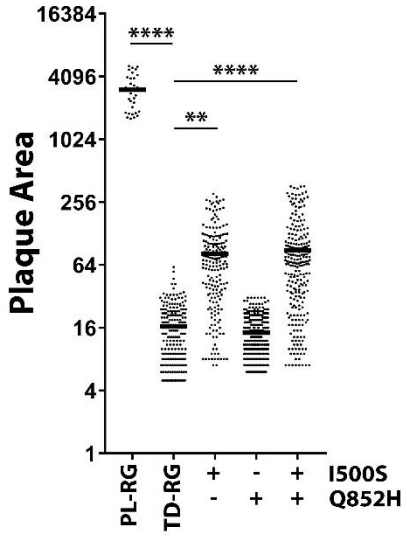
16384
4096
1024
256
64
16
4
1
Plaque Area
****
****
**
PL-RG
TD-RG
+ -
- +
+ +
I500S
Q852H

Figure 2.29: Identifying polymorphisms in S4, M1 and L3 genes that contribute towards T3D-PL large plaque phenotype. T3D-PL polymorphisms were inserted into T3D-TD backbone plasmids using QuikChange II XL Site-Directed Mutagenesis Kit (Agilent Technologies), and modified plasmids were used to generate reverse genetics reassortant. Cell lysates were collected and following 3 freeze/thaw cycles, plaqued onto L929 cells. A), C), E) Plaques were visualized following crystal violet staining and B), D), F) quantified using ImageQuantTL colony counting add-on. One-way ANOVA with Dunnett's multiple comparisons test, * $p < 0.03$, *** $p < 0.0002$, **** $p < 0.0001$.

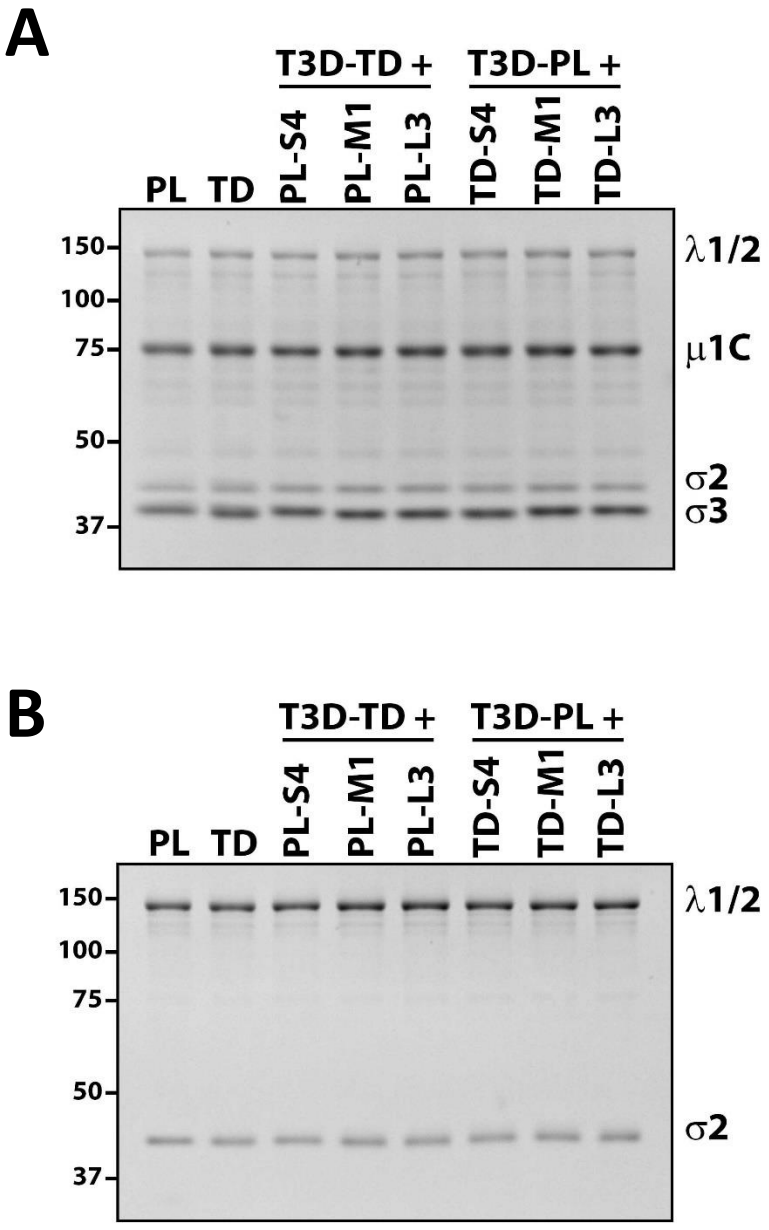
A
T3D-TD +
T3D-PL +
PL
TD
PL-S4
PL-M1
PL-L3
TD-S4
TD-M1
TD-L3
150
100
75
50
37
λ1/2
μ1C
σ2
σ3
B
T3D-TD +
T3D-PL +
PL
TD
PL-S4
PL-M1
PL-L3
TD-S4
TD-M1
TD-L3
150
100
75
50
37
λ1/2
σ2

C

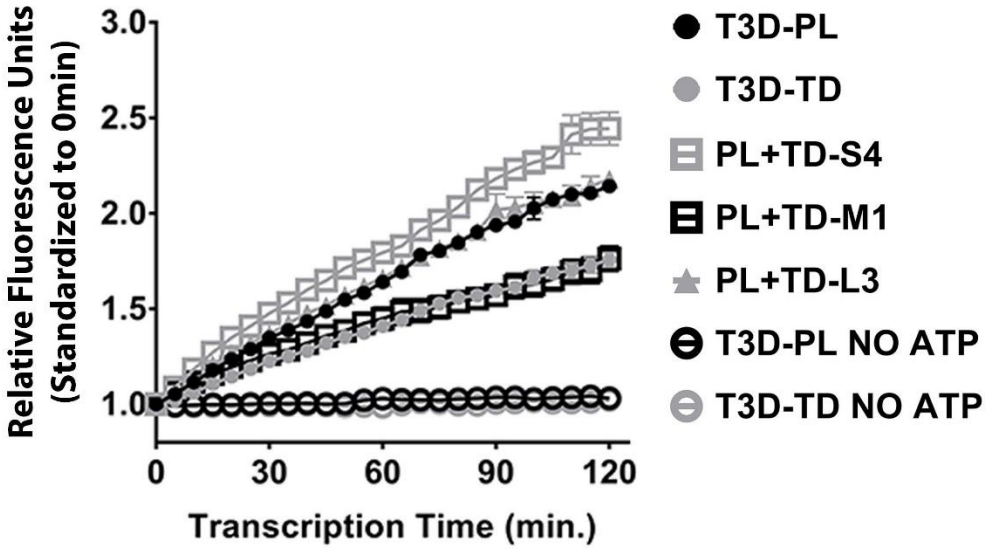
Relative Fluorescence Units
(Standardized to 0min)
3.0
2.5
2.0
1.5
1.0
0
30
60
90
120
Transcription Time (min.)
T3D-PL
T3D-TD
PL+TD-S4
PL+TD-M1
PL+TD-L3
T3D-PL NO ATP
T3D-TD NO ATP

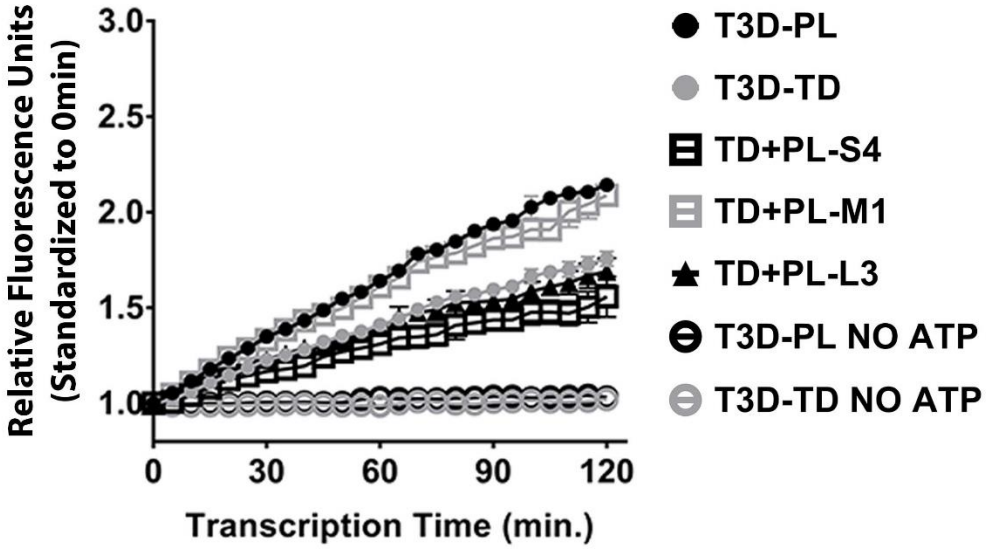
Relative Fluorescence Units
(Standardized to 0min)
3.0
2.5
2.0
1.5
1.0
0
30
60
90
120
Transcription Time (min.)
T3D-PL
T3D-TD
TD+PL-S4
TD+PL-M1
TD+PL-L3
T3D-PL NO ATP
T3D-TD NO ATP

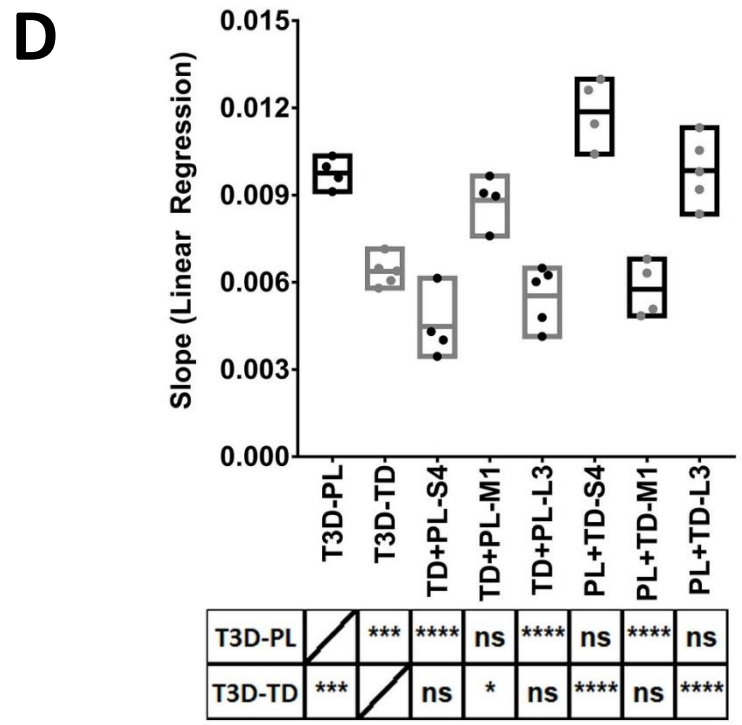

Figure 2.30: The M1 gene is the determinant of core transcriptase differences between T3D-PL and T3D-TD. A) CsCl purified parental $T3D^{PL}$ or $T3D^{TD}$, and S4, M1 and L3 gene monoreassortant $T3D^{PL}$ or $T3D^{TD}$ viruses were denatured in protein sample buffer, separated using SDS-PAGE, and proteins stained using Imperial^{TM} Coomassie stain. B) Viruses used in A) were incubated with chymotrypsin for 2 hours at 37°C. Reactions were stopped with addition of protease inhibitors and viral cores were pelleted with high speed centrifugation (100,000g) for 2 hours at 4°C. Viral cores were resuspended in 100mM Tris pH 8 and stored at 4°C. Proteins were separated and stained similar to A). C) Purified viral cores from B) were added to transcription buffer (with or without ATP), spiked with SYBR green II dye and incubated at 40°C. Fluorescene was monitored in real-time using a Biorad CFX96. D) Linear regression analysis performed on data from C). In D), $n \geq 4$, One-way ANOVA with Tukey's multiple comparisons test, * $p < 0.03$, *** $p < 0.0002$, **** $p < 0.0001$, ns > 0.05

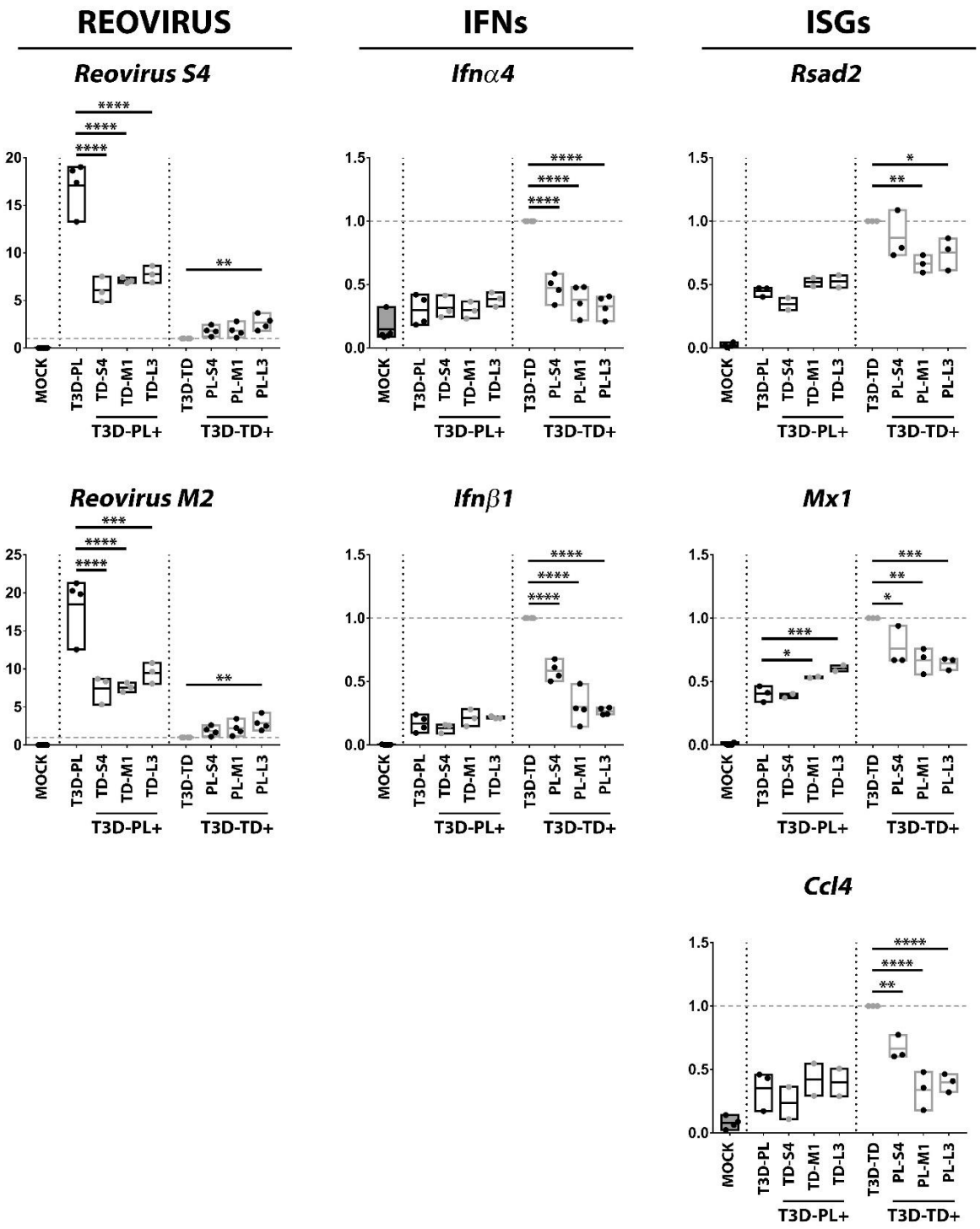
REOVIRUS
IFNs
ISGs
Reovirus S4
Ifnα4
Rsad2
Reovirus M2
Ifnβ1
Mx1
Ccl4
MOCK
T3D-PL
TD-S4
TD-M1
TD-L3
T3D-TD
PL-S4
PL-M1
PL-L3
T3D-PL+
T3D-TD+

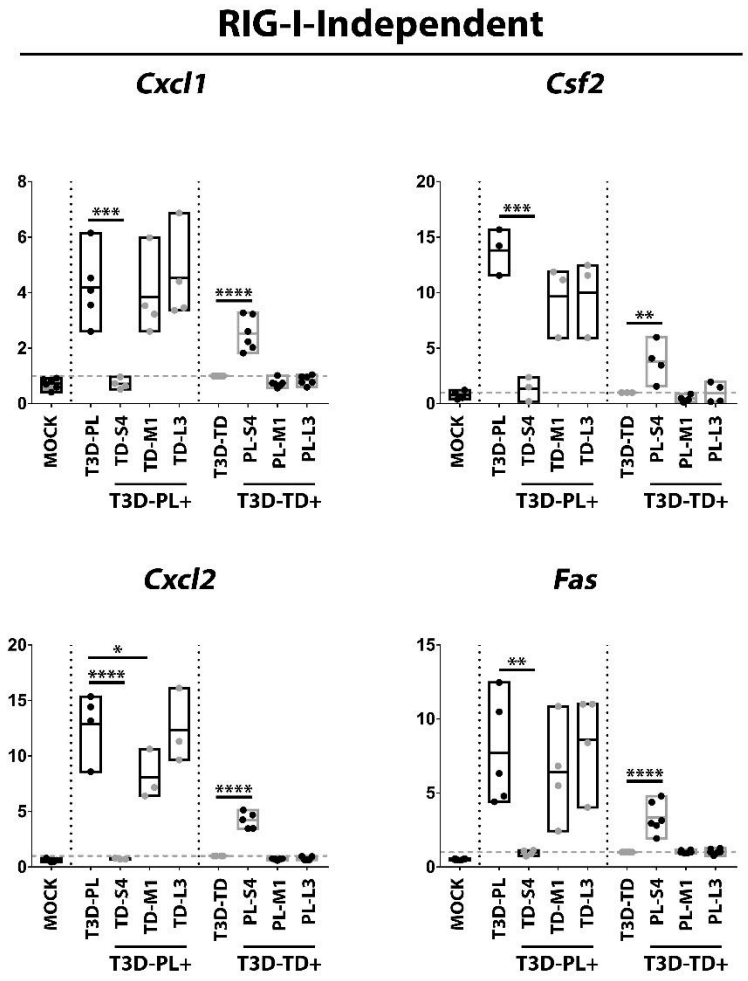

Figure 2.31: The S4 gene is the determinant of IFN-independent gene expression differences between T3D-PL and T3D-TD. Standardized for equal infection, L929 cells were infected with purified parental $T3D^{PL}$ or $T3D^{TD}$, and S4, M1 and L3 gene monoreassortant $T3D^{PL}$ or $T3D^{TD}$ viruses. At 12hpi, samples were collected for RNA extraction, cDNA synthesis and RT-PCR using gene-specific primers (corrected for *GAPDH*). $n \geq 3$, One-way ANOVA with Dunnett's multiple comparisons test, * $p < 0.03$, *** $p < 0.0002$, **** $p < 0.0001$, ns > 0.05

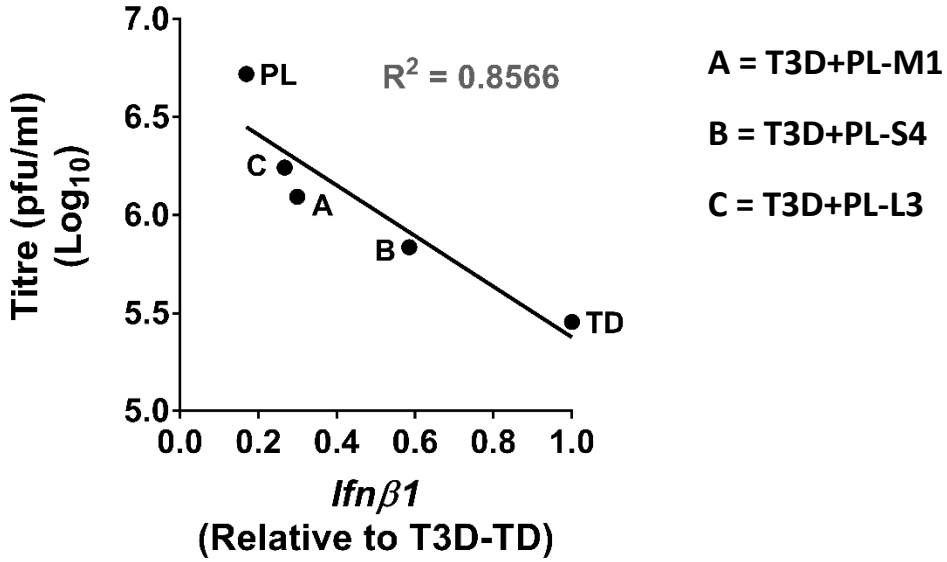

Figure 2.32: Reovirus replication correlates with IFNβ activation. Similar to Fig 2.9, L929 cells were infected with parental $T3D^{PL}$ or $T3D^{TD}$, and S4, M1 and L3 gene monoreassortants in a $T3D^{TD}$ backbone, at a MOI 1. Titres at 12hpi were determined by plaque assay on L929 cells with crystal violet staining. X-axis represents average value of *Ifnβ1* mRNA levels obtained from Fig 2.30.

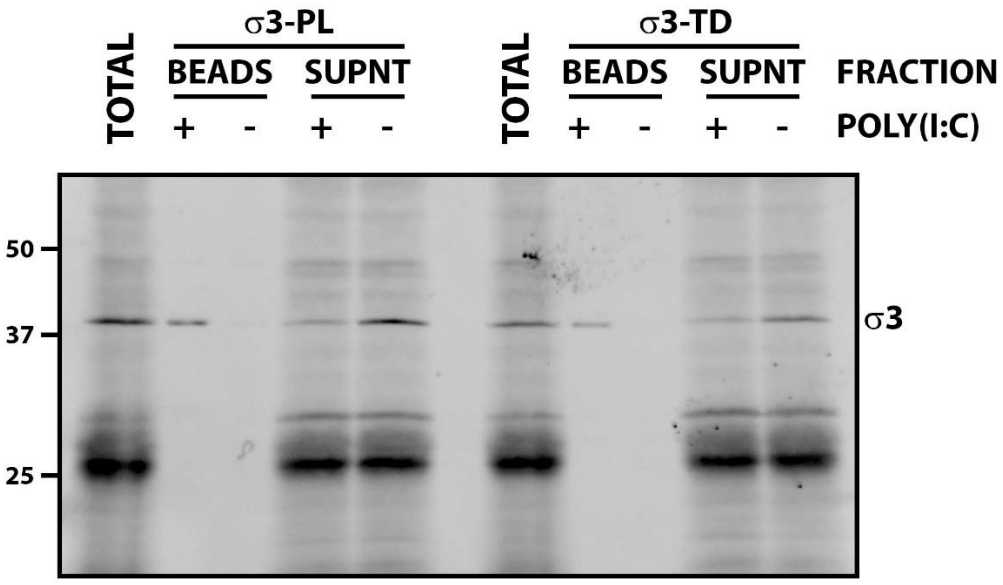

Figure 2.33. T3D-PL and T3D-TD σ3 bind poly(I:C) to similar levels. The TNT® Quick Coupled Transcription/Translation System was used to generate σ3-PL and σ3-TD proteins from PL-S4 and PL-TD plasmids, respectively. TNT® reactions were incubated with respective plasmids for 4hrs at 25°C. Streptavidin conjugated beads were bound to biotin tagged Poly(I:C) (HMW) and incubated with TNT® reactions for 2hrs at 4°C. Supernatant (SUPNT) and bead fractions were separated and Western blot analysis using σ3 specific antibody (mAb 4F2) was performed.

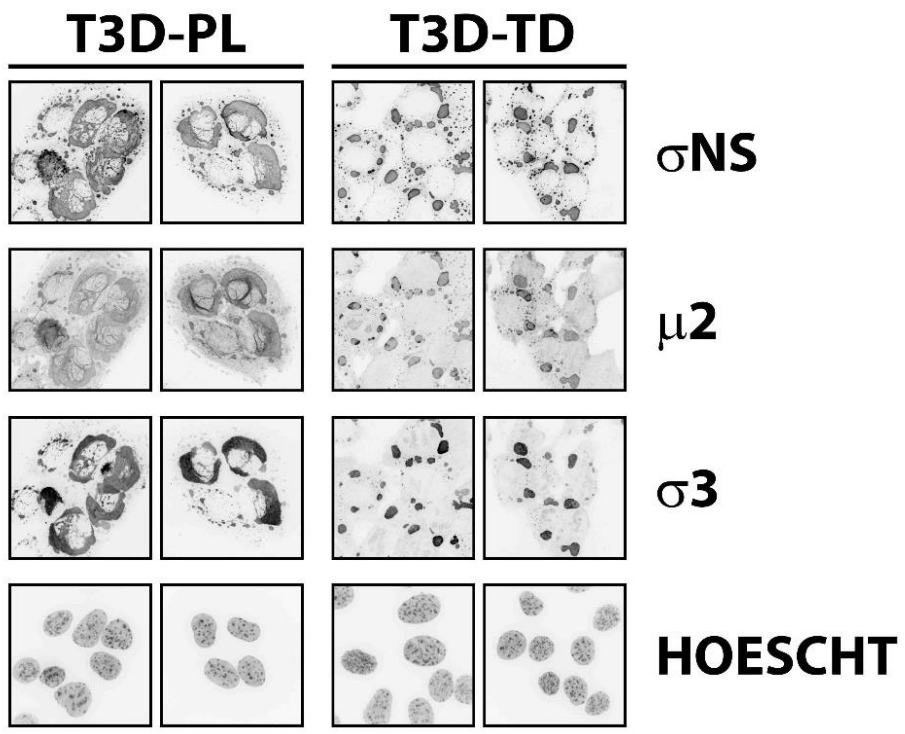
T3D-PL
T3D-TD
σNS
μ2
σ3
HOESCHT

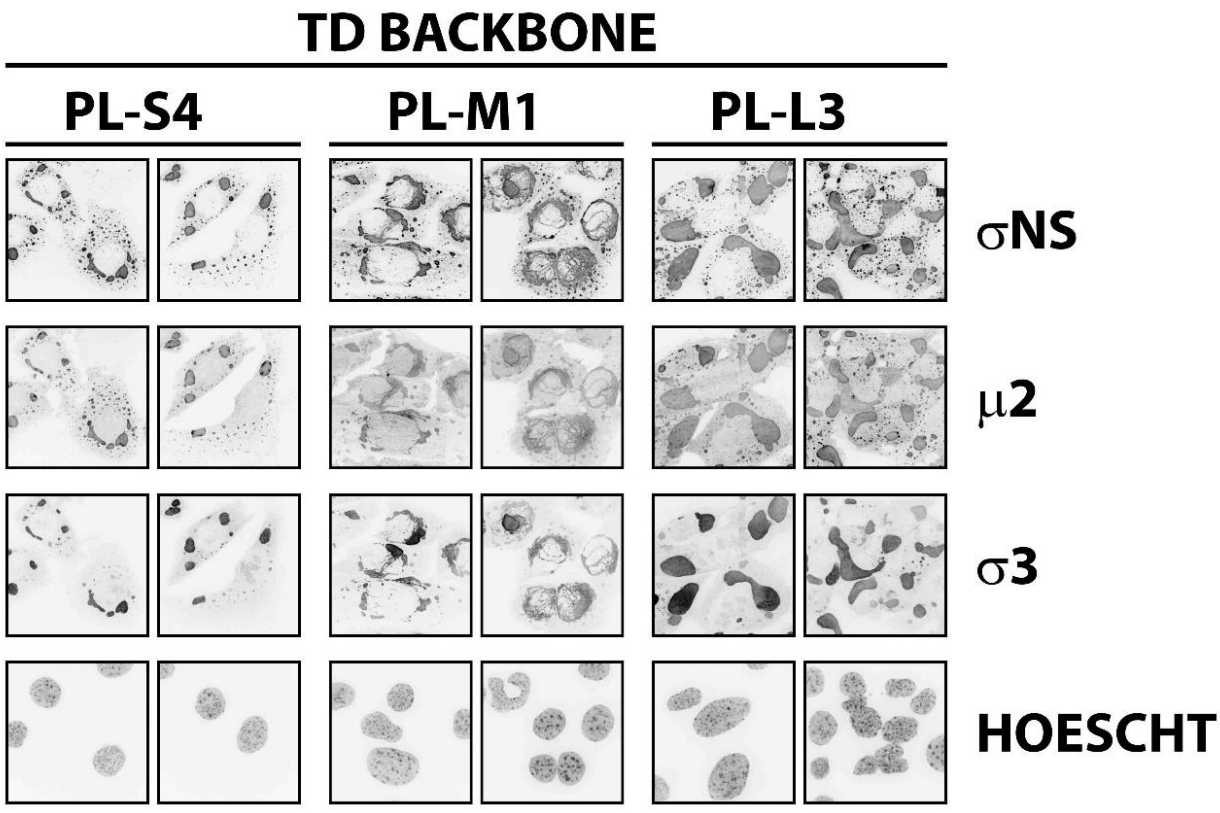
TD BACKBONE
PL-S4
PL-M1
PL-L3
σNS
μ2
σ3
HOESCHT

Figure 2.34: The M1 and L3 genes are determinants of virus factory morphology and size, respectively, differences between T3D-PL and T3D-TD. ID8 cells were infected with parental $T3D^{PL}$ or $T3D^{TD}$, and S4, M1 and L3 gene monoreassortants in a $T3D^{TD}$ backbone, at MOI 3 for 20hpi. Cells were fixed, stained with reovirus protein specific antibodies (σNS mAb , μ2 pAb, σ3 mAb 10G10), and nuclei (HOESCHT 33342), and imaged using confocal microscopy.

	T3DJB		T3D-RH		T3D-SB		T3D-RG	
Gene	Acccession #	Depositor	Acccession #	Depositor	Acccession #	Depositor	Acccession #	Depositor
S1	HM159619.1	John C. Bell	GU991665.1	Rob C. Hoeben	P208810.1	Guy Lemay	EF494441.1	Terence S. Dermody
S2	HM159620.1		GU991666.1		KP208811.1		EF494442.1	
S3	HM159621.1		GU991667.1		KP208812.1		EF494443.1	
S4	HM159622.1		GU991668.1		KP208813.1		EF494444.1	
M1	HM159616.1		GU991662.1		KP208807.1		EF494438.1	
M2	HM159617.1		GU991663.2		KP208808.1		EF494439.1	
M3	HM159618.1		GU991664.1		KP208809.1		EF494440.1	
L1	HM159613.1		GU991659.1		KP208804.1		EF494435.1	
L2	HM159614.1		GU991660.1		KP208805.1		EF494436.1	
L3	HM159615.1		GU991661.1		KP208806.1		EF494437.1	

	T1L-RG		T1L		T2J		T3A	
Gene	Acccession #	Depositor	Acccession #	Depositor	Acccession #	Depositor	Acccession #	Depositor
S1	Addgene #33292	Terence S. Dermody	Ref. 243	Wolfgang K. Joklik	Ref. 243	Wolfgang K. Joklik	GU589583.1	John C. Bell
S2	Addgene #33293		L19774.1	Bernard N. Fields	L19775.1	Bernard N. Fields	GU589584.1	
S3	Addgene #33294		M14325.1	Charles E. Samuel	M18390.1	Wolfgang K. Joklik	GU589585.1	
S4	Addgene #33295		M13139.1	Charles E. Samuel	X60066.1	Aaron J. Shatkin	GU589586.1	
M1	Addgene #33289		X59945.1	Earl G. Brown	AF124519.1	Kevin C. Coombs	GU589580.1	
M2	Addgene #33290		M19345.1	Wolfgang K. Joklik	M19355.1	Wolfgang K. Joklik	GU589581.1	
M3	Addgene #33291		AF174382.1	Max N. Nibert	AF174383.1	Max N. Nibert	GU589582.1	
L1	Addgene #33286		Ref. 244	Wolfgang K. Joklik	M31057.1	Wolfgang K. Joklik	GU589577.1	
L2	Addgene #33287		AF378003.1	Max N. Nibert	AF378005.1	Max N. Nibert	GU589578.1	
L3	Addgene #33288		AF129820.1	Max N. Nibert	AF129821.1	Max N. Nibert	GU589579.1	

	REOLYSIN®		T3D-PL, T3D-MS, T3D-KC, T3D-TD		T3D-PARENT	
Gene	Acccession #	Depositor	Acccession #	Depositor	Acccession #	Depositor
S1	Ref. 291	Matt Coffey	This study	Maya Shmulevitz	NC_004277.1	Wolfgang K. Joklik
S2					NC_004279.1	Wolfgang K. Joklik
S3					NC_004283.1	Yasuhiro Furuichi
S4					NC_004276.1	Aaron J. Shatkin
M1					NC_004280.1	Wolfgang K. Joklik
M2					NC_004278.1	Malcolm A. McCrae
M3					NC_004281.1	Wolfgang K. Joklik
L1					NC_004282.4	Wolfgang K. Joklik
L2					NC_004275.1	Aaron J. Shatkin
L3					NC_004274.1	Max N. Nibert

Table 2.1. Reovirus gene sequence accession numbers.

GENE	PROTEIN	POSITION	T3D-PL, T3D-MS, REOLYSIN®	T3D-TD, T3D-RG	T3D-PARENT	T3D-KC	T3D-JB	T3D-SB	T3D-RH	T3A	T3D-JOKLIK	T3D-CASHDOLLAR
S1	σ1	22	A	V	A	V	V	V	V	I		
		408	A	T	A	T	T	A	A	A		
	σ1s	3	H	Y	H	Y	Y	Y	Y	Y		
S2	σ2	-	-	-	-	-	-	-	-	-		
S3	σNS	-	-	-	-	-	-	-	-	-		
S4	σ3	133	R	W	R	W	W	W	W	W		
		198	K	G	E	G	G	G	G	E		
		229	D	E	E	E	E	E	E	E		
M1	μ2	150	R	Q	R	Q	Q	Q	Q	Q		R
		208	P	S	P	S	S	P	P	P		P
		342	Q	R	Q	Q	Q	Q	Q	Q		Q
		528	S	A	A	A	A	A	A	A		A
M2	μ1	73	D	E	E	E	E	E	E	E		
M3	μNS	180	E	K	E	K	K	E	E	E	E	
		705	V	A	V	A	A	V	A	V	V	
		707	D	G	D	G	G	G	G	G	D	
L1	λ3	979	L	M	M	M	M	M	M	M		
		1045	R	S	S	S	S	S	S	S		
		1048	S	N	S	N	N	S	S	S		
L2	λ2	504	E	G	E	G	G	E	E	E		
		509	R	G	R	G	G	G	G	G		
L3	λ1	500	S	I	I	I	I	S	S	S	S	
		852	H	Q	Q	Q	Q	Q	Q	Q	H	

Table 2.2: Amino acid differences between T3D laboratory strains. Protein sequences were aligned using Geneious® and amino acid differences between $T3D^{PL}$ and $T3D^{TD}$ were identified among other T3D laboratory strain sequences.

2.3 DISCUSSION

2.3.1 History and divergence of T3D laboratory strains

Our findings demonstrate that reovirus T3D laboratory strains differ in their oncolytic capacity both *in-vitro* and *in-vivo*. Genetically, the laboratory strains are highly similar with more than 99% nucleotide sequence similarity amongst them. We identified distinct polymorphisms that segregated with the historical laboratory origin of the strain. Differences among laboratory strains could have arisen from different virus passaging methodologies, or simply by an individual picking an "atypical" plaque during propagations when the original stock was depleted.

Our in-depth genetic analysis of reovirus T3D laboratory strains demonstrated that the original isolate of T3D has diverged into 3 main branches whose roots can be traced to either one of Wolfgang K. Joklik laboratory ($T3D^{PL}$, REOLYSIN®), Bernard N. Fields laboratory ($T3D^{TD}$, $T3D^{KC}$, $T3D^{JB}$) or ATCC ($T3D^{SB}$, $T3D^{RH}$) (Fig 2.22A-D). Upon further investigation, we discovered key differences in reovirus propagation protocols that could potentially account for and explain the observed differences between T3D laboratory strains. As further discussed below, our findings are impactful because they stress the importance of carefully interpreting findings among laboratories with distinct reovirus source, as this can clearly impact virus-host interactions and virus oncolysis.

Selection pressures such as a change is host species, are one of the major drivers of virus adaptation [269]. The initial LLC-MK2 cell propagated isolates of reovirus were found to be non-pathogenic in newborn mice. However, when these initial LLC-MK2 isolates were passaged in mice or used in very high concentrations, pathogenicity in newborn mice was observed [69].

Serotype and inoculation route dependent pathogenesis in newborn mice have been extensively characterized using L929 cell passaged reovirus stocks [270, 271]. It is highly possible that reovirus adaptation in mouse L929 cells altered and biased the pathogenicity of reovirus in *in-vivo* mouse studies [272]. A study published in 1989 from the Bernard N. Fields laboratory recognized discrepancies in the myocarditic capacity between their laboratory T3D strain and previously published T3D studies from other laboratories. They concluded that other laboratories' extensive virus propagation in tissue culture (14-23 passages), high virus inoculum doses and/or differing mouse strains were potential explanations for the observed discrepancies in myocarditic capacity [273]. These are some of the earliest reported differences between laboratory reovirus strains.

Despite early research showing the adaptability of reovirus in L929 cells, subsequent research still used L929 cells since the virion architecture of the T3D variant was similar to that of the original T3D and reovirus studies at the time were primarily focussed on understanding reovirus replication basics rather than host determinants of reovirus replication. The T3D stock obtained by the Wolfgang K. Joklik laboratory in 1967 had already been previously passaged at least 5 times in L cells, and therefore could likely have been a mouse L cell adapted virus stock [274, 275]. The T3D stock of the Bernard N. Fields laboratory originated from the Wolfgang K. Joklik laboratory and was continued to be propagated in L cells, however the reason for its further divergence is unknown [215, 216]. A genetic study in 2004 on the M1 gene from laboratory and environmental reovirus strains concluded that the T3D strain from the Bernard N. Fields laboratory had diverged away from the prototypical T3D strain sometime between 1973 and 1979 [203]. Therefore, laboratory strains of T3D are likely L929 cell adapted, and have further diverged between laboratories.

Given independent divergence of T3D laboratory strains, we sought to determine the divergence of our laboratory $T3D^{PL}$ strain from the earliest published T3D sequences. The first complete sequence of T3D ($T3D^{PARENT}$) was determined as a collaborative effort (NCBI Bioproject PRJNA14861) between the various laboratories working with T3D. S1, S2, S3, M1, M2, M3 and L1 genes were contributed by Wolfgang K. Joklik and affiliated laboratories. S4 and L2 genes were contributed by the Aaron J. Shatkin laboratory, while the L3 gene was contributed by the Max. L. Nibert laboratory. The origin of the T3D stock of Aaron J. Shatkin could not be traced through a literature review. The T3D stock of Max. L. Nibert originated from the laboratory of Bernard N. Fields (Table 2.1). The sequenced T3D stocks were propagated in L cells in all three laboratories; Wolfgang K. Joklik, Aaron J. Shatkin and Max. L. Nibert. Therefore, the earliest available sequences are from T3D stocks repeatedly passaged in L cells. Furthermore, at the time the $T3D^{PARENT}$ genes were sequenced, inter-laboratory reovirus divergence was not recognized. As a result, the individual $T3D^{PARENT}$ gene sequences likely contain laboratory specific genetic variations and should be ideally analyzed as independent sequences rather than sequences from the same virus.

Most laboratories currently studying T3D have inherited their virus stock from a parental laboratory that can be traced back to Wolfgang K. Joklik, Aaron J. Shatkin or Bernard N. Fields. However, a T3D stock is also available through ATCC ($T3D^{ATCC}$). $T3D^{ATCC}$ was deposited by W. Adrian Chappell, a researcher with the Centre for Disease Control and no affiliations with any reovirus publications found in the literature. According to ATCC guidelines, $T3D^{ATCC}$ should be propagated in LLC-MK2 cells [276]. Whether the deposited strain was previously only propagated in LLC-MK2 cells is unknown, but if that was the scenario, $T3D^{ATCC}$ may represent the closest representative stock to the original clinical isolate of T3D propagated only in LLC-

MK2 cells. Upon request, ATCC was not willing to disclose their records on the passage history of their T3D strain (personal communication). Two laboratory T3D strains ($T3D^{RH}$ and $T3D^{SB}$) obtained from ATCC have their complete sequences published. However, $T3D^{RH}$ and $T3D^{SB}$ sequences may not represent that of $T3D^{ATCC}$, since these stocks were propagated, and plaque isolated in alternate cell lines. $T3D^{SB}$ was propagated in the mouse fibroblast L929 cell line while $T3D^{RH}$ was propagated in an adenovirus (79-5789kb) transformed human embryonic retinoblast 911 cell line [277, 278]. Genetic analysis identified 6 silent and 11 missense variations between $T3D^{SB}$ and $T3D^{RH}$, further supporting our proposition of reovirus cell line-dependent adaptation. We recently purchased the $T3D^{ATCC}$ stock and are currently sequencing the virus directly from the original lysate to determine the unadapted sequence of $T3D^{ATCC}$.

Given the previous examples of T3D being propagated in alternate cell lines and potentially unknowingly adapting T3D, in one instance, T3D was intentionally adapted to an alternate cell line. Oncolytic Biotech Inc was established to further pursue and develop initial findings of T3D oncolytic activity from the Patrick Lee laboratory. According to a patent filed by Oncolytic Biotech Inc, REOLYSIN® was isolated following 3 passages in adenovirus (1-4500kb) transformed human embryonic kidney HEK293 cell line, with a large plaque isolated after every passage. The reasoning for HEK293 passaging was to intentionally adapt a mouse L929 cell line propagated T3D strain to better infect human cell lines for optimal oncolytic activity. However, the reported HEK293 adaptation changes were obtained by comparing the REOLYSIN® sequence to T3D gene sequences previously published by other laboratories (Patent# EP2952583A1). It would have been highly beneficial if the T3D sequence used for comparison was obtained prior to HEK293 adaptation, as it currently remains unknown if REOLYSIN is actually different from the original virus obtained from Patrick Lee's laboratory.

Large scale commercial manufacturing of REOLYSIN® is also performed in HEK293 cells, albeit a suspension adapted version. A recent publication by Oncolytic Biotech Inc demonstrated maintenance of REOLYSIN® sequence homogeneity from a single plaque pick to the purified batch culture virus stock, all performed in HEK293 cells [279]. Our T3D laboratory strain ($T3D^{PL}$) originated from the Patrick Lee laboratory and is identical in amino acid sequence to REOLYSIN®. However, there is no evidence in the literature supporting HEK293 passaging of T3D in the Patrick Lee laboratory (in communication with Dr. Patrick Lee). Given the evidence that when propagated at low MOI (1-3) and low passage (1-4) reovirus stably maintains its sequence and that reovirus adapts upon passaging in a different cell line, there remains the possibility that T3D reovirus does not adapt to the HEK293 cell line; although this question could be experimentally investigated [258, 279].

In addition to the evidence gathered from various publications that support the theory that current laboratory stocks of T3D are high passage stocks, we also discovered genetic evidence to support this theory. The $T3D^{PL}$ and $T3D^{PARENT}$ S4 gene that encodes the σ3 outer capsid protein differs at only 3 nucleotide positions; A74G, A624G, T719G. The A74G change is silent while the A624G and T719G changes are missense (Table 2.2). A624G (W133R) represents a major amino acid change from an acidic aspartic acid to a basic lysine. On the other hand, the T719G (D229E) is a conservative change, switching the amino acid from glutamic acid to aspartic acid. By monitoring passaging of T3D (Wolfgang K. Joklik laboratory) in cell culture, it was demonstrated that A74G and A624G S4 gene changes were absent immediately after plaque purification but were introduced with increasing incidence with successive passaging of reovirus [258]. All steps in propagation with our laboratory T3D ($T3D^{PL}$) isolate were performed using low MOI (1-3), hence I suspect that the A74G and A624G (W133R) changes in the S4 gene were

introduced at two possible stages: i) reports of REOLYSIN® (identical to $T3D^{PL}$ and $T3D^{MS}$) being repeatedly passaged with large plaque selection in HEK293 cells and/or ii) our laboratory reovirus isolate was initially obtained from a late passage virus stock.

The S4 gene polymorphisms in A74G and A624G were also observed to have a functional impact on specific virus infectivity and reovirus genome packaging accuracy (discussed later) [258]. Reovirus particle to pfu ratios have been proposed to be influenced by uncoating restrictions imposed by the host cell rather than defects in virions. Supporting this theory are findings that reovirus ISVPs are more infectious that virions and in some instances ISVPs have a 1:1 particle to pfu ratio [232-234]. Our in-house laboratory $T3D^{PL}$ and $T3D^{TD}$ virus stocks had average particle/pfu ratios of 119 and 195, respectively. In the recent (10 years) literature, the particle/pfu ratios of T3D laboratory strains range from 150 to 1000 [257, 280]. These particle/pfu ratios are notably higher than the 60:1 to 2:1 ratios observed for T3D stocks in the late 1980s to early 1990s [127, 281]. We speculated that current T3D laboratory stocks have much lower specific virus infectivity and could potentially implicate the aforementioned S4 gene polymorphisms in A74G and A624G.

2.3.2 Implications of differential immune signaling between $T3D^{PL}$ and $T3D^{TD}$ on *in-vivo* oncolytic potency

Previous studies comparing T3D laboratory strains have characterized differences in viral factory morphology and *in-vivo* dissemination [201, 203, 212]. Prior to our study, replication differences between T3D laboratory strains comparisons ($T3D^{F/N}$ and $T3D^{C}$) had not been observed or reported [211, 213]. Using a plaque assay as an overall assessment of virus replication, we observed that $T3D^{PL}$ formed larger plaques than $T3D^{KC}$, $T3D^{TD}$ and $T3D^{ATCC}$ in

L929 cells, which were used for virus propagation (Fig 2.1A, 2.1B). From an oncolytic virus perspective, $T3D^{PL}$ not only formed larger plaques that $T3D^{KC}$ and $T3D^{TD}$ in a panel of mouse and human cancer cell lines, but $T3D^{PL}$ also demonstrated enhanced *in-vivo* tumor regression relative to $T3D^{TD}$ (Fig 2.1C, 2.2A-C). These results are congruent with our previous findings that plaque size in vitro also correlated with improved in-vivo oncolytic efficacy in vivo for novel $T3D^{PL}$ variants (T3v1 and T3v2), relative to $T3D^{PL}$ [218].

This study presents an interesting conundrum between $T3D^{PL}$ and $T3D^{TD}$. $T3D^{PL}$ has accelerated replication and diminished interferon activation, while $T3D^{TD}$ has retarded replication and enhanced interferon activation (Fig 2.9, 2.10A, 2.10B, 2.12A, 2.12B). The profile of cytokines activated during $T3D^{PL}$ infection are primarily IFN-independent (*Csf2, Cxcl2)* while the $T3D^{TD}$ induced cytokine profile is largely IFN-dependent *(Cxcl10, Ccl4)* (Fig 2.19, 2.21A-C). It is yet unknown whether an IFN-independent or IFN-dependent cytokine profile is more beneficial for stimulating an anti-tumor immune response. Our $T3D^{PL}$ and $T3D^{TD}$ mono-reassortant comparisons identified the S4 gene encoding σ3 protein as being necessary for mediating IFN-independent signaling (Fig 2.31). Therefore, an *in-vivo* comparison between $T3D^{PL}$ with either PL-S4 versus TD-S4 with temporal monitoring of tumor regression, immune cell infiltration and cytokine profiling would hint towards the potential benefits of IFN-independent signaling in oncolytic efficacy. Additional studies in alternate tumor models such as the highly immunogenic 4T1 breast and CT26 colon cancer model systems could decipher the impact of differing immune signaling on $T3D^{PL}$ and $T3D^{TD}$ oncolytic potency [282]. Furthermore, the use of a bilateral tumor model or tumor re-challenge experiments, would amplify the impact of $T3D^{PL}$ and $T3D^{TD}$ stimulation of an anti-tumor immune response.

Combinatorial administration of $T3D^{PL}$ and $T3D^{TD}$ could potentially be utilized to activate both arms of the immune system either together or in a specific order.

2.3.3 Molecular basis for T3D strain-associated differences in innate signaling

Given the role of σ3 in dsRNA binding and PKR signaling, we explored the possibility that differential σ3-dsRNA interactions could explain the distinct $T3D^{PL}$ and $T3D^{TD}$ cytokine signaling [106, 263]. During reovirus infection, σ3 binds dsRNA formed by viral RNA secondary structure and inhibits activation of dsRNA cytoplasmic sensors (RLRs and PKR) [263, 283]. The dsRNA binding activity of σ3 has been mapped to the Zn finger motif (amino acid 51-71) and dsRNA binding domain (amino acid 233-305). Mutations to C51, C45, R236, R239, K291 and K293 diminish dsRNA binding capacity of σ3 [252, 284, 285]. Distinct from the outer capsid heterohexameric $\sigma3_3\mu1_3$ complex, dimers of σ3 have been proposed to contribute towards dsRNA binding [250]. Of the three σ3 residues that differ between $T3D^{PL}$ and $T3D^{TD}$, E229D is positioned adjacent to dsRNA binding residues R236, R239, and could potentially impact σ3 dsRNA binding activity (Fig 2.28B). Preliminary results using streptavidin beads bound to biotin labeled poly(I:C) to immunoprecipitated in-vitro generated σ3 demonstrated a minimal 12% decrease in $T3D^{PL}$-σ3 binding to poly(I:C) relative to $T3D^{TD}$-σ3 (Fig 2.33). The poly(1:C) used in the experiment was a high molecular weight version which constituted of annealed homopolymers of inosine poly(I) and cytidine poly(C) with an average size ranging from 1.5kb to 8kb [286]. Reovirus genes range from 1.2kb to 3.9kb, so the longest possible fragment of secondary RNA structure assuming perfect homology would be 1.95kb, which is highly unlikely [287]. Therefore, the high molecular weight poly(I:C) fragments used were too large to be physiologically relevant and could have resulted in saturation of σ3 binding

capacity. An ideal scenario would utilize reovirus positive sense RNA as the binding template to test if $T3D^{PL}$ and $T3D^{TD}$ differ in their capacity of σ3 in binding viral RNA secondary structure.

Sequestering σ3 away from the cytoplasm and allowing activation of RLRs and PKR could potentially benefit reovirus replication at later stages. When IFN signaling was monitored up to 24hpi, we observed that at later timepoints (18 and 24hpi), *Ifnb1* expression reduced in $T3D^{TD}$ and increased in $T3D^{PL}$, relative to 12hpi. Cells were infected with $T3D^{PL}$ and $T3D^{TD}$ to permit >90% infection, so that IFN signaling at late timepoints would not be a consequence of the second round of replication (Fig 2.13A, 2.13B). The increase in IFN signaling at later timepoints during $T3D^{PL}$ infection could by explained by unavailability of cytoplasmic σ3 due to μ1 complex formation for capsid assembly in viral factories. Additionally, apoptosis induction by PKR signaling at later timepoints could be also beneficial for enhancing $T3D^{PL}$ spread. At later timepoints during $T3D^{TD}$ infection, when sufficient σ3 is available, IFN signaling can be restricted. To further confirm these predictions, $T3D^{TD}$ infection should be monitored for 36-48hpi, to determine if IFN signaling increases again at the end of the $T3D^{TD}$ replication cycle. Novel techniques of monitoring RNA levels (e.g Invitrogen™ PrimeFlow™ RNA Assay) by flow cytometry, would further complement these studies, and enable identification on a per-cell basis of reovirus infected, apopotosis induced and IFN expressing cells.

2.3.4 Impact of S4 gene polymorphisms on virion stability

In addition to its role in dsRNA binding, host signaling and virus genome packaging, the S4 gene encoding σ3 protein is also important in virus stability. The outermost capsid of reovirus is composed of stable heterohexameric $\sigma3_3\mu1_3$ complexes [236, 288]. When exposed to digestive (trypsin, chymotrypsin) or lysosomal (cathepsin B, cathepsin L) enzymes, cleavage of σ3 is

initiated at a protease hypersensitive domain located between amino acids 208-244 [166]. All three σ3 residues (W133R, G198K, E229D) differing between $T3D^{PL}$ and $T3D^{TD}$ mapped very close to the protease hypersensitive domain on the σ3 crystal structure (Fig 2.28A). In L929 cells, intracellular uncoating of σ3 was similar between $T3D^{PL}$ and $T3D^{TD}$ (Fig 2.5A, 2.5B). However, due to limitations of Western blotting, and the overall average assessment of an infected cell lysate, it may have been difficult to detect small changes in σ3 uncoating. As an alternative approach, when we monitored viral uncoating in the presence of CHT, $T3D^{TD}$ and $T3D^{KC}$ had a 2-fold faster rate of σ3 uncoating relative to $T3D^{PL}$ (Fig 2.6A, 2.6B). Therefore, $T3D^{PL}$ σ3 is less sensitive to protease (CHT) cleavage compared to $T3D^{TD}$ and $T3D^{KC}$. An additional experiment using purified Cathepsin B and L instead of CHT will need to be performed to determine if cleavage of $T3D^{PL}$, $T3D^{KC}$ and $T3D^{TD}$ σ3 also differs in the presence of lysosomal proteases.

T3D variants that possess an unstable σ3 outer capsid have been identified from i) persistently infected cells ii) cells infected in the presence of reovirus uncoating inhibitors (E64 pan-cysteine protease inhibitor or ammonium chloride) and iii) T3A σ3 sequence alignment [176, 255-257, 289]. A polymorphism at in σ3 at Y354H was identified as a determinant of σ3 outer capsid stability. The σ3 Y354H residue maps close to the protease hypersensitive domain (Fig 2.28A) and a $T3D^{TD}$ variant with a single site change at σ3 Y354H demonstrated highly diminished capsid stability in the presence of CHT, during intracellular uncoating [257, 289]. The $T3D^{TD}$ σ3 Y354H variant also demonstrated σ3 instability in the presence of heat (55°C), suggesting a potential impact on structural stability rather than protease sensitivity [257]. The σ3 Y354H residue is outside facing and could potentially be important in interaction with neighbouring $\sigma3_3\mu1_3$ complexes. In addition to σ3 Y354H, a second site residue change at σ3

G198E was also observed in some variants [176, 255-257, 289]. The σ3 G198E residue maps adjacent to σ3 Y354H and was observed to have a compensatory effect. Variants that had both σ3 G198E and σ3 Y354H mutations had capsid stability similar to that of parental $T3D^{TD}$.

There have been no reports of σ3 G198E and σ3 Y354H mutations having any impact on $T3D^{TD}$ replication or plaque size [257]. The residues that differ (W133R, G198K and E229D) in σ3 between $T3D^{PL}$ and $T3D^{TD}$ are outward facing and solute accessible, similar to Y354H, and could potentially alter protease accessibility and sensitivity. When $\sigma3_3\mu1_3$ complex crystal structures were aligned in a six-fold axis resembling the outer capsid, the W133R and G198K variations were located in regions that have the capacity to interfere with σ3 – σ3 interactions (Fig 2.28A). Based on our single-site studies, we observed that σ3 W133R variant had a large plaque phenotype which was reduced when combined with G198K and/or E229D. The G198K had a greater reduction on W133R plaque size compared to E229D (Fig 2.29A, 2.29B). Given the findings from the σ3 Y354H and G198E studies, we could hypothesize that G198K and E229D could also act as stabilizing compensatory mutations specific to the destabilizing W133R. Since reovirus intracellular uncoating is a rate-limiting step during infection, the large plaque phenotype of $T3D^{TD}$+PL-S4-W133R could potentially be the consequence of an unstable outer reovirus capsid. Future experiments could focus on assessing capsid stability of σ3 W133R in combination with G198K and E229D in the presence of proteases, heat and low pH.

2.3.5 Contributions of M1 gene polymorphisms on viral factories

Reovirus factories have been shown to exhibit either globular or filamentous morphology. Except for T3D laboratory strains originating from the Bernard N. Fields laboratory (e.g $T3D^{N}$, $T3D^{F}$, $T3D^{TD}$, $T3D^{KC}$) and 1 human clinical isolate (T3C12), that form globular

factories, all other reovirus isolates, irrespective of serotype, form filamentous factories. The M1 gene encoding μ2 protein is the determinant of viral factory morphology. Specifically, the proline to serine polymorphism at amino acid position 208 dictates microtubule association of μ2 [201, 203]. In one report, a leucine to proline polymorphism at amino acid position 383 in μ2 was capable of determining factory morphology. Interestingly, the L383P variant was not present in any laboratory of environmental isolates but was rather identified from a cDNA plasmid clone of T1L M1 gene that differed in sequence from the parental T1L M1 sequence from the same laboratory, at positions L383P and F302L [204]. Whether the L383P variation was introduced during the cloning process or selected for during a different step is yet unknown.

One hypothesis would simply be that filamentous factories are determinants of enhanced $T3D^{PL}$ replication relative to $T3D^{TD}$ globular factories. The importance of filamentous versus globular factory morphologies during reovirus replication remains controversial. Microtubule depolymerizing agents (e.g nocodazole, vinblastine, colchicine) inhibit cellular microtubule formation and have been used to study the role of microtubules during reovirus infection. The consistent trend across multiple laboratories is that in the presence of microtubule depolymerizing agents, filamentous viral factories are disrupted and form globular factories, while globular viral factories remain globular but increase in number and reduce in size [198, 205, 210, 290]. However, inconsistencies have been observed with respect to virus replication. While some studies show evidence that microtubule disrupting agents reduce virus replication in both T3D and T1L, some studies do not observe any differences in virus replication upon treatment with microtubule disrupting agents [198, 210, 226, 291].

Since microtubules have also been shown to be important for virus entry and vesicle trafficking, reduction in virus infectivity following treatment with microtubule disrupting agents

cannot be directly associated with observed changes in viral factory morphology. In our studies, μ2 was a major determinant of plaque size differences between $T3D^{PL}$ and $T3D^{TD}$. We linked μ2 to having a role in viral core transcriptase activity and being a determinant of viral factory morphology (Fig 2.30C, 2.30D, 2.34). Additionally, of the four (R150Q, P208S, Q342R, S528A) μ2 polymorphisms between $T3D^{PL}$ and $T3D^{TD}$, the P208S polymorphism had the greatest individual impact on plaque size (Fig 2.29C, 2.29D). It was previously observed that the μ2 P208S polymorphism did not impact virus replication, in a similar $T3D^{TD}$ background, initial MOI and L929 cell line, as our experiment [204]. In our studies, the plaque size of $T3D^{TD}$+PL-M1 and $T3D^{TD}$+TD-M1+P208S were similar in size to each other and were both larger than $T3D^{TD}$ (Fig 2.29C, 2.29D). Viral titres at 12hpi in $T3D^{TD}$+PL-M1 were higher than $T3D^{TD}$ (Fig 2.32), however we will need to perform viral growth curves with the individual μ2 polymorphisms in order to specifically associate P208S to the observed increase in plaque size.

2.3.6 Contributions of μ2 and λ1 on viral core NTPase activity

Most functional characterizations of μ2 have been performed using T1L and T3D strains originating from the Bernard N Fields laboratory. Studies elucidating the function of μ2 as a NTPase and its role in viral RNA transcription have used the observation of a temperature-dependent difference between the functions of T1L μ2 and T3D μ2. Specifically, the NTPase activity and viral transcriptase activity of T1L and T3D viral cores segregated with the M1 gene in a temperature dependent manner [192, 266]. These studies were published prior to the observation that the M1 gene from $T3D^{N}$ (Bernard N. Fields laboratory strain) was a temperature sensitive variant [260]. A follow up study using a baculovirus expression system, purified T1L μ2 was shown to have NTPase activity, albeit still in a temperature dependent manner, suggesting that μ2 does indeed have NTPase activity [265]. However, since μ2 associates with

microtubules and is a major component of viral factories, we cannot exclude the possibility that the NTPase activity of μ2 is not virion associated and performs its NTPase function in the context of cellular cytoskeleton rearrangement and/or cell signaling. Therefore, the enzymatic properties currently assigned to μ2 in the viral core (NTPase and viral transcriptase activity) could potentially be due to the temperature sensitive nature of μ2 rather than the true function of μ2. Validation of these finding using a non-temperature sensitive T3D strain (e.g $T3D^{PL}$) need to be performed.

The L3 gene encodes the λ1 protein, which in addition to being the major core capsid protein, is capable of binding dsRNA, has NTPase, RTPase and helicase activity [119, 193, 267, 268, 292, 293]. Unlike μ2, the λ1 sequence contains motifs that closely resemble prototypic RNA helicases and NTPases [267]. T1L and T3D reassortant viral core analysis identified that λ1 segregates with differential NTPase activity [193]. These studies also observed temperature dependent NTPase activity differences between T1L and T3D cores [193, 267, 268]. However, the temperature (35°C) used in these NTPase studies had previously been shown to produce similar T1L and T3D core transcriptase activities [266]. Therefore, the λ1 NTPase activity was independent of differential T1L and T3D core RNA transcriptase activity. Additional studies using yeast purified λ1 demonstrated *in-vitro* helicase activity, NTPase activity and specific RTPase activity at the 5'-γ-phosphate of triphosphate end-terminated RNAs [267, 268]. In agreement with the sequence, function, structure and localization of other similar viral proteins, λ1 has been proposed to act as a viral core RNA helicase and serve as a terminal GTPase prior to mRNA capping by the λ2 pentameric complex. Our studies did not identify λ1 as a determinant of enhanced $T3D^{PL}$ viral core transcriptase activity, implying a potential non-NTPase λ1 functional difference between $T3D^{PL}$ and $T3D^{TD}$.

2.3.7 Contributions of L3 gene polymorphisms on viral factories

Apart from the proposed core NTpase activity of λ1, functions outside of the viral core have yet to be identified. A temperature sensitive λ1 mutant was previously isolated and characterized. At the restricted temperature (37°C), the temperature sensitive λ1 mutant formed small viral factories with structures resembling abnormally assembled virus particles lacking an outer capsid [294, 295]. The σ2 protein also constitutes the viral core and functions as a clamp for the λ1 capsid. Based on the viral core crystal structure, the temperature sensitive mutation (V1019G) was located at the interface between λ1 and σ2 and was therefore proposed to interfere with correct assembly of viral cores at the restricted temperature (37°C) [294, 295]. In our studies, the L3 gene was one of three genes that segregated with the observed replication differences between $T3D^{PL}$ and $T3D^{TD}$ (Fig 2.23A, 2.23B, 2.25A, 2.25B, 2.26A, 2.26B). Of the two missense amino acid (S5001, H852Q) changes between $T3D^{PL}$ and $T3D^{TD}$, S500I was found to be the important λ1 plaque size determinant. The location of S5001 on the viral core crystal structure was at the interface between λ1 and σ2 (2.29E, 2.29F) and can be predicted to have an impact on viral core assembly and/or stability, similar to the previously identified temperature sensitive mutant (V1019G). Interestingly, when assessing virus factory morphology, there was a striking increase in virus factory size in $T3D^{TD}$+PL-L3 relative to $T3D^{TD}$ (Fig 2.34). It would be valuable to delineate the mechanism by which λ1 mediated viral factory size.

Finally, the crystal structures available were extremely useful in localizing the variations between $T3D^{PL}$, $T3D^{TD}$, and predicting their potential structural impact. However, I felt it is important to point out that the virus strain/serotype for the crystal structures, as this could alter the proposed variation impact; heterohexameric $\sigma3_3\mu1_3$ (T1L), $\sigma3_2$ ($T3D^{N}$), $\sigma2_2\lambda1_2$ ($T3D^{N}$).

In conclusion, we have identified and characterized previously unreported replication differences among T3D laboratory strains. Relative to $T3D^{TD}$, $T3D^{KC}$ and $T3D^{ATCC}$, our $T3D^{PL}$ laboratory strain had enhanced replication in various cell lines *in-vitro*. In an *in-vivo* tumor model, $T3D^{PL}$ demonstrated improved tumor regression compared to $T3D^{TD}$. Since $T3D^{PL}$ was identical in amino acid sequence to the clinically relevant REOLYSIN®, oncolytic research performed by laboratories using strains other than $T3D^{PL}$ should be cautious in suggesting concluding relevance to REOLYSIN®. An in-depth characterization between $T3D^{PL}$ and $T3D^{TD}$ identified S4, M1 and L3 genes as genetic determinants of replication differences. Furthermore, sequence analysis suggested a historical divergence of T3D laboratory strains.

CHAPTER 3: ROLE OF P38 MAPK SIGNALING DURING REOVIRUS INFECTION

3.1 RESULTS

3.1.1 P38 MAPK signaling promotes establishment of reovirus infection

Several viruses have been demonstrated to activate the p38 MAPK stress-induced signaling pathway during infection. The role of p38 MAPK during virus infection can either be restricting or promoting, and depends highly on the virus and context in question [239, 296-299]. Previous studies observed that during reovirus infection of A549 human lung cancer cells, inhibition of p38 MAPK signaling suppressed IFN production and enhanced reovirus spread at 72 hours post-infection (hpi) [239]. It was also observed that inhibition of p38 MAPK signaling diminished reovirus replication in constitutively-active Ras transformed NIH/3T3 cells at 48hpi [300]. However, no studies have assessed the role of p38 MAPK in reovirus replication during a single round of infection. One round of reovirus replication is complete in approximately 24 hours, with progeny virus production commonly saturated by 12-15hpi and cell death (virus release) maximal at 18-24hpi. To understand the role of p38 directly on reovirus replication, we therefore focused on the previously unstudied role of p38 MAPK during the initial 12hrs of reovirus replication. In previous studies using NIH/3T3 cells, reovirus infection at 12hpi was associated with increased levels of phosphorylated p38 MAPK (P-p38) [239], although these studies did not exclude potential effects of other stress-inducing conditions during infection such as temperature or media change. Hence, we first assessed whether reovirus infection directly induces P-p38, using the tumorigenic L929 mouse fibroblast cell line, which is the most common susceptible cell line for reovirus studies. L929 cells were exposed to reovirus without change of media or temperature, and collected at 12hpi for assessment of P-p38 by Western blot analysis.

The reovirus dose used for infections was determined by immunocytochemistry to infect most (>80%) of the cells and ensure the phenotypes observed were primarily due to reovirus infected cells and not due to the response from uninfected cell population (Fig 3.4A; MOI 3). Reovirus infection produced a minimal increase in P-p38, and downstream signalling targets p-MSK1 (mitogen and stress activated protein kinase 1), p-MNK1 (MAP kinase-interacting serine/threonine-protein kinase 1), p-eEF2 (Eukaryotic elongation factor 2), and p-ATF2 (Cyclic AMP-dependent transcription factor 2) (Fig 3.1A; compare lane 1 and lane 5). There was however basal phosphorylation (activity) of p38 and downstream kinases that could affect reovirus replication (Fig 3.1A).

Given that basal activity of p38 MAPK was noted during reovirus infection, and that p38 MAPK is known to affect replication of other viruses [239, 296-299], we sought to determine if p38 MAPK signaling also influences reovirus replication. To manipulate p38 MAPK activity we applied compounds commonly used in p38 MAPK studies; p38 MAPK inhibitors (SB202190, SB203580, BIRB796), inactive p38 MAPK inhibitor analogue (SB202474), and a global MAPK activator (anisomycin). Since DMSO was a diluent for the various compounds, DMSO treatment was used as a negative control, and added at a similar volume as the compound. The p38 MAPK inhibitors SB202190 and SB203580 bind to p38 MAPK isoforms p38α and p38β and interrupt the ATP-binding active site but not the phosphorylation site [301]. Hence, p38α and p38β phosphorylation can still occur but downstream target phosphorylation is inhibited. Anisomycin activates MKK3/6 and MKK4/6, upstream kinases of p38 and JNK MAPK, respectively [302].

Our first priority was to determine if the 4 compounds modulate p38 MAPK signalling as expected, in L929 cells and the absence of reovirus infection. L929 cells were treated with

various combinations of p38 MAPK activator (anisomycin), inhibitors (SB202190, SB203580) or inactive analogue (SB202474). SB202190, SB203580 and SB202474 were added 1hr prior to the 30min anisomycin treatment. Cell lysates were collected and processed for Western blot analysis. As expected, anisomycin increased the phosphorylation status of MKK3/6, the upstream kinase that phosphorylates p38, increased P-p38, and also increased p38 downstream targets MSK1 and ATF2 (Fig 3.1B). Furthermore, our observation that P-eEF2 levels decreased following anisomycin treatment is congruent with previously findings that suggest p38 MAPK signaling inhibits eEF2K, the upstream kinase of eEF2 (Fig 3.1B, [303]). Together, our results suggest that animosmycin is a reliable inducer of p38 MAPK and some of its downstream pathways in L929 cells (MSK1, ATF2, eEF2). Importantly, both SB202190 and SB203580 p38 MAPK inhibitors, but not the inactive SB202474 analogue, effectively prevented phosphorylation of MSK1, and MNK1, and restored phosphorylation of eEF2. Therefore, MSK1, MNK1 and eEF2 are proteins likely regulated by p38 MAPK activity. SB202190 and SB203580 did not prevent ATF2 phosphorylation, suggesting that in L929 cells, ATF-2 is likely regulated by anisomycin activated MAPKs other than p38 MAPK, such as JNK and/or ERK. (Fig 3.1B) Altogether, our results demonstrate that p38 MAPK signalling can effectively manipulated with anisomycin or SB202190/SB203580 in L929 cells. Furthermore, the ability of anisomycin to increase P-p38 suggests that the lack of P-p38 induction during reovirus infection is not a consequence of unavailability or saturation of p38 MAPK, but rather that the infection does not potently activate p38 MAPK signalling in L929 cells.

Before proceeding with the use of the p38 MAPK modulating compounds, we also performed cellular toxicity assays to determine if compound concentrations and treatment durations were inherently toxic. Since our data indicated that SB202190 was the more potent p38

MAPK inhibitor, we used it as a representative compound for our toxicity trials. Cells were treated with various concentrations of DMSO, SB202190 or hydrogen peroxide (H_2O_2) as a positive control for 12hrs. Following a media change, cellular toxicity assessed after an additional 12hrs using resazurin dye fluorescence, an indirect measurement of cellular metabolism. Even though most of our assays were performed within 12 hours, we assessed cellular toxicity at 24 hours post treatment to permit ample time for cell death, if any, to occur. H_2O_2 demonstrated a dose-dependent decrease in cell viability with increasing H_2O_2 concentration, confirming functionality of the resazurin assay. At all tested concentrations (5-40 μM) of SB202190 and DMSO, minimal cellular toxicity was observed, suggesting the safe use of 10-20μM SB202190 in our L929 cell line model (Fig 3.2).

Having validated functional p38 MAPK signaling in L929 cells and the specificity and safety of p38 MAPK inhibitors, we assessed the role of p38 MAPK in the context of reovirus infection. Cells were pre-treated with p38 MAPK inhibitors or the inactive analogue for 1hr prior to addition of reovirus. Cell lysates were collected at 12hpi and assessed using Western blot analysis for both indicators of p38 signalling status and reovirus protein expression. Phosphorylation of p38 MAPK downstream targets MNK1 and MSK1 was similar between mock and reovirus infection, validating our observation that reovirus infection does not induce p38 activation in L929 cells. Treatment with p38 MAPK inhibitors reduced P-MSK1 and P-MNK1, further confirming their downstream position with regards to p38 MAPK signaling. Analysis of reovirus structural proteins μ1C and σ3, showed that treatment with p38 MAPK inhibitors markedly reduced reovirus protein expression relative to untreated and inactive analogue treated samples (Fig 3.1A). To demonstrate a dose-dependent relationship between reovirus infection and p38 MAPK signaling, reovirus protein expression levels were monitored

following treatment with various concentrations of SB202190, SB203580 and SB202474 (Fig 3.3). SB202190 and SB203580 reduced viral protein (μ1C and σ3) in a dose dependent manner, with SB202190 being the more potent inhibitor. Treatment at respective doses of SB202474 had minimal reduction in viral protein (μ1C and σ3), further confirming inhibitor specificity (Fig 3.3). In summary, our results demonstrate that basal p38 MAPK signaling is beneficial during the initial 12hrs of the reovirus infection cycle.

The reduced levels of reovirus proteins following p38 MAPK inhibitor treatment could reflect two possibilities: i) the number of cells infected by reovirus was reduced or ii) reovirus protein synthesis was inhibited in equivalent infected cells. To distinguish these possibilities and evaluate the effect of the p38 MAPK inhibitors on the proportion of reovirus infected cells, L929 cells were exposed to reovirus for 1hr and supplemented with media containing p38 MAPK inhibitors at various doses for 12hrs. Samples were then fixed and reovirus-infected cells were visualized using immunocytochemistry (Fig 3.4A) or quantified using flow cytometry (Fig 3.4B). Reovirus infection in the untreated sample was similar to DMSO treated samples, suggesting that DMSO did not affect reovirus infection. Both p38 MAPK inhibitors SB202190 and SB203580 reduced reovirus infection in a concentration dependent manner, with SB202190 exhibiting most-potent effects. Samples treated with the inactive p38 MAPK inhibitor analogue SB202474 did not reduce reovirus infection, suggesting that off-target effects of SB203580 and SB202190 are not likely the cause of reovirus inhibition (Fig 3.4A, 3.4B). Furthermore, a clinically-relevant p38 MAPK inhibitor BIRB796 [304] also inhibited the number of cells productively infected by reovirus (Fig 3.4A).

The observed differences in p38 MAPK activation between NIH/3T3 [239] and L929 (this study) cell lines during reovirus infection, indicate potential cell-specific phenotypes and

therefore we determined if inhibition of p38 MAPK also reduced reovirus infection in a diverse cell line panel. Using immunocytochemistry similar to Figure 3.4A, reovirus infection in the presence of SB202190 was assessed in mouse B16-F10 melanoma cells, mouse NIH/3T3 non-transformed fibroblast cells, human H1299 non-small cell lung carcinoma, and human T47D breast ductal carcinoma cells. In all four cell lines tested, p38 MAPK inhibition by SB202190 reduced reovirus infection (Fig 3.5). Overall, immunohistochemical and Western blot analysis demonstrated that inhibition of p38 MAPK suppressed initial reovirus infection in multiple cell types.

3.1.2 P38 MAPK signaling does not affect reovirus replication steps

P38 MAPK signaling is important in numerous cellular processes such as endocytosis and endosomal trafficking [305-307]. We hypothesized that treatment with p38 MAPK inhibitors prior to reovirus infection could potentially affect receptor expression on the cell surface and thereby reduce reovirus-cell binding. To evaluate if p38 MAPK signaling affects cell attachment of reovirus, L929 cells were pretreated for 1hr with SB202190, anisomycin, or left untreated, and then reovirus was adsorbed at 4°C to permit attachment but not entry. Unbound reovirus particles were removed by repeated rinsing and cell lysates were subjected to Western blot analysis for reovirus outer capsid proteins μ1C and σ3 (reflects cell-bound virus) or β actin (loading control). In both virus doses used, cell bound virus levels were unchanged between untreated and SB202190 or anisomycin treated samples (Fig 3.6A). As an alternative approach, attachment of S^{35} radiolabelled reovirus to L929 cells pre-treated with SB202190 was measured by liquid scintillation counting of total cell lysates. At all three reovirus dilutions, SB202190 treatment did not affect reovirus attachment (Fig 3.6B). Therefore, reduction in reovirus infection following inhibition of p38 MAPK signaling likely does not occur due to diminished reovirus-cell binding.

Cellular entry of avian reovirus via dynamin and cavelion mediated endocytosis is p38 MAPK dependent [308]. Since *Mammalian orthoreovirus* (reovirus) also shares these endocytosis pathways [146, 148, 228], we assessed whether reovirus entry also depends on p38 MAPK signaling. Cells were pre-treated with SB202190 for 1hr followed by reovirus binding at 4°C for 1hr. Samples were processed immediately after binding (0hpi) and at 2hpi at 37°C (Fig 3.7A). Extracellular virions were labelled using anti-reovirus antibodies and respective secondary antibodies conjugated to Alexa Fluor™ 647. Stained samples were fixed and imaged using confocal microscopy. The percent of reovirus internalization was determined with the quantification of the number of Alexa Fluor™ 647 spots at 0 and 2hpi. At 2hpi, SB202190 treated samples had an average of 30% virion internalization, while untreated samples had an average of 62% virion internalization, suggesting that p38 MAPK signaling was important in efficient reovirus endocytosis (Fig 3.7A).

3.1.3 Reovirus endosomal trafficking is facilitated by p38 MAPK signaling

Reovirus infected samples treated with SB202190 had 8 to 10-fold fewer infected cells relative to untreated samples. However, we only observed a 2-fold reduction in virus internalization (Fig 3.7A), suggesting that a downstream step following reovirus entry was also being inhibited during SB202190 treatment. To enable tracking of reovirus internalization, a purified reovirus preparation was labelled with an Alexa Fluor™ 546 succinimidyl ester dye which covalently binds to virion outer capsid proteins. Cells were pre-treated with SB202190 and exposed to Alexa Fluor™ 546 labelled virions at 4°C for 1hr. Similar to the endocytosis assay, external virions were identified using anti-reovirus antibodies and Alexa Fluor™ 647 secondary antibody staining. In this experiment however, internalized particles were also monitored using Alexa Fluor™ 546. At 0 and 1hpi, samples were visualized using confocal

microscopy. In both untreated and SB202910 treated samples, 1hpi internalized Alexa Fluor™ 546 spots were larger in area compared to Alexa Fluor™ 647 spots, resembling endosomal compartments with either multiple virions and/or dissociation of outer capsid fluorescent proteins. Interestingly, we observed that the area of internalized Alexa Fluor™ 546 spots were larger in the SB202190 samples than the untreated samples, suggesting potential defects in endosomal trafficking (Fig 3.7B) that will be further delineated in upcoming results.

For reovirus to establish an infection in the absence of digestive enzymes, it must transverse to the lysosome where proteolytic digestion of outer capsid proteins facilitates production of intermediate subviral particles (ISVPs) capable of penetrating the membrane and gain access to the cytoplasm [178, 225, 226, 228, 309]. The easiest strategy to detect a deficiency in endosomal trafficking and/or lysosomal-mediated processing of reovirus is therefore to monitor reovirus capsid disassembly (uncoating) using Western blot analysis for degradation of σ3 and cleavage of μ1C to δ. Accordingly, we assessed the status of reovirus uncoating following SB202190 treatment in various mouse (L929, B16-F10) and human (H1299, T-47D, HCT116) cell lines. Cells were pre-treated with SB202190, bound by reovirus at 4°C and lysates were collected at every hour until 5hpi. At 0hpi, equivalent viral capsid proteins were observed between untreated and SB202190 treated samples, validating our previous observation that SB202190 does not alter virus-cell attachment (Fig 3.6A, 3.6B, 3.8). In all cell lines tested, reovirus uncoating (μ1C to δ cleavage) was delayed in SB202190 treated samples, relative to untreated samples. Additionally, using *de-novo* μ1 as an indication of new viral protein synthesis, untreated samples had detectable *de-novo* μ1 as early as 3hpi, while no detectable *de-novo* μ1 was observed in SB202190 treated samples as late as 5hpi. Similar trends were observed

in all cell lines tested (Fig 3.8). Therefore, p38 MAPK signaling corresponds with efficient reovirus uncoating, resulting in earlier initiation of viral protein synthesis.

Following endocytosis, reovirus enclosed in endosomes are trafficked via microtubules to late endosomes and endo-lysosomes where reovirus undergoes uncoating [225, 226]. The diminished reovirus uncoating observed in the presence of SB202190 could be due to delayed trafficking, hindered lysosome establishment, or reduced lysosomal protease activity. While some studies have demonstrated that reovirus utilizes microtubules for trafficking and infection [225, 226], some studies have demonstrated that reovirus infection does not depend on microtubule trafficking [198, 291]. We tested the impact of two drugs, a microtubule stabilizer (paclitaxel) and a microtubule destabilizer (nocodazole), on initial virus infection. L929 cells were pre-treated for 30min at various concentration (10μM to 0.001μM) of the microtubule inhibiting drugs (nocodazole and paclitaxel) to ensure microtubule assembly/disassembly was blocked prior to virus entry. Virus was adsorbed onto cells and collected at 3hpi to assess virus uncoating and at 12hpi to determine virus infection. Virus uncoating was evaluated using Western blot analysis, while virus infection was visualized using immunocytochemistry. Both drugs (nocodazole and paclitaxel) at all concentrations tested had similar levels of uncoating (μ1C to δ conversion and σ3 cleavage) compared to untreated samples, suggesting that inhibition of microtubule function does not affect reovirus uncoating (Fig 3.9A). Reovirus infection in all treatment conditions remains either unchanged or even increased slightly, strongly suggesting that microtubule function is not required for reovirus infection (Fig 3.9B). These results suggest that inhibition of reovirus uncoating and subsequent infection by p38 MAPK inhibitor SB202190, may not be occurring through impedance of orderly microtubule function.

Early endosomes (pH 6.0-6.5) transition to late endosomes (pH 5.0-5.5) by means of a pH change mediated by the membrane traversing vacuolar ATPase (V-ATPase) [310]. Fusion of protease containing vesicles and additional activity of the V-ATPase facilitate the progression of the late endosome to an endo-lysosome (pH 4.5-5.0) [310-312]. When cells are incubated at a low temperature (18-20°C), endocytosis and transition to late endosomes occur normally, but lysosome formation is inhibited, presumably due to vesicle fusion inhibition [313, 314]. Since lysosome formation is necessary for reovirus uncoating, we first determined if low temperature incubation (19°C) blocked reovirus uncoating. L929 cells were bound by reovirus and reovirus uncoating was monitored at 0-7hpi using Western blot analysis for reovirus outer capsid proteins. At 37°C, reovirus uncoating proceeded with σ3 degradation and μ1C to δ cleavage. However, at 19°C reovirus uncoating (σ3 degradation and μ1C cleavage) was inhibited (Fig 3.10A). When the temperature was increased from 19°C to 37°C, reovirus progressed towards uncoating the observed σ3 degradation and μ1C to δ cleavage in a similar rate compared to only 37°C incubation, suggesting a temperature-dependent reversible block in reovirus uncoating (Fig 3.10A). Therefore, low (19°C) temperature incubation likely blocks reovirus uncoating by trapping virions in late endosomes incapable of accessing proteolytic lysosomal enzymes. The use of early endosome, late endosome and lysosome markers will need to be utilized to confirm that 19°C halts trafficking at the late endosome stage.

The ability to trap virions in uncoating-incapable late endosomes, enabled us to assess if p38 MAPK signaling facilitates reovirus uncoating by promoting either late endosome-to-endo-lysosome progression or preceding endosome trafficking steps. Reovirus was bound to L929 cells and incubated at 37°C and/or 19°C with or without SB202190 in various combinations and processed using Western blot analysis to measure reovirus uncoating. Cells were not pre-treated

with SB202190 but instead treated for 30min prior to temperature shift. Similar to our previous results, when maintained at 37°C, SB202190 treatment diminishes reovirus uncoating relative to untreated samples. Reovirus uncoating in L929 cells initiates between 1 and 3hpi (Fig 3.10B). Samples were therefore incubated at 19°C for either 1hr or 3hr to trap virions in late endosomes, followed by incubation at 37°C to initiate uncoating. Relative to DMSO treated samples, SB202190 treated samples had diminished reovirus uncoating in samples pre-incubated at 19°C followed by 37°C incubation (Fig 3.10C). Collectively, our results suggest that i) as expected, reovirus requires access to lysosomes for initiation and completion of outer capsid uncoating, and ii) p38 MAPK signaling facilitates efficient reovirus uncoating by modulating late endosome to lysosome transition. Future studies will be focussed on deciphering whether p38 MAPK signaling influences lysosomal protease containing vesicle formation, or their fusion with late-endosomes.

3.1.4 In addition to promoting early reovirus entry steps, p38 MAPK signaling also enhances post-reovirus uncoating steps

Downstream substrates of p38 MAPK include factors involved in modulating protein translation (e.g MNK1/2 and MK2/3) [315]. Since reovirus utilizes the host translation machinery for viral protein synthesis, we proposed that p38 MAPK signaling could impact the protein translation stage during reovirus infection. Since our data demonstrated that SB202190 treatment inhibited reovirus endocytosis and uncoating steps, we had to inhibit p38 MAPK after entry was complete in order to assess post-entry stages of reovirus replication. Accordingly, we initially determined the timepoint at which virion uncoating was complete. Ammonium chloride (NH_4Cl) is commonly used to neutralize lysosomal compartments, hence is capable of inhibiting reovirus uncoating [174, 256]. We added NH_4Cl at various timepoints post infection and

assessed reovirus infection at 12hpi using flow cytometry, reasoning that at the timepoint when the majority of uncoating was complete, NH_4Cl would no long affect infection. Addition of NH_4Cl at 0hpi had more than 90% inhibition on reovirus infection (Fig 3.11). Reovirus infection progressively increased with delayed addition of NH_4Cl. Only a 2-fold reduction in reovirus infection was observed when NH_4Cl was added at 2hpi. When NH_4Cl was added at timepoints after 3hpi, minimal-to-no inhibition on reovirus infection was observed, suggesting that uncoating of virions essential for reovirus infection was accomplished between 3 and 4hpi (Fig 3.11). Therefore, we could determine the effect of p38 MAPK signaling on post-reovirus uncoating steps by addition of SB202190 at timepoints after 3hpi.

Viral protein levels were quantified at 12hpi using Western blot analysis following addition of NH_4Cl and/or SB202190 at various timepoints post reovirus infection. In agreement with the levels of reovirus infection observed with flow cytometry, NH_4Cl addition at 0 and 1hpi had striking inhibition of viral proteins, addition at 2hpi had a 2 to 3-fold reduction in viral proteins, and addition at or after 3hpi had minimal to no effect on viral proteins (Fig 3.12A). At every given timepoint, we combined NH_4Cl and SB202190 to ensure that only virions that have undergone complete uncoating at the time of SB202190 addition contribute to the viral protein pool. As anticipated, addition of SB202190 at the onset on infection (1 and 2hpi) had more than 90% inhibition of viral proteins, suggesting that pre-reovirus uncoating steps are inhibited by SB202190. Interestingly, when added at 3hpi or later, when reovirus uncoating was close to completion, reovirus protein synthesis was still inhibited by SB202190, albeit to a lesser extent compared to addition of SB202190 prior to 3hpi (Fig 3.12A). Therefore, p38 MAPK signaling plays a role in post-reovirus uncoating steps that impact reovirus protein synthesis.

As an alternate strategy of circumventing the endocytic pathway during reovirus infection, we utilized reovirus ISVPs, that have been previously demonstrated to bypass the lysosomal pathway by either direct entry into the cytoplasm from the external cell membrane or cytoplasmic entry from the early endosomal vesicles [148, 149]. ISVPs consist of virions lacking outer capsid proteins σ3 and μ1 pre-cleaved to δ, and can be generated by in-vitro exposure of reovirus particles to chymotrypsin [154, 163]. We reasoned that by infecting cells with reovirus ISVPs, the endocytosis and uncoating steps that are inhibited by SB202190 would be bypassed, and the effect of p38 MAPK signaling on post-uncoating steps of reovirus infection would be revealed. Reovirus ISVPs were generated using chymotrypsin digestion, L929 cells were infected with or without SB202190 treatment for 15hours, and reovirus proteins were monitored by Western blot analysis. NH_4Cl treatment did not inhibit reovirus ISVP infection protein synthesis, confirming that ISVPS infection is lysosome-independent. Treatment with SB202190 inhibited reovirus ISVP proteins synthesis, relative to untreated or NH_4Cl treated samples (Fig 3.12B). Therefore, both time-of-addition and ISVP experiments suggest that p38 MAPK signaling is also important in post-reovirus uncoating steps that affect viral protein synthesis.

3.1.5 Generating cell lines with stable p38 MAPK isoform knockdown

The p38 MAPK family consists of four isoforms, p38α, p38β, p38δ and p38γ [315]. The p38 MAPK inhibitors used in the study bind to two or more isoforms; SB202190 and SB203580 bind p38α and p38β [301], BIRB796 binds p38α, p38β, p38δ and p38γ [316]. For a more targeted approach, we used an shRNA knockdown strategy to reduce expression of specific p38 MAPK isoforms. Limitations of this strategy were discovered in hindsight and will be examined in detail in the discussion section. Since the human whole genome shRNA library was available in-house, we switched from the L929 mouse fibroblast cell line in subsequent experiments and

performed the knockdown experiments in the H1299 human lung carcinoma cell line. We had previously demonstrated that p38 MAPK inhibition using SB202190 suppressed reovirus uncoating and reovirus infection in H1299 cells (Fig 3.5, 3.8). Plasmid vectors containing shRNA sequences were purified and transfected along with packaging and envelope plasmid vectors into HEK293T cells to generate lentivirus encoding shRNAs. For each p38 MAPK isoform, 5 shRNAs constructs targeting different regions of the mRNA were used. Constructs encoding either no shRNA (shEMPTY) or shRNA targeting GFP (shGFP) were used as non-targeting controls. H1299 cells were transduced with a dilution series of each lentivirus, followed by puromycin selection. Knockdown of each p38 MAPK isoform was verified at the mRNA and protein level using RT-PCR and western blot analysis, respectively. At the protein level, p38α shRNA constructs #1 and #2 knocked down expression of p38α by more than 80%, with minimal effect on p38β. For p38β, shRNA constructs #7, #8 and #10 knocked down p38β expression by more than 70%, without affecting p38α (Fig 3.13A).

Since SB202190 and SB203580 target both p38α and p38β, we decided to generate a double p38α and p38β knockdown. We selected various combinations of shRNA constructs #1, #2, #7, #8 and #10 that had the best individual isoform specific knockdowns. H1299 cells were also transduced with a MOI of 3 of each lentivirus encoding constructs to promote integration of both shRNAs into the same cell genome, and stable cells were selected using puromycin. All combinations of shRNA constructs against p38α and p38β (#1+#7, #1+#8, #2+#8, #2+#10) had more than 80% and 60% knockdown in p38α and p38β, respectively (Fig 3.13A). For p38γ, constructs #12, #14, #15 and #16 had more than 70% p38γ knockdown. Assessment of p38δ levels were uncertain, as none of the p38δ constructs showed any significant level of knockdown at the predicted p38δ band size (Fig 3.13B). This could be due to either inefficient shRNA

construct targeting and/or non-specific p38δ Western blot antibodies. We selected the following shRNA knockdown constructs for subsequent experiments: #1 and #2 for p38α, #8 and #10 for p38β, #1+8 for p38α and p38β double knockdown and #12 and #16 for p38γ. At the mRNA level, all constructs selected demonstrated at least 60% gene specific knockdown. All constructs except #8 had minimal impact on non-specific p38 isoform expression. Construct #8 targeting p38β, had a small increase in p38γ expression, relative to the empty vector control (Fig 3.13C).

3.1.6 Knockdown of p38β and p38δ MAPK isoforms inhibit reovirus protein synthesis

Our previous data demonstrated that p38 MAPK inhibition diminished reovirus uncoating and overall infection. Using our p38 MAPK isoform knockdown cell lines, we assessed the rate of reovirus uncoating, early (4hpi) viral protein synthesis and overall infection at 12hpi. Following binding at 4°C, cells were incubated at 37°C, and i) lysates collected at 1 and 4hpi and processed for reovirus uncoating using Western blot analysis or ii) fixed at 12hpi and virus infection quantified using flow cytometry. Following Western blot analysis, we did not observe any noticeable differences in reovirus uncoating (1hpi) or early viral protein synthesis (4hpi) in all the p38 MAPK isoform knockdowns (Fig 3.14A). Following flow cytometry analysis, reovirus infection at 12hpi in the various p38 MAPK isoform knockdown cell lines had no changes in overall reovirus infection (Fig 3.14B). As a high throughput measure of reovirus protein accumulation over 12hpi, we used a colorimetric ELISA, which utilizes a combination of anti-reovirus primary antibody, alkaline phosphatase secondary antibody and a p-nitrophenyl-phosphate (pNPP) substrate (Fig 3.15). The colorimetric clear to yellow color change of pNPP was monitored using a plate reader and was an indirect measure of the total amount of reovirus protein accumulation. Knockdown cell lines of p38β (#8, #10) had more than 70% reduction in viral proteins relative to the empty vector control. No noticeable differences were observed in

p38α knockdown cell lines (#1, #2). The combination of p38α and p38β knockdown cell lines (#1+#8) had an intermediate reduction in viral proteins of about 50%. Compared to the empty vector control, reduction of viral protein in the p38γ knockdown cell lines was 40% in construct #12 and 70% in construct #16 (Fig 3.15). Therefore, in H1299, knockdown of p38 MAPK isoforms did not affect reovirus uncoating, early (4hpi) viral protein synthesis or overall virus infection, but with respect to late (12hpi) reovirus protein accumulation, knockdown of p38β had a significant reduction while p38γ knockdown had an intermediate reduction.

3.1.7 Expression of p38β and p38δ MAPK isoforms correlates with reovirus uncoating in a breast cancer cell line panel

In reovirus clinical trials, patient responses are highly variable, and majority of patients fail to show clinical response relative to control test arm. However, with the inclusion of biomarkers such as EGFR, Hras, Kras, Nras, Braf and/or p53 mutations, patients expressing one or more of these biomarkers show an improved response to reovirus therapy compared to patents lacking any of the biomarkers [63-67]. Recent findings have also implicated gender as a variable in patient responses to reovirus therapy; in a lung cancer trial, female patients had a better response to reovirus therapy relative to male patients [62]. Given the importance of biomarkers in improving the prediction of patient response to reovirus therapy, we performed a preliminary screen to determine if p38 MAPK status correlates with reovirus infection in a panel of breast cancer cells. Reovirus successfully completed a Phase II clinical trial in breast cancer with a statistically significant progression free survival response, almost doubling the survival time compared to the control group [62]. As a result, FDA approval for a Phase III trials was recently granted and is currently ongoing. We therefore focused on breast cancer cell lines (MDA-MB-468, MDA-MB-231, T-47D, Hs578T, BT-549, MCF7) from the NCI-60 cell line panel,

characterizing reovirus infection versus various potential biomarkers including kinases of the p38 MAPK family.

As a first step in the characterization, we determined the overall susceptibility of the breast cancer cell line panel to reovirus infection. Reovirus infection was allowed to proceed for 12-15hrs and infection was assessed using immunocytochemistry (Fig 3.16A, 3.16B). Reovirus dose required for approximately 50% infection was determined for the cell line panel. MDA-MB-468 and T-47D were highly susceptible, MDA-MB231 and MCF7 were intermediate, and Hs578T and BT-548 were highly resistant to initial reovirus infection. Relative to the other breast cancer cell lines in our panel, BT-549 cells had a long doubling time (~60hrs) and was therefore excluded from subsequent analysis to eliminate the confounding effects of cell division.

Reovirus binding was evaluated as a potential step for differential infection among breast cancer cells. Cells were exposed to reovirus at 4°C for 1hr, rinsed extensively, and subjected to Western blot analysis to measure levels of bound reovirus structural proteins. For each cell line, β-actin was normalized on a per cell basis and used as a correction factor to account for differences in cell size and hence plate seeding, between the cell lines. Reovirus exhibited the highest attachment to MDA-MB-468, intermediate binding to T-47D and MDA-MB-231, low binding towards MCF-7, and very low attachment to Hs578T cells (Fig 3.17). Therefore, resistance of Hs578T to reovirus infection is likely due to inability of the virus to bind to these cells. Using the European Molecular Biology Laboratory (EMBL) cancer cell line RNA-seq database, we extracted expression data for *F11R* (JAM-A), a primary reovirus cell binding receptor (Fig 3.18). Expression data was available as transcripts per kilobase million (TPM) values. While all the other cell lines had F11R expression varying from 10 to 101, Hs578T had

zero expression, suggesting, that lack of JAM-A on Hs578T could potentially contribute to poor reovirus binding (Fig 3.18). In summary, our data suggests that complete lack of JAM-A is a likely contributor towards reovirus resistance by restricting virus binding. Future studies will strengthen this prediction using the per cell based reovirus binding assay, and cell surface JAM-A expression, but quantified using flow cytometry. Reovirus binding to cells is therefore an initial hurdle for successful infection and including biomarkers such as JAM-A would benefit pre-screening efforts.

Since reovirus uncoating is a rate-limiting step during establishment of infection, we assessed whether reovirus uncoating levels are a determinant reovirus susceptibility in our cell line panel. Reovirus uncoating was monitored by quantifying μ1C to δ cleavage various timepoints post reovirus binding using Western blot analysis. Reovirus uncoating in MDA-MB-468 and T-47D occurred most-rapidly, while MDA-MB231 and MCF-7 supported intermediate reovirus uncoating rates (Fig 3.19). The relative rates of uncoating correlated well with the infectivity assessed in Figure 3.16. Even though low levels of reovirus were detected immediately after binding (0hpi) to Hs578T cells, no viral protein was detected at subsequent timepoints (1-5hpi), suggesting that the few bound virions had detached from the cell and were not internalized (Fig 3.19). It was previously demonstrated that following reovirus binding to JAM-A and sialic acid, signaling through β1 integrin initiates virion endocytosis [145, 147]. We therefore checked the gene expression profile of *ITGB1* (β1 integrin), which was high on Hs578T cells, suggesting that either integrins are not restrictive for reovirus entry in Hs578T cells or that integrin surface expression and/or signalling are impaired (Fig 3.20). Nevertheless, the overall trend suggested that given the ability of reovirus to attached to breast cancer cells, the rate of reovirus uncoating does correlate with overall reovirus infection.

Given that rates of uncoating correlated with susceptibility to reovirus infection (Fig 3.16A, 3.16B, 3.19), and that p38 MAPK signalling was required for efficient steps leading to uncoating (Fig 3.8, 3.10), we assessed if uncoating rates also correlate with p38 MAPK levels. The NCI-60 cell line panel used in experiments above has an open source database for various omics studies [317]. With recent advances in proteomics depth and quality, the NCI-60 proteomics data compiled 5 years ago is incomplete and is currently undergoing improvements [318, 319]. We therefore utilized a validated RNA-seq transcriptome database available though EMBL for correlation studies. Expression of p38 MAPK isoforms was plotted with reference to percent reovirus uncoating at 3hpi (Fig 3.21). In addition to the breast cancer panel, we strengthened the confidence of the correlation analysis by including available data for H1299 (human large cell lung carcinoma), A549 (human lung adenocarcinoma) and HCT116 (human colon carcinoma). Hs578T and BT-549 were excluded from the analysis since reovirus uncoating was not determined due to low binding or slow cell division, respectively. Correlation analysis by linear regression was then used to determine if p38 MAPK isoform expression could help predict reovirus uncoating efficiency. The following correlation R^2 groups were used: strong (>0.75), moderate (0.50-0.75), poor (0.25-0.50), none (0.25-0.00). Correlation R^2 values for MAPK14 (p38α) (0.1697) and MAPK12 (p38δ) (0.06998) were poor to none (Fig 3.21). MAPK13 (p38γ) isoform was at very low abundance in lung cancer cell lines (H1299 and A549), which interestingly was found to be an overall trend in the NCI-60 lung cell panel, relative to other tissues (Fig 3.22). The correlation R^2 value for MAPK13 was therefore calculated both with inclusion and exclusion of the lung cancer cells lines and was found to be poor (0.05117) or moderate (0.51020), respectively. For MAPK11 (p38β), there was a strong correlation R^2 value (0.9001) (Fig 3.21). Since RNA expression does not necessarily correspond to protein levels, the

protein expression of p38 MAPK isoforms was determined by Western blot analysis using isoform-specific antibodies. Similar to RNA levels (Fig 3.23), protein expression of p38β and p38δ were highly expressed in MDA-MB-468 and T-47D; the 2 cell lines with the fastest reovirus uncoating (Fig 3.19, 3.23). Together the correlation analysis suggests that the MAPK11 gene and its p38β protein isoform offer the strongest association with efficiency of reovirus uncoating and infection.

Finally, since previous studies demonstrated the importance of lysosomal enzymes cathepsin B and L for lysosome-mediated reovirus uncoating [177-180, 320], and since a correlation of cathepsin B and L activity to reovirus induced cell death in a panel of cancer cells was previously observed [321], we also determined if expression of CTBB (Cathepsin B), CTSL (Cathepsin L) and CTSS (Cathepsin S) correlated with reovirus uncoating in the cell panel used in this study. CTSB had a poor correlation (0.3467), while CTSL and CTSS had no correlation (0.23010 and 0.03846, respectively) (Fig 3.24). As will be discussed further, the discrepancy with previous results could reflect our use of different cancer cell types and/or our evaluation of reovirus entry and infection in a single replication round rather than cell death or cell-to-cell spread.

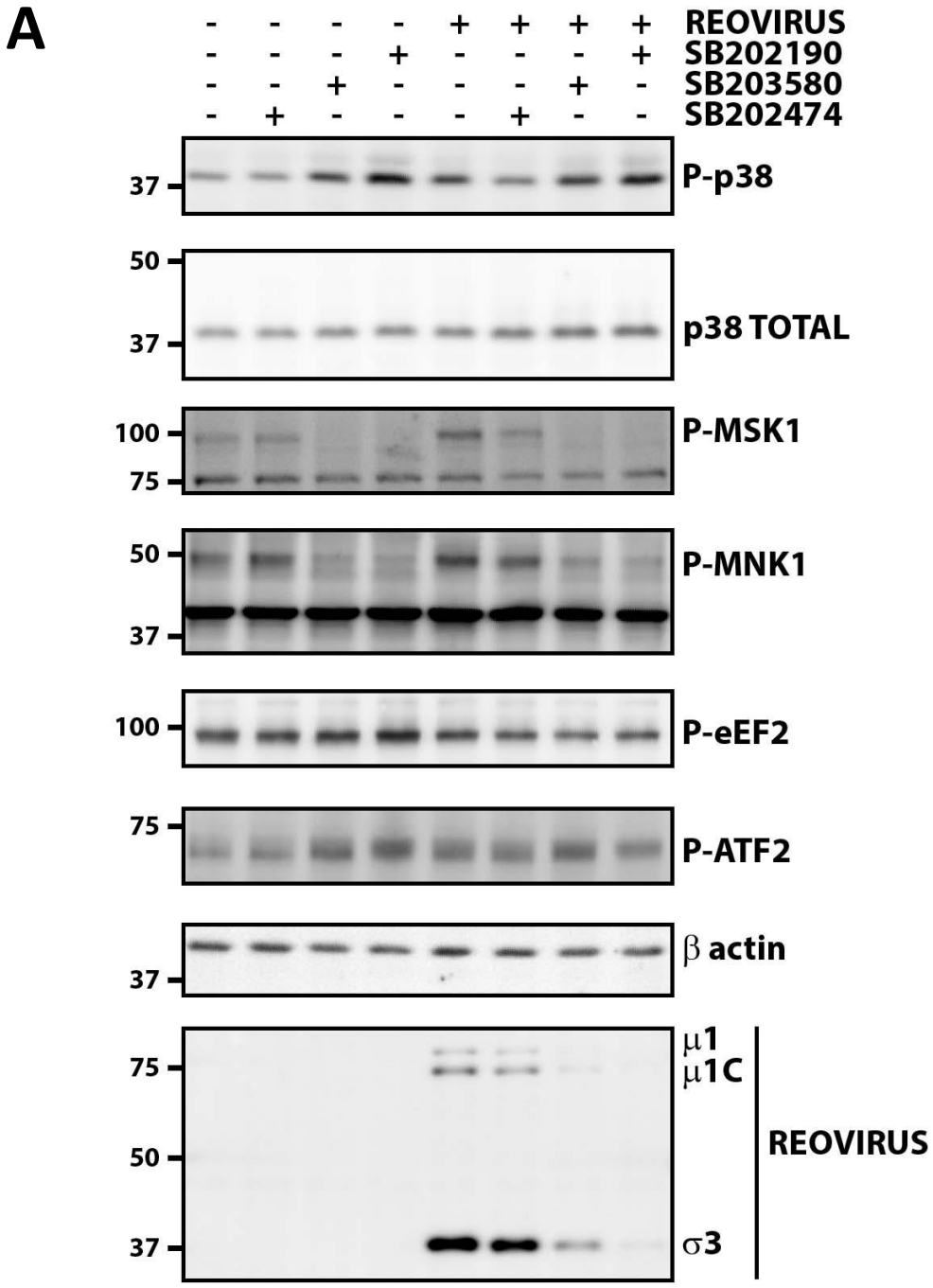
A
- - - - + + + + REOVIRUS
- - - + - - - + SB202190
- - + - - - + - SB203580
- + - - - + - - SB202474
37
P-p38
50
37
p38 TOTAL
100
75
P-MSK1
50
37
P-MNK1
100
P-eEF2
75
P-ATF2
37
β actin
75
50
37
μ1
μ1C
σ3
REOVIRUS

B

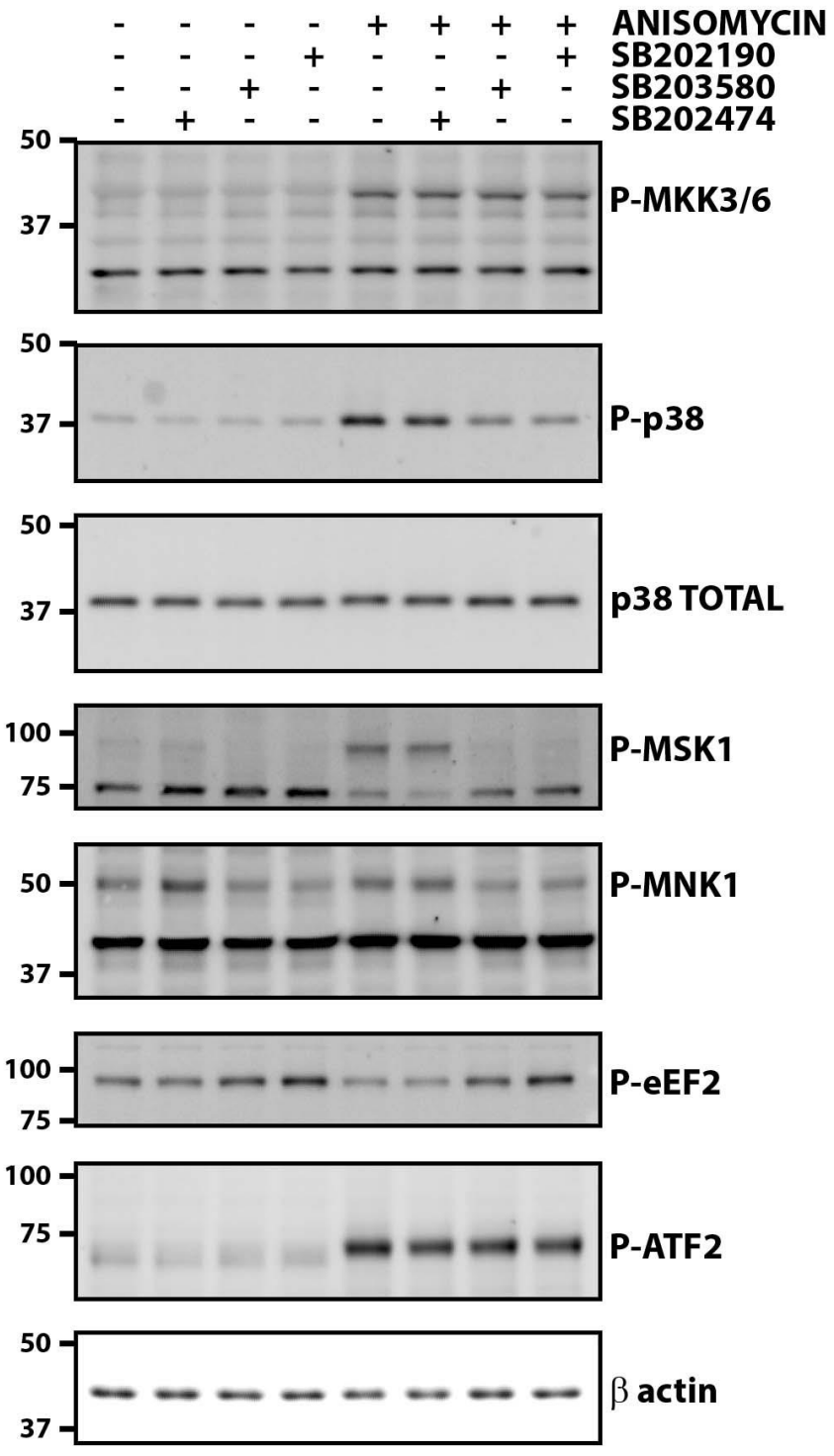
- - - - + + + + ANISOMYCIN
- - - + - - - + SB202190
- - + - - - + - SB203580
- + - - - + - - SB202474
50
37
P-MKK3/6
50
37
P-p38
50
37
p38 TOTAL
100
75
P-MSK1
50
37
P-MNK1
100
75
P-eEF2
100
75
P-ATF2
50
37
β actin

Figure 3.1. Reovirus does not activate p38 MAPK and downstream targets MNK1, MSK1 and eEF2. L929 cells were pre-treated with DMSO, SB202474, 202190 or 203580 for 1hr at 37°C, followed by A) addition of reovirus to the media for an additional 12 hours or B) addition of anisomycin for an additional 30 minutes, at 37°C. Cell lysates were collected in protein sample buffer, separated by SDS PAGE and Western blot analysis for p38 MAPK, downstream p38 MAPK targets (MNK1, MSK1, eEF2, ATF2), β actin (loading control), and reovirus. SB202190, SB203580 or SB202474 were added at a final concentration of 20μM. DMSO was added equivalent to the volume for master stock of SB202190, SB203580 or SB202474. Anisomycin was added at 0.5μM.

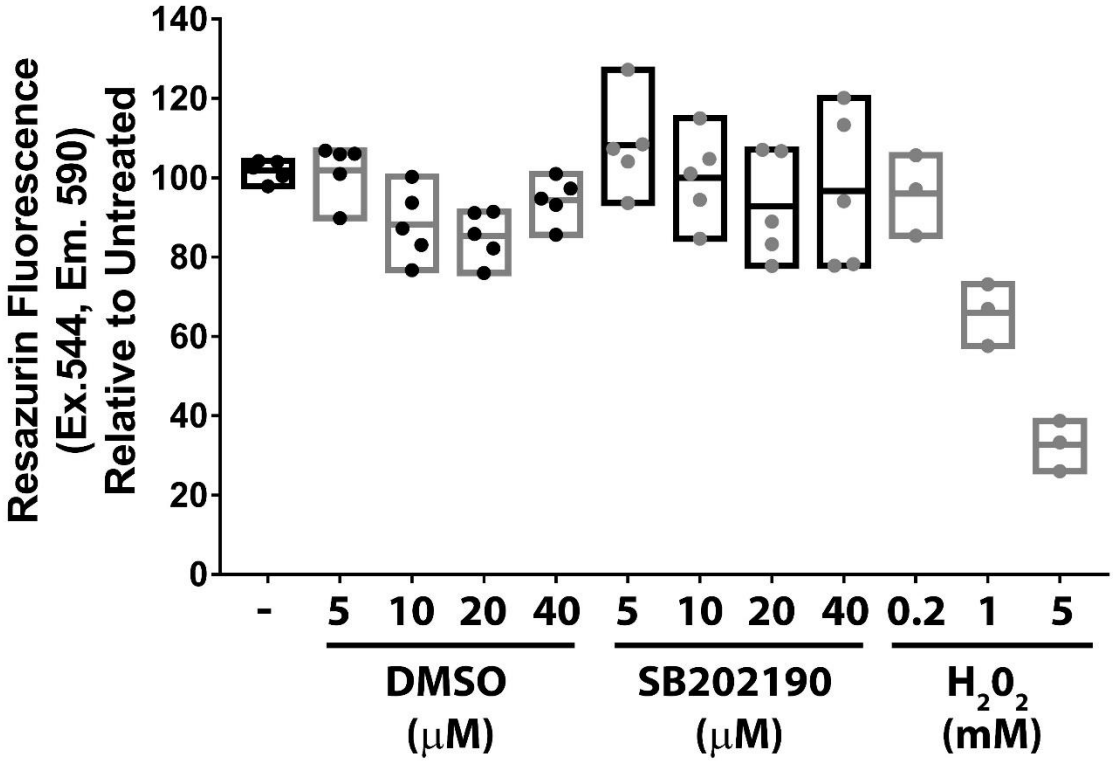

Figure 3.2. Inhibitor of p38 MAPK (SB202190) is non-toxic. L929 cells were treated with DMSO, SB202190 or H_2O_2, at indicated concentrations for 12hrs at 37°C. Media was replaced and incubated for an additional 12hrs at 37°C. Media was supplemented with resazurin dye at a final concentration of 4.4μM, incubated for 30min at 37°C, and fluorescence was measured on a plate reader. Untreated wells were used for standardization. $n \geq 3$

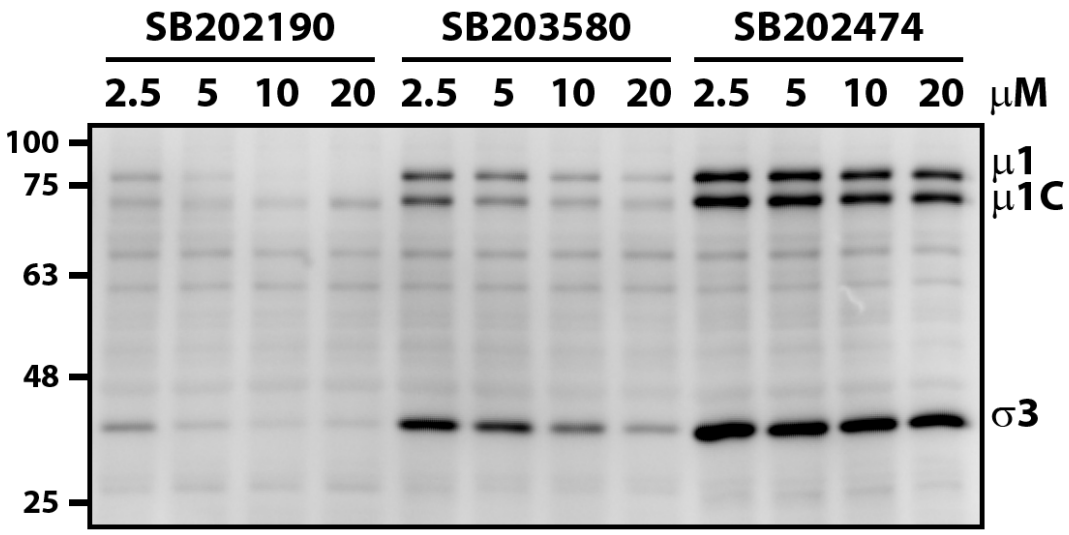

Figure 3.3. Reovirus proteins expression is repressed by p38 MAPK inhibitors (SB202190, SB20380), but unaffected by inactive inhibitor analogue (SB202474). Similar to Fig 3.1 A). SB202190, SB203580 or SB202474 were added at a final concentration as indicated. DMSO was added equivalent to the volume for master stock of SB202190, SB203580 or SB202474.

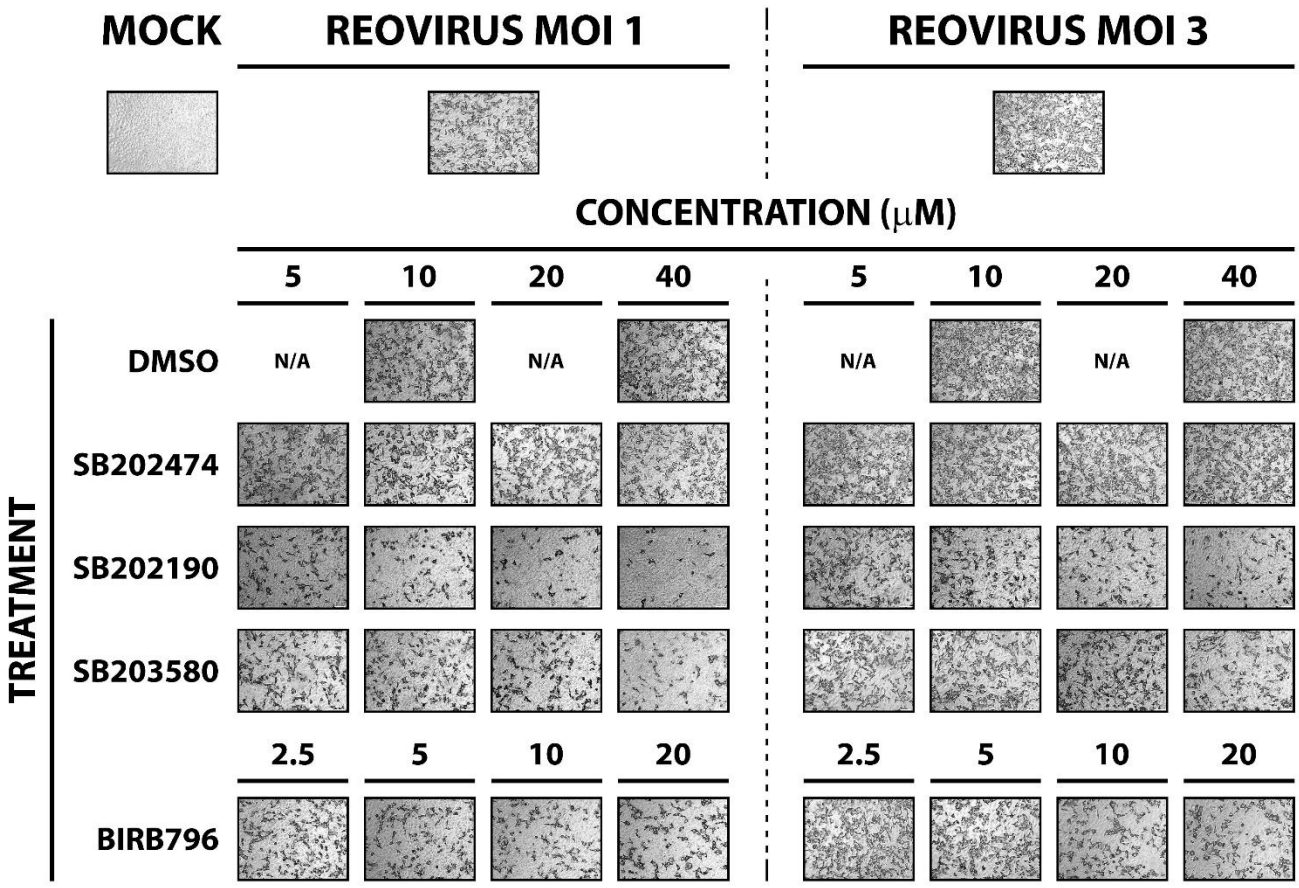
A
MOCK
REOVIRUS MOI 1
REOVIRUS MOI 3
CONCENTRATION (μM)
5
10
20
40
5
10
20
40
TREATMENT
DMSO
N/A
N/A
N/A
N/A
SB202474
SB202190
SB203580
2.5
5
10
20
2.5
5
10
20
BIRB796

B

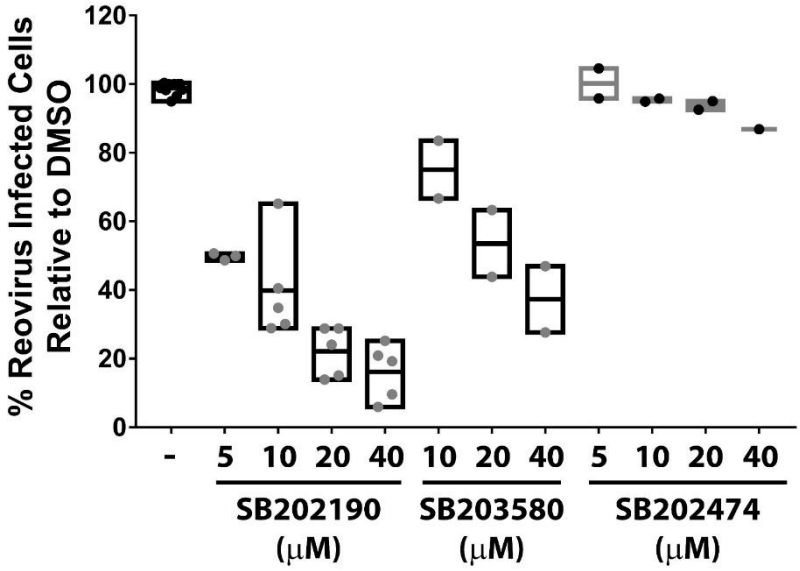

Figure 3.4. Reovirus infection is restricted by inhibition of p38 MAPK signaling. L929 cells were pre-treated with indicated concentrations of DMSO, SB202190, SB203580, SB202474 or BIRB796 for 1hr at 37°C. Media was removed and reovirus dilutions were added at either MOI 1 or MOI 3 for 1hr at 37°C. Virus was removed and media with corresponding compound was added for an additional 12 hours at 37°C. DMSO was added equivalent to the volume for master stock of SB202190, SB203580 or SB202474. Cells were fixed and reovirus infected cells were identified by either A) immunocytochemistry staining using reovirus specific primary antibody, alkaline phosphatase conjugated secondary antibody, and NBT/BCIP substrate, or B) reovirus specific primary antibody, Alexa Fluor 488 conjugated secondary antibody, and quantified using flow cytometry. Untreated wells were used for standardization. In B) $n \geq 1$

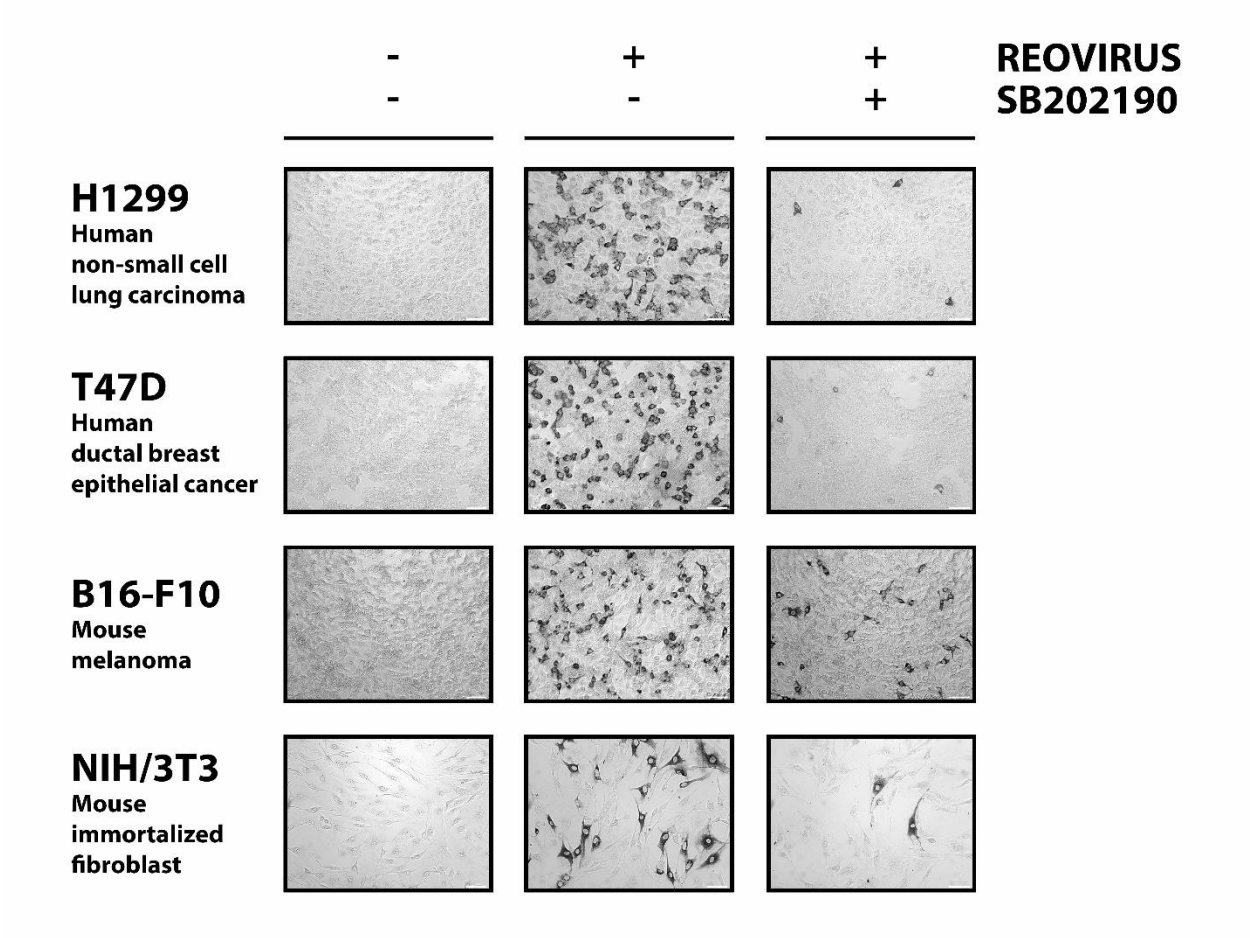

Figure 3.5. Restriction of reovirus infection by inhibition of p38 MAPK signaling, is cell line independent. H1299, T47D, B16-F10 and NIH/3T3 were pre-treated with SB202190, infected with reovirus, and processed for immunocytochemistry similar to Fig 3.4 A). SB202190 concentrations used were as follows: H1299 40μM, T47D 20μM, B16-F10 40μM, NIH/3T3 20μM.

A

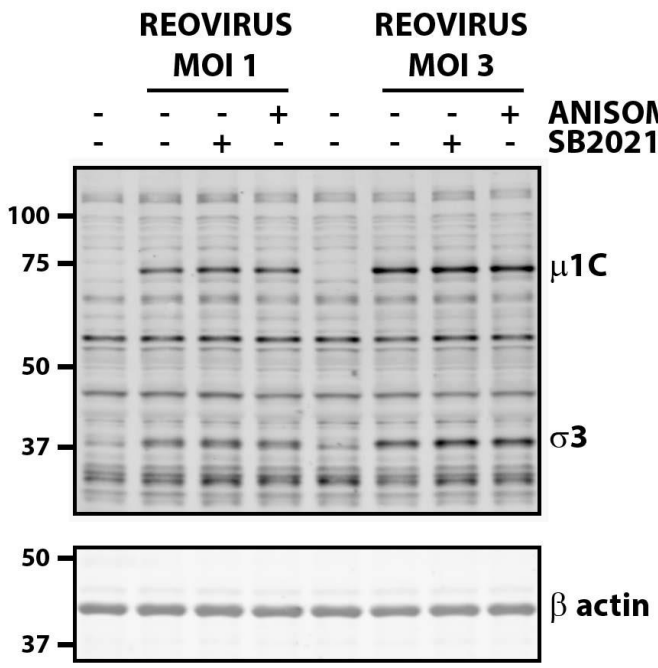
REOVIRUS MOI 1
REOVIRUS MOI 3
- - - + - - - + ANISOMYCIN
- - + - - - + - SB202190
100
75
50
37
μ1C
σ3
50
37
β actin

B

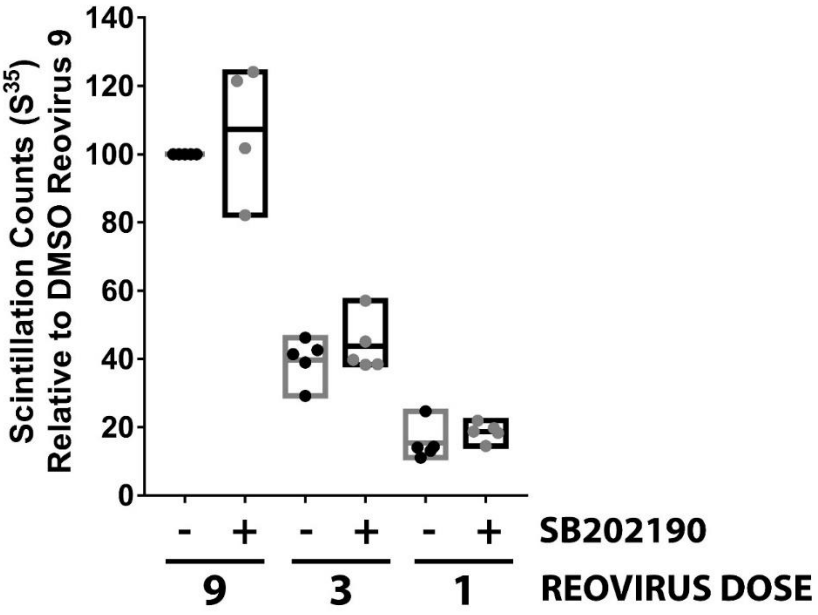
Scintillation Counts (S^{35}) Relative to DMSO Reovirus 9
140
120
100
80
60
40
20
0
- + - + - + SB202190
9 3 1 REOVIRUS DOSE

Figure 3.6. Reovirus-cell binding is not affected by p38 MAPK signaling. A) L929 cells were pre-treated with SB202190 (20μM) or anisomycin (0.5μM) for 1hr at 37°C. Following pre-chilling of cells at 4°C for 30 minutes, media was removed and reovirus dilutions were added. Virus was incubated at 4°C for 1hr, washed to remove unbound virus and cell lysates were processed for Western blot analysis using reovirus specific antibodies or β actin (loading control). B) L929 cells were pre-treated with SB202190 (20μM) and processed similar to A) except S^{35} labeled reovirus was used, and cell lysates were processed for scintillation counts. In B), $n \geq 4$

A

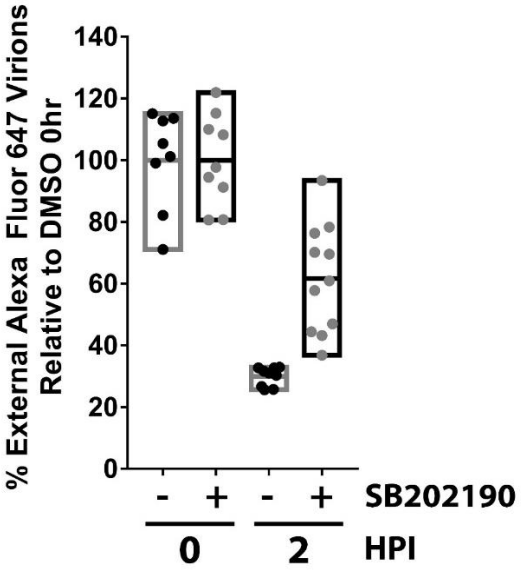
% External Alexa Fluor 647 Virions
Relative to DMSO 0hr
140
120
100
80
60
40
20
0
- + - +
SB202190
0 2
HPI

B

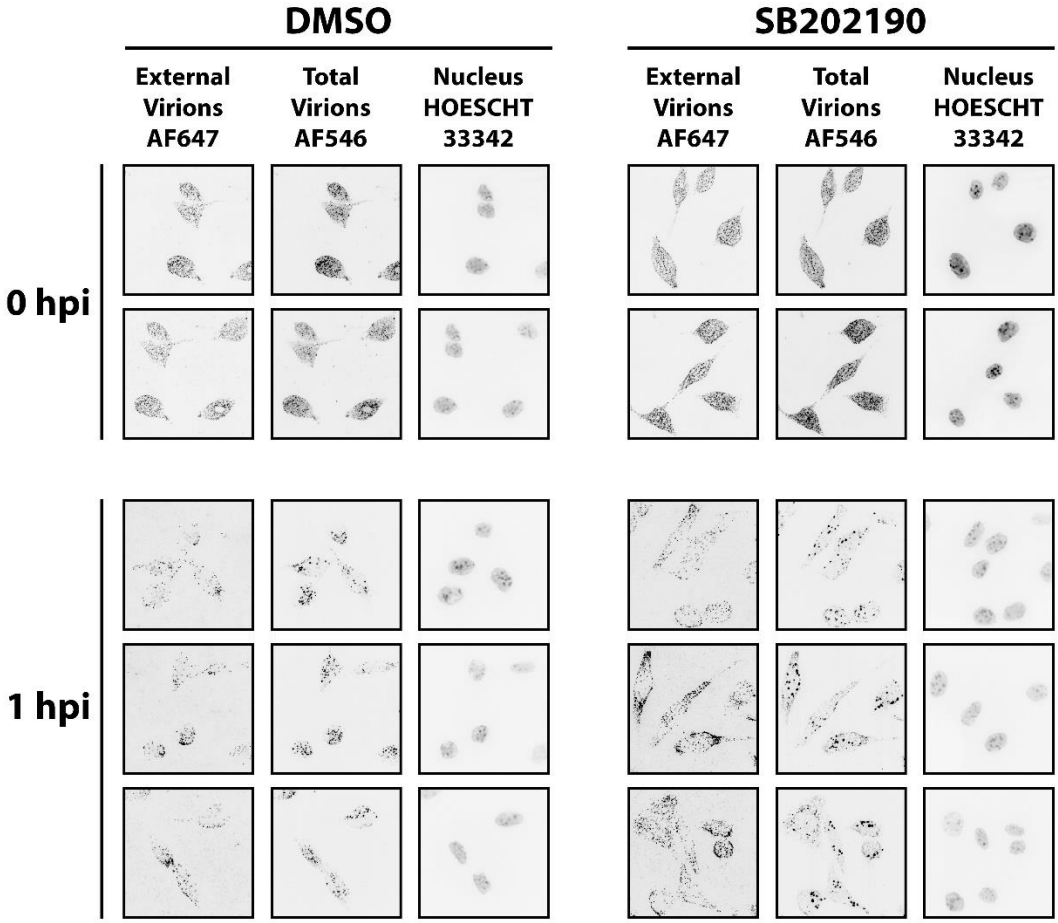
DMSO
SB202190
External Virions AF647
Total Virions AF546
Nucleus HOESCHT 33342
External Virions AF647
Total Virions AF546
Nucleus HOESCHT 33342
0 hpi
1 hpi

Figure 3.7. Inhibition of p38 MAPK signaling restricts reovirus entry and alters internalized reovirus trafficking. A and B) L929 cells were pre-treated with SB202190 (20μM) and processed similar to Fig 3.6 A), except Alexa Fluor 546 (AF546) succinimidyl ester labeled reovirus was used and samples were processed for confocal microscopy at 0hpi and 1hpi A) or 2hpi B) at 37°C. At each timepoint, cells were kept on ice and external virus was stained using reovirus specific antibodies and Alexa Fluor 647 (AF647) conjugated secondary antibodies, prior to paraformaldehyde fixation. A) Samples were imaged using the Operetta high-content imaging system and images were analyzed using the Columbus software for AF647 spot counting. % External Virions = External virus spots per cell per image/Average virus spots per cell in all images at 0hpi, B) Samples were imaged using confocal microscopy. In A), $n \geq 8$ images with ≥ 40 total cells per condition.

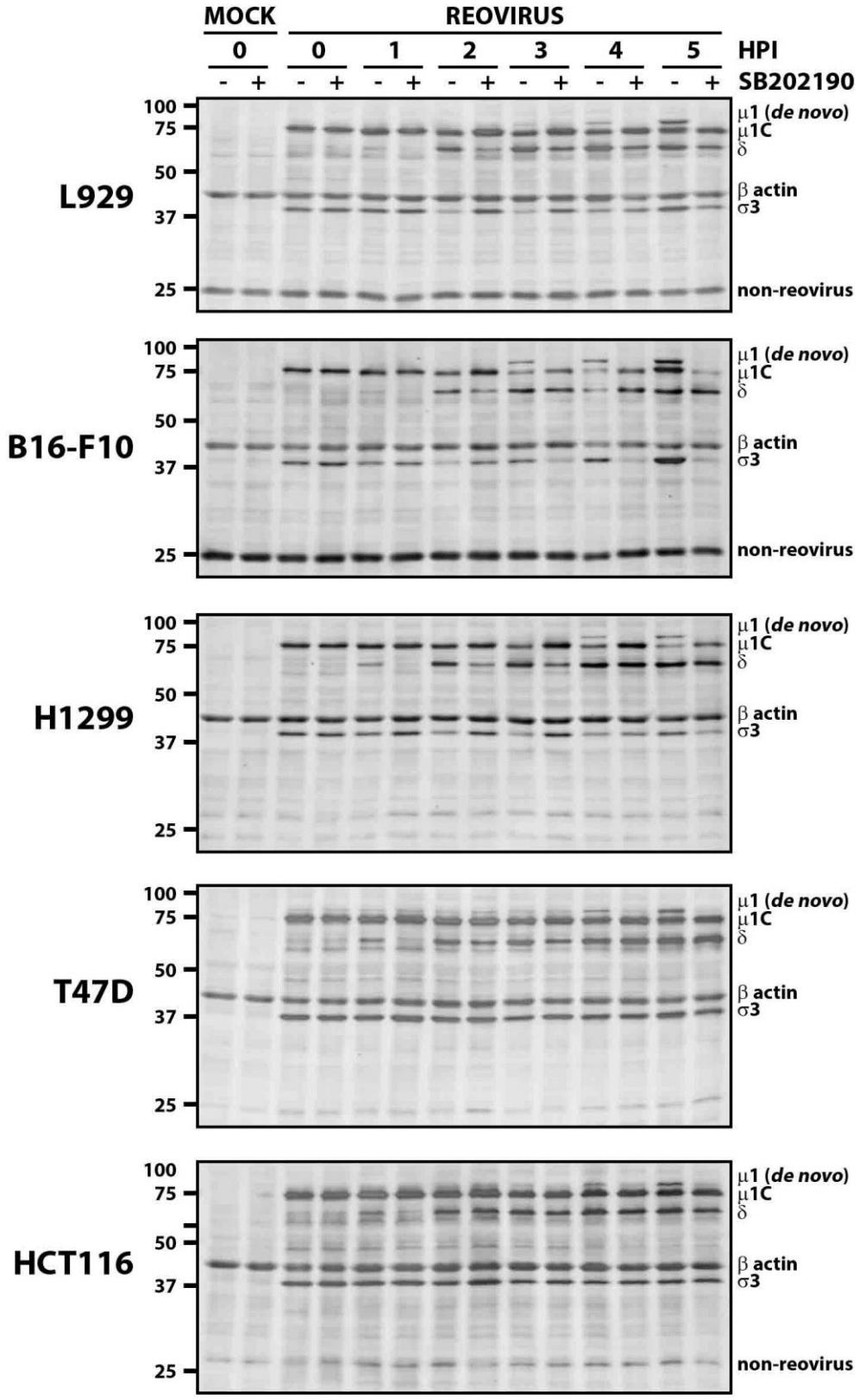
MOCK
REOVIRUS
0
0
1
2
3
4
5
HPI
- + - + - + - + - + - + - +
SB202190
L929
B16-F10
H1299
T47D
HCT116
100
75
50
37
25
μ1 (de novo)
μ1C
δ
β actin
σ3
non-reovirus

Figure 3.8. Efficient reovirus uncoating depends on p38 MAPK signaling. Cells were pre-treated with SB202190 and processed similar to Fig 3.6 A), in addition to sample collection every hour from 1hpi to 5hpi at 37°C. SB202190 concentrations used were as follows: L929 30μM, H1299 40μM, T47D 20μM, B16-F10 40μM, HCT116 40μM. Reovirus MOI used for each cell line were as follows: L929 (3), H1299 (3), T47D (3), B16-F10 (5), HCT116 (3).

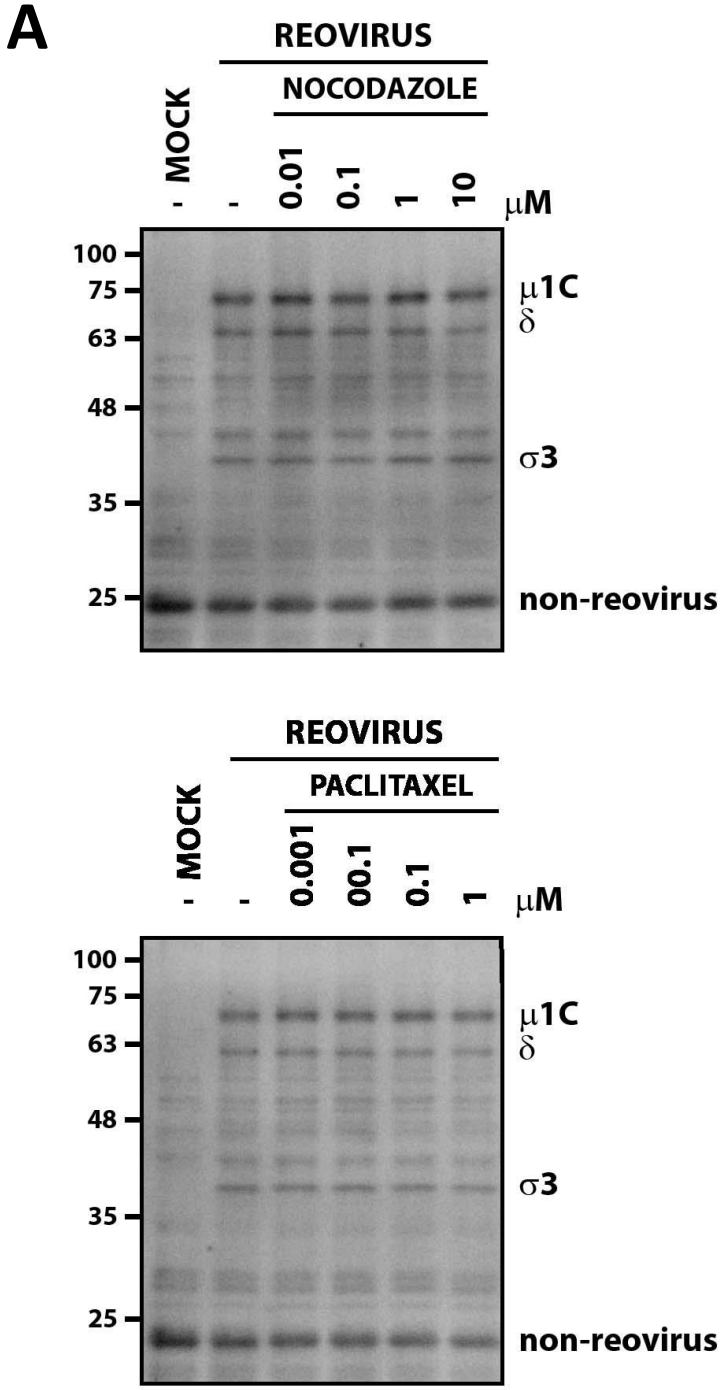
A
REOVIRUS
NOCODAZOLE
- MOCK
-
0.01
0.1
1
10
μM
100
75
63
48
35
25
μ1C
δ
σ3
non-reovirus
REOVIRUS
PACLITAXEL
- MOCK
-
0.001
00.1
0.1
1
μM
100
75
63
48
35
25
μ1C
δ
σ3
non-reovirus

B

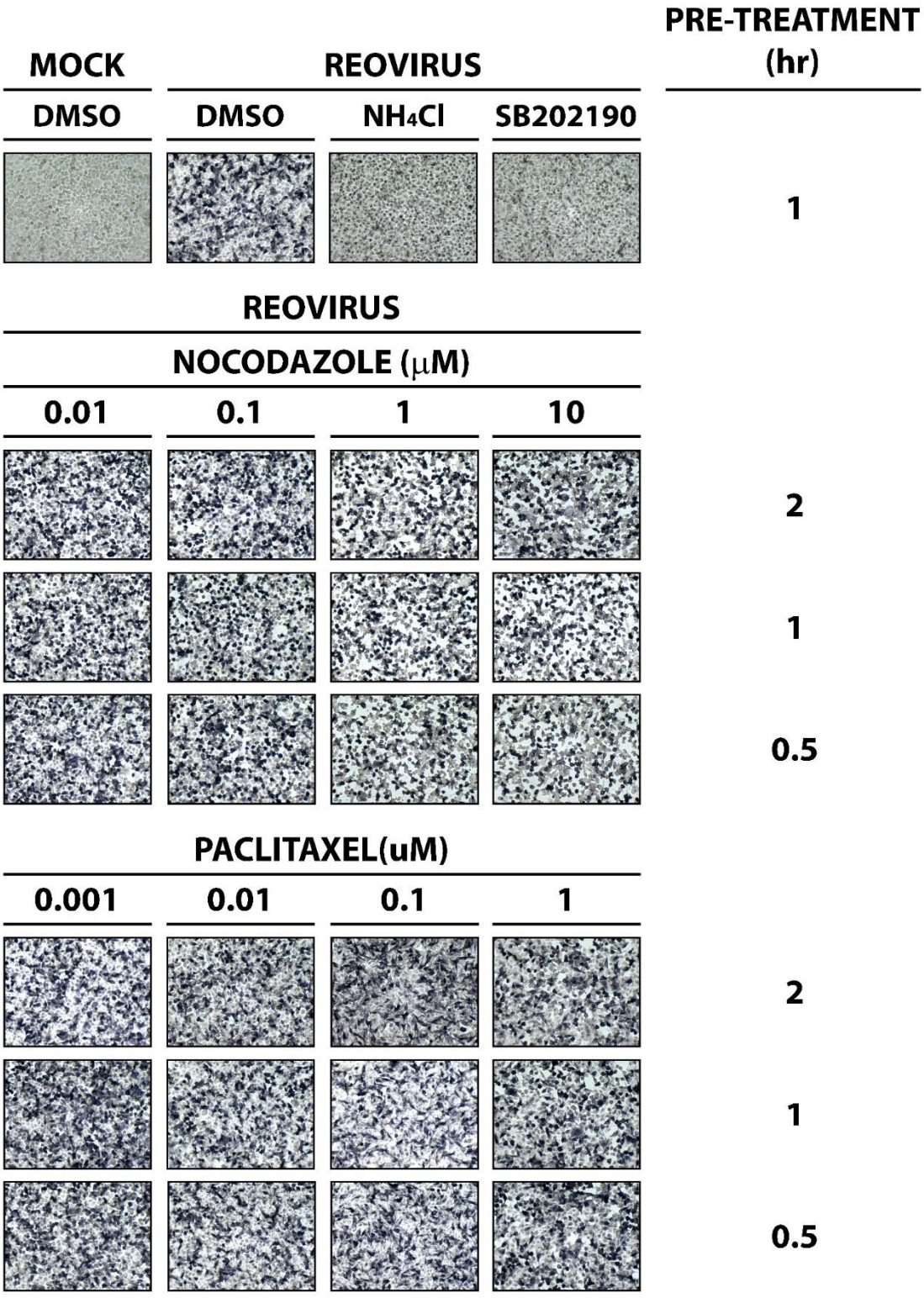
MOCK
REOVIRUS
PRE-TREATMENT (hr)
DMSO
DMSO
NH4Cl
SB202190
1
REOVIRUS
NOCODAZOLE (μM)
0.01
0.1
1
10
2
1
0.5
PACLITAXEL(uM)
0.001
0.01
0.1
1
2
1
0.5

Figure 3.9. Reovirus uncoating and infection occurs in the absence of microtubule function. A) L929 cells were pre-treated with indicated concentrations of DMSO, nocodazole and paclitaxel for 30 minutes at 37°C. Reovirus was added directly to the media a MOI 3 and incubated at 37°C for 3hrs. Cell lysates were collected and processed for Western blot analysis using reovirus specific antibodies. B) Similar to A) except, pre-treatment times varied, and samples were processed at 12hpi with immunocytochemistry staining using reovirus specific primary antibody, alkaline phosphatase conjugated secondary antibody, and NBT/BCIP substrate. SB202190 and NH_4Cl were pre-treated for 1hr prior to reovirus addition. SB202190 was used at 20μM, and NH_4Cl was used at 10mM.

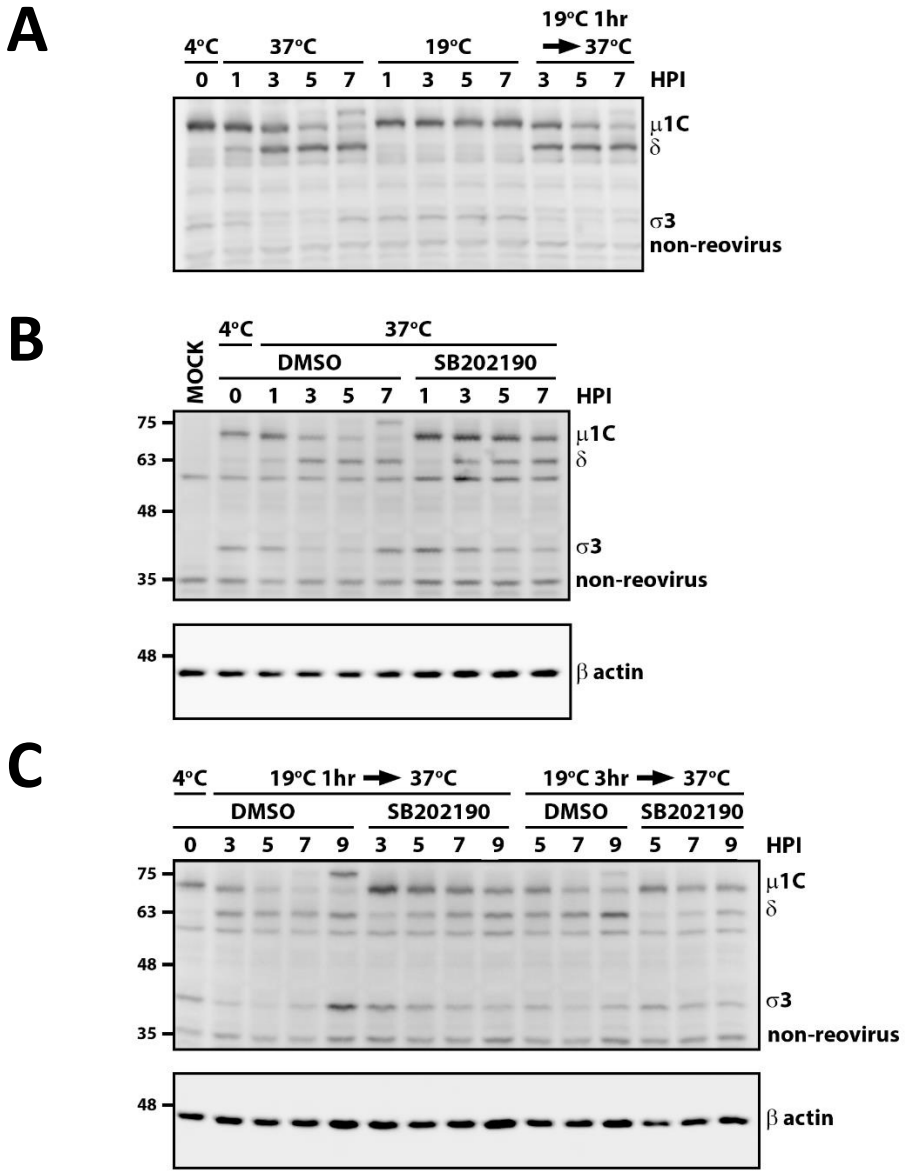

Fig 3.10. Late endosome to lysosome transition is mediated by p38 MAPK signaling. L929 cells were bound with reovirus (MOI 3) at 4°C and incubated at 19°C and/or 37°C, for the timepoints indicated. Media was supplemented with SB202190 (final 20μM) at various timepoints upon start of 19°C and/or 37°C incubation. Cell lysates were collected at the timepoints indicated (HPI) and processed for Western blot analysis using reovirus specific antibodies or β actin (loading control).

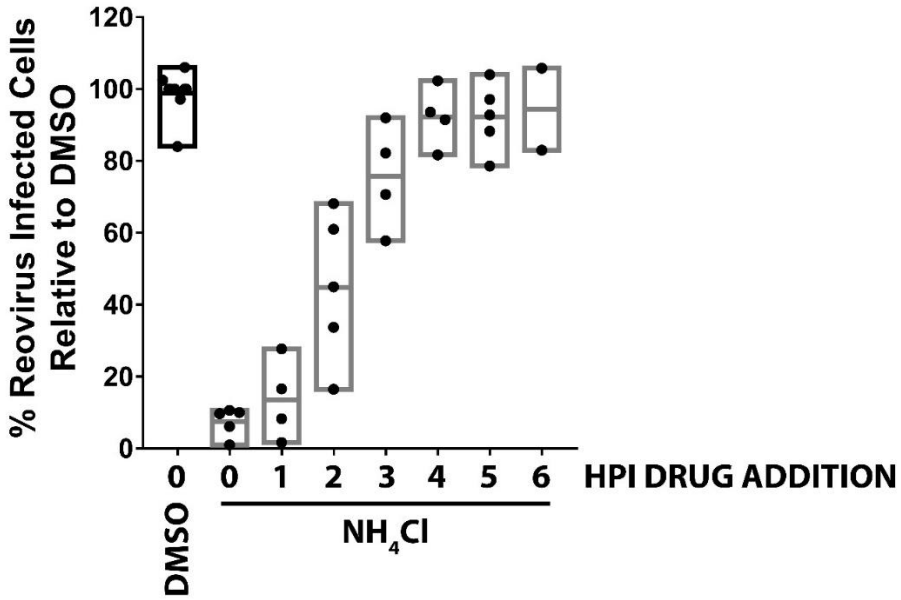

Fig 3.11. Reovirus endosomal escape sufficient for successful infection occurs after 3hpi. L929 cells were bound with reovirus (MOI 3) at 4°C and incubated at 37°C for 12hrs. Media was supplemented with NH_4Cl (final 10mM) at various timepoints upon start of 37°C incubation (0hpi). At 12hpi, samples were fixed and reovirus infected cells were quantified using flow cytometry. Untreated wells were used for standardization. $n \geq 2$

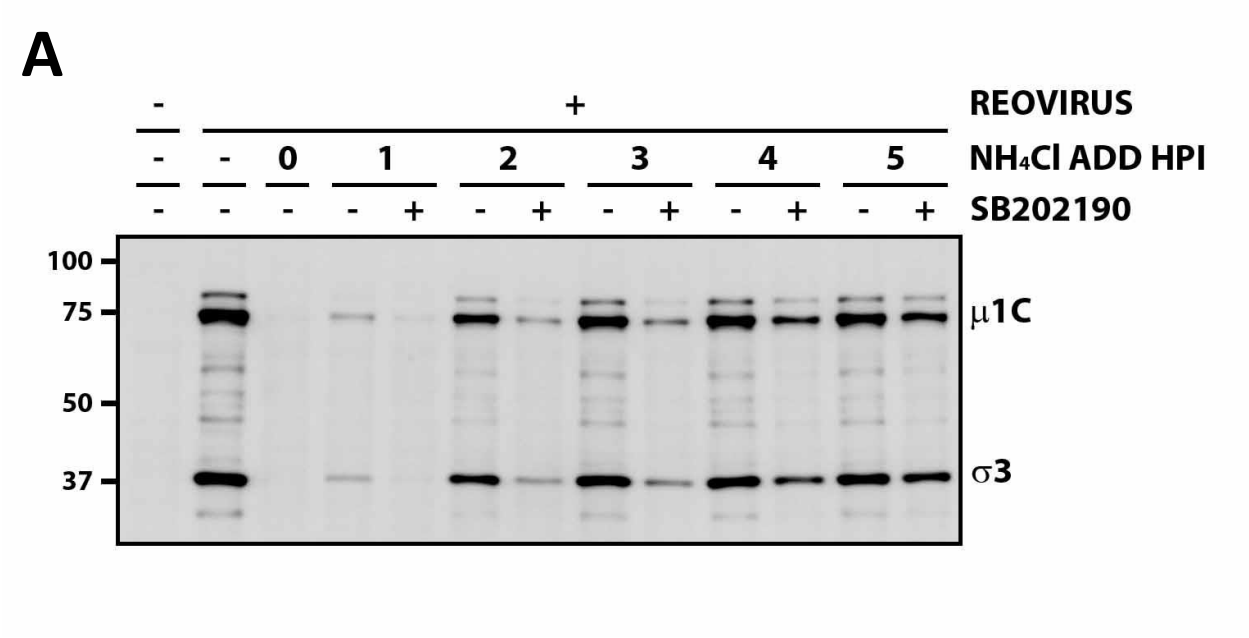
A
-
+
REOVIRUS
-
-
0
1
2
3
4
5
NH4Cl ADD HPI
-
-
-
-
+
-
+
-
+
-
+
-
+
SB202190
100
75
50
37
μ1C
σ3

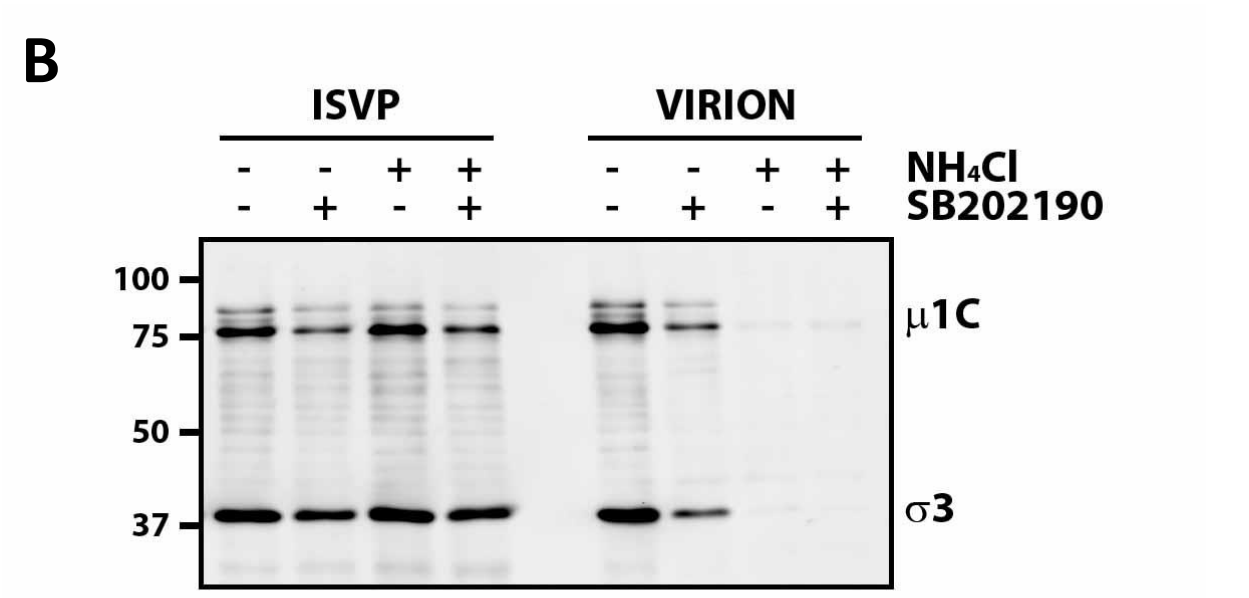
B
ISVP
VIRION
-
-
+
+
-
-
+
+
NH4Cl
-
+
-
+
-
+
-
+
SB202190
100
75
50
37
μ1C
σ3

Fig 3.12. A post uncoating step in reovirus infection is modulated by p38 MAPK signaling. A) L929 cells were bound with reovirus (MOI 3) at 4°C and incubated at 37°C for 12hrs. Media was supplemented with NH_4Cl (final 10mM) or NH_4Cl and SB202190 (20μM) at various timepoints upon start of 37°C incubation (0hpi). At 12hpi, cell lysates were collected and processed for Western blot analysis using reovirus specific antibodies. B) Similar to A), with the addition of ISVP infection, and NH_4Cl and/or SB202190 were only added at the start of infection.

A

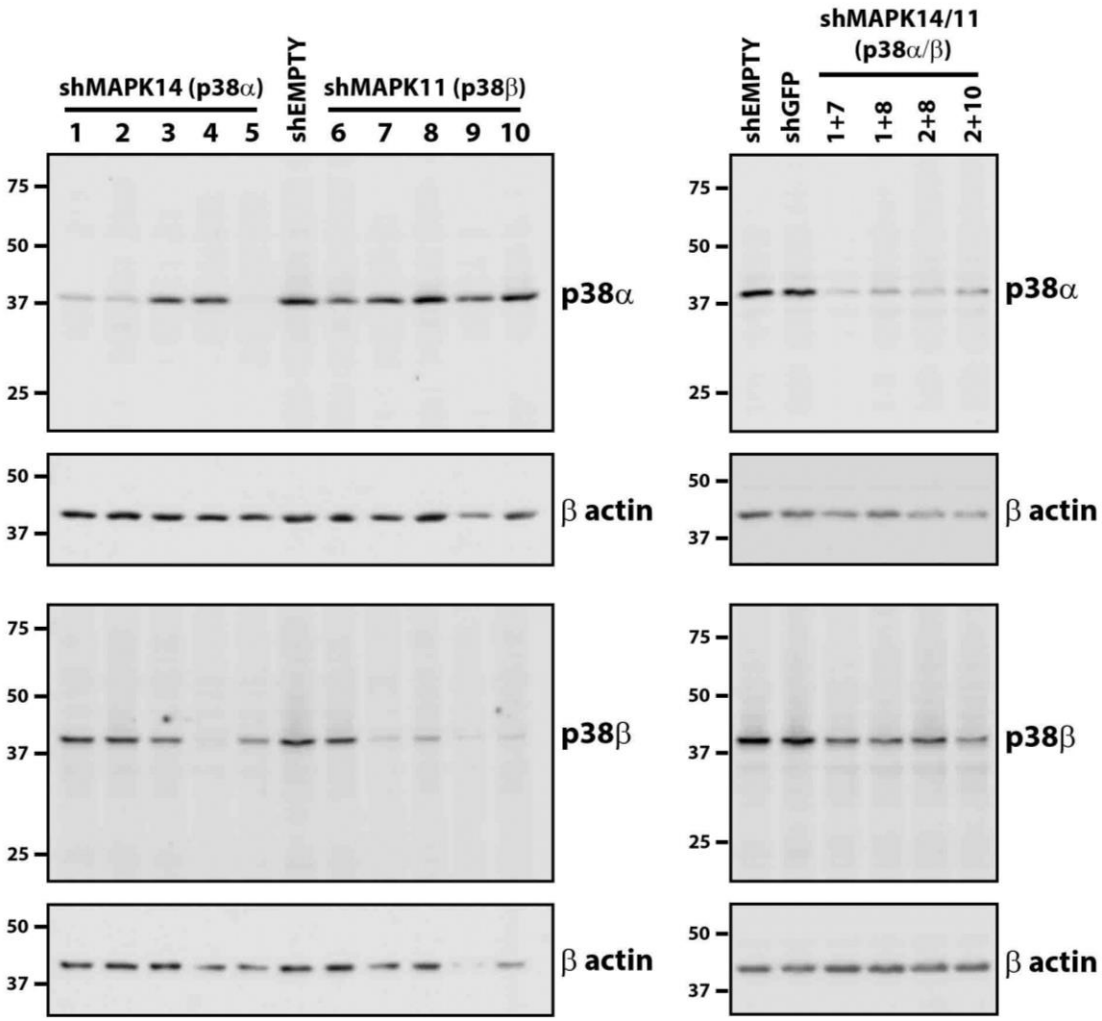
shMAPK14 (p38α)
1 2 3 4 5
shEMPTY
shMAPK11 (p38β)
6 7 8 9 10
shEMPTY
shGFP
shMAPK14/11 (p38α/β)
1+7
1+8
2+8
2+10
75
50
37
25
p38α
β actin
p38β

B

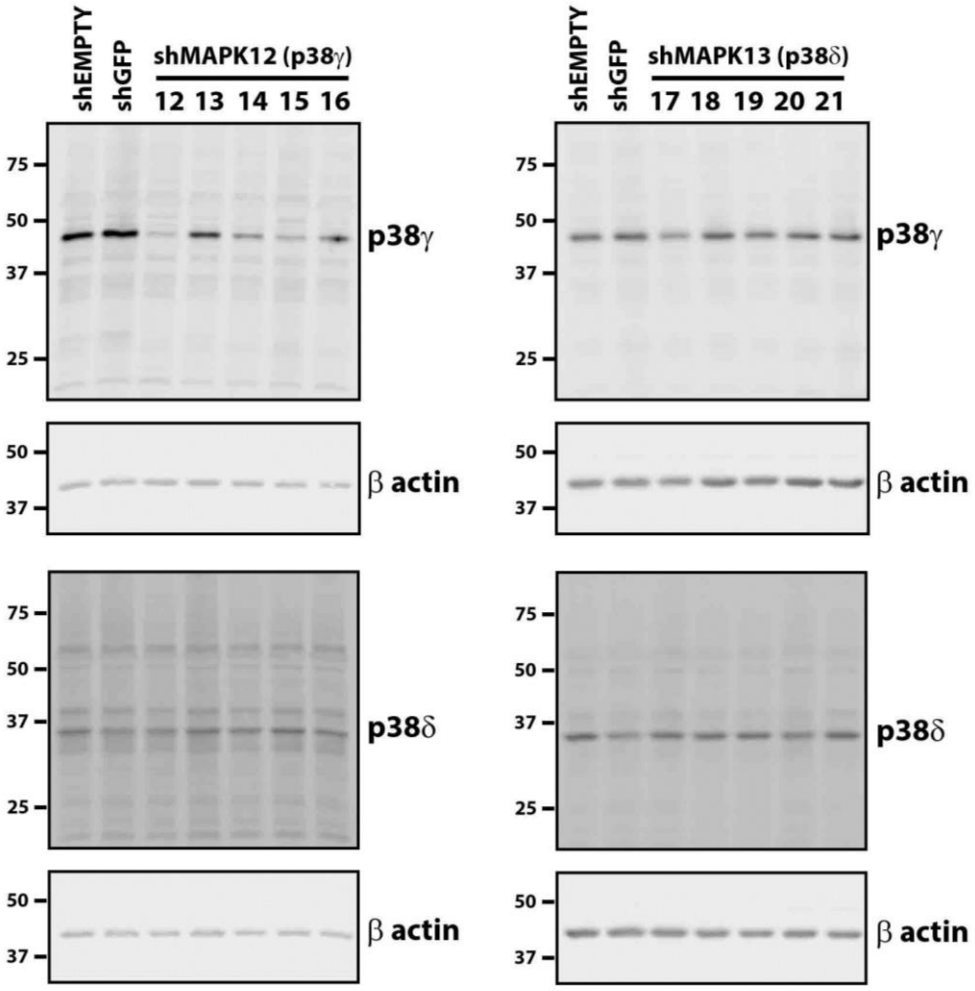
shEMPTY
shGFP
shMAPK12 (p38γ)
12 13 14 15 16
shMAPK13 (p38δ)
17 18 19 20 21
75
50
37
25
p38γ
β actin
p38δ

C

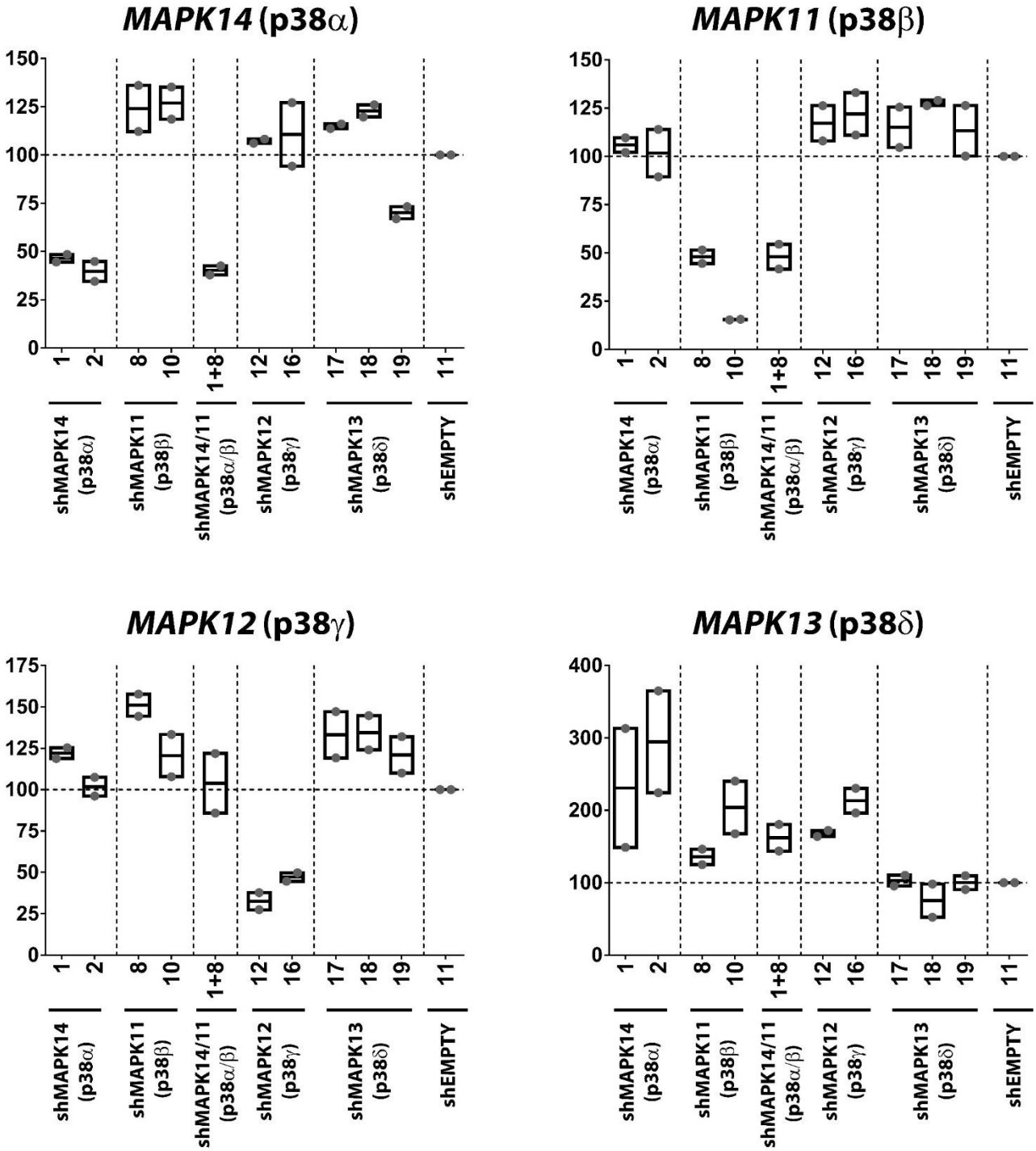
MAPK14 (p38α)
MAPK11 (p38β)
MAPK12 (p38γ)
MAPK13 (p38δ)
shMAPK14 (p38α)
shMAPK11 (p38β)
shMAPK14/11 (p38α/β)
shMAPK12 (p38γ)
shMAPK13 (p38δ)
shEMPTY
1
2
8
10
1+8
12
16
17
18
19
11

Fig 3.13. Stable knockdown assessment of p38 MAPK isoforms in H1299 cells. Lentivirus transduced and puromycin selected H1299 cells were collected for either A) Western blot analysis using isoform specific antibodies and β actin (loading control) or B) RT-PCR with isoform specific gene primers (corrected for *GAPDH*). $n \geq 2$

A

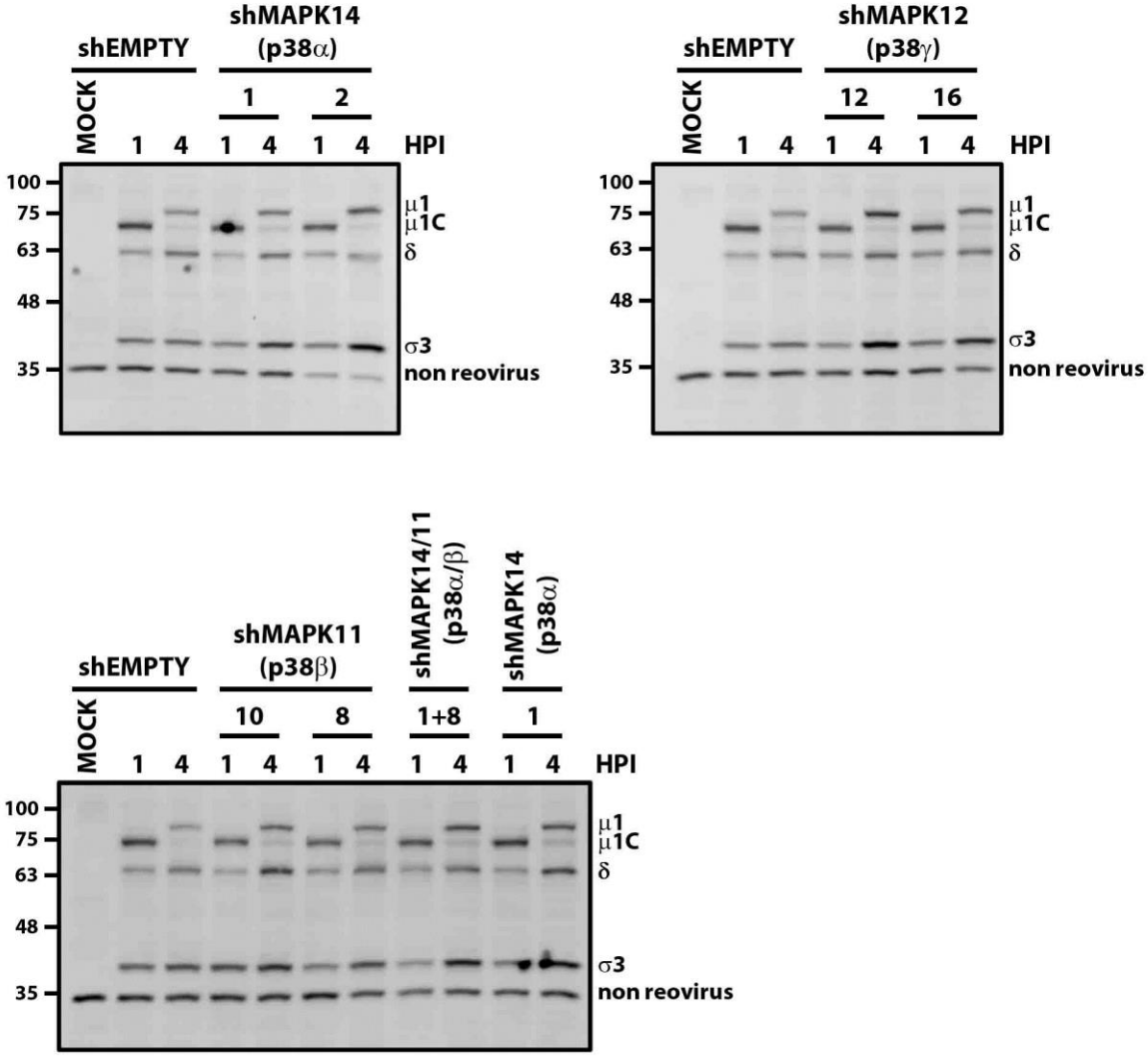
shEMPTY
shMAPK14 (p38α)
1
2
MOCK
1 4 1 4 1 4 HPI
100
75
63
48
35
μ1
μ1C
δ
σ3
non reovirus
shEMPTY
shMAPK12 (p38γ)
12
16
MOCK
1 4 1 4 1 4 HPI
100
75
63
48
35
μ1
μ1C
δ
σ3
non reovirus
shEMPTY
shMAPK11 (p38β)
shMAPK14/11 (p38α/β)
shMAPK14 (p38α)
10
8
1+8
1
MOCK
1 4 1 4 1 4 1 4 1 4 HPI
100
75
63
48
35
μ1
μ1C
δ
σ3
non reovirus

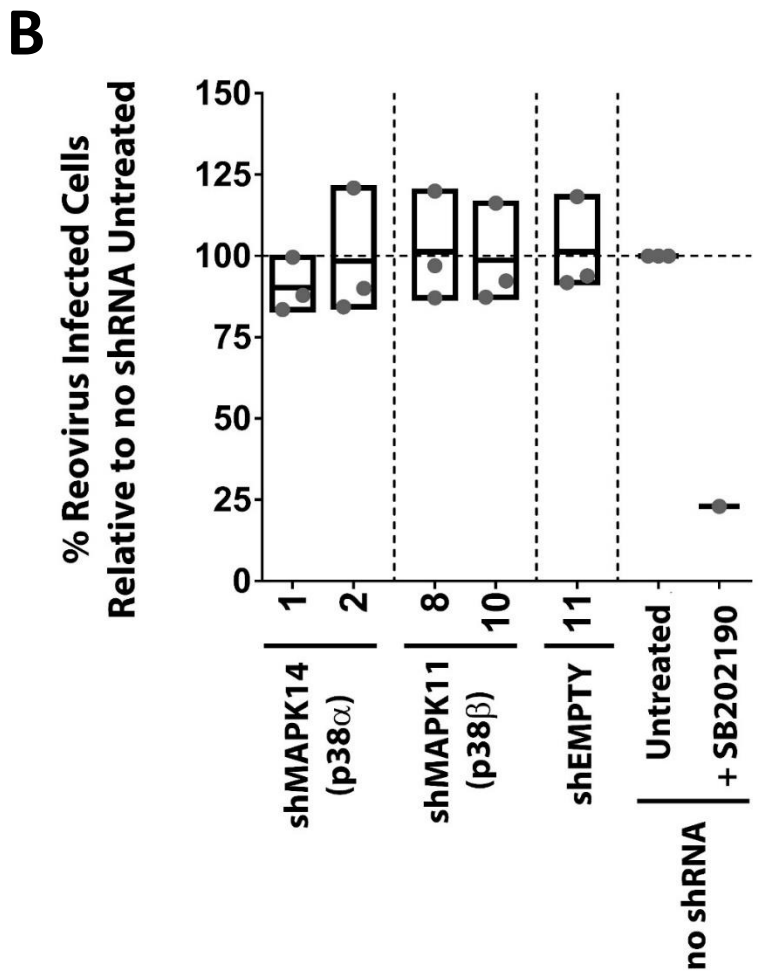

Fig 3.14. p38 MAPK isoform knockdown did not alter reovirus uncoating, early protein synthesis or number of infected cells. Lentivirus transduced and puromycin selected H1299 cells were infected with reovirus at an MOI 3, and samples were collected at A) 1hpi and 4hpi for Western blot analysis using reovirus specific antibodies, B) 12hpi for flow cytometry quantification of reovirus infected cells. $n \geq 1$

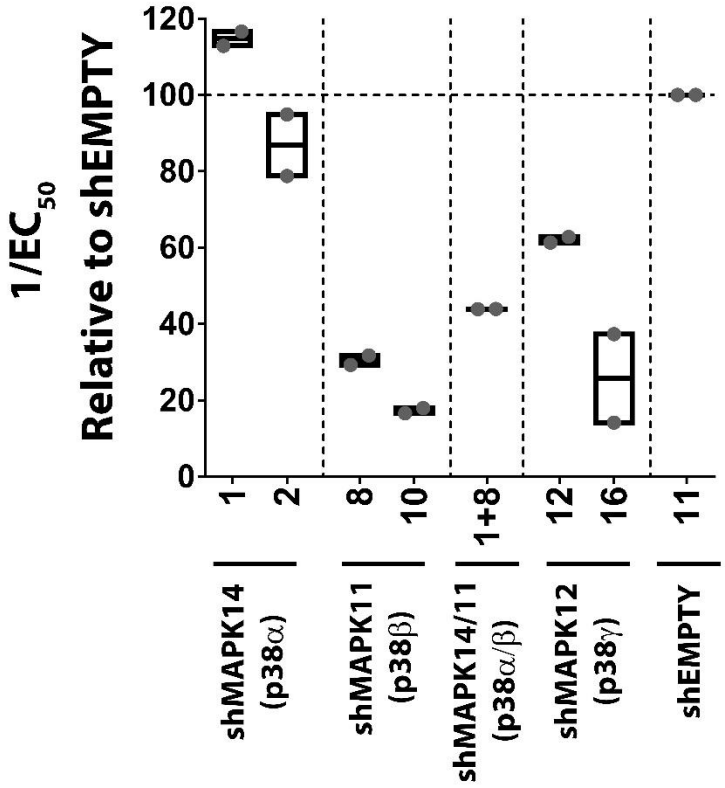

Fig 3.15. Knockdown of p38 MAPK isoforms (p38β and p38γ) inhibited accumulation of reovirus proteins late during infection. Lentivirus transduced and puromycin selected H1299 cells were infected with reovirus dilutions starting at MOI 6 and 10 × ¼ dilutions, for 1hr at 37°C. Virus was removed and fresh media was added. At 15hpi, samples were fixed, and incubated with reovirus specific primary antibody, alkaline phosphatase conjugated secondary antibody, and pNPP substrate. Substrate color change was measured using a plate reader. Titration curves were plotted with absorbance on the y axis and reovirus dilution on the x-axis. Half maximal effective concentration (EC50) values were determined using GraphPad Prism. n = 2

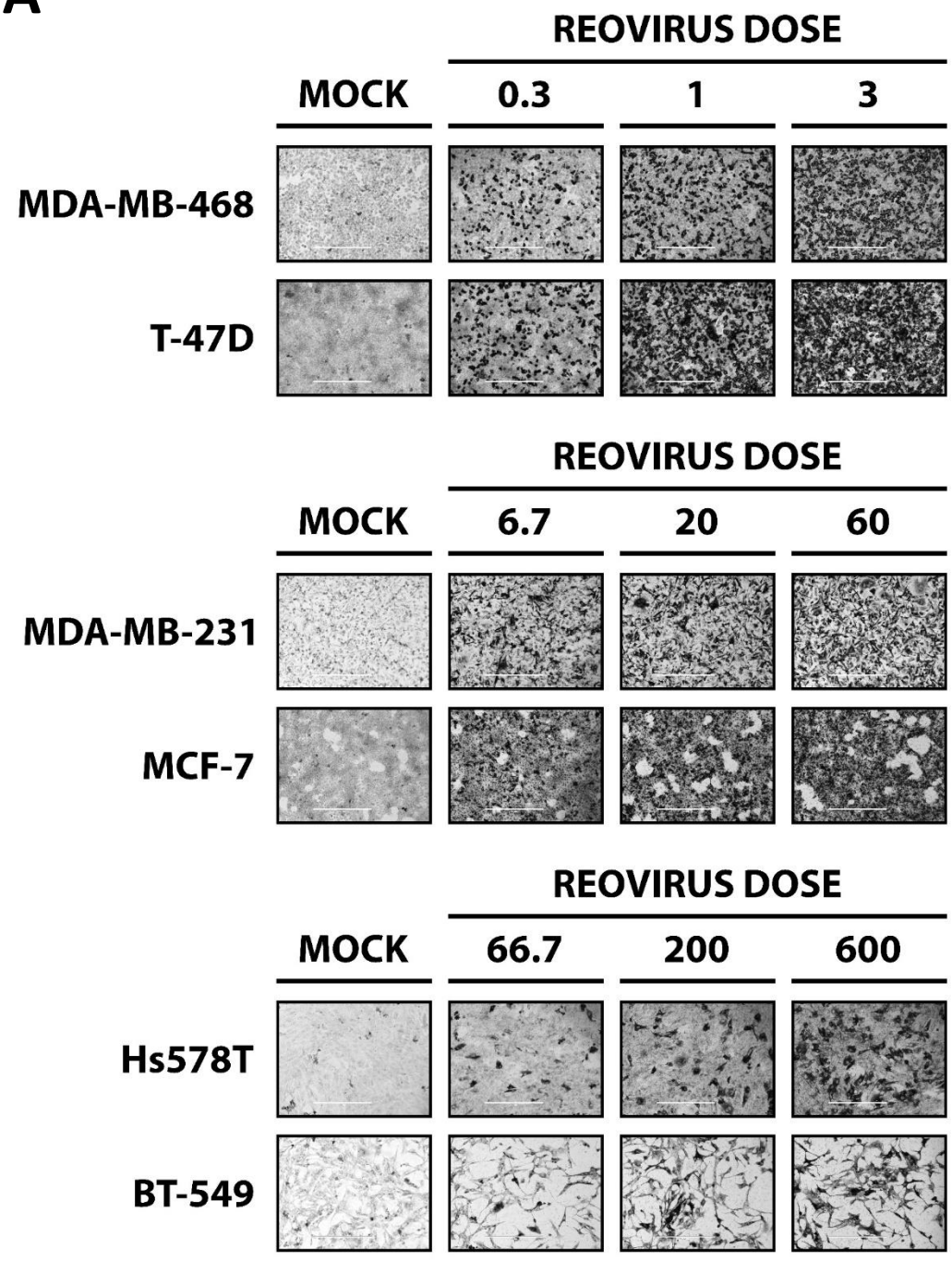
A
REOVIRUS DOSE
MOCK
0.3
1
3
MDA-MB-468
T-47D
REOVIRUS DOSE
MOCK
6.7
20
60
MDA-MB-231
MCF-7
REOVIRUS DOSE
MOCK
66.7
200
600
Hs578T
BT-549

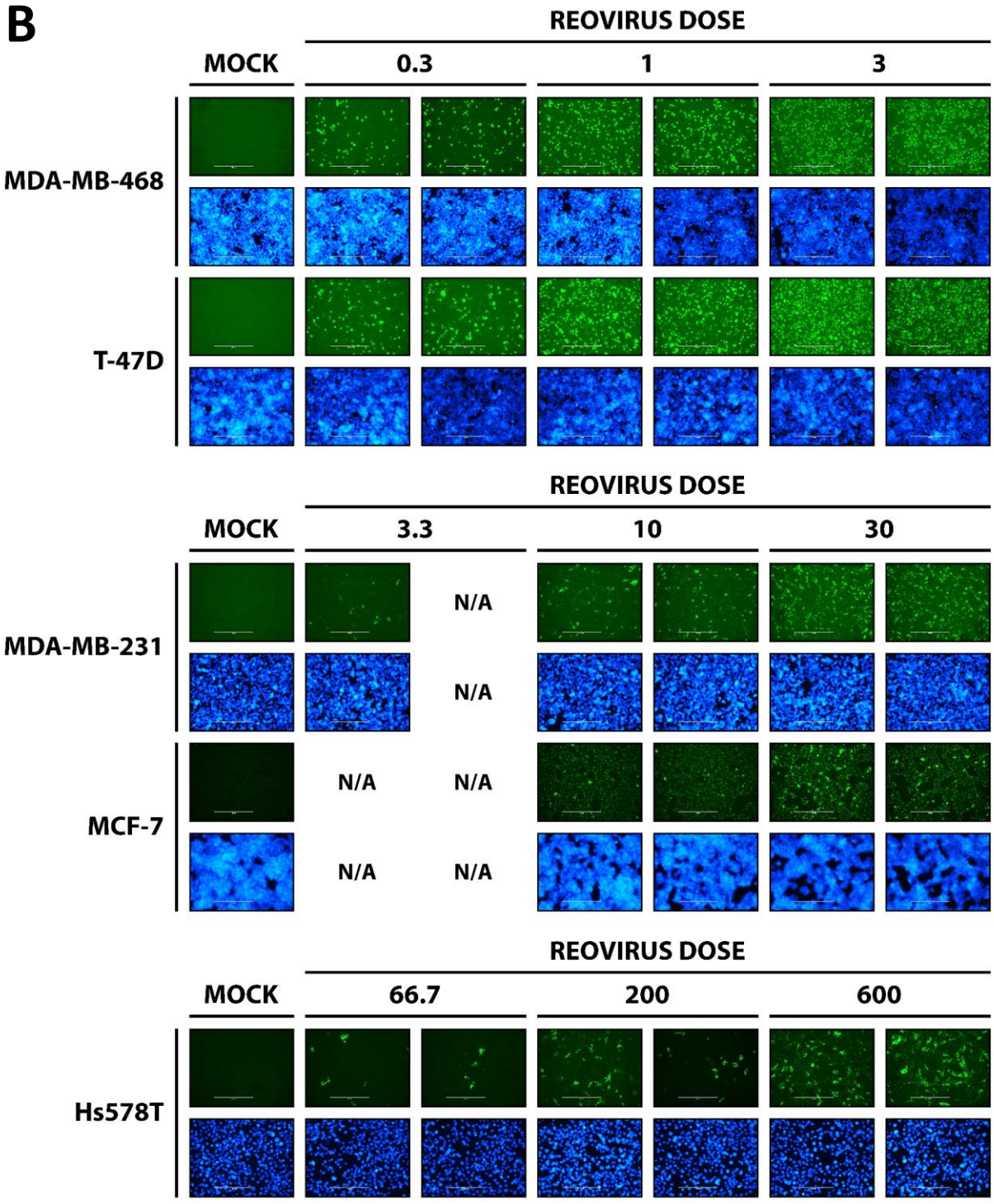
B
REOVIRUS DOSE
MOCK
0.3
1
3
MDA-MB-468
T-47D
REOVIRUS DOSE
MOCK
3.3
10
30
MDA-MB-231
MCF-7
N/A
N/A
N/A
N/A
N/A
N/A
REOVIRUS DOSE
MOCK
66.7
200
600
Hs578T

Figure 3.16: Reovirus susceptibility comparison in NCI-60 breast cancer cell lines. Cell line panel was infected reovirus at indicated dilutions and incubated at 37°C for 12hpi. Reovirus infected cells were identified using reovirus specific primary antibody and A) alkaline phosphatase conjugated secondary antibody, and NBT/BCIP substrate or B) Alexa Fluor 488 conjugated secondary antibody. Nuclei were stained with HOESCHT 33342 (Green staining represents reovirus infected cells, and blue staining represents cell nuclei).

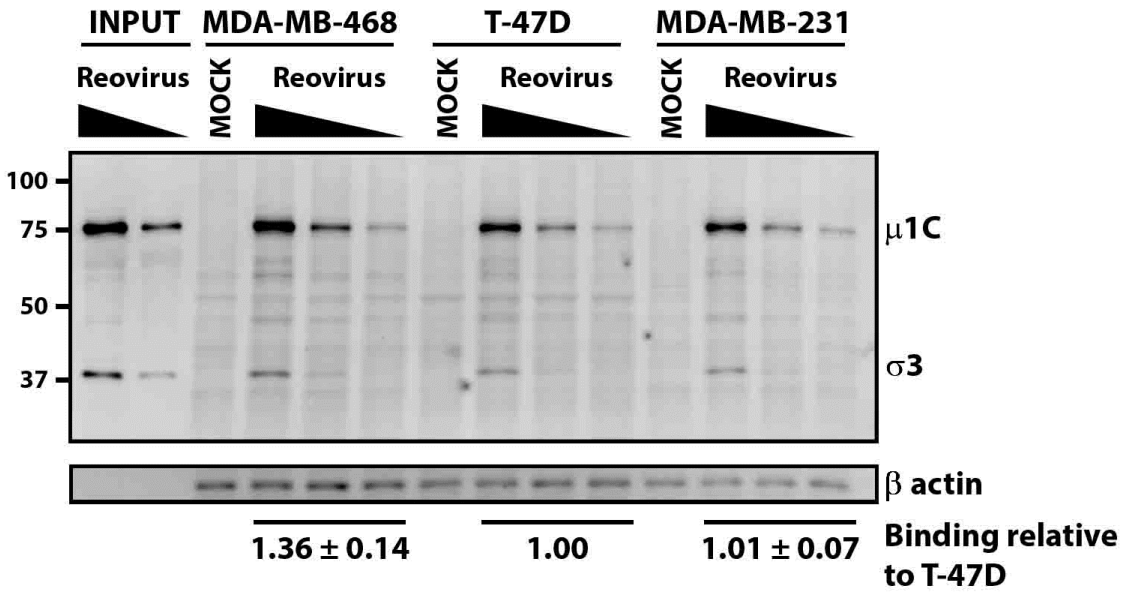
INPUT
MDA-MB-468
T-47D
MDA-MB-231
Reovirus
MOCK
Reovirus
MOCK
Reovirus
MOCK
Reovirus
100
75
50
37
μ1C
σ3
β actin
1.36 ± 0.14
1.00
1.01 ± 0.07
Binding relative to T-47D

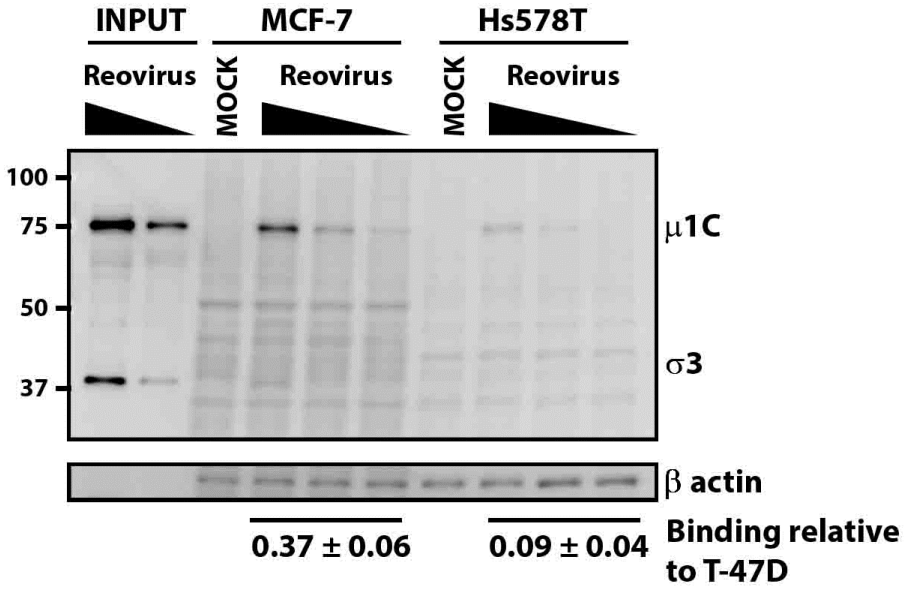
INPUT
MCF-7
Hs578T
Reovirus
MOCK
Reovirus
MOCK
Reovirus
100
75
50
37
μ1C
σ3
β actin
0.37 ± 0.06
0.09 ± 0.04
Binding relative to T-47D

Figure 3.17: Reovirus binding comparison in NCI-60 breast cancer cell lines. Cell line panel was pre-chilled at 4°C for 30 minutes, media was removed and reovirus dilutions were added. Virus was incubated at 4°C for 1hr, washed to remove unbound virus and cell lysates were processed for Western blot analysis using reovirus specific antibodies or β actin (loading control).

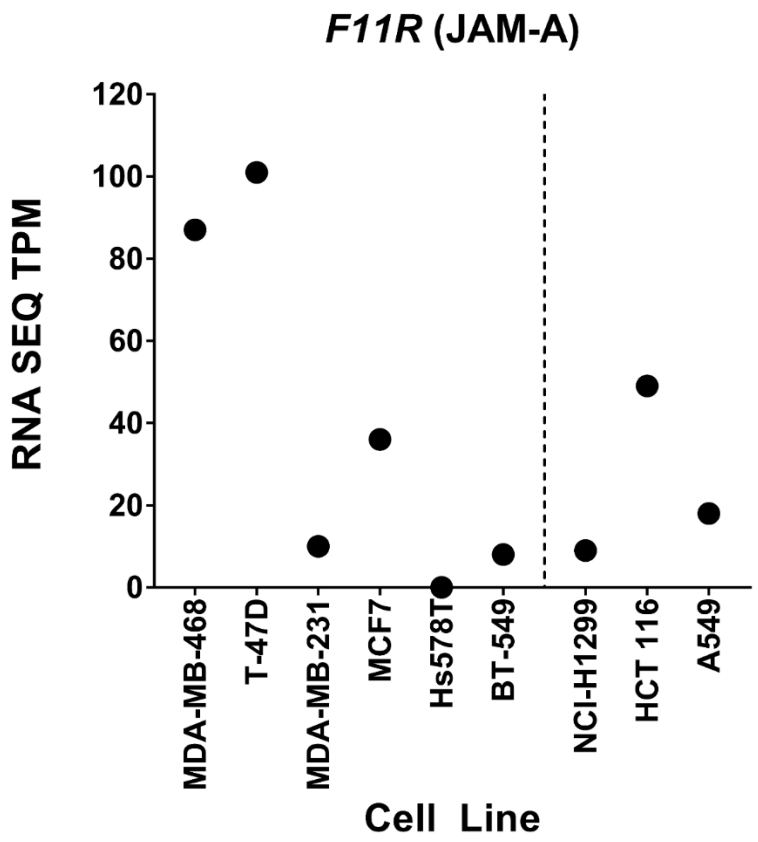

Figure 3.18: F11R (JAM-A) RNA-seq gene expression analysis. Source: EMBL expression atlas

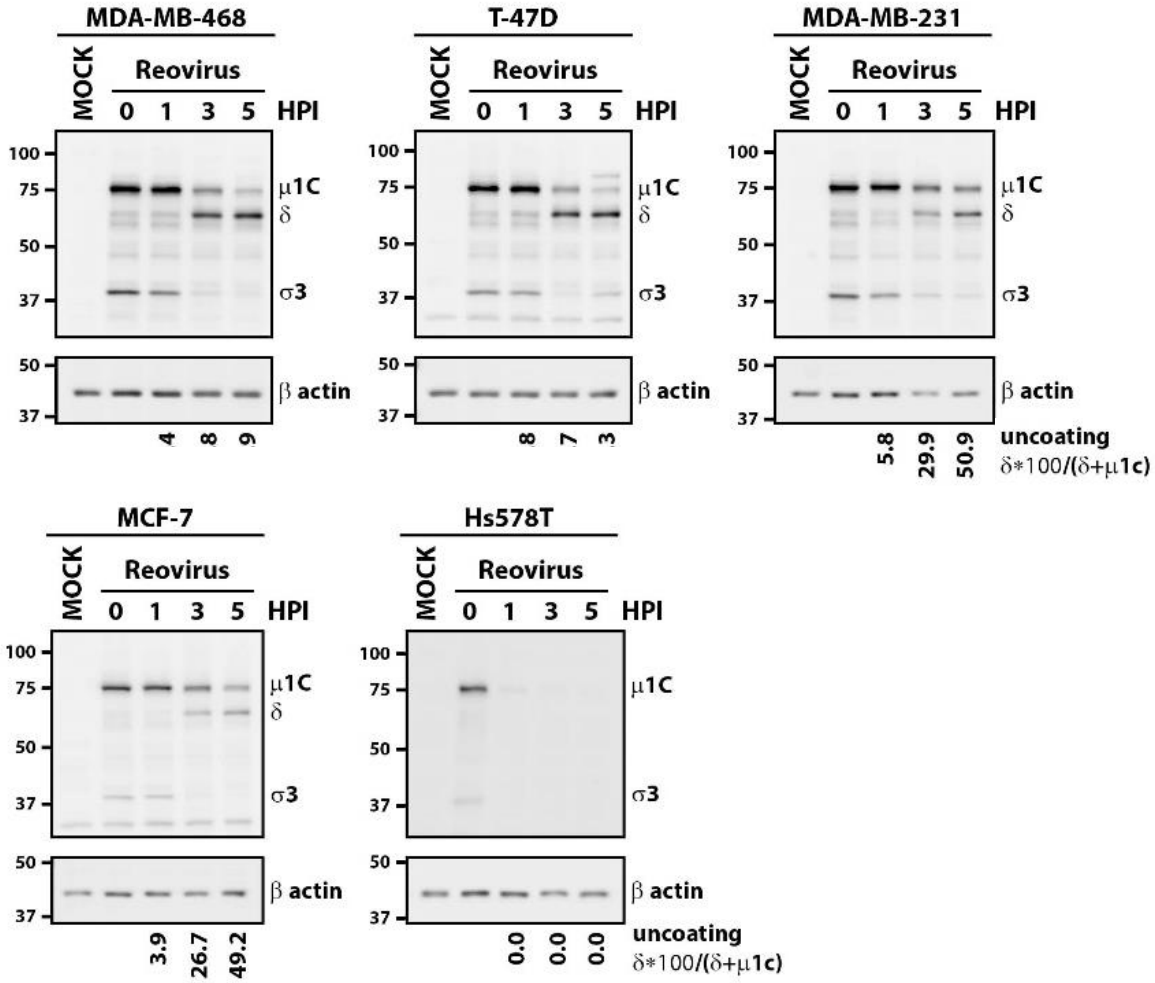

Figure 3.19: Reovirus intracellular uncoating comparison in NCI-60 breast cancer cell lines. Similar to Fig 3.17, except samples were incubated at 37°C and collected at 1hpi, 3hpi and 5hpi. Cell lysates were processed for Western blot analysis using reovirus specific antibodies or β actin (loading control).

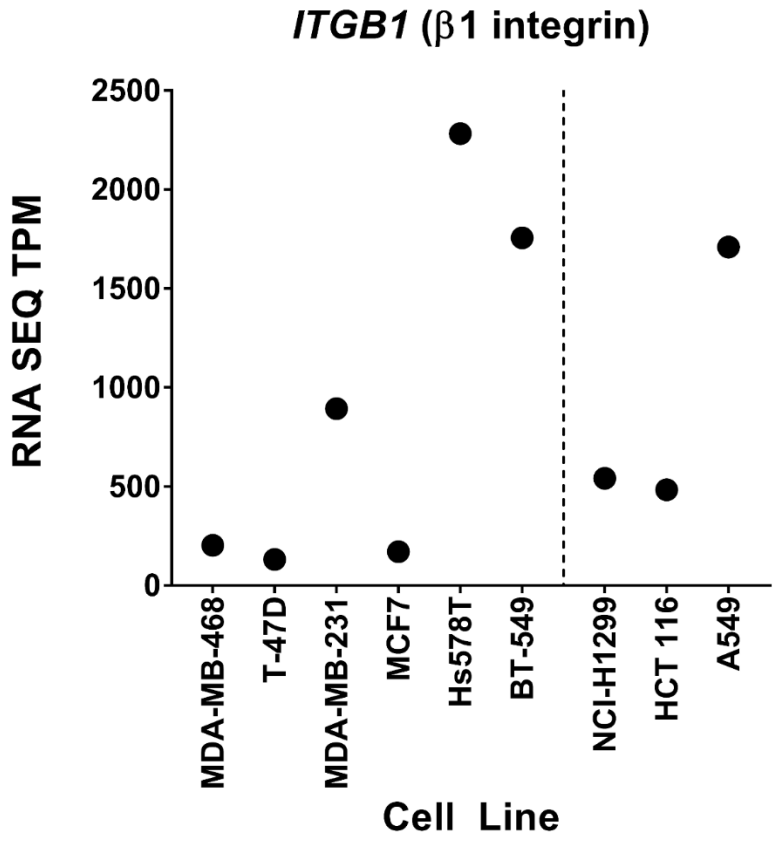

Figure 3.20: ITGB1 (β1 integrin) RNA-seq gene expression analysis. Source: EMBL expression atlas

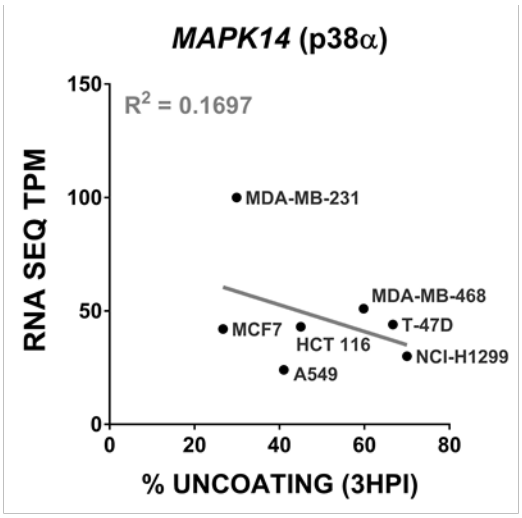
MAPK14 (p38α)
R2 = 0.1697
RNA SEQ TPM
% UNCOATING (3HPI)
MDA-MB-231
MDA-MB-468
MCF7
T-47D
HCT 116
NCI-H1299
A549

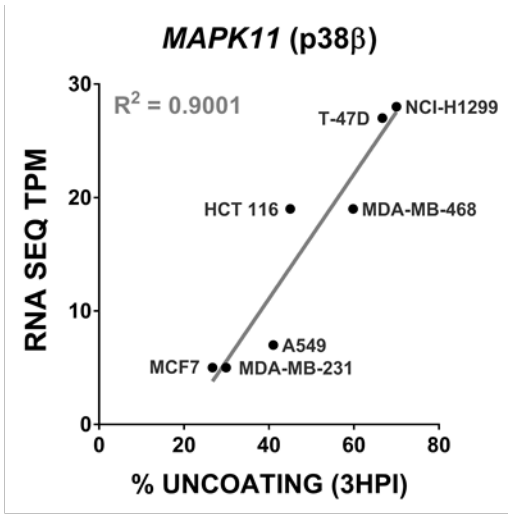
MAPK11 (p38β)
R2 = 0.9001
RNA SEQ TPM
% UNCOATING (3HPI)
T-47D
NCI-H1299
HCT 116
MDA-MB-468
A549
MCF7
MDA-MB-231

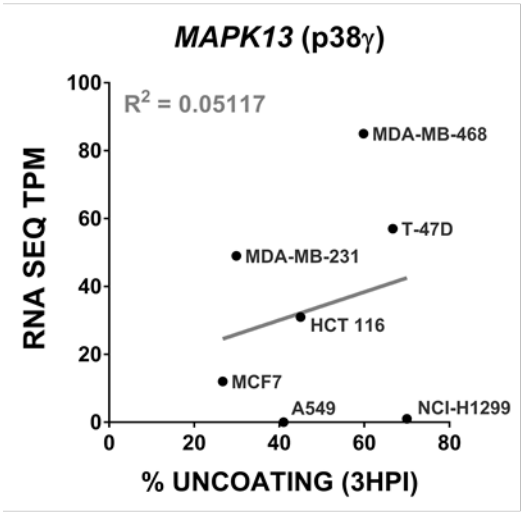
MAPK13 (p38γ)
R2 = 0.05117
RNA SEQ TPM
% UNCOATING (3HPI)
MDA-MB-468
T-47D
MDA-MB-231
HCT 116
MCF7
A549
NCI-H1299

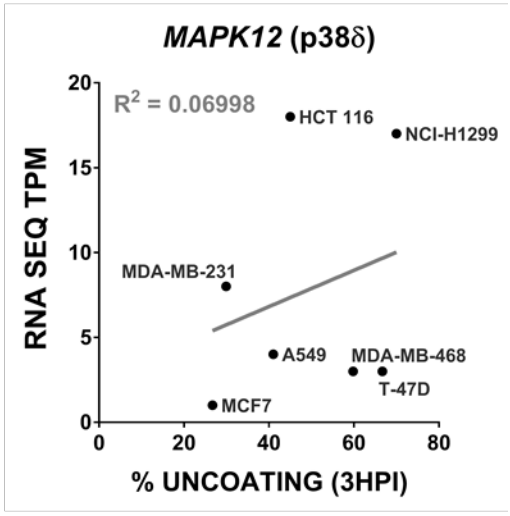
MAPK12 (p38δ)
R2 = 0.06998
RNA SEQ TPM
% UNCOATING (3HPI)
HCT 116
NCI-H1299
MDA-MB-231
A549
MDA-MB-468
T-47D
MCF7

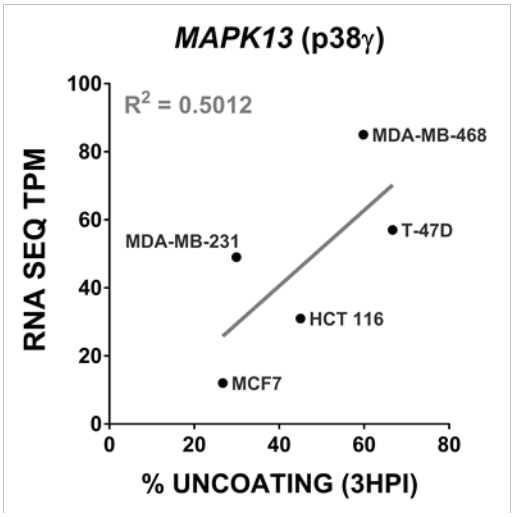
MAPK13 (p38γ)
R2 = 0.5012
RNA SEQ TPM
% UNCOATING (3HPI)
MDA-MB-468
MDA-MB-231
T-47D
HCT 116
MCF7

Figure 3.21: MAPK11 (p38β) isoform correlates with reovirus uncoating efficiency. Y-axis represents RNA-seq expression of p38 MAPK isoforms obtained from EMBL expression atlas. X-axis represents % reovirus uncoating [(δ/δ+μ1C)/100] calculated at 3hpi from Fig 3.18 (T-47D, MDA-MB-468, MDA-MB-231, MCF7), Fig 3.8 (L929, NCI-H1299, HCT 116) and data not shown (A549).

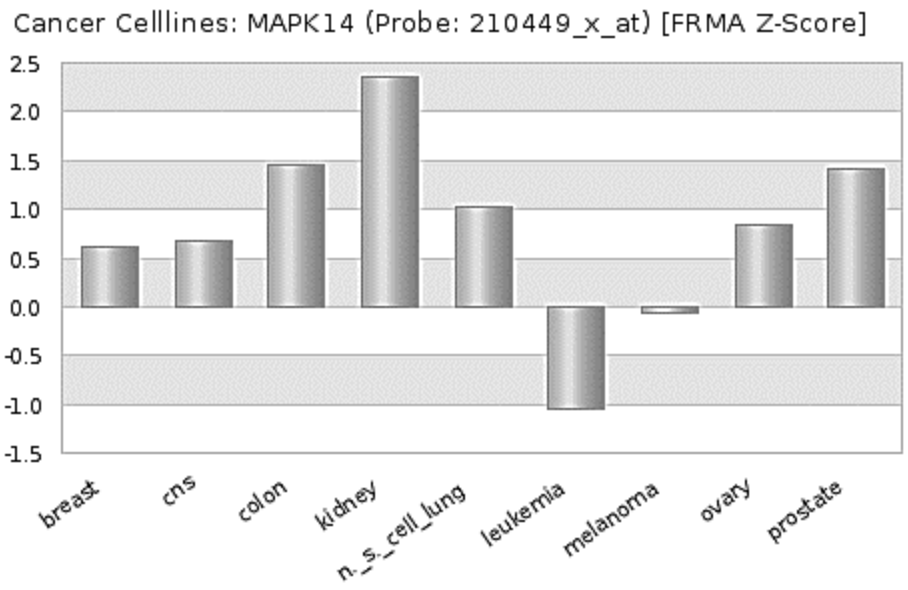
Cancer Celllines: MAPK14 (Probe: 210449_x_at) [FRMA Z-Score]
2.5
2.0
1.5
1.0
0.5
0.0
-0.5
-1.0
-1.5
breast
cns
colon
kidney
n._s._cell_lung
leukemia
melanoma
ovary
prostate

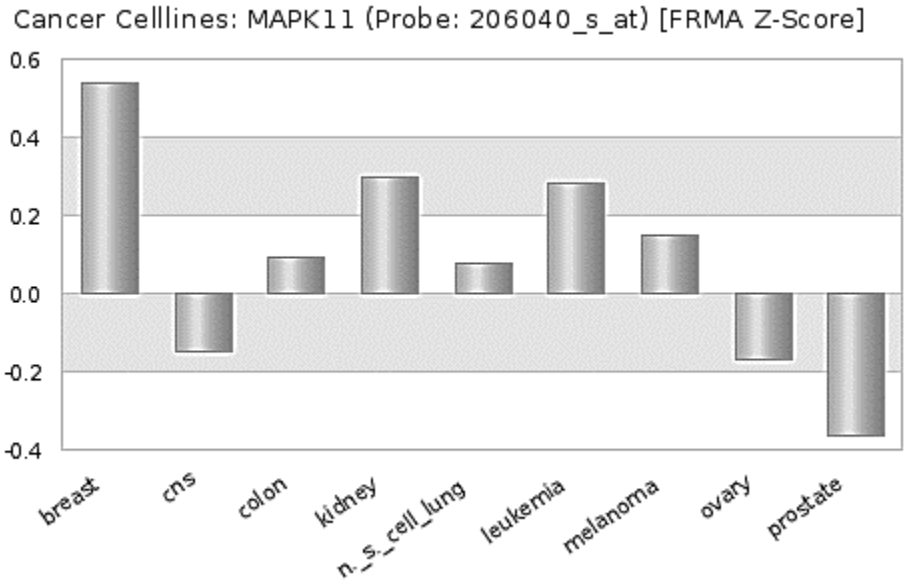
Cancer Celllines: MAPK11 (Probe: 206040_s_at) [FRMA Z-Score]
0.6
0.4
0.2
0.0
-0.2
-0.4
breast
cns
colon
kidney
n._s._cell_lung
leukemia
melanoma
ovary
prostate

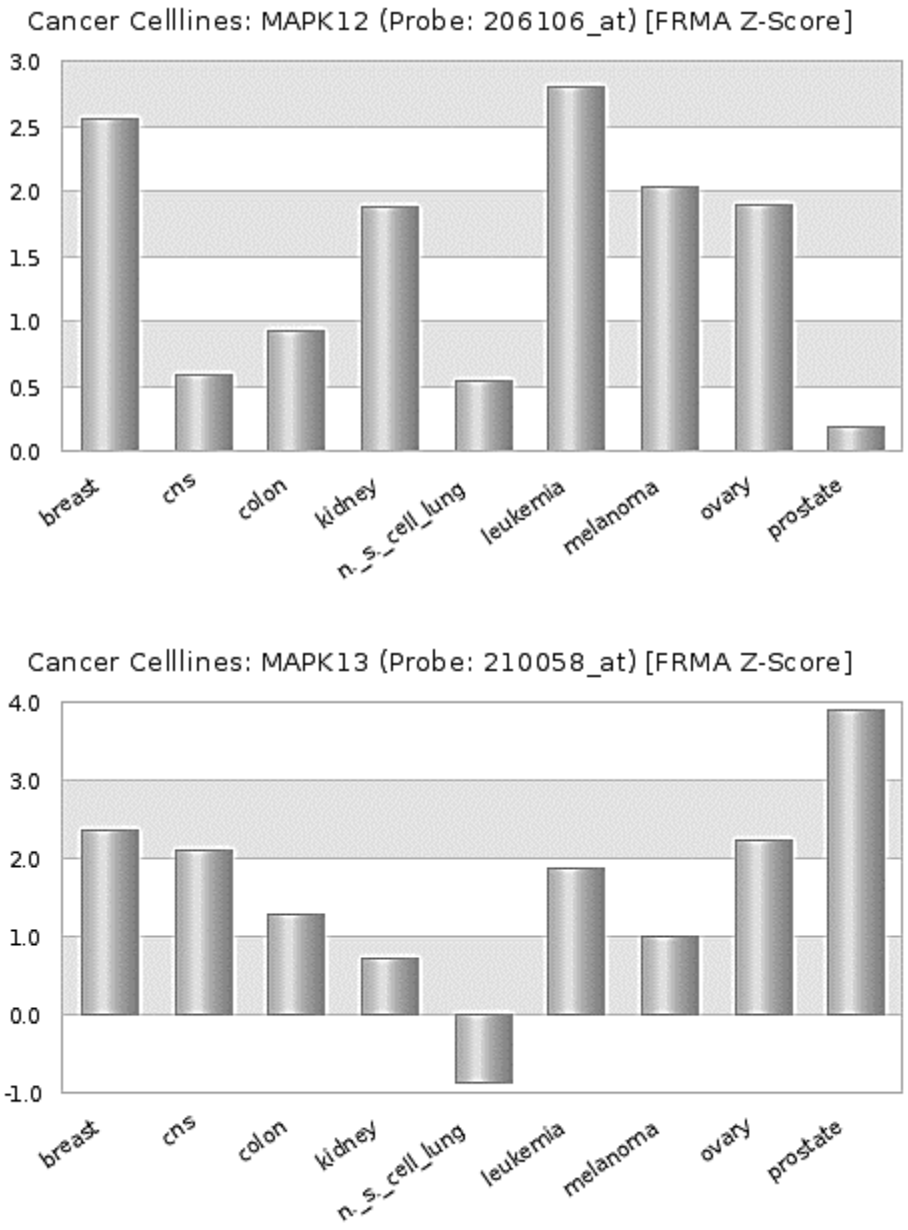

Figure 3.22: MAPK13 (p38γ) expression is lowest in the non-small (n.s) cell lung NCI-60 cell line panel. Source: Medicalgenomics – microarray -NCI-60 tumor cell lines

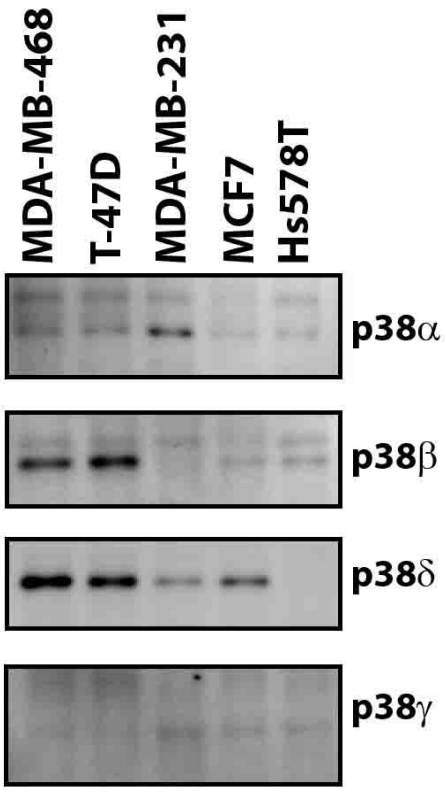

Figure 3.23. Assessment of p38 MAPK isoforms in NCI-60 breast cancer cell lines.

Equalized for cell number, cell lysates were collected and processed for Western blot analysis using p38 MAPK isoform specific antibodies.

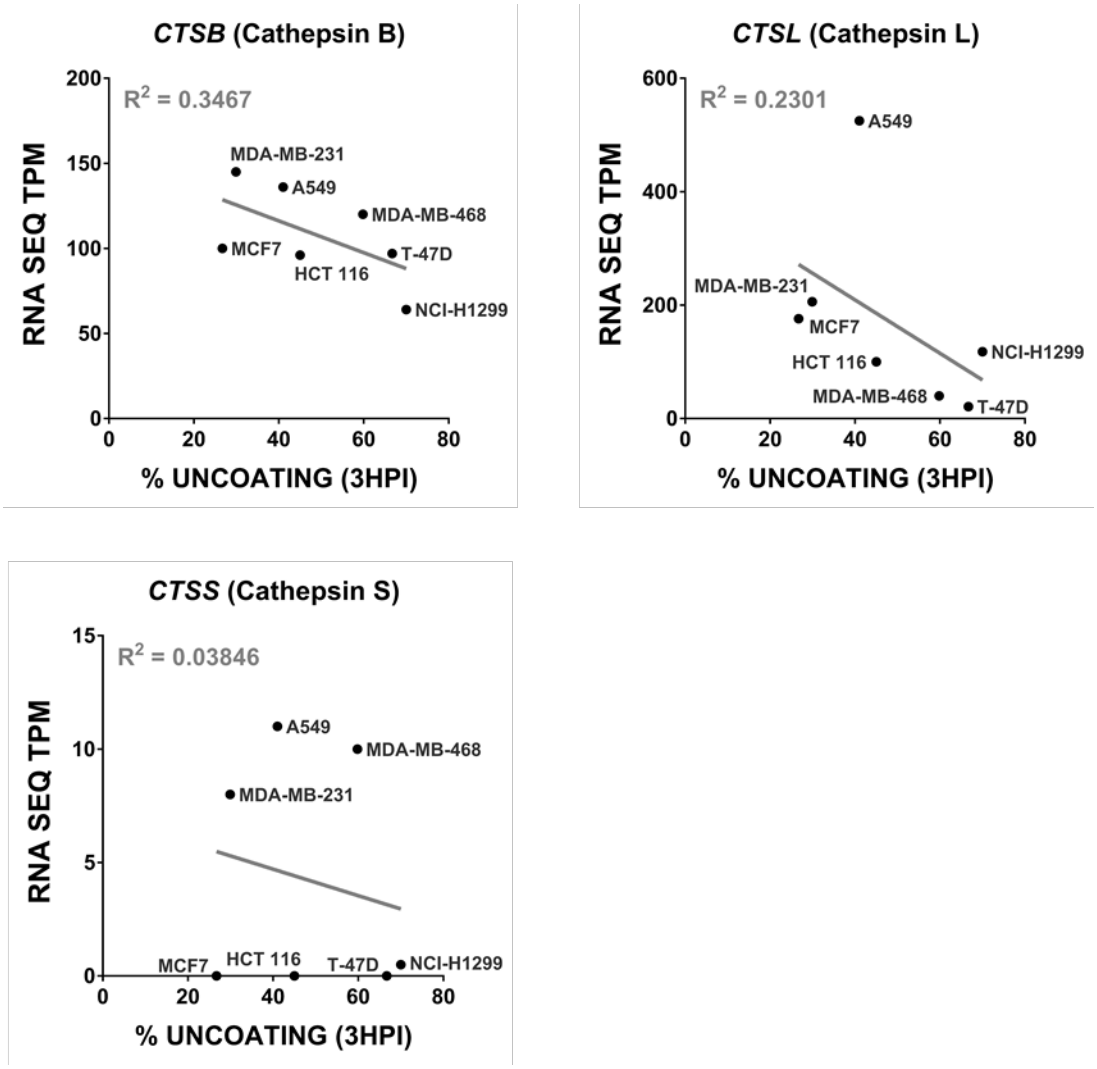

Figure 3.24: CTSB (cathepsin B) expression does not correlates with reovirus uncoating efficiency. Y-axis represents RNA-seq expression of cathepsins obtained from EMBL expression atlas. X-axis represents % reovirus uncoating [(δ/δ+μ1C)/100] calculated at 3hpi from Fig 3.18 (T-47D, MDA-MB-468, MDA-MB-231, MCF7), Fig 3.8 (L929, NCI-H1299, HCT 116) and data not shown (A549).

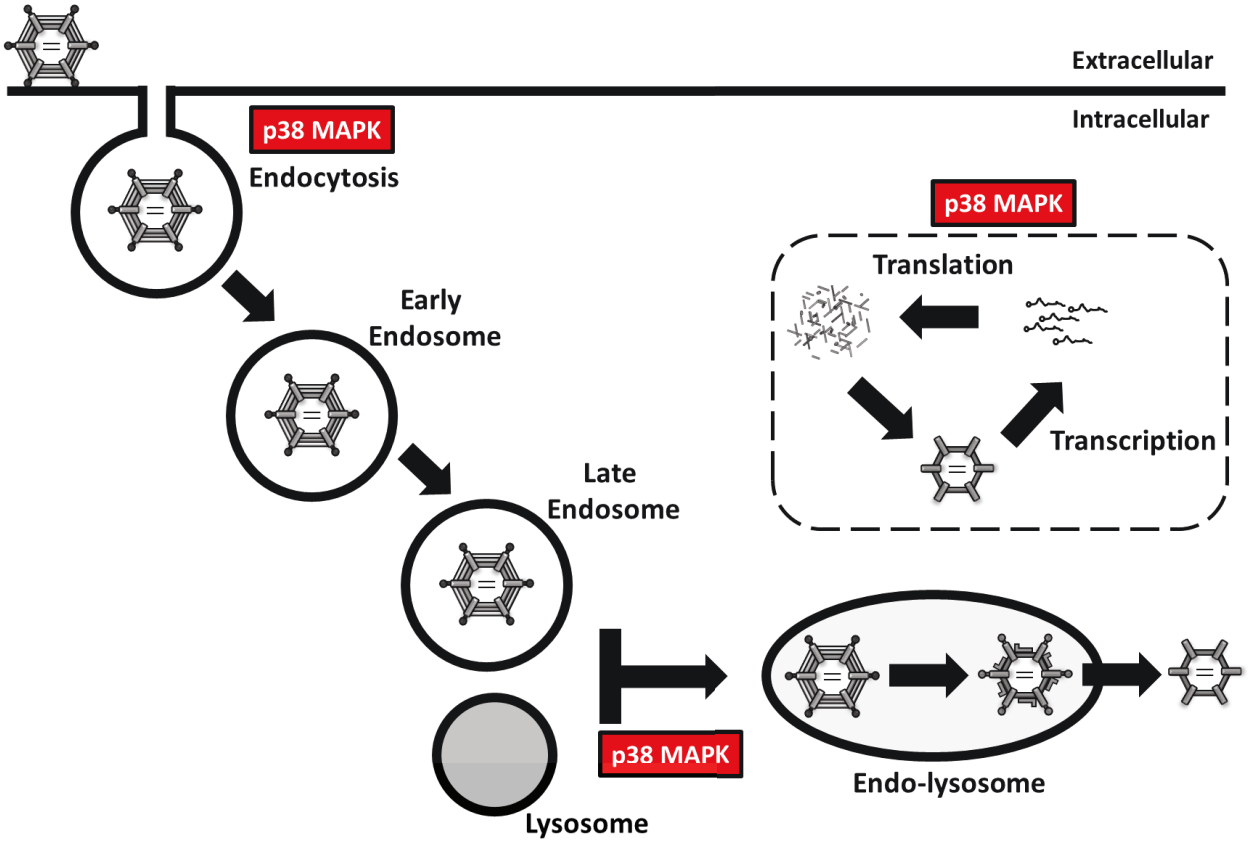

Figure 3.25: Steps during reovirus replication modulated by p38 MAPK signaling. Reovirus endocytosis, uncoating and post-uncoating steps are diminished during p38 MAPK inhibitor treatment.

3.2 DISCUSSION

Numerous host factors play roles during the entry, initiation, replication and dissemination steps of reovirus infection [228, 322-324]. Host signaling though p38 MAPK is involved in processes such as vesicle trafficking, mRNA transcription and stability, and protein translation [315, 325]. Using a panel of specific p38 MAPK inhibitors and an inactive inhibitor analogue, we demonstrate that p38 MAPK signaling is important for reovirus endocytosis, uncoating and viral protein synthesis. Our analysis identified a potential role of p38 MAPK signaling during late endosome and lysosome fusion and/or lysosome biogenesis. Additionally, using a breast cancer cell line panel we observed a strong correlation between p38β and reovirus uncoating. Our study elucidates the functional importance of p38 MAPK signaling during reovirus infection and identifies the p38β isoform as a potential biomarker for reovirus uncoating and overall susceptibly.

Previous work had established that p38 MAPK signaling triggers IFNβ expression upon reovirus infection and was therefore important in limiting reovirus spread [239]. Additional studies demonstrated that augmented reovirus infection in Ras transformed cells occurred via the Ras/Ral-GEF/p38 MAPK signaling axis [300]. However, the precise roles of p38 MAPK signaling during the initial reovirus infection cycle were unknown. Using multiple p38 MAPK inhibitors (SB202190, SB203580, BIRB796) we observed a dose-dependent reduction of initial reovirus infection at 12hpi (Fig 3.4A, 3.4B). Reovirus infection of both human (T47D breast, H1299 non-small cell lung) and mouse (B16-F10 melanoma) cancer cell lines was hindered by p38 MAPK inhibition (Fig 3.5). Our results suggest that p38 MAPK signaling facilitates initial reovirus infection, irrespective of cell type. Other viruses whose infection also depends on p38 MAPK signaling include a diverse range of DNA and RNA genome viruses, enveloped and non-

enveloped viruses, and nuclear and cytoplasmic replicating viruses; avian reovirus, Ebola virus, HSV-1 [308, 326, 327]. As will be discussed, p38 MAPK signaling is beneficial at specific steps of reovirus replication cycle, that are potentially conserved across many viruses.

We demonstrated that active p38 MAPK signaling does not enhance reovirus binding but rather promotes reovirus internalization. When cells were pre-treated with p38 inhibitor, reovirus bound to cells to a similar level as untreated cells at 0hpi (Fig 3.6A, 3.6B). However, at 2hpi, surface virions were 2-fold lower in untreated samples compared to p38 inhibitor treated samples (Fig 3.7A). Reovirus utilizes multiple routes of endocytic cell entry. It has been demonstrated that reovirus internalization and overall infection was reduced following treatment with various endocytosis pathway inhibitors; dynasore (dynamin inhibitor), chlorpromazine (inhibits clathrin assembly), genistein (Src kinase/cavelolin-1 inhibitor) and methyl-β-cyclodextrin (cholesterol/lipid raft depletion) [146, 148]. The p38 MAPK signaling cascade has been implicated in clathrin, caveolin-1 and dynamin mediated endocytic pathways. An extensive study with avian reovirus demonstrated that virus infection was facilitated by p38 MAPK and Src kinase activation, caveolin-1 and dynamin-2 mediated endocytosis, and Rab5 and microtubule dependent trafficking [308]. However, since this study did not specifically examine virus internalization, but instead only assessed viral protein and titres at 24hpi, the effect of p38 MAPK, Src kinase, caveolin-1 and dynamin-2, Rab5 and microtubules on later steps of virus infection cannot be excluded.

Following reovirus low affinity binding to sialic acid and high affinity binding to JAM-A, binding to β1 integrin triggers endocytosis through activation of Src kinase signaling [134, 139, 145, 147, 309]. Whether p38 MAPK signaling occurs downstream of Src kinase has yet to be delineated in the context of reovirus endocytosis. As has been demonstrated for human

rhinovirus, virus binding to intercellular adhesion molecule 1 (ICAM-1) triggers Src kinase activation and subsequent Syk-mediated endocytosis [328]. These studies also demonstrated that Src kinase mediated p38 MAPK signaling modulates IL8 cytokine expression following human rhinovirus-ICAM-1 binding [329]. Future studies could determine if Src kinase is the upstream regulator of p38 MAPK mediated reovirus endocytosis.

The p38 MAPK signaling pathway is involved in various aspects of endosome trafficking. Endosomes are classified in accordance with the presence of specific markers; Rab5 and early endosome antigen 1 (EEA1) for early endosomes, Rab7 and Rab9 for late endosome, Lysosomal-associated membrane protein 1 (LAMP1) and LAMP2 for lysosomes [310, 311]. Loading of Rab5 onto early endosome membranes occurs early during endosome formation and is facilitated by guanine nucleotide dissociation inhibitor (GDI). It has been demonstrated that phosphorylation of GDI by p38 MAPK results in formation of cytoplasmic P-GDI-Rab5 complexes which are required for Rab5 delivery, docking and loading onto early endosome membranes. Artificial activation of p38 MAPK using H_2O_2 or UV treatment increased internalization rates and early endosome formation, whereas inhibition of p38 MAPK using SB203580 or p38α knockout had the opposite phenotype of decreased internalization rates and early endosome formation [305, 307]. Therefore, our observation that p38 MAPK signaling modulates reovirus internalization could potentially be related to p38 MAPK-GDI-Rab5 mediated early endosome formation. Furthermore, our result of internalized fluorescent virions forming larger vesicles in the presence of a p38 MAPK inhibitor, could also be an indication of defective early endosome formation. Future experiments performed with co-localization of reovirus, Rab5 and EEA1 and p38 MAPK modulation, could delineate this hypothesis.

Reovirus uncoating occurs in protease containing acidic intracellular compartments, likely at the late endosome compartment. The following results suggest that p38 MAPK signaling mediates internalized reovirus vesicular trafficking to lysosomes: i) p38 inhibitor treatment restricts intracellular reovirus uncoating (Fig 3.8), ii) internalized virions reside in larger vesicles following p38 inhibitor treatment (Fig 3.7B) and iii) impedance of late endosome and lysosome fusion restricts reovirus uncoating in p38 inhibitor treated cells (Fig 3.10A-C). Extrusion of Rab5 from early endosome membranes occurs concurrently with loading of Rab7 resulting in the transition to late endosomes. Rab7 containing late endosomes are the site of lysosome fusion and subsequent degradation of endosome contents [310-312]. Incubation of cells at 4°C inhibits endocytosis, whereas incubation at 19°C allows endocytosis, early endosome to late endosome transition but does not permit lysosome fusion [313, 314]. At 19°C, our results demonstrate that reovirus does not undergo uncoating, indicating a block in access to lysosomal contents. When reovirus infected cells at 19°C were moved to 37°C, reovirus uncoating progressed, suggesting successful interaction of virions with lysosomal contents (Fig 3.10A-C). However, in the presence of a p38 MAPK inhibitor, reovirus uncoating did not occur when moved from 19°C to 37°C, proposing a p38 MAPK regulated defect in either i) late endosome/lysosome fusion and/or ii) lysosome biogenesis.

The role of p38 MAPK in lysosome fusion is yet unclear. During autophagy, it has been demonstrated that p38 MAPK inhibition reduces ATG5 activation and increases autophagosome numbers presumably due to inhibition of ATG5-mediated fusion to lysosomes [330]. Using reovirus as a model, we could decipher the role of p38 MAPK in late-endosome/lysosome fusion using compartment-unique markers and temperature (19°C and 37°C) controlled endosomal trafficking. The role of p38 MAPK in lysosome biogenesis is also not well studied. Low

lysosomal pH (4.5-5.0) is attained by two membrane pumps, vacuolar-type H + ATPase (V-ATPase) and two-pore channel subtype 2 (TPC2), the later of which has been demonstrated to be functionally controlled by MAPK (p38 and JNK) signaling [310, 311, 331]. TPC2 knockout cells exhibit higher lysosomal pH and diminished lysosomal enzyme activity [332]. In the context of reovirus, it is possible that p38 MAPK mediated TPC2 activity plays a role in reovirus uncoating by controlling lysosomal enzyme activity. During the endocytic pathway, endosome-lysosome fusion is mediated by lysosomal pH in an endosome cargo dependent manner [333]. Therefore, it is possible that p38 MAPK mediated TPC2 activity could alter lysosome fusion with reovirus containing endosomes. Interestingly, lysosomes are also known to activate signaling cascades by recruitment of protein complexes to the lysosomal membrane. During cellular stress, lysosomal membranes have been observed to recruit mammalian target of rapamycin complex 1 (mTORC1) and MKK4 [334, 335]. In the case of MKK4, recruitment to the lysosomal membrane resulted in p38 MAPK activation, subsequent phosphorylation of lysosomal membrane LAMP2A and downstream triggering of autophagy [335]. Reovirus has previously been shown to induce autophagy, but the mechanism of induction has yet to be determined [336]. Further investigations could characterize the relationship between p38 MAPK signaling, autophagy induction by reovirus and lysosomal-p38 MAPK.

The p38 MAPK family is composed of 4 isoforms; p38α (MAPK14), p38β (MAPK11), p38δ(MAPK13), p38(MAPK12). The p38 MAPK inhibitors used in the study inhibit two or more isoforms. SB202190 and SB20380 inhibit p38α and p38β while BIRB796 inhibits all 4 isoforms. To precisely delineate which isoform(s) contributes towards the p38 MAPK inhibitor mediated phenotypes observed during reovirus infection, an isoform-specific shRNA knockdown strategy was pursued. Successful stable knockdown cell lines were generated in H1299 cell lines

for p38α, p38β and p38γ. For p38δ, knockdown assessment at the RNA and protein level was unresolved (Fig 3.13A-C). Using the EMBL RNA-seq data set, H1299 cell line expression of p38δ (1) was considerably lower relative to the other isoforms; p38α (30), p38β (28) and p38γ (17). The low basal expression of p38δ could explain why we did not observe a further reduction following shRNA knockdown. Additional validation of our p38δ shRNA constructs could be performed on higher p38δ expressing cell lines such as MDA-MB-468 (85), T47-D (57) and MDA-MB-231 (49). None of the p38 MAPK isoform knockdown cell lines had any impact on reovirus uncoating, early (4hpi) reovirus protein translation and overall reovirus infection (Fig 3.14A, 3.14B). Using a high throughput colorimetric (pNPP) ELISA, we observed that p38β and p38δ knockdown cell lines had reduced accumulation of total reovirus proteins over a 12hr infection period, relative to EMPTY vector and p38α and p38γ knockdown cell lines (Fig 3.15). To confirm the pNPP ELISA observations, Western blot analysis at 12hpi would need to be performed to measure total reovirus protein accumulation. In addition to protein accumulation, viral RNA accumulation could also be monitored using RT-PCR.

In hindsight, the shRNA knockdown method may not have been the ideal strategy to pursue. P38 MAPK directly phosphorylates more than 100 proteins including kinases and transcription factors. Downstream p38 MAPK signaling is important in numerous cellular functions, such as RNA transcription, mRNA stability, protein translation, among others [337]. Therefore, permanent knockdown of p38 MAPK would negatively affect pathways crucial for normal cellular function. In addition to p38 MAPK specific inhibitors, *in-vivo* knockout mouse models generated for p38β, p38γ and p38δ, have been utilized to study the role of p38 MAPK isoforms. Knockout mouse models of p38α are embryonic lethal, however strategies such as conditional and tissue specific knockout have proven successful [338]. Knockout of p38δ or

p38γ resulted in enhanced MEF cell line migration, while p38γ knockout increased proliferation and tumorigenesis of K-Ras transformed MEF cells, suggesting a potential role of p38δ and p38γ in tumor suppression. Additionally, p38δ knockout MEF cells had abnormal tubulin localization, indicating potential defects in cytoskeletal functions [339]. Using a chemical induced skin tumor model, it was observed that p38δ knockout mice had reduced incidence of skin tumors and restricted epidermis cell proliferation [340]. These results suggest the importance of a potential balance in signaling between p38 MAPK isoforms is tissue dependent. Therefore, we need to be cautious in interpreting data that involves manipulation of upstream kinases such as p38 MAPK, with numerous downstream targets.

Several p38 MAPK inhibitors have been pursued in clinical trials for treating chronic inflammatory disorders such as rheumatoid arthritis, however their success has been limited. Using a wide panel of p38 MAPK inhibitors, including SB203580 and BIRB796, in combination with JNK and ERK inhibitors, a high throughput microscopy strategy was used to demonstrate the extensive cross talk between MAPK family members. Additionally, this cross talk was dependent on the stimuli, be it inflammatory (e.g tumor necrosis factor α (TNFα)) or a mitogen (e.g epidermal growth factor (EGF)). For example, p38 MAPK inhibitor treatment restricted phosphorylation of downstream p38 MAPK target, heat shock protein 27 (Hsp27), following stimulation with TNFα or EGF. However, TNFα stimulation with p38 MAPK inhibitor treatment resulted in elevated JNK, ERK and NFκB signaling, whereas EGF stimulation with p38 MAPK inhibitor had limited impact on ERK and NFκB signaling but elevated JNK signaling. The authors suggest and demonstrate the potential using combination therapies (p38 MAPK and CREB inhibition) to limit MAPK cross talk and off-target pathway activation [341]. In a separate study, it was determined that the kinetics of p38 MAPK activation were dependent on the

stimuli. For example, anisomycin treatment resulted in a more prolonged (up to 120 minutes) p38 MAPK activation, whereas TNFα resulted in a more transient (up to 15min) p38 MAPK activation. Additionally, microarray analysis demonstrated that gene regulation was also dependent on p38 MAPK activation stimuli. To determine gene dependency on p38 MAPK activation, cells were pretreated with p38 MAPK inhibitor (SB203580) prior to stimulation. Of the three stimuli (anisomycin, sodium chloride, TNFα) tested, anisomycin treatment had 88% of genes regulated in a p38 MAPK dependent manner, the highest of the 3 stimuli tested [342]. These studies demonstrate the complexities and intricacies of p38 MAPK signaling and need to be taken into account when studying p38 MAPK signaling. In our studies, reovirus infections were performed using conditioned cell culture media, to minimize serum growth factor stimulation from fresh media. Additionally, whenever possible, cell culture media manipulations were kept to a minimum. Reovirus and compound working stocks were made to 10 times the final dilution and spiked into the media rather than refreshing the media. However, for reovirus binding and uncoating assays, media manipulations were unavoidable. According to our standard operating protocols, reovirus infections were performed in serum free media with low volume (100ul per 12well) at 4°C for 1hr. Changes in temperature and serum concentrations have both been previously observed to alter p38 MAPK signaling [343-345]. Future experiments could determine if temperature and serum concentration changed have an impact in the context of p38 MAPK signaling during reovirus infection.

Following assessment of various stages of initial reovirus replication in a panel of breast cancer cell lines (Fig 3.16, 3.17, 3.19), we identified 2 potential predictive markers; i) F11R (JAM-A) for reovirus binding (Fig 3.18) and ii) MAPK11 (p38β) for reovirus uncoating (Fig 3.21). Hs578T cells lacked expression of F11R and had almost no reovirus-cell binding (Fig

3.17, 3.18). Following initial low affinity binding to sialic acids, reovirus interacts with JAM-A with high affinity [134, 136, 137, 346, 347]. Hence, lack of JAM-A expression could potentially explain poor reovirus binding in Hs578T cells. However, F11R expression did not correlate with reovirus binding in the cell line panel (Fig 3.18), suggesting that other factors such as sialic acids could play a role in predicting reovirus binding efficacy. Furthermore, whether F11R expression correlates with surface expression of JAM-A has yet to de determined. Our data suggested that p38 MAPK signaling enhanced various steps during reovirus entry, and eventual reovirus uncoating. A strong correlation was observed between MAPK11 (p38β) and reovirus uncoating (Fig 3.21). Additionally, Western blot analysis validated MAPK11 expression with p38β protein levels among the cell line panel (Fig 3.23).

In conclusion, our data demonstrates that p38 MAPK signaling is important during various steps of reovirus replication. Specifically, p38 MAPK signaling enhances reovirus endocytosis, uncoating, and post-uncoating steps. Furthermore, our results support the use of reovirus entry as a model system to further delineate the function of p38 MAPK signaling in late endosome to endo-lysosome transition stage of endosome trafficking. Finally, we illustrate the potential of using p38β MAPK isoform as a predictive marker for reovirus uncoating and overall reovirus infection.

CHAPTER 4: PERSPECTIVES AND FUTURE DIRECTIONS

4.1 REOVIRUS CELL CULTURE ADAPTATION

RNA viruses have high mutation rates due to their error prone viral polymerase, resulting in rapid virus adaptation. RNA virus polymerase errors can range from 10^{-6} to 10^{-4} substitutions per nucleotide per round of replication [348]. The generality is that approximately 1 mutation

arises per progeny for all viruses; given that RNA viruses have lower fidelity but also smaller genomes. Environmental and host selection pressures exerted during virus replication drive virus adaptation and evolution [269]. A given population of viruses exists as a range of genetically distinct viruses, percentages of which are highly dependent on viral fitness under the specific selection pressures [349]. The consequence of virus adaptation can explain important virology concepts such as antiviral drug resistance, host specific pathogenicity and live attenuated vaccines [350-352]. In a clinical setting, virus adaptation is a well recognized phenomenon and is taken into consideration during drug discovery and development. Influenza virus evolution and HIV diversity are two well known examples of the importance of virus adaption in viral pathogenesis and drug resistance [353, 354]. However, in laboratory scientific research, the importance of virus adaptation is much less emphasized. It is common practice for environmental and patient virus isolates to be initially cultured and amplified in cell lines in culture. To best maintain natural host virus specificity and limit virus adaptation, the cell line of preference is selected that not only closely matches the host species but also originates from the natural organ of virus infection. For example, poultry isolated reoviruses are initially cultured in chicken embryonic fibroblast (CEF) or chicken kidney (CK) cells and human isolated adenoviruses are initially cultured in human lung adenocarcinoma (A549) cells or human lung fibroblast (MRC-5) cells [355, 356]. The decision of a laboratory to alter the cell line used for virus propagation can be i) intentional adaptation of the virus ii) convenience of alternate cell line availability iii) virus identification studies iv) lack of cell culture virus adaptation knowledge.

During virus propagation in cell culture, changing the cell line host species can result in virus adaptation to the new cell line host and attenuation in the previous cell line host. The clinical isolate of T3D obtained in 1955 by Albert B. Sabin and Manuel Ramos-Alvarez, was

initially propagated in a rhesus monkey kidney (LLC-MK2) cell line [357]. The LLC-MK2 cell line is highly susceptible to a broad range of enteric viruses and was routinely used for initial identification and propagation of clinical virus isolates [358]. Research laboratories studying T3D following its isolation continued to propagate the virus in LLC-MK2 cells. However, due to the increased popularity of *in-vivo* mouse models to study virus pathogenesis and companion mouse-specific reagents, such as purified IFN and antibodies, L cells and the clonal L929 cell line became a common cell line to explore various aspects of replication for several viruses, including reovirus. Reovirus replication kinetics were similar in L cells relative to LLC-MK2 cells and virion architecture as determined by electron microscopy was also similar between the two cell lines [359]. Importantly, it was observed that as few as four passages in L cells was sufficient to generate a T3D variant that differed in replication kinetics to the parental LLC-MK2 passaged T3D. Relative to the parental T3D, the variant described had reduced virus release and diminished sensitivity to T3D antibodies [359, 360]. However, it was not reported how the variant was identified, in other words, whether they observed a difference in plaque size. The isolation of a reovirus variant in only four cell line passages is a classical example of the ability of reovirus to evolve and adapt.

4.2 REOVIRUS PROPAGATION METHODS

In addition to cell line dependent virus adaptation, factors during virus propagation such as plaque selection, inoculum passage and inoculation MOI, can impact the rate of virus adaptation. Plaque selection is performed to maintain virus homogeneity and bias towards large or small plaques should be avoided if possible. Seed stocks are usually passaged 2-3 times to obtain sufficient amount of inoculum for large scale amplification. To reduce virus adaptation and minimize the amplification of defective interfering virions, cell cultures are commonly

inoculated with virus at an MOI of 1-3. A brief investigation of the literature demonstrates that a virus propagation protocol cited by a majority of laboratories utilize an MOI of 5-20 [126, 169]. Whether this high MOI during reovirus propagation has contributed to the laboratory specific reovirus strains has yet to be determined. Together with our data, historical evidence supports the importance of recognizing the concept of reovirus laboratory adaptation and the urgent need for the reovirus field to standardize laboratory strain and virus propagation protocols.

4.3. TUMOR MODELS FOR ASSESSING ONCOLYTIC REOVIRUS EFFICACY

Our current study and the previous T3v1/v2 study utilized the syngeneic B16-F10 melanoma model with hind flank subcutaneous tumor inoculation and intratumoral reovirus administration [218]. Since the B16-F10 melanoma model is highly aggressive and results in tumor volumes increasing very rapidly, it was used as a model to compare the oncolytic efficacy of $T3D^{PL}$ and $T3D^{TD}$ primarily on the basis of virus replication and less on the basis of reovirus induced anti-tumor immune responses [282]. Additionally, B16-F10 tumors are classified as poorly immunogenic. Not only do B16-F10 tumors harbor low basal levels of innate and adaptive immune cells, in the event of immune cell recruitment during stimulated (e.g oncolytic virus administration), low expression of cytokines (e.g GM-CSF) and high expression of immune inhibitory molecules (PD-L1) by tumor cells suppress immune cell recruitment and activation. The B16-F10 tumor therefore creates a highly immunosuppressive microenvironment and is not an ideal model to study immunological aspects viral oncolysis but is a good model for assessing direct oncolytic virus potency [282, 361].

Our subsequent finding of differential cytokine activation profiles between $T3D^{PL}$ and $T3D^{TD}$ justify the use of alternate *in-vivo* tumor model systems. In recent years, the importance

of the host immune system in potentiating oncolytic virus therapy has become increasingly appreciated. A multitude of oncolytic viruses in clinical trials, including the FDA approved HSV-1 (T-VEC®), have been modified to express potent cytokines, commonly GM-CSF [52, 53]. It was demonstrated that oncolytic virus-elicited tumor cell lysis stimulates a tumor specific immune response by exposing antigen presenting cells to previously concealed tumor antigens, resulting in both tumor clearance and long-term anti-tumor immunity [361, 362]. In addition, cytokines (chemokines) released by the virus infected tumor cells promote recruitment of immune cells to the tumor microenvironment and enhance their activation [363, 364]. However, virus-induced cytokines such as interferons act as potent-antivirals and hamper oncolytic virus dose escalation within the tumor. Oncolytic virus infection also enhances expression of immune cell inhibitory receptors (e.g PD-L1, CTLA-4) on the cancer cells, and restricts immune cell mediated cancer cell elimination [361, 364, 365]. For optimal oncolytic virus efficacy, there needs to be a fine balance between minimizing induction of the antiviral immune response and maximizing stimulation of the anti-tumor immune response [366-368].

4.4. ROLE OF σ3 IN DSRNA BINDING AND VIRAL GENOME PACKAGING

Inhibition of host protein translation during reovirus infection has been correlated to cellular localization rather than the amount of σ3. Specifically, infection with reovirus strains that strongly inhibit host protein translation, σ3 localized to perinuclear viral factories whereas diffuse cytoplasmic and nuclear localization of σ3 was observed in strains with poor inhibition of host protein translation. Interestingly, reovirus replication did not depend on the extent of host translation inhibition [369]. It was proposed that early during reovirus infection, prior to the establishment of viral factories, σ3 binds to virus dsRNA and inhibits RLR and PKR signaling, allowing translation of reovirus proteins and inhibition of antiviral signaling. Later during

infection, σ3 is complexed to μ1 and is restricted to viral factories. Cytoplasmic viral dsRNA is unbound and can therefore be detected by RLRs and PKR to initiate downstream signaling [264, 369]. It would be beneficial to determine the temporo-spatial organization of σ3 in the context of μ1 and dsRNA during reovirus infection to delineate the proposed model.

The previously discussed S4 gene polymorphisms (A74G and A624G) were also demonstrated to play an important role in reovirus genome packaging fidelity. Interestingly, the A74G and A624G variations in the S4 gene have yet to be reported in the T3D strains originating from the Bernard Fields laboratory, including our in-house virus sequences of $T3D^{TD}$ and $T3D^{KC}$ (Fig 2.2). Reovirus genome assembly is an intricate process where each virion is packaged with a single copy of each of the 10 reovirus genes. The observation that reovirus particle to pfu ratios can be as low as 1, supports the notion that a systematic rather than random assortment of gene segments occurs [234]. During infection, reovirus ssRNA segments are rapidly associated with μNS and σNS and/or σ3 [208]. As aforementioned, $T3D^{PL}$ and $T3D^{PARENT}$ S4 genes differ at only 3 nucleotide positions; A74G, A624G, T719G. The A74G and A624G (W133R) changes are of particular interest and have been very eloquently characterized with respect to correct packaging of reovirus genome segments. Defective interfering (DI) virions harboring truncated gene segments can be generated during high MOI infection, and can be dominantly maintained in the presence of low (1%) levels of helper complete virions. Using the reovirus infectious RNA system to characterize the genetic determinants of a L1-T3D-DI virus, the S4-T3D-DI gene not only permitted efficient DI virus formation but was also sufficient in preventing infectious virus formation when combined with 9 genes from T3D. When sequenced, the S4-T3D-DI gene had only 2 changes compared to S4-T3D, namely A74G and A624G (W133R). Moreover, formation of intertypic T2J mono- and multi-reassortants in a T3D backbone are exclusively dependent on

the S4-T3D gene with A74G and A624G (W133R) changes. Furthermore, it was also demonstrated that A74G and A624G (W133R) changes have their functional impact at the σ3 protein level and not the S4 gene level [258]. Therefore, it is likely that the A624G (W133R) missense change in σ3 allows for a more relaxed reovirus genome assembly criterion, facilitating packaging of adapted and evolved viral genes.

4.5. TEMPERATURE SENSITIVE μ2 VARIATION

It is very important to note that either most laboratories are unaware or fail to acknowledge that the $T3D^{TD}$ μ2 is a temperature sensitive variant, that is most likely determined by the P208S polymorphism. $T3D^{N}$, a strain originating from the Bernard N. Fields laboratory, forms filamentous viral factories at 31°C and globular viral factories at 37°C [260]. Transfecting a plasmid encoding P208 M1 gene encoding μ2 protein is capable interacting with microtubules from filamentous virus-like inclusions. However, transfection of a plasmid encoding S208 M1 gene encoding μ2 protein results in cytoplasmic globular virus-like inclusions [205, 260]. When a $T3D^{N}$ M1 (S208) encoding plasmid, which is identical to $T3D^{TD}$ M1, was transfected into cells, filamentous virus-like inclusions were formed at 31°C and globular inclusions were formed at 37°C. Expression of μ2 from a plasmid encoding T1L M1 (P208) transfected into cells, localizes to filamentous structures at both 31°C and 37°C [260].

Since functional virions are still produced to a high titre in $T3D^{TD}$, albeit at a reduced rate relative to $T3D^{PL}$, we can predict that $T3D^{TD}$ μ2 at 37°C could either be partially misfolded or constitute of a mixed proportion of misfolded and properly folded protein. This observation raises an interesting possibility: if μ2 is misfolded during virus replication, is the μ2 packaged in the virus core also misfolded? Having partially misfolded μ2 present in the viral core could

potentially explain the deficiency of $T3D^{TD}$ core transcriptase activity. It would be interesting to generate a $T3D^{TD}$ virus preparation at 31°C and assess its core transcriptase activity relative to a $T3D^{TD}$ virus preparation generated at 37°C. Using a T1L μ2 temperature sensitive mutant, it was demonstrated that infection at the non-restricted temperature (32°C) was capable of producing viral RNA and proteins similar to parental T1L. At early timepoints (<6hpi) at the restricted temperature (39°C), the μ2 temperature sensitive mutant produced viral RNA and proteins to a similar level as parental T1L. At later timepoints (6-24hpi) at the restricted temperature (39°C), no viral dsRNA and reduced viral proteins were observed in the μ2 temperature sensitive mutant, relative to parental T1L [196]. These results suggest that packaging a properly folded μ2 is important for conversion of viral ssRNA to progeny dsRNA.

4.6. P38 MAPK DEPENDENT SIGNALING INITIATING REOVIRUS ENDOCYTOSIS

A direct role of p38 MAPK signaling and receptor mediated internalization has been characterized with respect to G protein-coupled receptors (GPCR). Ligand-GPCR binding results in the activation of second messenger dependent signaling cascades. Inhibition of GPCR signaling is facilitated by the recruitment of β-arrestins to the active GPCR. Additional functions following β-arrestin recruitment include i) clathrin mediated receptor internalization, ii) GPCR-independent signaling, and iii) Ubiquitin ligase adaptor. GPCR-independent signaling is orchestrated by β-arrestins that can act as a scaffold protein for MKKs and serve as a site for MAPK (p38, JNK, ERK) signal activation [370]. This cascade has been demonstrated with platelet activating factor (PAF) and cognate PAF receptor (PAFR), a GPCR. PAF-PAFR binding results in β-arrestin mediated p38 MAPK recruitment and activation. Subsequent p38 MAPK signaling facilitates clathrin complex and actin bundle formation, and internalization of PAR-PAFR [306]. Reovirus binding has yet to be associated with any GPCRs, however cell entry of

other viruses such filovirus family members (Ebola virus, Marburg virus) have been reported to be mediated by GPCRs [326]. Our observation that p38 MAPK signaling modulates reovirus internalization opens the possibility of identifying a novel GPCR-p38 MAPK-dependent reovirus entry pathway.

4.7. CLINICAL BIOMARKERS FOR PREDICTING REOLYSIN® EFFICACY

Clinical trials involving REOLYSIN® have had limited success. Currently, biomarkers previously demonstrated to enhance reovirus infection in cell lines, are used for stratifying patients that could benefit from REOLYSIN® therapy in clinical trials include. These biomarkers include EGFR, Hras, Kras, Nras, Braf and/or p53. Even with these biomarkers, REOLYSIN® therapeutic efficacy still need improvement [62, 64]. Our data suggests a revisit to the current choice of biomarkers. We propose that biomarkers should be selected based on various stages of reovirus replication rather than global biomarkers. Future studies should focus on expanding the cell panel for which reovirus replication, similar to our NCI-60 breast cancer panel. Generation of an if/then biomarker formula would be a better prognostic determinant. For example, *IF* a cell line expresses F11R (JAM-A), *THEN* assess MAPK11 (p38β) expression. A cell line than expresses no F11R (JAM-A) would have poor reovirus binding and infectivity irrespective of other biomarkers important for other steps of reovirus replication.

REFERENCES

1. World Health Organization. *Cancer*. 2018; Available from: www.who.int/news-room/fact-sheets/detail/cancer.
2. World Health Organization. *Cardiovascular diseases (CVDs)*. 2017; Available from: www.who.int/news-room/fact-sheets/detail/cardiovascular-diseases-(cvds).
3. Canadian Cancer Society. *Canadian Cancer Statistics*. 2017; Available from: www.cancer.ca/Canadian-CancerStatistics-2017-EN.pdf.
4. Brownell, C., *Less than half of charities' funds go toward fighting disease*, in *Calgary Herald*. 2017.
5. National Cancer Institute. *Types of Cancer Treatment*. 2017; Available from: www.cancer.gov/about-cancer/treatment/types.
6. National Cancer Institute. *Cancer Staging*. 2015; Available from: www.cancer.gov/about-cancer/diagnosis-staging/staging.
7. Begg, K., Tavassoli, M. *Biomarkers towards personalised therapy in cancer*. Drug Target Review, 2017.
8. National Cancer Institute. *Targeted Cancer Therapies*. 2018; Available from: www.cancer.gov/about-cancer/treatment/types/targeted-therapies/targeted-therapies-fact-sheet.
9. National Cancer Institute. *Biological Therapies for Cancer*. 2018; Available from: www.cancer.gov/about-cancer/treatment/types/immunotherapy/bio-therapies-fact-sheet#q6.
10. McCarthy, E.F., *The toxins of William B. Coley and the treatment of bone and soft-tissue sarcomas.* Iowa Orthop J, 2006. **26**: p. 154-8.
11. Hobohm, U., *Fever and cancer in perspective.* Cancer Immunol Immunother, 2001. **50**(8): p. 391-6.
12. Deidier, A., *Dissertation medicinal et Chirurgical sur les Tumeurs.* 1725.
13. Coley, W.B., *II. Contribution to the Knowledge of Sarcoma.* Ann Surg, 1891. **14**(3): p. 199-220.
14. Coley, W.B., *The treatment of malignant tumors by repeated inoculations of erysipelas. With a report of ten original cases. 1893.* Clin Orthop Relat Res, 1991(262): p. 3-11.
15. Coley, W.B., *The Treatment of Inoperable Sarcoma by Bacterial Toxins (the Mixed Toxins of the Streptococcus erysipelas and the Bacillus prodigiosus).* Proc R Soc Med, 1910. **3**(Surg Sect): p. 1-48.
16. Starnes, C.O., *Coley's toxins in perspective.* Nature, 1992. **357**(6373): p. 11-2.
17. Coley, W.B., *The Erysipelas Toxins—A Reply to the Editorial of Dec. 15, 1894.* JAMA, 1895. **XXIV**(1): p. 1.
18. *The Failure of the Erysipelas Toxins.* JAMA, 1894. **XXIII**(24): p. 1.
19. Hoption Cann, S.A., J.P. van Netten, and C. van Netten, *Dr William Coley and tumour regression: a place in history or in the future.* Postgrad Med J, 2003. **79**(938): p. 672-80.
20. Johnston, B.J. and E.T. Novales, *Clinical effect of Coley's toxin. II. A seven-year study.* Cancer Chemother Rep, 1962. **21**: p. 43-68.
21. Nauts, H.C. and J.R. McLaren, *Coley toxins--the first century.* Adv Exp Med Biol, 1990. **267**: p. 483-500.
22. Nauts, H.C., W.E. Swift, and B.L. Coley, *The treatment of malignant tumors by bacterial toxins as developed by the late William B. Coley, M.D., reviewed in the light of modern research.* Cancer Res, 1946. **6**: p. 205-16.

23. Kramer, M.G., et al., *Bacterial Therapy of Cancer: Promises, Limitations, and Insights for Future Directions.* Front Microbiol, 2018. **9**: p. 16.
24. Torres, W., Lameda, V., Olivar, L.C., Navarro, C., Fuenmayor, J., Pérez, A., Mindiola, A., Rojas, M., Martínez, M.S., Velasco, M., Rojas, J., Bermudez, V., *Bacteria in cancer therapy: beyond immunostimulation.* J Cancer Metastasis, 2018. **4**(4).
25. De Pace, N., *Sulla scomparsa di un enorme cancro vegetante del callo dell'utero senza cura chirurgica.* Ginecologia, 1912. **9**(82).
26. Nemunaitis, J. *Live Viruses in Cancer Treatment*. 2002. **16**.
27. Webb, H.E. and C.E. Smith, *Viruses in the treatment of cancer.* Lancet, 1970. **1**(7658): p. 1206-8.
28. Kelly, E. and S.J. Russell, *History of oncolytic viruses: genesis to genetic engineering.* Mol Ther, 2007. **15**(4): p. 651-9.
29. Hoster, H.A., R.P. Zanes, Jr., and E. Von Haam, *Studies in Hodgkin's syndrome; the association of viral hepatitis and Hodgkin's disease; a preliminary report.* Cancer Res, 1949. **9**(8): p. 473-80.
30. Southam, C.M. and A.E. Moore, *Clinical studies of viruses as antineoplastic agents with particular reference to Egypt 101 virus.* Cancer, 1952. **5**(5): p. 1025-34.
31. Georgiades, J., et al., *Research on the oncolytic effect of APC viruses in cancer of the cervix uteri; preliminary report.* Biul Inst Med Morsk Gdansk, 1959. **10**: p. 49-57.
32. Asada, T., *Treatment of human cancer with mumps virus.* Cancer, 1974. **34**(6): p. 1907-28.
33. Moore, A.E., *The destructive effect of the virus of Russian Far East encephalitis on the transplantable mouse sarcoma 180.* Cancer, 1949. **2**(3): p. 525-34.
34. Moore, A.E., *Effect of inoculation of the viruses of influenza A and herpes simplex on the growth of transplantable tumors in mice.* Cancer, 1949. **2**(3): p. 516-24.
35. Moore, A.E. and S. O'Connor, *Further studies on the destructive effect of the virus of Russian Far East encephalitis on the transplantable mouse sarcoma 180.* Cancer, 1950. **3**(5): p. 886-90.
36. Moore, A.E., *Enhancement of oncolytic effect of Russian encephalitis virus.* Proc Soc Exp Biol Med, 1951. **76**(4): p. 749-54.
37. Moore, A.E., *Inhibition of growth of five transplantable mouse tumors by the virus of Russian Far East encephalitis.* Cancer, 1951. **4**(2): p. 375-82.
38. Moore, A.E., *The destructive effects of viruses on transplantable mouse tumors.* Acta Unio Int Contra Cancrum, 1951. **7**(2): p. 279-81.
39. Moore, A.E., *Viruses with oncolytic properties and their adaptation to tumors.* Ann N Y Acad Sci, 1952. **54**(6): p. 945-52.
40. Moore, A.E. and L.C. Diamond, *Influence of hemagglutinating viruses on tumor cell suspensions. I. Growth inhibition and reversal of the effect.* Proc Soc Exp Biol Med, 1952. **79**(4): p. 663-9.
41. Moore, A.E., et al., *Influence of hemagglutinating viruses on tumor cell suspensions. II. Newcastle disease virus and Ehrlich carcinoma.* Proc Soc Exp Biol Med, 1952. **81**(2): p. 498-501.
42. Toolan, H.W. and A.E. Moore, *Oncolytic effect of Egypt virus on a human epidermoid carcinoma grown in x-irradiated rats.* Proc Soc Exp Biol Med, 1952. **79**(4): p. 697-702.
43. Moore, A.E. and L.C. Diamond, *Factors influencing the effect of hemagglutinating viruses on tumor cell suspensions.* J Immunol, 1953. **71**(6): p. 441-5.
44. Moore, A.E., *Effects of viruses on tumors.* Annu Rev Microbiol, 1954. **8**: p. 393-410.
45. Diamond, L.C. and A.E. Moore, *Changes in activity of Newcastle disease virus after adaption to Ehrlich ascites tissue culture.* J Immunol, 1956. **77**(2): p. 81-6.
46. Moore, A.E., *Present status of oncolytic viruses and their effect on tumors in mouse, man and tissue culture.* Acta Unio Int Contra Cancrum, 1956. **12**(4): p. 491-4.
47. Moore, A.E., *Oncolytic properties of viruses.* Tex Rep Biol Med, 1957. **15**(3): p. 588-99; discussion 599-602.
48. Moore, A.E., *The oncolytic viruses.* Prog Exp Tumor Res, 1960. **1**: p. 411-39.

49. Russell, L. and K.W. Peng, *The emerging role of oncolytic virus therapy against cancer.* Chin Clin Oncol, 2018. **7**(2): p. 16.
50. RIGVIR Ltd. *First oncolytic virotherapy*. 2018; Available from: www.rigvir.com.
51. Liang, M., *Oncorine, the World First Oncolytic Virus Medicine and its Update in China.* Curr Cancer Drug Targets, 2018. **18**(2): p. 171-176.
52. Rehman, H., et al., *Into the clinic: Talimogene laherparepvec (T-VEC), a first-in-class intratumoral oncolytic viral therapy.* J Immunother Cancer, 2016. **4**: p. 53.
53. Lawler, S.E., et al., *Oncolytic Viruses in Cancer Treatment: A Review.* JAMA Oncol, 2017. **3**(6): p. 841-849.
54. MDCPartners. *Oncolytic virus therapies in clinical trials*. 2017; Available from: https://www.mdcpartners.be/get-free-ta-scan-download-immuno-oncology-summit-2017/.
55. Liu, B.L., et al., *ICP34.5 deleted herpes simplex virus with enhanced oncolytic, immune stimulating, and anti-tumour properties.* Gene Ther, 2003. **10**(4): p. 292-303.
56. Chou, J., et al., *Mapping of herpes simplex virus-1 neurovirulence to gamma 134.5, a gene nonessential for growth in culture.* Science, 1990. **250**(4985): p. 1262-6.
57. Hill, A., et al., *Herpes simplex virus turns off the TAP to evade host immunity.* Nature, 1995. **375**(6530): p. 411-5.
58. Poppers, J., et al., *Inhibition of PKR activation by the proline-rich RNA binding domain of the herpes simplex virus type 1 Us11 protein.* J Virol, 2000. **74**(23): p. 11215-21.
59. Cassady, K.A., M. Gross, and B. Roizman, *The herpes simplex virus US11 protein effectively compensates for the gamma1(34.5) gene if present before activation of protein kinase R by precluding its phosphorylation and that of the alpha subunit of eukaryotic translation initiation factor 2.* J Virol, 1998. **72**(11): p. 8620-6.
60. Taneja, S., et al., *Enhanced antitumor efficacy of a herpes simplex virus mutant isolated by genetic selection in cancer cells.* Proc Natl Acad Sci U S A, 2001. **98**(15): p. 8804-8.
61. Yan, W.L., et al., *Recent progress in GM-CSF-based cancer immunotherapy.* Immunotherapy, 2017. **9**(4): p. 347-360.
62. Oncolytics Biotech Inc. *REOLYSIN - Innately Adaptive*. Corporate Presentation 2018; Available from: https://ir.oncolyticsbiotech.com/events-presentations.
63. Clements, D., et al., *Reovirus in cancer therapy: an evidence-based review.* Oncolytic Virother, 2014. **3**: p. 69-82.
64. Bradbury, P.A., et al., *Canadian Cancer Trials Group (CCTG) IND211: A randomized trial of pelareorep (Reolysin) in patients with previously treated advanced or metastatic non-small cell lung cancer receiving standard salvage therapy.* Lung Cancer, 2018. **120**: p. 142-148.
65. Jonker, D.J., et al., *A Randomized Phase II Study of FOLFOX6/Bevacizumab With or Without Pelareorep in Patients With Metastatic Colorectal Cancer: IND.210, a Canadian Cancer Trials Group Trial.* Clin Colorectal Cancer, 2018.
66. Cohn, D.E., et al., *Randomized phase IIB evaluation of weekly paclitaxel versus weekly paclitaxel with oncolytic reovirus (Reolysin(R)) in recurrent ovarian, tubal, or peritoneal cancer: An NRG Oncology/Gynecologic Oncology Group study.* Gynecol Oncol, 2017. **146**(3): p. 477-483.
67. Noonan, A.M., et al., *Randomized Phase 2 Trial of the Oncolytic Virus Pelareorep (Reolysin) in Upfront Treatment of Metastatic Pancreatic Adenocarcinoma.* Mol Ther, 2016. **24**(6): p. 1150-1158.
68. Bernstein, V., Ellard, S., Dent, S.F., Gelmon, K.A., Dhesy-Thind, S.K., Mates, M., Salim, M., Panasci, L., Song, X., Clemons, M., Tu, D., Hagerman, L.J., Seymour, L. *CT131: A Randomized (RCT) Phase II Study of Oncolytic Reovirus (Pelareorep) plus Standard Weekly Paclitaxel (P) as Therapy for Metastatic Breast Cancer (mBC)*. in *American Association for Cancer Research*. 2017. Washington, D.C. .

69. Sabin, A.B., *Reoviruses. A new group of respiratory and enteric viruses formerly classified as ECHO type 10 is described.* Science, 1959. **130**(3386): p. 1387-9.
70. Banerjee, A.K. and A.J. Shatkin, *Guanosine-5'-diphosphate at the 5' termini of reovirus RNA: evidence for a segmented genome within the virion.* J Mol Biol, 1971. **61**(3): p. 643-53.
71. Loh, P.C., H.R. Hohl, and M. Soergel, *Fine Structure of Reovirus Type 2.* J Bacteriol, 1965. **89**: p. 1140-4.
72. Mayor, H.D., et al., *Reoviruses. Ii. Structure and Composition of the Virion.* J Bacteriol, 1965. **89**: p. 1548-56.
73. Vieler, E., et al., *Characterization of a reovirus isolate from a rattle snake, Crotalus viridis, with neurological dysfunction.* Arch Virol, 1994. **138**(3-4): p. 341-4.
74. Duncan, R., F.A. Murphy, and R.R. Mirkovic, *Characterization of a novel syncytium-inducing baboon reovirus.* Virology, 1995. **212**(2): p. 752-6.
75. Duncan, R., *Extensive sequence divergence and phylogenetic relationships between the fusogenic and nonfusogenic orthoreoviruses: a species proposal.* Virology, 1999. **260**(2): p. 316-28.
76. Shmulevitz, M., J. Salsman, and R. Duncan, *Palmitoylation, membrane-proximal basic residues, and transmembrane glycine residues in the reovirus p10 protein are essential for syncytium formation.* J Virol, 2003. **77**(18): p. 9769-79.
77. Cheng, L.T., R.K. Plemper, and R.W. Compans, *Atypical fusion peptide of Nelson Bay virus fusion-associated small transmembrane protein.* J Virol, 2005. **79**(3): p. 1853-60.
78. Salsman, J., et al., *Extensive syncytium formation mediated by the reovirus FAST proteins triggers apoptosis-induced membrane instability.* J Virol, 2005. **79**(13): p. 8090-100.
79. Kohl, C., et al., *Isolation and characterization of three mammalian orthoreoviruses from European bats.* PLoS One, 2012. **7**(8): p. e43106.
80. Hu, T., et al., *Characterization of a novel orthoreovirus isolated from fruit bat, China.* BMC Microbiol, 2014. **14**: p. 293.
81. Lorusso, A., et al., *A new member of the Pteropine Orthoreovirus species isolated from fruit bats imported to Italy.* Infect Genet Evol, 2015. **30**: p. 55-58.
82. Malherbe, H. and R. Harwin, *The cytopathic effects of vervet monkey viruses.* S Afr Med J, 1963. **37**: p. 407-11.
83. Hartley, J.W., W.P. Rowe, and R.J. Huebner, *Recovery of reoviruses from wild and laboratory mice.* Proc Soc Exp Biol Med, 1961. **108**: p. 390-5.
84. Rosen, L. and F.R. Abinanti, *Natural and experimental infection of catle with human types of reoviruses.* Am J Hyg, 1960. **71**: p. 250-7.
85. Kasza, L., *Isolation and characterisation of a reovirus from pigs.* Vet Rec, 1970. **87**(22): p. 681-6.
86. Stanley, N.F., *Reovirus--a ubiquitous orphan.* Med J Aust, 1961. **48(2)**: p. 815-8.
87. Minuk, G.Y., R.W. Paul, and P.W. Lee, *The prevalence of antibodies to reovirus type 3 in adults with idiopathic cholestatic liver disease.* J Med Virol, 1985. **16**(1): p. 55-60.
88. Minuk, G.Y., et al., *Reovirus type 3 infection in patients with primary biliary cirrhosis and primary sclerosing cholangitis.* J Hepatol, 1987. **5**(1): p. 8-13.
89. Rubin, D., et al., *Immunologic tolerance after oral administration of reovirus: requirement for two viral gene products for tolerance induction.* J Immunol, 1981. **127**(4): p. 1697-701.
90. Cashdollar, L.W., et al., *Sequences of the S1 genes of the three serotypes of reovirus.* Proc Natl Acad Sci U S A, 1985. **82**(1): p. 24-8.
91. Shatkin, A.J., J.D. Sipe, and P. Loh, *Separation of ten reovirus genome segments by polyacrylamide gel electrophoresis.* J Virol, 1968. **2**(10): p. 986-91.
92. Dermody, T.S., et al., *Sequence diversity in S1 genes and S1 translation products of 11 serotype 3 reovirus strains.* J Virol, 1990. **64**(10): p. 4842-50.

93. Rosen, L., et al., *Observations on a newly recognized virus (Abney) of the reovirus family.* Am J Hyg, 1960. **71**: p. 258-65.
94. Rosen, L., H.E. Evans, and A. Spickard, *Reovirus infections in human volunteers.* Am J Hyg, 1963. **77**: p. 29-37.
95. Masillamony, R.P. and T.J. John, *Experimental reovirus infection in monkeys. I. Clinical and virological studies.* Am J Epidemiol, 1970. **91**(4): p. 446-52.
96. Masillamony, R.P. and T.J. John, *Experimental reovirus infection in monkeys. II. Serologic studies.* Am J Epidemiol, 1974. **99**(2): p. 155-63.
97. Lou, T.Y., Wenner, H.A., Mcmillen, J. , *Natural and Experimental Infection of Dogs with Reovirus, Type 1: Pathogenicity of the Strain for other Animals.* American Journal of Epidemiology, 1963. **77**(3): p. 11.
98. Hermann, L., et al., *Reovirus type 2 isolated from cerebrospinal fluid.* Pediatr Infect Dis J, 2004. **23**(4): p. 373-5.
99. Jiang, J., L. Hermann, and K.M. Coombs, *Genetic characterization of a new mammalian reovirus, type 2 Winnipeg (T2W).* Virus Genes, 2006. **33**(2): p. 193-204.
100. Tyler, K.L., et al., *Isolation and molecular characterization of a novel type 3 reovirus from a child with meningitis.* J Infect Dis, 2004. **189**(9): p. 1664-75.
101. Chua, K.B., et al., *A previously unknown reovirus of bat origin is associated with an acute respiratory disease in humans.* Proc Natl Acad Sci U S A, 2007. **104**(27): p. 11424-9.
102. Chua, K.B., et al., *Identification and characterization of a new orthoreovirus from patients with acute respiratory infections.* PLoS One, 2008. **3**(11): p. e3803.
103. Cheng, P., et al., *A novel reovirus isolated from a patient with acute respiratory disease.* J Clin Virol, 2009. **45**(1): p. 79-80.
104. Loh, P.C. and A.J. Shatkin, *Structural proteins of reoviruses.* J Virol, 1968. **2**(11): p. 1353-9.
105. Graziadei, W.D., 3rd and P. Lengyel, *Translation of in vitro synthesized reovirus messenger RNAs into proteins of the size of reovirus capsid proteins in a mouse L cell extract.* Biochem Biophys Res Commun, 1972. **46**(5): p. 1816-23.
106. Huismans, H. and W.K. Joklik, *Reovirus-coded polypeptides in infected cells: isolation of two native monomeric polypeptides with affinity for single-stranded and double-stranded RNA, respectively.* Virology, 1976. **70**(2): p. 411-24.
107. Wiener, J.R., J.A. Bartlett, and W.K. Joklik, *The sequences of reovirus serotype 3 genome segments M1 and M3 encoding the minor protein mu 2 and the major nonstructural protein mu NS, respectively.* Virology, 1989. **169**(2): p. 293-304.
108. McCutcheon, A.M., T.J. Broering, and M.L. Nibert, *Mammalian reovirus M3 gene sequences and conservation of coiled-coil motifs near the carboxyl terminus of the microNS protein.* Virology, 1999. **264**(1): p. 16-24.
109. Darzynkiewicz, E. and A.J. Shatkin, *Assignment of reovirus mRNA ribosome binding sites to virion genome segments by nucleotide sequence analyses.* Nucleic Acids Res, 1980. **8**(2): p. 337-50.
110. Miura, K., et al., *The 5'-terminal nucleotide sequences of the double-stranded RNA of human reovirus.* Proc Natl Acad Sci U S A, 1974. **71**(10): p. 3979-83.
111. Roner, M.R., K. Bassett, and J. Roehr, *Identification of the 5' sequences required for incorporation of an engineered ssRNA into the Reovirus genome.* Virology, 2004. **329**(2): p. 348-60.
112. Antczak, J.B., et al., *Sequence at both termini of the 10 genes of reovirus serotype 3 (strain Dearing).* Virology, 1982. **121**(2): p. 307-19.
113. Roner, M.R. and J. Roehr, *The 3' sequences required for incorporation of an engineered ssRNA into the Reovirus genome.* Virol J, 2006. **3**: p. 1.

114. Roner, M.R. and B.G. Steele, *Localizing the reovirus packaging signals using an engineered m1 and s2 ssRNA.* Virology, 2007. **358**(1): p. 89-97.
115. Demidenko, A.A., et al., *Engineering recombinant reoviruses with tandem repeats and a tetravirus 2A-like element for exogenous polypeptide expression.* Proc Natl Acad Sci U S A, 2013. **110**(20): p. E1867-76.
116. Roner, M.R. and W.K. Joklik, *Reovirus reverse genetics: Incorporation of the CAT gene into the reovirus genome.* Proc Natl Acad Sci U S A, 2001. **98**(14): p. 8036-41.
117. Roner, M.R. and B.G. Steele, *Features of the mammalian orthoreovirus 3 Dearing l1 single-stranded RNA that direct packaging and serotype restriction.* J Gen Virol, 2007. **88**(Pt 12): p. 3401-12.
118. Luongo, C.L., et al., *Localization of a C-terminal region of lambda2 protein in reovirus cores.* J Virol, 1997. **71**(10): p. 8035-40.
119. Reinisch, K.M., M.L. Nibert, and S.C. Harrison, *Structure of the reovirus core at 3.6 A resolution.* Nature, 2000. **404**(6781): p. 960-7.
120. Dryden, K.A., et al., *Early steps in reovirus infection are associated with dramatic changes in supramolecular structure and protein conformation: analysis of virions and subviral particles by cryoelectron microscopy and image reconstruction.* J Cell Biol, 1993. **122**(5): p. 1023-41.
121. Kim, J., et al., *The hydrophilic amino-terminal arm of reovirus core shell protein lambda1 is dispensable for particle assembly.* J Virol, 2002. **76**(23): p. 12211-22.
122. Zhang, X., et al., *Reovirus polymerase lambda 3 localized by cryo-electron microscopy of virions at a resolution of 7.6 A.* Nat Struct Biol, 2003. **10**(12): p. 1011-8.
123. Coombs, K.M., *Stoichiometry of reovirus structural proteins in virus, ISVP, and core particles.* Virology, 1998. **243**(1): p. 218-28.
124. Zhang, X., et al., *Features of reovirus outer capsid protein mu1 revealed by electron cryomicroscopy and image reconstruction of the virion at 7.0 Angstrom resolution.* Structure, 2005. **13**(10): p. 1545-57.
125. Odegard, A.L., et al., *Disulfide bonding among micro 1 trimers in mammalian reovirus outer capsid: a late and reversible step in virion morphogenesis.* J Virol, 2003. **77**(9): p. 5389-400.
126. Furlong, D.B., M.L. Nibert, and B.N. Fields, *Sigma 1 protein of mammalian reoviruses extends from the surfaces of viral particles.* J Virol, 1988. **62**(1): p. 246-56.
127. Larson, S.M., J.B. Antczak, and W.K. Joklik, *Reovirus exists in the form of 13 particle species that differ in their content of protein sigma 1.* Virology, 1994. **201**(2): p. 303-11.
128. Gilmore, R., et al., *Co-translational trimerization of the reovirus cell attachment protein.* EMBO J, 1996. **15**(11): p. 2651-8.
129. Rosen, L., *Serologic grouping of reoviruses by hemagglutination-inhibition.* Am J Hyg, 1960. **71**: p. 242-9.
130. Roizman, B. and P.R. Roane, Jr., *Studies of polyoma virus. I. Hemagglutination as a measure of virus mass and antibody to the virus.* J Immunol, 1960. **85**: p. 418-28.
131. Ungar, J. and P.W. Muggleton, *The relationship of the aluminium phosphate precipitation of organisms of Haemophilus pertussis strains to their other biological properties.* J Gen Microbiol, 1949. **3**(3): p. 353-60.
132. Armstrong, G.D., R.W. Paul, and P.W. Lee, *Studies on reovirus receptors of L cells: virus binding characteristics and comparison with reovirus receptors of erythrocytes.* Virology, 1984. **138**(1): p. 37-48.
133. Reiss, K., et al., *The GM2 glycan serves as a functional coreceptor for serotype 1 reovirus.* PLoS Pathog, 2012. **8**(12): p. e1003078.
134. Barton, E.S., et al., *Utilization of sialic acid as a coreceptor enhances reovirus attachment by multistep adhesion strengthening.* J Biol Chem, 2001. **276**(3): p. 2200-11.

135. Reiter, D.M., et al., *Crystal structure of reovirus attachment protein sigma1 in complex with sialylated oligosaccharides.* PLoS Pathog, 2011. **7**(8): p. e1002166.
136. Barton, E.S., et al., *Utilization of sialic acid as a coreceptor is required for reovirus-induced biliary disease.* J Clin Invest, 2003. **111**(12): p. 1823-33.
137. Helander, A., et al., *The viral sigma1 protein and glycoconjugates containing alpha2-3-linked sialic acid are involved in type 1 reovirus adherence to M cell apical surfaces.* J Virol, 2003. **77**(14): p. 7964-77.
138. Barton, E.S., et al., *Junction adhesion molecule is a receptor for reovirus.* Cell, 2001. **104**(3): p. 441-51.
139. Campbell, J.A., et al., *Junctional adhesion molecule a serves as a receptor for prototype and field-isolate strains of mammalian reovirus.* J Virol, 2005. **79**(13): p. 7967-78.
140. Antar, A.A., et al., *Junctional adhesion molecule-A is required for hematogenous dissemination of reovirus.* Cell Host Microbe, 2009. **5**(1): p. 59-71.
141. He, X.L., et al., *Structure of the Nogo receptor ectodomain: a recognition module implicated in myelin inhibition.* Neuron, 2003. **38**(2): p. 177-85.
142. Fournier, A.E., T. GrandPre, and S.M. Strittmatter, *Identification of a receptor mediating Nogo-66 inhibition of axonal regeneration.* Nature, 2001. **409**(6818): p. 341-6.
143. Konopka-Anstadt, J.L., et al., *The Nogo receptor NgR1 mediates infection by mammalian reovirus.* Cell Host Microbe, 2014. **15**(6): p. 681-91.
144. Hunt, D., R.S. Coffin, and P.N. Anderson, *The Nogo receptor, its ligands and axonal regeneration in the spinal cord; a review.* J Neurocytol, 2002. **31**(2): p. 93-120.
145. Maginnis, M.S., et al., *Beta1 integrin mediates internalization of mammalian reovirus.* J Virol, 2006. **80**(6): p. 2760-70.
146. Schulz, W.L., A.K. Haj, and L.A. Schiff, *Reovirus uses multiple endocytic pathways for cell entry.* J Virol, 2012. **86**(23): p. 12665-75.
147. Maginnis, M.S., et al., *NPXY motifs in the beta1 integrin cytoplasmic tail are required for functional reovirus entry.* J Virol, 2008. **82**(7): p. 3181-91.
148. Boulant, S., et al., *Similar uptake but different trafficking and escape routes of reovirus virions and infectious subvirion particles imaged in polarized Madin-Darby canine kidney cells.* Mol Biol Cell, 2013. **24**(8): p. 1196-207.
149. Borsa, J., et al., *Two modes of entry of reovirus particles into L cells.* J Gen Virol, 1979. **45**(1): p. 161-70.
150. Lucia-Jandris, P., J.W. Hooper, and B.N. Fields, *Reovirus M2 gene is associated with chromium release from mouse L cells.* J Virol, 1993. **67**(9): p. 5339-45.
151. Owen, R.L., *Sequential uptake of horseradish peroxidase by lymphoid follicle epithelium of Peyer's patches in the normal unobstructed mouse intestine: an ultrastructural study.* Gastroenterology, 1977. **72**(3): p. 440-51.
152. Owen, R.L. and A.L. Jones, *Epithelial cell specialization within human Peyer's patches: an ultrastructural study of intestinal lymphoid follicles.* Gastroenterology, 1974. **66**(2): p. 189-203.
153. Wolf, J.L., et al., *Intestinal M cells: a pathway for entry of reovirus into the host.* Science, 1981. **212**(4493): p. 471-2.
154. Amerongen, H.M., et al., *Proteolytic processing of reovirus is required for adherence to intestinal M cells.* J Virol, 1994. **68**(12): p. 8428-32.
155. Wolf, J.L., et al., *Adherence to and penetration of the intestinal epithelium by reovirus type 1 in neonatal mice.* Gastroenterology, 1987. **92**(1): p. 82-91.
156. Knoop, K.A., et al., *RANKL is necessary and sufficient to initiate development of antigen-sampling M cells in the intestinal epithelium.* J Immunol, 2009. **183**(9): p. 5738-47.

157. Gonzalez-Hernandez, M.B., et al., *Efficient norovirus and reovirus replication in the mouse intestine requires microfold (M) cells.* J Virol, 2014. **88**(12): p. 6934-43.
158. Lai, C.M., et al., *Directional release of reovirus from the apical surface of polarized endothelial cells.* MBio, 2013. **4**(2): p. e00049-13.
159. Wolf, J.L., et al., *Determinants of reovirus interaction with the intestinal M cells and absorptive cells of murine intestine.* Gastroenterology, 1983. **85**(2): p. 291-300.
160. Kauffman, R.S., et al., *The sigma 1 protein determines the extent of spread of reovirus from the gastrointestinal tract of mice.* Virology, 1983. **124**(2): p. 403-10.
161. Chappell, J.D., et al., *Cleavage susceptibility of reovirus attachment protein sigma1 during proteolytic disassembly of virions is determined by a sequence polymorphism in the sigma1 neck.* J Virol, 1998. **72**(10): p. 8205-13.
162. Bodkin, D.K., M.L. Nibert, and B.N. Fields, *Proteolytic digestion of reovirus in the intestinal lumens of neonatal mice.* J Virol, 1989. **63**(11): p. 4676-81.
163. Bass, D.M., et al., *Intraluminal proteolytic activation plays an important role in replication of type 1 reovirus in the intestines of neonatal mice.* J Virol, 1990. **64**(4): p. 1830-3.
164. Freeman, H.J. and Y.S. Kim, *Digestion and absorption of protein.* Annu Rev Med, 1978. **29**: p. 99-116.
165. Yeung, M.C., et al., *The cell attachment proteins of type 1 and type 3 reovirus are differentially susceptible to trypsin and chymotrypsin.* Virology, 1989. **170**(1): p. 62-70.
166. Mendez, II, et al., *Digestion pattern of reovirus outer capsid protein sigma3 determined by mass spectrometry.* Virology, 2003. **311**(2): p. 289-304.
167. Sargent, M.D., D.G. Long, and J. Borsa, *Functional analysis of the interactions between reovirus particles and various proteases in vitro.* Virology, 1977. **78**(1): p. 354-8.
168. Middleton, J.K., et al., *Thermostability of reovirus disassembly intermediates (ISVPs) correlates with genetic, biochemical, and thermodynamic properties of major surface protein mu1.* J Virol, 2002. **76**(3): p. 1051-61.
169. Berard, A. and K.M. Coombs, *Mammalian reoviruses: propagation, quantification, and storage.* Curr Protoc Microbiol, 2009. **Chapter 15**: p. Unit15C 1.
170. Ward, R.L. and C.S. Ashley, *pH modification of the effects of detergents on the stability of enteric viruses.* Appl Environ Microbiol, 1979. **38**(2): p. 314-22.
171. Nygaard, R.M., J.W. Golden, and L.A. Schiff, *Impact of host proteases on reovirus infection in the respiratory tract.* J Virol, 2012. **86**(2): p. 1238-43.
172. Golden, J.W. and L.A. Schiff, *Neutrophil elastase, an acid-independent serine protease, facilitates reovirus uncoating and infection in U937 promonocyte cells.* Virol J, 2005. **2**: p. 48.
173. Martinez, C.G., et al., *The entry of reovirus into L cells is dependent on vacuolar proton-ATPase activity.* J Virol, 1996. **70**(1): p. 576-9.
174. Maratos-Flier, E., et al., *Ammonium inhibits processing and cytotoxicity of reovirus, a nonenveloped virus.* J Clin Invest, 1986. **78**(4): p. 1003-7.
175. Kothandaraman, S., et al., *No role for pepstatin-A-sensitive acidic proteinases in reovirus infections of L or MDCK cells.* Virology, 1998. **251**(2): p. 264-72.
176. Baer, G.S. and T.S. Dermody, *Mutations in reovirus outer-capsid protein sigma3 selected during persistent infections of L cells confer resistance to protease inhibitor E64.* J Virol, 1997. **71**(7): p. 4921-8.
177. Johnson, E.M., et al., *Genetic and pharmacologic alteration of cathepsin expression influences reovirus pathogenesis.* J Virol, 2009. **83**(19): p. 9630-40.
178. Ebert, D.H., et al., *Cathepsin L and cathepsin B mediate reovirus disassembly in murine fibroblast cells.* J Biol Chem, 2002. **277**(27): p. 24609-17.

179. Baer, G.S., et al., *Mutant cells selected during persistent reovirus infection do not express mature cathepsin L and do not support reovirus disassembly.* J Virol, 1999. **73**(11): p. 9532-43.
180. Ebert, D.H., S.A. Kopecky-Bromberg, and T.S. Dermody, *Cathepsin B Is Inhibited in Mutant Cells Selected during Persistent Reovirus Infection.* J Biol Chem, 2004. **279**(5): p. 3837-51.
181. Chandran, K. and M.L. Nibert, *Protease cleavage of reovirus capsid protein mu1/mu1C is blocked by alkyl sulfate detergents, yielding a new type of infectious subvirion particle.* J Virol, 1998. **72**(1): p. 467-75.
182. Chandran, K., D.L. Farsetta, and M.L. Nibert, *Strategy for nonenveloped virus entry: a hydrophobic conformer of the reovirus membrane penetration protein micro 1 mediates membrane disruption.* J Virol, 2002. **76**(19): p. 9920-33.
183. Borsa, J., et al., *Specific monovalent cation effects on modification of reovirus infectivity by chymotrypsin digestion in vitro.* J Virol, 1973. **11**(6): p. 1017-9.
184. Zhang, L., et al., *Reovirus mu1 structural rearrangements that mediate membrane penetration.* J Virol, 2006. **80**(24): p. 12367-76.
185. Odegard, A.L., et al., *Putative autocleavage of outer capsid protein micro1, allowing release of myristoylated peptide micro1N during particle uncoating, is critical for cell entry by reovirus.* J Virol, 2004. **78**(16): p. 8732-45.
186. Ivanovic, T., et al., *Peptides released from reovirus outer capsid form membrane pores that recruit virus particles.* EMBO J, 2008. **27**(8): p. 1289-98.
187. Tillotson, L. and A.J. Shatkin, *Reovirus polypeptide sigma 3 and N-terminal myristoylation of polypeptide mu 1 are required for site-specific cleavage to mu 1C in transfected cells.* J Virol, 1992. **66**(4): p. 2180-6.
188. Both, G.W., S. Lavi, and A.J. Shatkin, *Synthesis of all the gene products of the reovirus genome in vivo and in vitro.* Cell, 1975. **4**(2): p. 173-80.
189. Tao, Y., et al., *RNA synthesis in a cage--structural studies of reovirus polymerase lambda3.* Cell, 2002. **111**(5): p. 733-45.
190. Luongo, C.L., et al., *Binding site for S-adenosyl-L-methionine in a central region of mammalian reovirus lambda2 protein. Evidence for activities in mRNA cap methylation.* J Biol Chem, 1998. **273**(37): p. 23773-80.
191. Shatkin, A.J., *Methylated messenger RNA synthesis in vitro by purified reovirus.* Proc Natl Acad Sci U S A, 1974. **71**(8): p. 3204-7.
192. Noble, S. and M.L. Nibert, *Core protein mu2 is a second determinant of nucleoside triphosphatase activities by reovirus cores.* J Virol, 1997. **71**(10): p. 7728-35.
193. Noble, S. and M.L. Nibert, *Characterization of an ATPase activity in reovirus cores and its genetic association with core-shell protein lambda1.* J Virol, 1997. **71**(3): p. 2182-91.
194. Smith, R.E., H.J. Zweerink, and W.K. Joklik, *Polypeptide components of virions, top component and cores of reovirus type 3.* Virology, 1969. **39**(4): p. 791-810.
195. Dryden, K.A., et al., *Internal/structures containing transcriptase-related proteins in top component particles of mammalian orthoreovirus.* Virology, 1998. **245**(1): p. 33-46.
196. Coombs, K.M., *Identification and characterization of a double-stranded RNA- reovirus temperature-sensitive mutant defective in minor core protein mu2.* J Virol, 1996. **70**(7): p. 4237-45.
197. Chow, N.L. and A.J. Shatkin, *Blocked and unblocked 5' termini in reovirus genome RNA.* J Virol, 1975. **15**(5): p. 1057-64.
198. Desmet, E.A., L.J. Anguish, and J.S. Parker, *Virus-mediated compartmentalization of the host translational machinery.* MBio, 2014. **5**(5): p. e01463-14.
199. Silverstein, S.C. and P.H. Schur, *Immunofluorescent localization of double-stranded RNA in reovirus-infected cells.* Virology, 1970. **41**(3): p. 564-6.

200. Ooms, L.S., et al., *Reovirus replication protein mu2 influences cell tropism by promoting particle assembly within viral inclusions.* J Virol, 2012. **86**(20): p. 10979-87.
201. Parker, J.S., et al., *Reovirus core protein mu2 determines the filamentous morphology of viral inclusion bodies by interacting with and stabilizing microtubules.* J Virol, 2002. **76**(9): p. 4483-96.
202. Becker, M.M., T.R. Peters, and T.S. Dermody, *Reovirus sigma NS and mu NS proteins form cytoplasmic inclusion structures in the absence of viral infection.* J Virol, 2003. **77**(10): p. 5948-63.
203. Yin, P., et al., *Comparisons of the M1 genome segments and encoded mu2 proteins of different reovirus isolates.* Virol J, 2004. **1**: p. 6.
204. Kobayashi, T., et al., *Identification of functional domains in reovirus replication proteins muNS and mu2.* J Virol, 2009. **83**(7): p. 2892-906.
205. Broering, T.J., et al., *Mammalian reovirus nonstructural protein microNS forms large inclusions and colocalizes with reovirus microtubule-associated protein micro2 in transfected cells.* J Virol, 2002. **76**(16): p. 8285-97.
206. Broering, T.J., et al., *Reovirus nonstructural protein mu NS recruits viral core surface proteins and entering core particles to factory-like inclusions.* J Virol, 2004. **78**(4): p. 1882-92.
207. Broering, T.J., et al., *Reovirus nonstructural protein muNS binds to core particles but does not inhibit their transcription and capping activities.* J Virol, 2000. **74**(12): p. 5516-24.
208. Antczak, J.B. and W.K. Joklik, *Reovirus genome segment assortment into progeny genomes studied by the use of monoclonal antibodies directed against reovirus proteins.* Virology, 1992. **187**(2): p. 760-76.
209. Chandran, K., et al., *In vitro recoating of reovirus cores with baculovirus-expressed outer-capsid proteins mu1 and sigma3.* J Virol, 1999. **73**(5): p. 3941-50.
210. Eichwald, C., M. Ackermann, and M.L. Nibert, *The dynamics of both filamentous and globular mammalian reovirus viral factories rely on the microtubule network.* Virology, 2018. **518**: p. 77-86.
211. Berard, A.R., A. Severini, and K.M. Coombs, *Comparative proteomic analyses of two reovirus T3D subtypes and comparison to T1L identifies multiple novel proteins in key cellular pathogenic pathways.* Proteomics, 2015. **15**(12): p. 2113-35.
212. Nygaard, R.M., et al., *Genetic determinants of reovirus pathogenesis in a murine model of respiratory infection.* J Virol, 2013. **87**(16): p. 9279-89.
213. Berard, A.R., A. Severini, and K.M. Coombs, *Differential Reovirus-Specific and Herpesvirus-Specific Activator Protein 1 Activation of Secretogranin II Leads to Altered Virus Secretion.* J Virol, 2015. **89**(23): p. 11954-64.
214. Fields, B.N., R. Laskov, and M.D. Scharff, *Temperature-sensitive mutants of reovirus type 3: studies on the synthesis of viral peptides.* Virology, 1972. **50**(1): p. 209-15.
215. Cross, R.K. and B.N. Fields, *Temperature-sensitive mutants of reovirus type 3: studies on the synthesis of viral RNA.* Virology, 1972. **50**(3): p. 799-809.
216. Fields, B.N., *Temperature-sensitive mutants of reovirus type 3 features of genetic recombination.* Virology, 1971. **46**(1): p. 142-8.
217. Fields, B.N. and W.K. Joklik, *Isolation and preliminary genetic and biochemical characterization of temperature-sensitive mutants of reovirus.* Virology, 1969. **37**(3): p. 335-42.
218. Shmulevitz, M., et al., *Reovirus variants with mutations in genome segments S1 and L2 exhibit enhanced virion infectivity and superior oncolysis.* J Virol, 2012. **86**(13): p. 7403-13.
219. Doyle, J.D., et al., *Diminished reovirus capsid stability alters disease pathogenesis and littermate transmission.* PLoS Pathog, 2015. **11**(3): p. e1004693.
220. Sarkar, P. and P. Danthi, *The mu1 72-96 loop controls conformational transitions during reovirus cell entry.* J Virol, 2013. **87**(24): p. 13532-42.

221. Coombs, K.M., *Reoviruses*, in *eLS*. 2011, John Wiley & Sons, Ltd.
222. Hrdy, D.B., L. Rosen, and B.N. Fields, *Polymorphism of the migration of double-stranded RNA genome segments of reovirus isolates from humans, cattle, and mice.* J Virol, 1979. **31**(1): p. 104-11.
223. Ramig, R.F., R.K. Cross, and B.N. Fields, *Genome RNAs and polypeptides of reovirus serotypes 1, 2, and 3.* J Virol, 1977. **22**(3): p. 726-33.
224. Mohamed, A., et al., *Reduction of virion-associated sigma1 fibers on oncolytic reovirus variants promotes adaptation toward tumorigenic cells.* J Virol, 2015. **89**(8): p. 4319-34.
225. Mainou, B.A. and T.S. Dermody, *Transport to late endosomes is required for efficient reovirus infection.* J Virol, 2012. **86**(16): p. 8346-58.
226. Mainou, B.A., et al., *Reovirus cell entry requires functional microtubules.* MBio, 2013. **4**(4).
227. Danthi, P., et al., *Reovirus receptors, cell entry, and proapoptotic signaling.* Adv Exp Med Biol, 2013. **790**: p. 42-71.
228. Danthi, P., et al., *From touchdown to transcription: the reovirus cell entry pathway.* Curr Top Microbiol Immunol, 2010. **343**: p. 91-119.
229. Danthi, P., et al., *Independent regulation of reovirus membrane penetration and apoptosis by the mu1 phi domain.* PLoS Pathog, 2008. **4**(12): p. e1000248.
230. Agosto, M.A., T. Ivanovic, and M.L. Nibert, *Mammalian reovirus, a nonfusogenic nonenveloped virus, forms size-selective pores in a model membrane.* Proc Natl Acad Sci U S A, 2006. **103**(44): p. 16496-501.
231. Nibert, M.L., et al., *Putative autocleavage of reovirus mu1 protein in concert with outer-capsid disassembly and activation for membrane permeabilization.* J Mol Biol, 2005. **345**(3): p. 461-74.
232. Alain, T., et al., *Proteolytic disassembly is a critical determinant for reovirus oncolysis.* Mol Ther, 2007. **15**(8): p. 1512-21.
233. Golden, J.W., et al., *Addition of exogenous protease facilitates reovirus infection in many restrictive cells.* J Virol, 2002. **76**(15): p. 7430-43.
234. Spendlove, R.S., M.E. McClain, and E.H. Lennette, *Enhancement of reovirus infectivity by extracellular removal or alteration of the virus capsid by proteolytic enzymes.* J Gen Virol, 1970. **8**(2): p. 83-94.
235. Skehel, J.J. and W.K. Joklik, *Studies on the in vitro transcription of reovirus RNA catalyzed by reovirus cores.* Virology, 1969. **39**(4): p. 822-31.
236. Shing, M. and K.M. Coombs, *Assembly of the reovirus outer capsid requires mu 1/sigma 3 interactions which are prevented by misfolded sigma 3 protein in temperature-sensitive mutant tsG453.* Virus Res, 1996. **46**(1-2): p. 19-29.
237. Xu, P., S.E. Miller, and W.K. Joklik, *Generation of reovirus core-like particles in cells infected with hybrid vaccinia viruses that express genome segments L1, L2, L3, and S2.* Virology, 1993. **197**(2): p. 726-31.
238. Tyler, K.L., et al., *Differences in the capacity of reovirus strains to induce apoptosis are determined by the viral attachment protein sigma 1.* J Virol, 1995. **69**(11): p. 6972-9.
239. Shmulevitz, M., et al., *Oncogenic Ras promotes reovirus spread by suppressing IFN-beta production through negative regulation of RIG-I signaling.* Cancer Res, 2010. **70**(12): p. 4912-21.
240. Loo, Y.M., et al., *Distinct RIG-I and MDA5 signaling by RNA viruses in innate immunity.* J Virol, 2008. **82**(1): p. 335-45.
241. Goubau, D., et al., *Antiviral immunity via RIG-I-mediated recognition of RNA bearing 5'-diphosphates.* Nature, 2014. **514**(7522): p. 372-375.
242. Kato, H., et al., *Length-dependent recognition of double-stranded ribonucleic acids by retinoic acid-inducible gene-I and melanoma differentiation-associated gene 5.* J Exp Med, 2008. **205**(7): p. 1601-10.

243. Henderson, D.R. and W.K. Joklik, *The mechanism of interferon induction by UV-irradiated reovirus.* Virology, 1978. **91**(2): p. 389-406.
244. Duncan, R., et al., *Identification of conserved domains in the cell attachment proteins of the three serotypes of reovirus.* Virology, 1990. **174**(2): p. 399-409.
245. Wiener, J.R. and W.K. Joklik, *The sequences of the reovirus serotype 1, 2, and 3 L1 genome segments and analysis of the mode of divergence of the reovirus serotypes.* Virology, 1989. **169**(1): p. 194-203.
246. Kobayashi, T., et al., *A plasmid-based reverse genetics system for animal double-stranded RNA viruses.* Cell Host Microbe, 2007. **1**(2): p. 147-57.
247. Komoto, S., et al., *A plasmid-based reverse genetics system for mammalian orthoreoviruses driven by a plasmid-encoded T7 RNA polymerase.* J Virol Methods, 2014. **196**: p. 36-9.
248. Boehme, K.W., et al., *Reverse genetics for mammalian reovirus.* Methods, 2011. **55**(2): p. 109-13.
249. Liemann, S., et al., *Structure of the reovirus membrane-penetration protein, Mu1, in a complex with is protector protein, Sigma3.* Cell, 2002. **108**(2): p. 283-95.
250. Olland, A.M., et al., *Structure of the reovirus outer capsid and dsRNA-binding protein sigma3 at 1.8 A resolution.* EMBO J, 2001. **20**(5): p. 979-89.
251. Jane-Valbuena, J., et al., *Sites and determinants of early cleavages in the proteolytic processing pathway of reovirus surface protein sigma3.* J Virol, 2002. **76**(10): p. 5184-97.
252. Denzler, K.L. and B.L. Jacobs, *Site-directed mutagenic analysis of reovirus sigma 3 protein binding to dsRNA.* Virology, 1994. **204**(1): p. 190-9.
253. Wang, Q., et al., *Site-directed mutagenesis of the double-stranded RNA binding domain of bacterially-expressed sigma 3 reovirus protein.* Virus Res, 1996. **41**(2): p. 141-51.
254. Mabrouk, T., C. Danis, and G. Lemay, *Two basic motifs of reovirus sigma 3 protein are involved in double-stranded RNA binding.* Biochem Cell Biol, 1995. **73**(3-4): p. 137-45.
255. Ebert, D.H., et al., *Adaptation of reovirus to growth in the presence of protease inhibitor E64 segregates with a mutation in the carboxy terminus of viral outer-capsid protein sigma3.* J Virol, 2001. **75**(7): p. 3197-206.
256. Clark, K.M., et al., *Reovirus variants selected for resistance to ammonium chloride have mutations in viral outer-capsid protein sigma3.* J Virol, 2006. **80**(2): p. 671-81.
257. Doyle, J.D., et al., *Molecular determinants of proteolytic disassembly of the reovirus outer capsid.* J Biol Chem, 2012. **287**(11): p. 8029-38.
258. Roner, M.R., et al., *Identification of signals required for the insertion of heterologous genome segments into the reovirus genome.* Proc Natl Acad Sci U S A, 1995. **92**(26): p. 12362-6.
259. Mbisa, J.L., et al., *Reovirus mu2 protein determines strain-specific differences in the rate of viral inclusion formation in L929 cells.* Virology, 2000. **272**(1): p. 16-26.
260. Miller, C.L., et al., *Increased ubiquitination and other covariant phenotypes attributed to a strain- and temperature-dependent defect of reovirus core protein mu2.* J Virol, 2004. **78**(19): p. 10291-302.
261. Zurney, J., et al., *Reovirus mu2 protein inhibits interferon signaling through a novel mechanism involving nuclear accumulation of interferon regulatory factor 9.* J Virol, 2009. **83**(5): p. 2178-87.
262. Irvin, S.C., et al., *A single-amino-acid polymorphism in reovirus protein mu2 determines repression of interferon signaling and modulates myocarditis.* J Virol, 2012. **86**(4): p. 2302-11.
263. Yue, Z. and A.J. Shatkin, *Double-stranded RNA-dependent protein kinase (PKR) is regulated by reovirus structural proteins.* Virology, 1997. **234**(2): p. 364-71.
264. Smith, J.A., et al., *Involvement of the interferon-regulated antiviral proteins PKR and RNase L in reovirus-induced shutoff of cellular translation.* J Virol, 2005. **79**(4): p. 2240-50.

265. Kim, J., et al., *Nucleoside and RNA triphosphatase activities of orthoreovirus transcriptase cofactor mu2.* J Biol Chem, 2004. **279**(6): p. 4394-403.
266. Yin, P., M. Cheang, and K.M. Coombs, *The M1 gene is associated with differences in the temperature optimum of the transcriptase activity in reovirus core particles.* J Virol, 1996. **70**(2): p. 1223-7.
267. Bisaillon, M., J. Bergeron, and G. Lemay, *Characterization of the nucleoside triphosphate phosphohydrolase and helicase activities of the reovirus lambda1 protein.* J Biol Chem, 1997. **272**(29): p. 18298-303.
268. Bisaillon, M. and G. Lemay, *Characterization of the reovirus lambda1 protein RNA 5'-triphosphatase activity.* J Biol Chem, 1997. **272**(47): p. 29954-7.
269. Schneider, W.L. and M.J. Roossinck, *Genetic diversity in RNA virus quasispecies is controlled by host-virus interactions.* J Virol, 2001. **75**(14): p. 6566-71.
270. Mann, M.A., et al., *Type 3 reovirus neuroinvasion after intramuscular inoculation: viral genetic determinants of lethality and spinal cord infection.* Virology, 2002. **303**(2): p. 213-21.
271. Tyler, K.L., et al., *Protective anti-reovirus monoclonal antibodies and their effects on viral pathogenesis.* J Virol, 1993. **67**(6): p. 3446-53.
272. Dalldorf, G., *Brief review of Coxsackie viruses in 1956.* Ann N Y Acad Sci, 1957. **67**(8): p. 209-11.
273. Sherry, B., et al., *Derivation and characterization of an efficiently myocarditic reovirus variant.* J Virol, 1989. **63**(11): p. 4840-9.
274. Bellamy, A.R., et al., *Studies on reovirus RNA. I. Characterization of reovirus genome RNA.* J Mol Biol, 1967. **29**(1): p. 1-17.
275. Gomatos, P.J. and I. Tamm, *The Secondary Structure of Reovirus Rna.* Proc Natl Acad Sci U S A, 1963. **49**(5): p. 707-14.
276. American Type Culture Collection. *Reovirus 3 (ATCC® VR-824™)*. 2018; Available from: www.atcc.org/en/Products/All/VR-824.aspx#history.
277. Sandekian, V. and G. Lemay, *A single amino acid substitution in the mRNA capping enzyme lambda2 of a mammalian orthoreovirus mutant increases interferon sensitivity.* Virology, 2015. **483**: p. 229-35.
278. van den Wollenberg, D.J., et al., *Isolation of reovirus T3D mutants capable of infecting human tumor cells independent of junction adhesion molecule-A.* PLoS One, 2012. **7**(10): p. e48064.
279. Chakrabarty, R., et al., *Evaluation of homogeneity and genetic stability of REOLYSIN (pelareorep) by complete genome sequencing of reovirus after large scale production.* Appl Microbiol Biotechnol, 2014. **98**(4): p. 1763-70.
280. Bokiej, M., et al., *Optimum length and flexibility of reovirus attachment protein sigma1 are required for efficient viral infection.* J Virol, 2012. **86**(19): p. 10270-80.
281. Ahmed, R. and B.N. Fields, *Reassortment of genome segments between reovirus defective interfering particles and infectious virus: construction of temperature-sensitive and attenuated viruses by rescue of mutations from DI particles.* Virology, 1981. **111**(2): p. 351-63.
282. Lechner, M.G., et al., *Immunogenicity of murine solid tumor models as a defining feature of in vivo behavior and response to immunotherapy.* J Immunother, 2013. **36**(9): p. 477-89.
283. Beattie, E., et al., *Reversal of the interferon-sensitive phenotype of a vaccinia virus lacking E3L by expression of the reovirus S4 gene.* J Virol, 1995. **69**(1): p. 499-505.
284. Schiff, L.A., et al., *Distinct binding sites for zinc and double-stranded RNA in the reovirus outer capsid protein sigma 3.* Mol Cell Biol, 1988. **8**(1): p. 273-83.
285. Mabrouk, T. and G. Lemay, *Mutations in a CCHC zinc-binding motif of the reovirus sigma 3 protein decrease its intracellular stability.* J Virol, 1994. **68**(8): p. 5287-90.
286. InvivoGen. *Poly(I:C) (HMW) Biotin*. 2018; Available from: www.invivogen.com/polyic-biotin.

287. Imai, M., et al., *Molecular cloning of double-stranded RNA virus genomes.* Proc Natl Acad Sci U S A, 1983. **80**(2): p. 373-7.
288. Schiff, L.A., *Reovirus capsid proteins sigma 3 and mu 1: interactions that influence viral entry, assembly, and translational control.* Curr Top Microbiol Immunol, 1998. **233**(Pt 1): p. 167-83.
289. Wilson, G.J., et al., *A single mutation in the carboxy terminus of reovirus outer-capsid protein sigma 3 confers enhanced kinetics of sigma 3 proteolysis, resistance to inhibitors of viral disassembly, and alterations in sigma 3 structure.* J Virol, 2002. **76**(19): p. 9832-43.
290. Shah, P.N.M., et al., *Genome packaging of reovirus is mediated by the scaffolding property of the microtubule network.* Cell Microbiol, 2017. **19**(12).
291. Carvalho, J., M.M. Arnold, and M.L. Nibert, *Silencing and complementation of reovirus core protein mu2: functional correlations with mu2-microtubule association and differences between virus- and plasmid-derived mu2.* Virology, 2007. **364**(2): p. 301-16.
292. Lemay, G. and C. Danis, *Reovirus lambda 1 protein: affinity for double-stranded nucleic acids by a small amino-terminal region of the protein independent from the zinc finger motif.* J Gen Virol, 1994. **75 (Pt 11)**: p. 3261-6.
293. Harrison, S.J., et al., *Mammalian reovirus L3 gene sequences and evidence for a distinct amino-terminal region of the lambda1 protein.* Virology, 1999. **258**(1): p. 54-64.
294. Morgan, E.M. and H.J. Zweerink, *Reovirus morphogenesis. Corelike particles in cells infected at 39 degrees with wild-type reovirus and temperature-sensitive mutants of groups B and G.* Virology, 1974. **59**(2): p. 556-65.
295. Lemay, G. and M. Bisaillon, *Further characterization and determination of the single amino acid change in the tsI138 reovirus thermosensitive mutant.* Can J Microbiol, 2012. **58**(5): p. 589-95.
296. Zhu, S., et al., *p38MAPK plays a critical role in induction of a pro-inflammatory phenotype of retinal Muller cells following Zika virus infection.* Antiviral Res, 2017. **145**: p. 70-81.
297. Hirasawa, K., et al., *Effect of p38 mitogen-activated protein kinase on the replication of encephalomyocarditis virus.* J Virol, 2003. **77**(10): p. 5649-56.
298. Johnson, J.C., et al., *Pyridinyl imidazole inhibitors of p38 MAP kinase impair viral entry and reduce cytokine induction by Zaire ebolavirus in human dendritic cells.* Antiviral Res, 2014. **107**: p. 102-9.
299. Borgeling, Y., et al., *Inhibition of p38 mitogen-activated protein kinase impairs influenza virus-induced primary and secondary host gene responses and protects mice from lethal H5N1 infection.* J Biol Chem, 2014. **289**(1): p. 13-27.
300. Norman, K.L., et al., *Reovirus oncolysis: the Ras/RalGEF/p38 pathway dictates host cell permissiveness to reovirus infection.* Proc Natl Acad Sci U S A, 2004. **101**(30): p. 11099-104.
301. Wilson, K.P., et al., *The structural basis for the specificity of pyridinylimidazole inhibitors of p38 MAP kinase.* Chem Biol, 1997. **4**(6): p. 423-31.
302. Kang, Y.J., et al., *Multiple activation mechanisms of p38alpha mitogen-activated protein kinase.* J Biol Chem, 2006. **281**(36): p. 26225-34.
303. Knebel, A., et al., *Stress-induced regulation of eukaryotic elongation factor 2 kinase by SB 203580-sensitive and -insensitive pathways.* Biochem J, 2002. **367**(Pt 2): p. 525-32.
304. van den Blink, B., et al., *P38 mitogen activated protein kinase is involved in the downregulation of granulocyte CXC chemokine receptors 1 and 2 during human endotoxemia.* J Clin Immunol, 2004. **24**(1): p. 37-41.
305. Felberbaum-Corti, M., V. Cavalli, and J. Gruenberg, *Capture of the small GTPase Rab5 by GDI: regulation by p38 MAP kinase.* Methods Enzymol, 2005. **403**: p. 367-81.
306. McLaughlin, N.J., et al., *Platelet-activating factor-induced clathrin-mediated endocytosis requires beta-arrestin-1 recruitment and activation of the p38 MAPK signalosome at the plasma membrane for actin bundle formation.* J Immunol, 2006. **176**(11): p. 7039-50.

307. Cavalli, V., et al., *The stress-induced MAP kinase p38 regulates endocytic trafficking via the GDI:Rab5 complex.* Mol Cell, 2001. **7**(2): p. 421-32.
308. Ji, W.T., et al., *AMP-activated protein kinase facilitates avian reovirus to induce mitogen-activated protein kinase (MAPK) p38 and MAPK kinase 3/6 signalling that is beneficial for virus replication.* J Gen Virol, 2009. **90**(Pt 12): p. 3002-9.
309. Mainou, B.A. and T.S. Dermody, *Src kinase mediates productive endocytic sorting of reovirus during cell entry.* J Virol, 2011. **85**(7): p. 3203-13.
310. Huotari, J. and A. Helenius, *Endosome maturation.* EMBO J, 2011. **30**(17): p. 3481-500.
311. Scott, C.C., F. Vacca, and J. Gruenberg, *Endosome maturation, transport and functions.* Semin Cell Dev Biol, 2014. **31**: p. 2-10.
312. Poteryaev, D., et al., *Identification of the switch in early-to-late endosome transition.* Cell, 2010. **141**(3): p. 497-508.
313. Punnonen, E.L., K. Ryhanen, and V.S. Marjomaki, *At reduced temperature, endocytic membrane traffic is blocked in multivesicular carrier endosomes in rat cardiac myocytes.* Eur J Cell Biol, 1998. **75**(4): p. 344-52.
314. Baravalle, G., et al., *Transferrin recycling and dextran transport to lysosomes is differentially affected by bafilomycin, nocodazole, and low temperature.* Cell Tissue Res, 2005. **320**(1): p. 99-113.
315. Cuadrado, A. and A.R. Nebreda, *Mechanisms and functions of p38 MAPK signalling.* Biochem J, 2010. **429**(3): p. 403-17.
316. Kuma, Y., et al., *BIRB796 inhibits all p38 MAPK isoforms in vitro and in vivo.* J Biol Chem, 2005. **280**(20): p. 19472-9.
317. Shankavaram, U.T., et al., *CellMiner: a relational database and query tool for the NCI-60 cancer cell lines.* BMC Genomics, 2009. **10**: p. 277.
318. Gholami, A.M., et al., *Global proteome analysis of the NCI-60 cell line panel.* Cell Rep, 2013. **4**(3): p. 609-20.
319. Guruceaga, E., et al., *Enhanced Missing Proteins Detection in NCI60 Cell Lines Using an Integrative Search Engine Approach.* J Proteome Res, 2017. **16**(12): p. 4374-4390.
320. Mainou, B.A. and T.S. Dermody, *In search of cathepsins: how reovirus enters host cells.* DNA Cell Biol, 2012. **31**(12): p. 1646-9.
321. Terasawa, Y., et al., *Activity levels of cathepsins B and L in tumor cells are a biomarker for efficacy of reovirus-mediated tumor cell killing.* Cancer Gene Ther, 2015. **22**(4): p. 188-97.
322. Gong, J. and M.M. Mita, *Activated ras signaling pathways and reovirus oncolysis: an update on the mechanism of preferential reovirus replication in cancer cells.* Front Oncol, 2014. **4**: p. 167.
323. Shmulevitz, M., P. Marcato, and P.W. Lee, *Unshackling the links between reovirus oncolysis, Ras signaling, translational control and cancer.* Oncogene, 2005. **24**(52): p. 7720-8.
324. Marcato, P., M. Shmulevitz, and P.W. Lee, *Connecting reovirus oncolysis and Ras signaling.* Cell Cycle, 2005. **4**(4): p. 556-9.
325. Cargnello, M. and P.P. Roux, *Activation and function of the MAPKs and their substrates, the MAPK-activated protein kinases.* Microbiol Mol Biol Rev, 2011. **75**(1): p. 50-83.
326. Cheng, H., et al., *Inhibition of Ebola and Marburg Virus Entry by G Protein-Coupled Receptor Antagonists.* J Virol, 2015. **89**(19): p. 9932-8.
327. Chen, Y., et al., *p38 inhibition provides anti-DNA virus immunity by regulation of USP21 phosphorylation and STING activation.* J Exp Med, 2017. **214**(4): p. 991-1010.
328. Lau, C., et al., *Syk associates with clathrin and mediates phosphatidylinositol 3-kinase activation during human rhinovirus internalization.* J Immunol, 2008. **180**(2): p. 870-80.

329. Wang, X., et al., *Syk is downstream of intercellular adhesion molecule-1 and mediates human rhinovirus activation of p38 MAPK in airway epithelial cells.* J Immunol, 2006. **177**(10): p. 6859-70.
330. Keil, E., et al., *Phosphorylation of Atg5 by the Gadd45beta-MEKK4-p38 pathway inhibits autophagy.* Cell Death Differ, 2013. **20**(2): p. 321-32.
331. Jha, A., et al., *Convergent regulation of the lysosomal two-pore channel-2 by Mg(2)(+), NAADP, PI(3,5)P(2) and multiple protein kinases.* EMBO J, 2014. **33**(5): p. 501-11.
332. Lin, P.H., et al., *Lysosomal two-pore channel subtype 2 (TPC2) regulates skeletal muscle autophagic signaling.* J Biol Chem, 2015. **290**(6): p. 3377-89.
333. Morano, K.A. and D.J. Klionsky, *Differential effects of compartment deacidification on the targeting of membrane and soluble proteins to the vacuole in yeast.* J Cell Sci, 1994. **107 (Pt 10)**: p. 2813-24.
334. Settembre, C., et al., *A lysosome-to-nucleus signalling mechanism senses and regulates the lysosome via mTOR and TFEB.* EMBO J, 2012. **31**(5): p. 1095-108.
335. Li, W., et al., *Phosphorylation of LAMP2A by p38 MAPK couples ER stress to chaperone-mediated autophagy.* Nat Commun, 2017. **8**(1): p. 1763.
336. Thirukkumaran, C.M., et al., *Reovirus modulates autophagy during oncolysis of multiple myeloma.* Autophagy, 2013. **9**(3): p. 413-4.
337. Zer, C., G. Sachs, and J.M. Shin, *Identification of genomic targets downstream of p38 mitogen-activated protein kinase pathway mediating tumor necrosis factor-alpha signaling.* Physiol Genomics, 2007. **31**(2): p. 343-51.
338. del Barco Barrantes, I., et al., *Genetic analysis of specific and redundant roles for p38alpha and p38beta MAPKs during mouse development.* Proc Natl Acad Sci U S A, 2011. **108**(31): p. 12764-9.
339. Cerezo-Guisado, M.I., et al., *Evidence of p38gamma and p38delta involvement in cell transformation processes.* Carcinogenesis, 2011. **32**(7): p. 1093-9.
340. Schindler, E.M., et al., *p38delta Mitogen-activated protein kinase is essential for skin tumor development in mice.* Cancer Res, 2009. **69**(11): p. 4648-55.
341. Jones, D.S., et al., *Inflammatory but not mitogenic contexts prime synovial fibroblasts for compensatory signaling responses to p38 inhibition.* Sci Signal, 2018. **11**(520).
342. Ferreiro, I., et al., *Whole genome analysis of p38 SAPK-mediated gene expression upon stress.* BMC Genomics, 2010. **11**: p. 144.
343. Cao, W., et al., *p38 mitogen-activated protein kinase is the central regulator of cyclic AMP-dependent transcription of the brown fat uncoupling protein 1 gene.* Mol Cell Biol, 2004. **24**(7): p. 3057-67.
344. Shimizu, Y., et al., *Activation of mitogen-activated protein kinase by norepinephrine in brown adipocytes from rats.* Endocrinology, 1997. **138**(1): p. 248-53.
345. Lu, C., et al., *Serum starvation induces H2AX phosphorylation to regulate apoptosis via p38 MAPK pathway.* FEBS Lett, 2008. **582**(18): p. 2703-8.
346. Coyne, C.B., *The distinct roles of JAM-A in reovirus pathogenesis.* Cell Host Microbe, 2009. **5**(1): p. 3-5.
347. Lai, C.M., et al., *Endothelial JAM-A promotes reovirus viremia and bloodstream dissemination.* J Infect Dis, 2015. **211**(3): p. 383-93.
348. Sanjuan, R., et al., *Viral mutation rates.* J Virol, 2010. **84**(19): p. 9733-48.
349. Eigen, M., *On the nature of virus quasispecies.* Trends Microbiol, 1996. **4**(6): p. 216-8.
350. Gaudieri, S., et al., *Hepatitis C virus drug resistance and immune-driven adaptations: relevance to new antiviral therapy.* Hepatology, 2009. **49**(4): p. 1069-82.
351. Shi, Y., et al., *Enabling the 'host jump': structural determinants of receptor-binding specificity in influenza A viruses.* Nat Rev Microbiol, 2014. **12**(12): p. 822-31.

352. Sabin, A.B., *Oral poliovirus vaccine: history of its development and use and current challenge to eliminate poliomyelitis from the world.* J Infect Dis, 1985. **151**(3): p. 420-36.
353. Bonhoeffer, S., E.C. Holmes, and M.A. Nowak, *Causes of HIV diversity.* Nature, 1995. **376**(6536): p. 125.
354. Taubenberger, J.K. and J.C. Kash, *Influenza virus evolution, host adaptation, and pandemic formation.* Cell Host Microbe, 2010. **7**(6): p. 440-51.
355. Nwajei, B.N., A.A. Afaleq, and R.C. Jones, *Comparison of chick embryo liver and vero cell cultures for the isolation and growth of avian reoviruses.* Avian Pathol, 1988. **17**(4): p. 759-66.
356. Smith, C.D., et al., *Alternative cell line for virus isolation.* J Clin Microbiol, 1986. **24**(2): p. 265-8.
357. Ramos-Alvarez, M. and A.B. Sabin, *Enteropathogenic viruses and bacteria; role in summer diarrheal diseases of infancy and early childhood.* J Am Med Assoc, 1958. **167**(2): p. 147-56.
358. Hull, R.N., W.R. Cherry, and O.J. Tritch, *Growth characteristics of monkey kidney cell strains LLC-MK1, LLC-MK2, and LLC-MK2(NCTC-3196) and their utility in virus research.* J Exp Med, 1962. **115**: p. 903-18.
359. Gomatos, P.J., et al., *Reovirus type 3: physical characteristics and interaction with L cells.* Virology, 1962. **17**: p. 441-54.
360. Gomatos, P.J. and I. Tamm, *Base composition of the RNA of a reovirus variant.* Science, 1963. **140**(3570): p. 997-8.
361. Zamarin, D., et al., *PD-L1 in tumor microenvironment mediates resistance to oncolytic immunotherapy.* J Clin Invest, 2018. **128**(4): p. 1413-1428.
362. Potts, K.G., et al., *Deletion of F4L (ribonucleotide reductase) in vaccinia virus produces a selective oncolytic virus and promotes anti-tumor immunity with superior safety in bladder cancer models.* EMBO Mol Med, 2017. **9**(5): p. 638-654.
363. Samson, A., et al., *Intravenous delivery of oncolytic reovirus to brain tumor patients immunologically primes for subsequent checkpoint blockade.* Sci Transl Med, 2018. **10**(422).
364. Ribas, A., et al., *Oncolytic Virotherapy Promotes Intratumoral T Cell Infiltration and Improves Anti-PD-1 Immunotherapy.* Cell, 2017. **170**(6): p. 1109-1119 e10.
365. Kelly, K.R., et al., *Oncolytic reovirus sensitizes multiple myeloma cells to anti-PD-L1 therapy.* Leukemia, 2018. **32**(1): p. 230-233.
366. Bommareddy, P.K., M. Shettigar, and H.L. Kaufman, *Integrating oncolytic viruses in combination cancer immunotherapy.* Nat Rev Immunol, 2018.
367. Marelli, G., et al., *Oncolytic Viral Therapy and the Immune System: A Double-Edged Sword Against Cancer.* Front Immunol, 2018. **9**: p. 866.
368. Achard, C., et al., *Lighting a Fire in the Tumor Microenvironment Using Oncolytic Immunotherapy.* EBioMedicine, 2018. **31**: p. 17-24.
369. Schmechel, S., et al., *Preferential translation of reovirus mRNA by a sigma3-dependent mechanism.* Virology, 1997. **232**(1): p. 62-73.
370. Srivastava, A., et al., *Emerging Functional Divergence of beta-Arrestin Isoforms in GPCR Function.* Trends Endocrinol Metab, 2015. **26**(11): p. 628-642.